



This work is protected by copyright and other intellectual property rights and duplication or sale of all or part is not permitted, except that material may be duplicated by you for research, private study, criticism/review or educational purposes. Electronic or print copies are for your own personal, non-commercial use and shall not be passed to any other individual. No quotation may be published without proper acknowledgement. For any other use, or to quote extensively from the work, permission must be obtained from the copyright holder/s.

Expression and functionality of
beta-chemokines in endothelial
cells of the rheumatoid
synovium

Lisa Rump-Goodrich

A thesis submitted for the
award of Doctor of Philosophy

March 2016

Keele University

Contents

Dedication	I
Acknowledgments	II
List of figures	III
List of Tables	XI
Abstract	XIV
Published abstracts	XV
Abbreviations	XVI
Chapter 1 – Introduction	1
1. Rheumatoid Arthritis (RA)	2
1.1 What is RA?	2
1.2 Autoimmunity	8
1.3 Cells involved in RA	11
1.3.1 Macrophages	11
1.3.2 Synovial fibroblasts	12
1.3.3 Dendritic cells (DCs)	16
1.3.4 Neutrophils	16
1.3.5 B cells	17
1.3.6 T-cells	18
1.3.7 Pannocytes (PCs)	19
1.3.8 Chondrocytes	19
1.1.9 Osteoclasts	20
1.3.10 Endothelial cells (ECs)	20
1.3.11 Cell populations in acidic environments.	24

1.4	Angiogenesis in RA	25
1.5.	Structure of the synovium	26
1.6.	Function of the synovium	28
1.6.1	Cartilage lubrication	28
1.6.2	Tissue surface maintenance	29
1.6.3	Chondrocyte nutrition	30
1.6.4	Synovial fluid composition and volume control	30
1.7.	Leukocyte infiltration into the synovium	31
1.7.1	Chemokines and transendothelial migration (TEM)	32
1.7.1.1	Chemoattraction and Integrin activation	32
1.7.1.2	Activation	38
1.7.1.3	Leukocyte capture and rolling	36
1.7.1.4	Arrest and firm adhesion	38
1.7.1.5	Crawling	40
1.7.1.6	Podosome formation and conformational changes	40
1.7.1.7	Transmigration	42
1.7.1.8	Transcellular migration	42
1.7.1.9	Paracellular migration	43
1.8.	Chemokines and chemokine receptors	45
1.8.1	Chemokines	45
1.8.2	Chemokine receptors	46
1.8.3	Chemokine involvement in rheumatoid arthritis	49
1.8.3.1	Inflammatory chemokines	49
1.8.3.2	Constitutive chemokines	50

2.4.2	Protein synthesis arrest	95
2.4.3	Immunofluorescent staining of cultured HBMECs and HDLECs	98
2.4.3.1	Whole cell staining in chamber slides	98
2.4.3.2	Cell surface staining in chamber slides	99
2.4.4	Quantitation of Immunofluorescence	100
2.5	Materials and methods used in chapter 5	100
2.5.1	Isolation of cells from human blood	100
2.5.1.1	Peripheral Blood Mononuclear Cell (PBMC) isolation	100
2.5.2	Transmigration	101
2.5.2.1	Stimulation of inflammatory conditions in transwell systems for transmigration analysis across cultured cell monolayers	101
2.5.2.2	Optimisation of chemokine concentrations for transmigration analysis	102
2.5.2.3	Transmigration of mononuclear cells across HBMEC monolayers in response to human CCL7, CCL14, CCL16 and CCL22	104
2.5.3	Sample preparation for transmission electron microscopy (EM)	105
2.5.3.1	Buffers	105
2.5.3.2	Preparation of filters for EM	105
2.5.3.3	Post fixation and Spurr embedding of cells on filters.	106
2.5.3.4	Staining of ultrathin sections for EM	107
2.6	Materials and methods used in chapter 6	108
2.6.1	RA and non-RA blood samples.	108

2.6.2 Transmigration of mononuclear cells across HDLEC monolayers in response to human CCL7	109
2.6.3 Flow Cytometry	110
2.6.3.1 Chemokine receptor staining of leukocytes from human Blood	110
2.6.3.2 CD marker staining of leukocytes from human blood	110
2.7 Materials and methods used in chapter 7	112
2.7.1 Matched blood and synovial fluid for ELISA analysis	112
2.7.2 ELISA of matched synovial fluid and serum samples	113
2.7.3 Plate Preparation	113
2.7.4 Assay procedure	113
 Chapter 3 – Immunofluorescent analysis of synovial tissue	 115
3.1 Introduction and Aims	116
3.2 Materials and Methods	118
3.2.1 Quantitation of results	118
3.3 Results	119
3.3.1 Beta chemokines on synovial ECs	119
3.3.1.1 CCL1 in RA synovial tissue	119
3.3.1.2 CCL2 in RA synovial tissue	120
3.3.1.3 CCL3 in RA synovial tissue	120
3.3.1.4 CCL4 in RA and non-RA synovial tissue	120
3.3.1.5 CCL5 in RA synovial tissue	121

3.3.1.6	CCL7 and VWF in RA and non-RA synovial tissue	130
3.3.1.7	CCL7 and LYVE-1 in RA and non-RA synovial tissue	130
3.3.1.8	CCL8 and VWF staining in RA synovial tissue	136
3.3.1.9	CCL10 and VWF staining in RA synovial tissue	136
3.3.1.10	CCL11 and VWF staining in RA synovial tissue	136
3.3.1.11	CCL12 and VWF staining in RA synovial tissue	141
3.3.1.12	CCL13 and VWF staining in RA synovial tissue	141
3.3.1.13	CCL14 and VWF staining in RA and non-RA synovial tissue	141
3.3.1.14	CCL14 and LYVE-1 staining in RA and non-RA synovial tissue	142
3.3.1.15	CCL15 and VWF staining in RA synovial tissue	142
3.3.1.16	CCL16 and VWF staining in RA and non-RA synovial tissue	150
3.3.1.17	CCL16 and LYVE-1 staining in RA and non-RA synovial tissue	150
3.3.1.18	CCL17 and VWF staining in RA synovial tissue	150
3.3.1.19	CCL18 and VWF staining in RA synovial tissue	151
3.3.1.20	CCL19 and VWF staining in RA and non-RA synovial tissue	151
3.3.1.21	CCL20 and VWF staining in RA synovial tissue	160
3.3.1.22	CCL21 and VWF staining in RA synovial tissue	160
3.3.1.23	CCL22 and VWF staining in RA and non-RA synovial tissue	160
3.3.1.24	CCL22 and LYVE-1 staining in RA and non-RA	

synovial tissue	161
3.3.1.25 CCL23 and VWF staining in RA synovial tissue	161
3.3.1.26 CCL24 and VWF staining in RA synovial tissue	161
3.3.1.27 CCL25 and VWF staining in RA synovial tissue	170
3.3.1.28 CCL26 and VWF staining in RA synovial tissue	170
3.3.1.29 CCL27 and VWF staining in RA synovial tissue	170
3.3.1.30 CCL28 and VWF staining in RA synovial tissue	170
3.4 Iron and aluminium content of RA tissue	175
3.5 Discussion.	177

Chapter 4 - Analysis of ICAM-1 and chemokine levels in cultured endothelial

cells	183
4.1 Introduction and Aims	184
4.2 Materials and methods	185
4.2.1 Quantitation of results	186
4.3 Results	187
4.3.1 Cell surface ICAM-1 intensity following 16 hour simulation of HBMECs	187
4.3.1.1 Stimulation of HBMECs with 100ng/ml TNF- α	187
4.3.1.2 Stimulation of HBMECs with 100ng/ml IFN- γ	187
4.3.1.3 Stimulation of HBMECs with 100ng/ml TNF- α and 100ng/ml IFN- γ	188
4.3.2 Time dependent stimulation of HBMECs with 100ng/ml TNF- α	193
4.4 Chemokine generation at activated HBMECs	196
4.4.1 Time dependent CCL7 generation at HBMECs in	

the absence and presence of 10ug/ml cycloheximide	196
4.4.2 Time dependent CCL14 generation at HBMECs in the absence and presence of 10ug/ml cycloheximide	201
4.4.3 Time dependent CCL16 generation at HBMECs in the absence and presence of 10µg/ml cycloheximide	205
4.4.4 Time dependent CCL22 generation at HBMECs in the absence and presence of 10µg/ml cycloheximide	205
4.5 Cell surface ICAM-1 intensity following 16 hour simulation of HDLECs	211
4.5.1 Stimulation of HDLECs with 100ng/ml TNF-α	211
4.5.2 Stimulation of HDLECs with 100ng/ml IFN-γ	211
4.5.3 Stimulation of HDLECs with 100ng/ml TNF-α and 100ng/ml IFN-γ	211
4.5.4 Time dependent stimulation of HDLECs with 100ng/ml TNF-α and 100ng/ml IFN-γ	216
4.5.5 ELISA testing of conditioned medium for CCL7, CCL14, CCL16 and CCL22	216
4.6 Discussion	219
Chapter 5 – Transmission electron microscopy	226
5.1 Introduction and Aims	227
5.2 Materials and Methods	229
5.2.1 Quantitation of results	230
5.3 Results	231
5.3.1 Transmission electron micrograph description	231
5.3.1.1 Microstructures on mononuclear cells and HBMECs	231
5.3.1.2 Interactions between mononuclear cells and ECs	232
5.3.2 Microvilli generation on mononuclear cells in response to	

chemokines	238
5.3.3 Microvilli generation on HBMECs	238
5.3.4 Filopodia generation on TNF- α stimulated HBMECs in the presence of chemokine	241
5.3.5 Podosome generation, migration and adherence of mononuclear cells	241
5.4 Discussion	244
Chapter 6 – Chemokine receptor expression and transendothelial migration	248
6.1 Introduction and aims	249
6.2 Materials and Methods	251
6.2.1 Quantitation of results	251
6.3 Results	252
6.3.1 CD and CCR analysis	252
6.3.1.1 Establishing T-cell, B-cell and monocyte populations by flow cytometry	252
6.3.1.2 Establishing the percentage of cells positive for each marker in the gated populations by FACs	253
6.4 Results of CD3+, CD14+ and CD20+ marker staining on peripheral blood mononuclear cells (PBMCs)	254
6.4.1 CD3+ marker staining on RA and non-RA PBMCs	254
6.4.2 CD14+ marker staining on RA and non-RA PBMCs	254
6.4.3 CD20+ marker staining on RA and non-RA PBMCs	255
6.4.4 Monocyte, T-cell and B-cell expression on RA and non-RA monocytes.	255
6.5 Results of CCR marker staining on PBMCs	258
6.5.1 CCR1 expression in RA and non-RA blood	258

6.5.2 CCR2 expression in RA and non-RA blood	259
6.5.3 CCR4 expression in RA and non-RA blood	259
6.5.4 CCR5 expression in RA and non-RA PBMCs	260
6.6 PBMC migrations through HBMEC's	269
6.6.1 Mononuclear cell migration across TNF- α activated HBMECs	269
6.7 CCL7 HDLEC dose response	272
6.8 Discussion	275
Chapter 7 - CCL7, CCL14, CCL16 and CCL22 in matched serum and synovial fluid	280
7.1 Introduction and Aims	281
7.2 Materials and Methods	282
7.2.1 Quantitation of results	282
7.3 Results	283
7.3.1 CCL7 in the serum and SF of RA, OA, PsA and ReA patients	283
7.3.2 CCL14 in the serum and SF of RA, OA, PsA and ReA sufferers	287
7.3.3 CCL16 in the serum and SF of RA, OA, PsA and ReA patients	289
7.3.4 CCL22 in the serum and SF of RA, OA, PsA and ReA sufferers	289
7.3.5 Analysis of correlations in RA, ReA and PsA SF and serum.	292
7.3.5.1 CCL7, CCL14, CCL16 and CCL22 in RA	292
7.3.5.2 CCL7, CCL14, CCL16 and CCL22 in ReA	292
7.3.5.3 CCL7, CCL14, CCL16 and CCL22 in PsA	292
7.3.5.4 CCL7, CCL14, CCL16 and CCL22 in OA	292
7.4 Discussion	294

Chapter 8 – Final discussion	297
8.1 General discussion	298
8.1.1 Background	298
8.1.2 RA and non-RA ECs and lymphatic presentation of CCL7, CCL14, CCL16 and CCL22	300
8.1.3 CCL7, CCL14, CCL16 and CCL22 in cultured cells	303
8.1.4 CCL7, CCL14, CCL16 and CCL22 matched serum and synovial fluid chemokines	309
8.2 Final conclusions	312
8.3 Further work	313
Chapter 9 – References	314
9.1 Journal references	315
9.2 Book references	341
9.3 Web site references	342
Appendix	343

Dedication

I would like to dedicate this thesis primarily to my wonderful Children, Quinton and Alexander. They were born while I was doing my PhD and have never known me to be anything other than a very busy mummy.

I dedicate it also to my amazing parents, Quinton and Judy, my sister Jody, and my friends and at the Robert Jones and Agnes Hunt NHS Foundation Trust for their unfailing support throughout my PhD.

Acknowledgments

I would like to thank Professor Jim Middleton for the opportunity to do this PhD and his hard work as supervisor throughout the first year of my studies and his ongoing role as a mentor from my second year onwards. I would then like to thank Dr Derek Matthey for stepping in as my supervisor and all his hard work, encouragement and support.

Additional thanks go to Dr Karen Wilson for her help and work with electron microscopy.

Special thanks go to Dr Oksana Kehoe (my PhD advisor), Dr Catherine Whittall, Dr Alison Cartwright and Dr Helen McCarthy, who have provided training, support, advice and comfort when I needed it most, as well as a drinking partner when required.

Thanks also go to The MRC and The Oswestry Rheumatology Association, without whose funding the work I have done would not have been possible.

Final thanks go to the Robert Jones and Agnes Hunt Orthopaedic Hospital surgeons and consultants without whose kind support the samples used for some of this work would not have been available to me.

List of figures

Chapter 1

Figure 1.1	Diagram of the normal and rheumatoid joint synovium	2
Figure 1.2	Overview of antibody mediated autoimmunity	8
Figure 1.3.	Autoimmunity in rheumatoid arthritis	10
Figure 1.4	Diagrammatic representations of the major synovium types	27
Figure 1.5	Diagrammatic representation of areolar synovium	27
Figure 1.6	Subcellular events in the endothelium during chemokine-directed leukocyte extravasation	35
Figure 1.7	Scanning electron microscope image of leukocyte rolling and adhesion to an EC monolayer	37
Figure 1.8.	Leukocyte adhesion cascade	39
Figure 1.9	Leukocyte crawling and transmigration	41
Figure 1.10	Schematic showing some inflammatory, constitutive, angiogenic and angiostatic chemokines designated to various different groups	53
Figure 1.11	Diagram showing basic blood-tissue-lymphatic exchange	56
Figure 1.12	Diagram showing regulation of HIF-1 and nuclear factor- κ B (NF- κ B) pathways by reactive oxygen species and cytokine Stimulation	60
Figure 1.13	Schematic showing the source of iron and ROS and the cell damaging effects of ROS in the synovium	63

Chapter 2

Figure 2.1	Schematic showing initial optimization carried out for primary Antibodies	75
Figure 2.2	Schematic showing double immunofluorescent staining process	81
Figure 2.3	Diagram showing field of view layout for immunofluorescent Quantification	84
Figure 2.4.	Schematic showing optimisation process for the activation solutions; TNF- α ; IFN- γ and TNF- α + IFN- γ prior to transmigration analysis using HBMECs and HDLECs	93-94
Figure 2.5	Schematic showing mononuclear cell isolation from whole blood	101
Figure 2.6	Schematic diagram showing transwell system used to study leukocyte migration	102
Figure 2.7	Schematic showing optimisation process for chemokines CCL7, CCL14, CCL16 and CCL22 prior to transmigration analysis using HBMECs and HDLECs	103

Chapter 3

Figure 3.1	CCL1 and VWF staining in RA synovium	125
Figure 3.2	CCL2 and VWF staining in RA synovium	126
Figure 3.3	CCL3 and VWF staining in RA synovium	127
Figure 3.4	CCL4 and VWF staining in RA synovium	128
Figure 3.5	CCL5 and VWF staining in RA synovium	129
Figure 3.6	CCL7 and VWF staining in RA synovium	131
Figure 3.7	CCL7 and VWF staining in non-RA synovium	132
Figure 3.8	CCL7 and LYVE-1 staining in RA synovium	133
Figure 3.9	CCL7 and LYVE-1 staining in RA synovium	134

Figure 3.10	CCL7 and LYVE-1 staining in non-RA synovium	135
Figure 3.11	CCL8 and VWF staining in RA synovium	137
Figure 3.12	CCL8 and VWF staining in non-RA synovium	138
Figure 3.13	CCL10 and VWF staining in RA synovium	139
Figure 3.14	CCL11 and VWF staining in RA synovium	140
Figure 3.15	CCL12 and VWF staining in RA synovium	143
Figure 3.16	CCL13 and VWF staining in RA synovium	144
Figure 3.17	CCL14 and VWF staining in RA synovium	145
Figure 3.18	CCL14 and VWF staining in non-RA synovium	146
Figure 3.19	CCL14 and LYVE-1 staining in RA synovium	147
Figure 3.20	CCL14 and LYVE-1 staining in non-RA synovium	148
Figure 3.21	CCL15 and VWF staining in RA synovium	149
Figure 3.22	CCL16 and VWF staining RA synovium	152
Figure 3.23	CCL16 and VWF staining in non-RA synovium	153
Figure 3.24	CCL16 and LYVE-1 staining in RA synovium	154
Figure 3.25	CCL16 and LYVE-1 staining in non-RA synovium	155
Figure 3.26	CCL17 and VWF staining in RA synovium	156
Figure 3.27	CCL18 and VWF staining in RA synovium	157
Figure 3.28	CCL19 and VWF staining in RA synovium	158
Figure 3.29	CCL19 and VWF staining in the non-RA synovium	159
Figure 3.30	CCL20 staining in RA synovium	162
Figure 3.31	CCL21 and VWF staining in RA synovium	163
Figure 3.32	CCL22 and VWF staining in RA synovium	164
Figure 3.33	CCL22 and VWF staining in non-RA synovium	165
Figure 3.34	CCL22 and LYVE-1 staining in RA synovium	166
Figure 3.35	CCL22 and LYVE-1 staining in non-RA synovium	167
Figure 3.36	CCL23 staining in RA synovium	168

Figure 3.37	CCL24 staining in RA synovium	169
Figure 3.38	CCL25 staining in the RA synovium	171
Figure 3.39	CCL26 staining in the RA synovium	172
Figure 3.40	CCL27 staining in RA synovium	173
Figure 3.41	CCL28 staining in the RA synovium	174
Chapter 4		
Figure 4.1	ICAM-1 staining of HBMECs stimulated for 16 hours with 100ng/ml TNF- α	190
Figure 4.2	ICAM-1 staining of HBMECs stimulated for 16 hours with 100ng/ml IFN- γ	191
Figure 4.3	ICAM-1 staining of HBMECs stimulated for 16 hours with 100ng/ml TNF- α /IFN- γ	192
Figure 4.4	Dot plot showing ICAM-1 staining intensity at 0-24 hour TNF- α stimulation of HBMECs	194
Figure 4.5	Image showing typical ICAM-1 staining of HBMECs stimulated with 100ng/ml TNF- α for 2 hours	195
Figure 4.6	CCL7, CCL14, CCL16 and CCL22 staining intensity at 0, 2, 3, 4, 5 and 6 hours TNF- α stimulation of HBMECs in the absence and presence of cycloheximide	198
Figure 4.7	Image showing typical CCL7 staining of HBMECs Stimulated with 100ng/ml TNF- α for 2 hours in the absence of cycloheximide	199
Figure 4.8	Image showing typical CCL7 staining of HBMECs stimulated with 100ng/ml TNF- α for 2 hours in the presence of cycloheximide	200
Figure 4.9	Image showing typical CCL14 staining of HBMECs stimulated with 100ng/ml TNF- α for 2 hours in the absence	

	of cycloheximide	203
Figure 4.10	Image showing typical CCL14 staining of HBMECs stimulated with 100ng/ml TNF- α for 2 hours in the presence of cycloheximide	204
Figure 4.11	Image showing typical CCL16 staining of HBMECs stimulated with 100ng/ml TNF- α for 2 hours in the absence of cycloheximide	208
Figure 4.12	Image showing typical CCL16 staining of HBMECs stimulated with 100ng/ml TNF- α for 2 hours in the presence of cycloheximide	209
Figure 4.13	Image showing typical CCL22 staining of HBMECs stimulated with 100ng/ml TNF- α for 3 hours in the absence of cycloheximide	210
Figure 4.14	ICAM-1 staining of HDLECs stimulated for 16 hours with 100ng/ml TNF- α	213
Figure 4.15	ICAM-1 staining of HDLECs stimulated for 16 hours with 100ng/ml IFN- γ	214
Figure 4.16	ICAM-1 staining of HDLECs stimulated for 16 hours with 100ng/ml TNF- α and 100ng/ml IFN- γ	215
Figure 4.17	Dot plot showing ICAM-1 staining intensity at 0-24 hour TNF- α /IFN- γ stimulation of HDLECs.	217
Figure 4.18	ICAM-1 staining of HDLECs stimulated for 2hours with 100ng/ml TNF- α and 100ng/ml IFN- γ	218
Figure 4.19	Mechanistic model of Cycloheximide inhibition of translation elongation	220

Chapter 5

- Figure 5.1** TNF- α stimulated HBMEC's (*EC*) grown on a 5 μ m transwell filter (*F*) in close association with mononuclear cell (*MC*) in the absence of chemokine 233
- Figure 5.2** Mononuclear cell (*MC*) with long (7500nm long) microvillus (*MCP*) like projection 233
- Figure 5.3** Mononuclear cell (*MC*) 234
- Figure 5.4** Mononuclear cell (*MC*) in the process of migrating through HBMEC monolayer (*EC*) in response to CCL7 234
- Figure 5.5** Mononuclear cell (*MC*) in close association with an EC with a filopodia like microstructure (*FP*) 235
- Figure 5.6** Mononuclear cell (*MC*) with microvilli like projections (*MCP*) 235
- Figure 5.7** TNF- α stimulated HBMEC's (*EC*) grown on a 5 μ m transwell filter (*F*) showing lack of microstructure formation 236
- Figure 5.8** Mononuclear cell (*MC*) with podosome like microstructures (*P*) protruding into an EC in the process of migrating through an HBMEC monolayer in response to CCL16 236
- Figure 5.9** A mononuclear cell (*MC*) near HBMEC's where CCL14 was added to the basal transwell filter compartment for 30 minutes 237
- Figure 5.10** A mononuclear cell (*MC*) in association with HBMEC's where CCL7 was added to the basal transwell filter compartment for 30 minutes 237

Chapter 6

- Figure 6.1** Sample dot plot showing forward scatter (FSC) versus side scatter (SSC) for freshly isolated RA mononuclear cells 252

Figure 6.2	Sample dot plots showing FSC versus fluorescence for isotype control and stained cells in PBMCs	253
Figure 6.3	Expression of (A) CD3+ on RA blood PBMCs and (B) non-RA blood PBMCs	256
Figure 6.4	Expression of (A) CD14+ on RA blood PBMCs and (B) non-RA blood PBMCs	256
Figure 6.5	Expression of (A) CD20+ on RA blood PBMCs and (B) non-RA blood PBMCs	257
Figure 6.6	Chart showing percentage of CD3+, CD14+ and CD20+ positive RA and non-RA PBMCs	257
Figure 6.7	Expression of CCR1 in RA and non-RA PBMCs	261
Figure 6.8	Expression of CCR2 in RA and non-RA PBMCs	262
Figure 6.9	Expression of CCR4 in RA and non-RA PBMCs	263
Figure 6.10	Expression of CCR5 in RA and non-RA PBMCs	264
Figure 6.11	Chart showing percentage of CCR1, CCR2, CCR4 and CCR5 positive monocytes in RA and non-RA monocytes	265
Figure 6.12	Chart showing percentage of CCR1, CCR2, CCR4 and CCR5 positive B/T cells in RA and non-RA PBMCs	266
Figure 6.13	Box plot showing mean fluorescent intensity (MFI) of CCR1, CCR2, CCR4 and CCR5 on RA and non-RA monocytes	267
Figure 6.14	Box plot showing mean fluorescent intensity (MFI) of CCR1, CCR2, CCR4 and CCR5 on RA and non-RA B/T-cells	268
Figure 6.15	Box plot showing numbers of monocytes migrated in response to 100ng/ml chemokine across TNF- α activated HBMECs	270
Figure 6.16	Box plot showing numbers of B/T-cells migrated in response to 100ng/ml chemokine across TNF- α activated HBMECs	271

Figure 6.17	Box plot showing numbers of monocytes migrated in response to CCL7 through TNF- α /IFN- γ activated HDLECs	273
Figure 6.18	Box plot showing numbers of B/T-cells migrated in response to CCL7 across TNF- α /IFN- γ activated HDLECs	274
Chapter 7		
Figure 7.1	CCL7 in RA, OA, ReA and PsA serum and synovial fluid	286
Figure 7.2	CCL14 in RA, OA, ReA and PsA serum and synovial fluid	288
Figure 7.3	CCL16 in RA, OA, ReA and PsA serum and synovial fluid	290
Figure 7.4	CCL22 in RA, OA, ReA and PsA serum and synovial fluid	291

List of tables

Chapter 1 - Introduction

Table 1.1	Risk factors and markers associated with RA	6
Table 1.2	The 2010 revised criteria for RA classification	8
Table 1.3	Macrophage function and potential role in RA	11
Table 1.4	Molecules expressed and/or released by macrophages	14
Table 1.5	Molecules secreted by macrophages	15
Table 1.6	Some characteristics of activated, angiogenic, apoptotic and leaky endothelial cells	23
Table 1.7	Proteins seen at tight and adherens junctions involved in paracellular transmigration	44
Table 1.8	Human chemokines and chemokine receptors	48
Table 1.9	Chemokines considered important in RA/expressed in RA joints	50
Table 1.10	Human chemokines present at RA microvascular ECs	54

Chapter 2 – Materials and methods

Table 2.1	showing patient details for the RA tissues samples used	68
Table 2.2	showing patient details for the non-RA tissues samples used	69
Table 2.3	showing the primary antibodies used for immunofluorescence	71-72
Table 2.4	showing the Secondary antibodies used for immunofluorescence	73
Table 2.5	showing solutions used for immunofluorescence	78-80
Table 2.6	showing solutions for the Duffy antigen receptor for chemokines (DARC) and VWF and CD68 with LYVE-1 staining	82
Table 2.7	showing solutions for TNF- α , IFN, and combination activation and staining of cultured cell monolayers	97
Table 2.8	showing recombinant proteins used in transmigration analysis	105

Table 2.9	showing reagents used for CD marker and chemokine receptor staining for FACS analysis	112
------------------	---	-----

Chapter 3 – Immunofluorescent analysis of synovial tissue

Table 3.1	Chemokine present at $\leq 59.9\%$ of VWF+ vessels in RA synovial tissue	122
Table 3.2	Chemokine present at (60% of VWF+ vessels in RA synovial tissue assessed on non-RA synovial tissue	123
Table 3.3	Chemokine with VWF, and chemokine with LYVE-1 in RA and non-RA tissue	124
Table 3.4	Iron (Fe) and aluminium (Al) content of RA samples	176

Chapter 4 - Analysis of ICAM-1 and chemokine levels in cultured endothelial cells

Table 4.1	Intensity of cell surface ICAM-1 staining following HBMEC stimulation with TNF- α , IFN- γ and TNF- α /IFN- γ for 16 hours	189
Table 4.2	Intensity of cell surface ICAM-1 staining following 16 hour stimulation of HDLECs with 100ng/ml TNF- α , 100ng/ml IFN- γ and 100ng/ml IFN- γ / TNF- α	197
Table 4.3	Intensity of CCL14 staining following time dependent stimulation of HBMECs by TNF- α in the absence and presence of cycloheximide	202
Table 4.4	Intensity of CCL16 staining following time dependent stimulation of HBMECs by TNF- α in the absence and presence of cycloheximide	206
Table 4.5	Intensity of CCL22 staining following time dependent stimulation of HBMECs by TNF- α in the absence and presence of cycloheximide	207

Table 4.6	Intensity of cell surface ICAM-1 staining following 16 hour Stimulation of HDLECs with 100ng/ml TNF- α , 100ng/ml IFN- γ and 100ng/ml IFN- γ /TNF- α	212
------------------	--	-----

Chapter 5 – Transmission electron microscopy

Table 5.1	Microvilli generation on mononuclear cells in the presence of TNF- α stimulated HBMECs with and without chemokines	239
Table 5.2	Microvilli generation on HBMECs in response to TNF- α stimulation in the presence of chemokines	240
Table 5.3	Data for podosome-like structure generation of mononuclear cells, mononuclear cells actively migrating and mononuclear cells adhered to HBMECs treated with TNF- α and in the presence of chemokines	242
Table 5.4	The generation of filopodia like structures on HBMECs in response to TNF- α stimulation in the presence of chemokines	243

Chapter 7 - CCL7, CCL14, CCL16 and CCL22 in matched serum and synovial fluid

Table 7.1	Chemokines present in serum and synovial fluid from RA and OA	284
Table 7.2	Chemokines present in serum and synovial fluid from ReA and PsA.	285
Table 7.3	List of correlations for serum and SF CCL7, CCL14, CCL16 and CCL22 in serum RA, ReA and PsA	293

Abstract

RA is a destructive and chronic autoimmune inflammatory disease. The inflammation of the synovium is associated with the local invasion of inflammatory cells across blood vessel endothelial cells (ECs), increases in synovial fluid volume and local pannus invasion of the connective tissues and bone. Synovial ECs in RA are involved in a wide range of processes, and chemokines are known mediators of inflammatory cell invasion into the tissue. Chemokines at the ECs of lymph vessels play a further role in attracting the infiltrates out of the tissue.

This study used immunofluorescence to investigate the presentation of a number chemokines in RA tissue ECs, and also the presentation of CCL7, CCL14, CCL16 and CCL22 in lymphatic ECs. A number of chemokines were newly identified in synovial ECs, and continued investigation showed a marked dysregulation in blood vessel and lymphatic vessel chemokine presentation, including CCL7. In vitro studies showed that the chemokines also preferentially generated microvilli which may facilitate transendothelial migration in vivo. Mononuclear cells expressed the receptors for the chemokines and transmigration analysis showed CCL7 (among others) to significantly chemoattract monocytes. This suggests that dysregulation of chemokines may have a functional role in RA pathology. Furthermore, the analysis of these chemokines in matched synovial fluid (DF) and serum indicates that EC chemokines may be inflammatory markers in arthritic diseases.

Overall, this study has shown that the EC interface between the influx and efflux of inflammatory cells in the RA synovium may offer currently unexplored therapeutic opportunities.

Published abstracts

Lisa Rump-Goodrich, Derek Matthey, Jim Middleton. (2012). An assessment of CC chemokines present on the microvasculature of synovial tissue in patients with rheumatoid arthritis. *Rheumatology*. 51 (suppl 3): iii140-iii184

Lisa Rump-Goodrich, Derek Matthey, Oksana Kehoe, Alison Cartwright, Jim Middleton. (2013). Differential Generation of CC Chemokines at Microvascular Endothelial Cells of Blood and Lymphatic Vessels Under Inflammatory Conditions. *Rheumatology*. 52 (suppl 1): i135-i172

Lisa Rump-Goodrich, Ayman Askari, Derek Matthey, Jim Middleton (2014). Dysregulation of CC Chemokines at Microvascular Endothelial Cells of Blood and Lymphatic Vessels Under Inflammatory Conditions. *Arthritis & Rheumatology*. Special Issue: ACR/ARHP Annual Meeting Abstract Supplement. 66, Issue S10, pages S1–S140

AG Kay , S Parida , A Stefan , L Rump , J Middleton , O Kehoe. (2015). Assessment of aggrecanase- and MMP-driven cartilage degradation following MSC treatment for Rheumatoid Arthritis. *European Cells and Materials*. Vol 29. Supp 3:70

Abbreviations

ACR	American College of Rheumatology
ACPA	Anti-citrullinated peptide antibodies
AKA	Anti-keratin antibodies
ANOVA	Analysis of variance
APC	Antigen presenting cell
BSA	Bovine serum albumin
CaCl ₂	Calcium chloride
CCL	C-C motif ligand
CCR	C-C motif receptor
CI	Confidence interval
CRP	C-reactive protein
DAF	Decay accelerating factor
DAPI	4', 6-diamidino-2-phenylindole
DARC	Duffy antigen receptor complex
DC	dendritic cell
DLEC	Dermal Lymphatic Endothelial Cell
DMEM-F12	Dublecco's modified eagle medium: nutrient mixture –F12
EBM-mv	Endothelial basal medium (microvascular bullitKit)
EC	Endothelial cell
ECM	Extracellular matrix
EDTA	Ethylene diamine tetra acetate
EGF	Epidermal growth factor
ELISA	Enzyme-Linked Immunosorbent Assay
EM	Endothelial cell microvilli like protrusions
ESR	Erythrocyte-sedimentary rate

ET	Endothelin
EULAR	European league against Rheumatism
FACs	Fluorescence activated cell sorter
FGF	Fibroblast growth factor
<i>F</i>	Filter
FSC	Forward scatter (forward angle light scatter)
GAGs	Glycosaminoglycan
GC	Germinal centre
GlyCAM	Glycosylated cell adhesion molecule
GTA	Glutaraldehyde
HBMECs	Human bone marrow endothelial cells
HDLECs	Human dermal lymphatic endothelial cells
HEVs	high endothelial venules
HIF	Hypoxia inducible factor
ICAM	Intra cellular adhesion molecule
IFN- γ	Interferon-gamma
Ig	Immunoglobulin
IL	Interleukin
iNOS	Inducible nitrous oxide
IPA	Isopentane alcohol
IQR	Inter-quartile range
IVIg	Intravenous immunoglobulin
JAM	Junctional adhesion molecule
<i>L</i>	Lymphocytes
LEC	Lymphatic endothelial cell
LF	Lymphoid follicle

LFA-1	Lymphocyte function antigen
LM	Lymphocyte microvilli like protrusions
LYVE-1	Lymphatic vessel endothelial HA receptor-1
MA	Macrophage
MCV	Mutated citrullinated vimentin
MHC	Major- histocompatibility complex
MMP	Matrix metalloproteinase
MO	Monocyte
mRNA	micro ribonucleic acid
NO	Nitrous oxide
NK	Natural killer cell
OA	Osteoarthritis
OR	Odds ratio
<i>P</i>	Pseudopodia
PAF	Platelet activating factor
PBMC	Peripheral blood mononuclear cell
PBS	Phosphate buffered saline
PCs	Pannocytes
PE	Phycoetherine
PECAM-1	Platelet endothelial cell adhesion molecule-1
RA	Rheumatoid arthritis
RF	Rheumatoid Factor
RNA	Ribonucleic acid
ROS	reactive oxygen species
RPMI	Roswell Park memorial institute (medium)
SD	standard deviation
SE	Standard error

SF	Synovial fluid
TEM	Transmission electron microscopy
TGF	Transforming growth factor
T H-GFAAS	Transverse Heated-Graphite Furnace Atomic Absorption Spectrometry
THGA	Transverse heated graphite atomiser
TM	Transmembrane
TLR	Toll like receptor
TNF- α	Tumour necrosis factor-alpha
tPO	Tissue oxygen pressure
VCAM-1	Vascular cell adhesion molecule-1
VEGF	vascular endothelial growth factor
VWF	von-Willebrand factor

Chapter 1

Introduction

1. Rheumatoid Arthritis (RA)

1.1 What is RA?

RA is a destructive and chronic autoimmune inflammatory disease. Typically the peripheral joints are affected with the most visible manifestation of joint destruction being at the diarthrodial joints of the feet and hands. The destruction of the bone and cartilage is predominantly due to the release of proteinases acting against the connective tissues which are generated at the invasive face of the synovium (Gravallese, 2002), termed the pannus, and occurs at periarticular and subchondral bone as well as the cartilage and bone margins (Goldring, 2003) (see figure 1.1). The inflammation of the synovium associated with the local invasion of inflammatory cells leads to increases in synovial fluid and local pannus invasion of the connective tissues and bone thus playing a lead role in RA pathology.

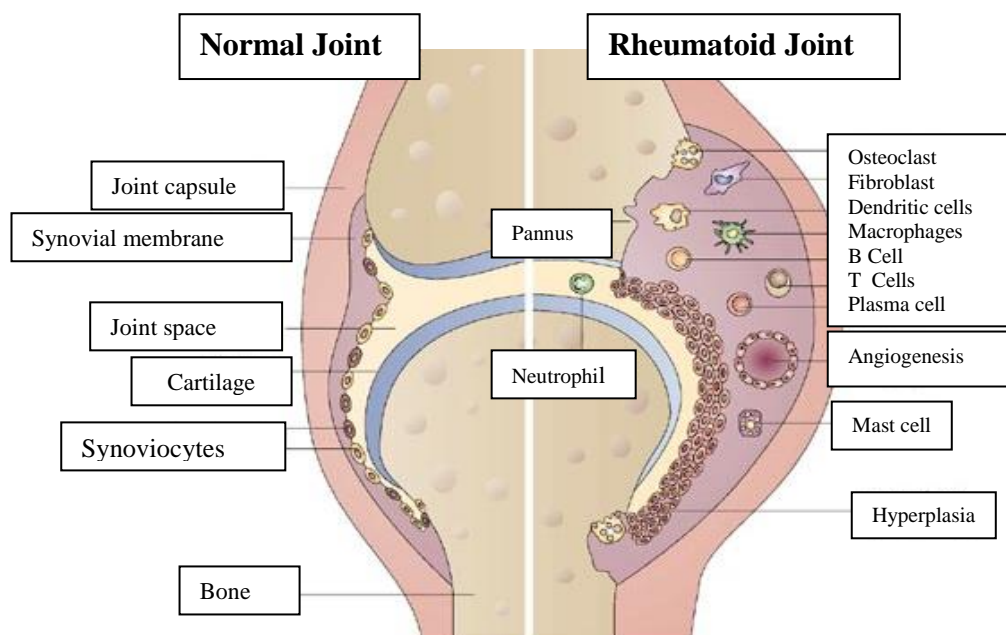


Figure 1.1 Diagram of the normal and rheumatoid joint synovium. Major cell types and processes involved in RA synovial inflammation are also shown. (Taken and adapted from Strand *et al*, 2007).

As seen in figure 1.1 the rheumatoid synovium is marked by severe inflammation leading to hyperplasia. This is associated with the generation of redundant folds and villi in the tissue of the synovial lining and extensive angiogenesis with massive increases in cellular infiltrates such as B and T-cells, macrophages and dendritic cells (among others), with the degree/type of cellular infiltration differing between disease stages and patients.

Innate immune responses such as dendritic cell (DC) activation are believed to be one of the primary events in RA (Smolen et al., 2007). These antigen presenting cells (APCs) present antigens to T-cells. This T-cell activation promotes increases in pro-inflammatory chemokine and cytokine generation leading to a 'feedback loop for additional T-cell, B-cell and macrophage interactions (Smolen and Steiner, 2003; Smolen *et al.*, 2007). Antigens are also presented by the B-cells, which also generate a range of cytokines (e.g. IL-6) and autoantibodies such as rheumatoid factor (RF) and anti-citrullinated peptides (anti-CCP). The autoantibodies can stimulate the generation of cytokines such as TNF- α (Smolen *et al.*, 2007). The synovial membrane also produces a range of inflammatory cytokines and matrix-metalloproteinases (MMPs) from activated fibroblast-like synoviocytes (FLS) which in turn facilitate the damage to bone and cartilage as the disease progresses (Smolen *et al.*, 2007) (figure 1.1).

In later stage RA the process of synovial inflammation is essentially the same as in early RA with differences in mediators/infiltrates, for example, being largely accounted for by differences such as medication and disease activity in different patients (Tak, 2001). However, differences have been noticed between early RA and late RA such as increased expression of Duffy antigen in early RA (disease duration ≤ 7 months) followed by decreased Duffy expression at disease duration of 9 years, and further decreases at 18 years disease duration. This indicated that Duffy was expressed preferentially by the newly

formed angiogenic vessels (Gardner *et al.*, 2006) and was primarily active in early, diffuse leukocyte transmigration.

The development of lymphoid like structures in the RA synovium, known as lymphoid follicles (LFs), is dependent on the organisation of the B and T-cell infiltrate (reviewed by Humby *et al.*, 2007). Regions of LFs can become more organised and resemble secondary lymphoid organs (SLOs). These organised structures can facilitate disease exacerbating immune responses such as antibody production by their role in directing B/T-cell responses and so have been referred to as both ectopic lymphoid-like structures (ELSs) and tertiary lymphoid organs (TLOs) (Aloisi and Pujol-Borrell, 2006; Neyt *et al.*, 2012). In RA 50% of cases show diffuse infiltration and 50% show the LFs. Of the cases where LF development has occurred only 50% of these have germinal centres (GCs). These GC LFs manifest as organised arrangements of T and B-cells within the synovium and therefore occur in ~20-40% of RA cases (Loetscher and Moser, 2002; Aloisi and Pujol-Borrell, 2006; Manzo *et al.*, 2010). The lack of LFs in greater numbers of RA sufferers raised the possibility that they were not of great importance in disease progression and pathogenesis; which was built upon by Thurlings *et al.*, (2008) who showed that disease phenotype is not correlated to the development of lymphoid follicles and that their development may well be based on an individuals response to cytokine regulation (reviewed by Edwards and Leandro, 2008). However, the importance of LF development in RA remains contentious as Cañete *et al.*, (2009) showed that RA patients with ELS were more likely to be non-responsive to anti-TNF therapy. Furthermore an RA synovial B-cell subset can generate pro-inflammatory cytokines such as TNF- α , IL-6 and RANKL (Yeo *et al.*, 2012).

It is still currently unknown if LFs/ELS are representative of persistent inflammation or are characteristic of individual pathological subsets present from very early RA (Pitzalis *et al.*, 2014).

The aetiology of RA had been quite elusive, however a range of risk factors has been identified (see table 1.1). In addition to the data in table 1.1 there is a huge range of genetic loci associated with RA susceptibility which are comprehensively listed/ by Yarwood *et al.*, (2014). The National Institute for Health and Care Excellence (NICE) states that there are ~400,000 RA sufferers in the UK with 5.1 people per 10,000 being diagnosed per year (1.5 men: 3.6 women). The diagnosis peaks in the over 70s population but develops in all age groups to some extent.

It is widely known that the rate of disease progression varies between sufferers and that the age of disease onset also shows a marked variation. It is accepted that whilst RA sufferers' immediate relatives appear to have a greater chance of developing the disease, an interplay of both genetic and environmental factors are more likely to be causal in its development (Hajalilou *et al.*, 2012). A range of arthropathies manifests with similar symptoms in the early stages and in order to better aid diagnosis the American College of Rheumatology (ACR) revised the criteria to be met for a diagnosis of RA in 1988 (Arnett *et al.*, 1988) and further revisions were done by the ACR, and the European League Against Rheumatism (EULAR) revised the criteria to be met for a diagnosis of RA (Aletaha *et al.*, 2010) (table 1.2). A score of $\geq 6/10$ is needed for classification of a patient as having definite RA.

Table 1.1 Risk factors and markers associated with RA.

Risk Factor	
Sex	3:1 females to males develop RA. Factors include (among others), hormonal change during pregnancy and/or menstruation and oral contraceptive use. (Oliver and Silman, 2009a).
Age	Usually between 40-50 years of age.
Environmental	<p>Diet; Lean mass of arms and legs (LMAL), total body fat mass (BFM) or truncal fat distribution (TFD) indicated that Low LMAL, high BFM and high TFD are present in early RA patients. (Book et al, 2009).</p> <p>Caffeine; Implicated in some RA studies but vindicated in others (Oliver and Silman, 2009b)</p> <p>Smoking; Time spent smoking and the amount smoked correlates to increased RA risk (Oliver and Silman, 2009b)</p> <p>Traffic pollution; Evidence from Hart <i>et al.</i>, (2009) and A recent review by Essouma and Noubiap , (2015) suggests that increased exposure to traffic pollution increases the risk of RA.</p> <p>Infectious agents; The lead viral candidate is Epstein Barr Virus (EBV), the genome of which has been found in the human synovial membrane. Also seen to be cross-reactivity between EBV proteins and human proteins (Toussirot and Roudier, 2008). Other pathogens are also being found to have a role in RA development such as Chikungunya virus (Becker and Winthrop, 2010). Bacterial infection may also be causal. Most recently the Proteus bacteria, active as an upper urinary tract infection, have been implicated (Ebringer and Rashid, 2009).</p>
Geographical	Worldwide distribution. Populations in the UK and certain American Indians have greatly increased risk of RA than many other European and American peoples. Between 25-50 per 100,000 in any given population (reviewed by Uhlig and Kevin, 2005)
Genetic risk factors (reviewed by Goronzy <i>et al.</i> , 2009)	
Familial	Sporadic but may affect several generations. Recently incidence of RA in families has been indicated to correlate with increased risk of other autoimmune diseases within the same family (Hemminki <i>et al.</i> , 2009)
HLA- DRB1	HLA-DRB1 encoding the shared epitope is the strongest risk factor of the HLA type susceptibilities. PAD14_94 have been associated with the European population and PAD14 polymorphisms in general associated with Asian populations. (Lee <i>et al.</i> ,2007)
PTPN22	Protein tyrosine phosphatase (PTPN22) has been shown to exert regulatory action on both B and T-cells in RA (Oliver and Silman, 2009b; reviewed by Imboden, 2009; Messemaker <i>et al.</i> ; 2015)
Other Genes	CTLA4 (Messemaker <i>et al</i> ; 2015), MHC2A and FCRL3 (Oliver and Silman, 2009b). WNT5A (Rauner <i>et al.</i> , 2012)
Markers	
Autoantibodies	<p>Rheumatoid Factor (RF); Autoantibodies reactive to the Fc portion of IgG, used as a diagnostic tool.</p> <p>ACPA; Anti-citrullinated peptide antibodies (also known as anti-citrullinated cyclic antibodies, anti-CCP) react with proteins where citrulline has replaced arginine, used as a diagnostic tool.</p> <p>AKA; Anti keratin antibodies (an ACPA subtype). Identified among other subtypes (reviewed by Song and Kang, 2009).</p>

Table 1.2 The 2010 revised criteria for RA classification

Revised ACR/EULAR criteria of RA classification	
Joint involvement	
1 large joint	0
2-10 large joints	1
1-3 small joints (with or without involvement of large joints)	2
4-10 small joints (with or without involvement of large joints)	3
>10 joints (at least 1 small joint)	5
Serology	
Negative RF <i>and</i> negative ACPA	0
Low-positive RF <i>or</i> low-positive ACPA	2
High-positive RF <i>or</i> high-positive ACPA	3
Acute-phase reactants (at least 1 test result required)	
Normal CRP and normal ESR	0
Abnormal CRP or abnormal ESR	1
Duration of symptoms	
<6 weeks	0
≥6 weeks	1

Table adapted from Aletaha *et al.*, (2010).

1.2 Autoimmunity

RA is the most common autoimmune joint disease (reviewed by El-Jawhari *et al.*, 2014). The immune system distinguishes the many cellular components of the human body (known as ‘self’) from the cells or components of invading organisms (non-self). The harmful ‘non-self’ should generate an immune response while ‘self’ should not. If the immune system does not recognize self-cells (or their constituents) and mounts an immune response, the result is autoimmune disease leading to self-cell damage/death (figure 1.2).

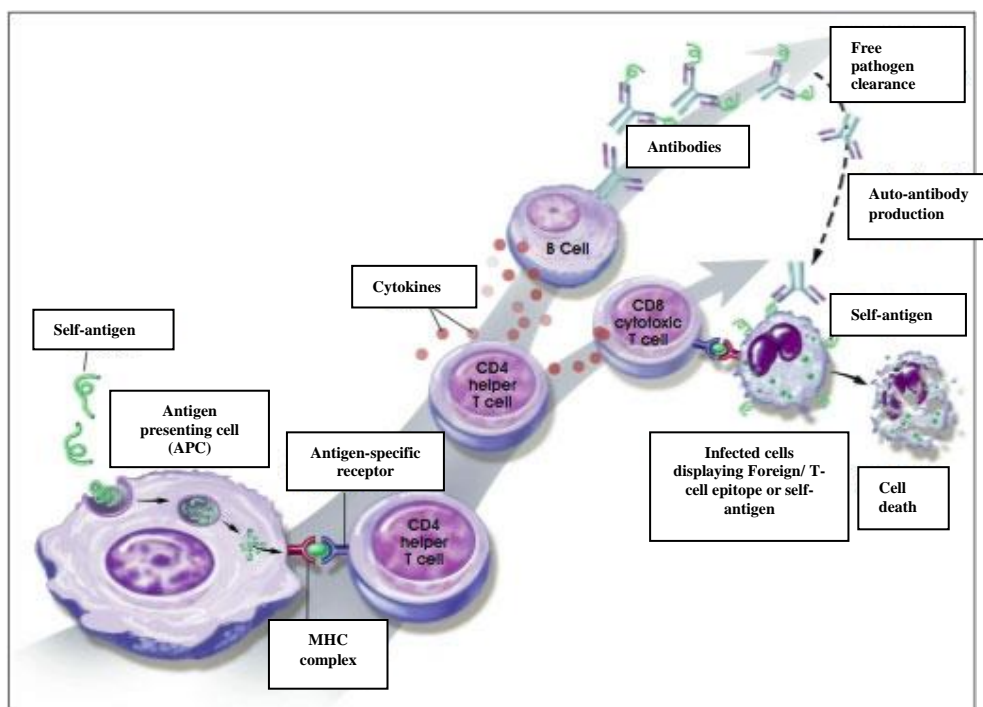


Fig 1.2 Overview of antibody mediated autoimmunity. (image adapted from

<http://stemcells.nih.gov/info/scireport/pages/chapter6.aspx>)

In RA, autoimmunity is due to the generation of ‘autoantibodies’ such as rheumatoid factor (RF) and anti-citrullinated antibodies (table 1.1). The presence of a number of these autoantibodies is used as a diagnostic tool.

In cell mediated autoimmune responses T-cells complex with self-antigens such as mutated citrullinated vimentin, (MCV) and activate other immune cells via the generation of soluble factors. Activated macrophages then ‘attack’ the synovial tissue and produce chemical messengers (cytokines) leading to the uncontrolled growth of synovial cells into the joint tissue, creating the pannus. Here they damage the cartilage and bone, and T-cells and macrophages interact further promoting the inflammation (figure 1.3A).

The inflammatory process begins with the entry of neutrophils, monocytes and macrophages. Local tissue damage is followed by ‘neo-autoantigen’ release, antigen priming, T-cell activation then autoantibody generation by B-cells and rheumatoid factor (RF) release. Neutrophils take up immune complexes and bind complement C5a, the neutrophils then generate inflammatory chemokines and cytokines. Joint infiltration starts with neutrophils expressing CD137 and its receptor, 4-1BB ligand (Mitter, 2004).

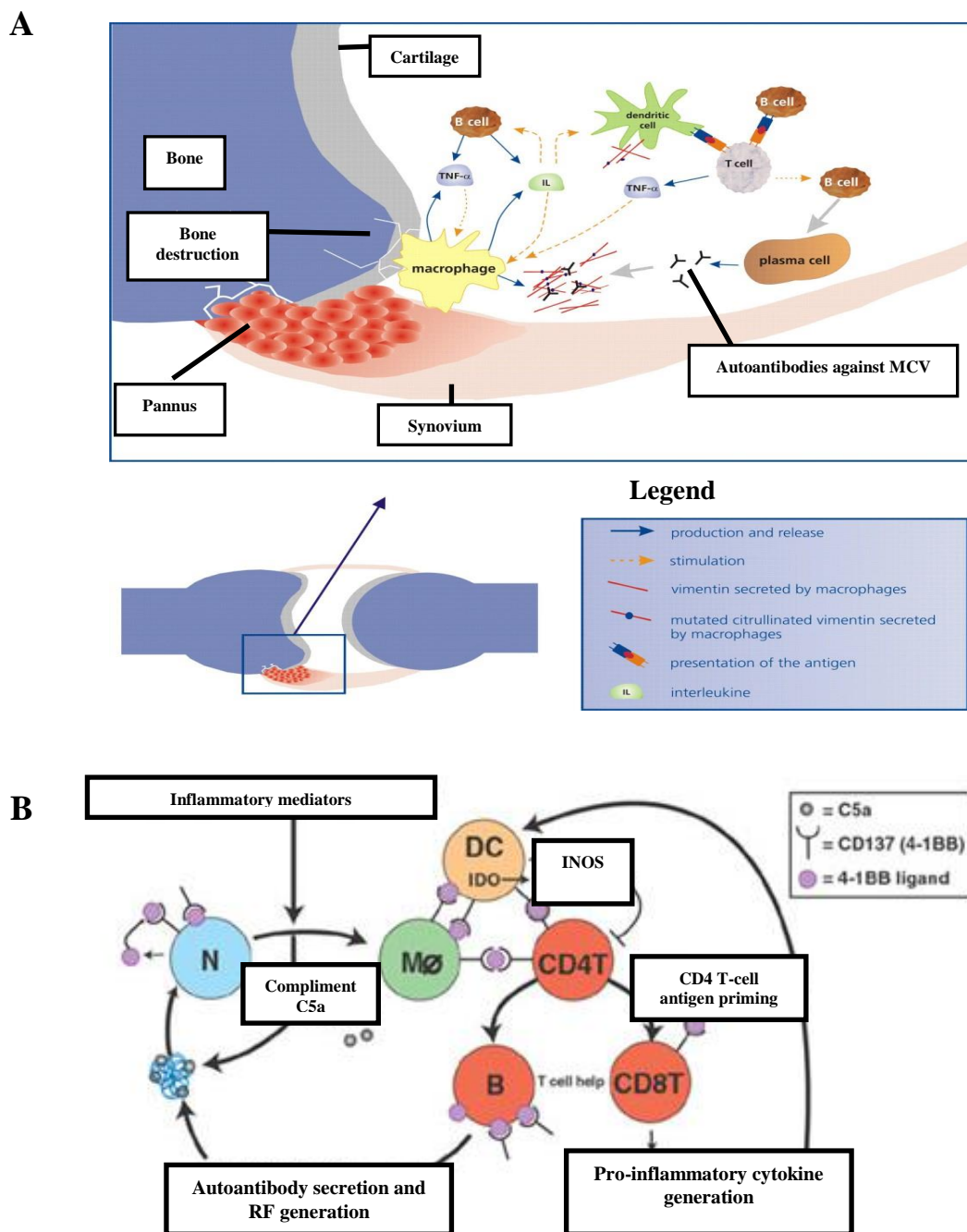


Figure 1.3. Autoimmunity in rheumatoid arthritis. (A) An overview of antibody-mediated immunity in RA. (B) An overview of cell-mediated autoimmunity in RA. Neutrophil (N), monocyte ($M\emptyset$), dendritic cell (DC) (figure 1.3A adapted from http://www.chemgapedia.de/vsengine/vlu/vsc/en/ch/25/orgentec/autoimmun.vlu/Page/vsc/en/ch/25/orgentec/autoimmun_ra_en.vscml.html © *Orgentec Diagnostika*; figure1.3B adapted from Mitter, 2004)

1.3 Cells involved in RA

1.3.1 Macrophages (see table 1.3)

Macrophages have long been known to be key factors in RA involved not only in inflammation initiation and perpetuation but also angiogenesis, matrix degradation and leukocyte adhesion/migration in RA. As well as expressing a range of chemokine receptors, adhesion molecules and surface antigens, they secrete a range of cytokines (a number of which increase macrophage activation, Drexler *et al.*, 2008), chemokines, growth factors, proteases and further mediators (Szekanecz and Koch, 2007). These are shown in tables 1.4 and 1.5).

Table 1.3 Macrophage function and potential role in RA (Drexler *et al.*, 2008; Kinne *et al.*, 2007)

Macrophage function	Potential role in RA
Cytokine and protease production	Activation and tissue destruction
Complement activation	Activated complement recognition. Promotion of phagocytosis and Monocyte activation
Particulate antigen phagocytosis	Antigen presentation and CD4+/CD8+ T cell activation (relevance to RA initiation/perpetuation)
Antigen processing/presentation	Important cognate functions upon antigen recognition via MHC-II molecule presentation.
Chemotaxis and Angiogenesis	Positive feedback between monocyte derived cytokines and chemotactic factors (i.e. IL-8 and MCP-1)
Lipid metabolism	Pro-inflammatory activity of PGE ₂ and PGI ₂
Intracellular pathogen/apoptotic cell clearance	Induction of monocyte derived cytokines by Bacterial toxins Persistence of intracellular obligate/facultative pathogens with arthritogenic potential.
Wound healing	Phagocytosis of matrix debris and endogenous IL-1 production.
Immune complex clearance	RF clearance. Further monocytes activation. Complement opsonisation of complexes.

Macrophages differentiate from monocytes and are present in large numbers in the cartilage-pannus junction and the inflamed synovium. Intimal macrophages are the minority cell type in the normal intimal layer, but in the diseased state the population can rise to 80%. Conceivably, the macrophages are continuously replaced from monocytes in the circulation (Bartholome *et al.*, 2004), however Thurlings *et al.*, (2009) obtained results indicating that while monocyte migration into the inflamed synovium is continuous the macrophage replacement rate is markedly slower. This may be partly due to the cytokine imbalance which occurs in RA joints, bone marrow and peripheral blood (Kinne *et al.*, 2007). As well as expressing a range of chemokines, cytokines (a number of which increase macrophage activation, Drexler *et al.*, 2008), chemokine receptors, adhesion molecules and surface antigens, they secrete a range of cytokines, chemokines, growth factors, proteases and further mediators (tables 1.4 and 1.5) (reviewed by Szekanecz and Koch, 2007). It has also been shown that anti-citrullinated protein autoantibody (ACPA) containing immune complexes can induce the generation of TNF- α secretion by synovial fluid-derived macrophages from RA patients which would further exacerbate the pathophysiology of RA (Laurent *et al.*, 2011).

1.3.2 Synovial fibroblasts

In normal tissue synovial fibroblasts provide the cavity of the joint and the adjacent cartilage with lubricating molecules (such as hyaluronic acid) and nutritive plasma proteins as well as the production of matrix components required for matrix remodelling. In RA tissue, together with macrophages, synovial fibroblasts are the most prolific cell type in the hyperplastic synovial intimal layer. Thus, they are a driving force behind RA joint degradation via generation of matrix-degrading molecules and inflammatory cytokines (Muller-Ladner *et al.*, 2007). Pretzel *et al.*, (2009) have also demonstrated the degree to

which synovial fibroblasts degrade the cartilage matrix via cartilage homeostasis disruption by suppressing anabolic matrix synthesis and by producing pro-inflammatory cytokines and catabolic enzymes.

Table 1.4 Molecules expressed and/or released by macrophages (data adapted from Szekanecz and Koch, 2007)

Macrophage Molecule		Ligand/function
Selectins	L-selectin	Sialylated carbohydrates, GLyCAM-1
Integrins	$\alpha_4\beta_1$ (VLA-4)	Fibronectin, VCAM-1
	$\alpha_5\beta_1$ (VLA-5)	Fibronectin
	$\alpha_L\beta_2$ (LFA-1, CD11a,CD18)	ICAM-1, ICAM-2, ICAM-3
	$\alpha_M\beta_2$ (Mac-1, CD11b,CD18)	ICAM-1, iC3b, fibrinogen
	$\alpha_X\beta_2$ (CD11c,CD18)	iC3b, fibrinogen
	$\alpha_V\beta_3$	Various ECM components
	$\alpha_V\beta_5$	Fibronectin, vitronectin
Immunoglobulin superfamily	ICAM-1 (CD54)	$\alpha_L\beta_2$, $\alpha_M\beta_2$, cd43
	ICAM-2 (CD102)	$\alpha_L\beta_2$
	ICAM-3 (CD50)	$\alpha_L\beta_2$
	VCAM-1 (CD106)	$\alpha_4\beta_1$, $\alpha_4\beta_7$
	PECAM-1 (CD31)	$\alpha_V\beta_3$
	LFA-3 (CD58)	CD2
Chemokine receptors	CXCR1	CXCL8, CXCL6
	CXCR2	CXCL1, CXCL2, CXCL3,CXCL5, CXCL6, CXCL7, CXCL8
	CXCR4	CXCL12
	CXCR5	CXCL13
	CCR1	CCL3, CCL5, CCL7, CCL14, CCL15, CCL16, CCL22
	CCR2	CCL2, CCL7, CCL8, CCL13
	CCR5	CCL3, CCL4, CCL5, CCL8, CCL14
	CCR7	CCL19, CCL21
	CCR8	CCL1, CCL4, CCL17
	XCR1	XCL1
	CX ₃ CR1	CX ₃ CL1

ECM - extracellular matrix; GlyCAM - glycosylated cell adhesion molecule; ICAM - intercellular cell adhesion molecule; LFA - lymphocyte function associated antigen; PECAM - platelet/endothelial cell adhesion molecule; VCAM - vascular cell adhesion molecule; VLA - very late antigen; BCA - B-cell-activating chemokine; CXCL, CXL, CX₃CL and CCL - chemokines[?]; CXCR, CXR , CX₃CR and CCR - chemokine receptors; IL – interleukin.

Table 1.5 Molecules secreted by macrophages (data adapted from Szekanecz and Koch, 2007 and references therein)

Secretory product		Function
Chemokines	CXCL1, CXCL5, CXCL7, CXCL8	Chemotactic for neutrophils, promote angiogenesis
	CXCL9, CXCL10	Possibly pro-inflammatory, are antiangiogenic
	CXCL16	Monocyte recruitment
	CCL2, CCL3, CCL5	Monocyte chemoattractants
	CCL18	Homeostatic, T-cell chemoattractant
	CX ₃ CL1	Chemoattractant for monocytes and lymphocytes
Cytokines	IL-1, TNF- α	Pro-inflammatory, induces macrophage interleukin and chemokine secretion
	IL-6, Oncostatin-M	Cytokine release and monocyte effector function
	IL-10	Pro-inflammatory
	IL-12, IL-15, IL-18	Th1 polarisation, IL-18 induces CCL2 secretion by macrophages
	B-lymphocyte-stimulator protein	Proliferation inducer
	Lymphotoxin- α	Induces adhesion molecule changes on ECs to allow phagocytes to bind to them. Previously known as TNF- β
	GM-CSF	Constitutively produced, major role in myeloid precursor proliferation and differentiation
	MIF	Macrophage cytokine release and angiogenesis. Secretion of TNF- α , IL-1, IL-6, CXCL8 and MMP production
Growth factors	PDGF-C, PDGF-D	-D isoform increased MMP-1 production
	VEGFR-1	Implicated in the activation of macrophages and angiogenesis
Proteinases	MMP-1, MMP-2, MMP-9	ECM degradation, tissue destruction
	Cathepsin G	Monocyte chemotactic mediated by SF
	TIMP-1, TIMP-4	MMP antagonisers

GM-CSF - granulocyte–monocyte colony-stimulating factor; PDGF - platelet derived growth factor; VEGFR, vascular endothelial growth factor receptor; TIMP - tissue inhibitors of MMPs; IL – interleukin; MMP – matrix-metalloproteinases; MIF – macrophage inhibitory factor; CXCL, CXL, CX₃CL and CCL - chemokines; CXCR, CXR, CX₃CR and CCR - chemokine receptors; TNF – tumour necrosis factor

1.3.3 Dendritic cells (DCs)

In normal conditions DCs are essential regulators of both the acquired and innate immune systems where they stimulate naive T-cell proliferation and act as accessory cells in the generation of primary antibody responses as well as being enhancers of natural killer (NK) T-cells and NK cell cytotoxicity (Lutzky *et al.*, 2007).

In RA DCs play a range of roles (reviewed by Lutzky *et al.*, 2007);

1. Priming MHC-restricted autoimmune responses in lymphoid organs.
2. Helping to perpetuate the disease by processing and presenting antigens locally following infiltration into synovial fluid and tissue. This initiation and perpetuation of RA by DC is by self tolerance abolition followed by the generation of lymphocytes, which are self-reactive (Lebre and Tak, 2009).
3. Drive the generation of ectopic lymphoid tissue (presumably also in the synovium).
4. Together with macrophages and synoviocytes they produce inflammatory mediators of the innate immune system.
5. Recent evidence suggests that DCs are contributors to atherosclerosis, an RA complication. A range of DC subsets have been characterised.

1.3.4 Neutrophils

Neutrophils are the most abundant and shortest lived leukocyte with a life span of around 24-48 hours in a normal individual before their apoptosis and death. It is the inhibition/suppression in the levels of neutrophil apoptosis which may lead to severe inflammatory conditions such as RA. Neutrophil apoptosis has been shown to be suppressed in RA synovial fluid from as little as <3 month disease duration (Raza *et al.*,

2006), and the reduction of neutrophil recruitment is a source of potential therapeutic avenues as they may be key factors in RA pathogenesis in a number of ways, including the secretion of MMP-8 and MMP-9 (Murphy and Nagase, 2008) as well as secreting granule enzymes (such as cathepsin G, and proteinase 3) which activate cytokines. They also play a role in the functional regulation of immune cells via the secretion of chemokines such as CCL2, CCL4, CCL20 and CXCL10 and cytokines such as IL-1 α , IL1- β and TGF- β (reviewed by Wright, Moots and Edwards, 2014). Furthermore neutrophils have been shown to produce neutrophil extracellular traps (NETs) which destroy extracellular bacteria and have been indicated as a source of autoantigens in autoimmune disease sufferers (reviewed by Wright, Moots and Edwards, 2014). A range of therapies which affect neutrophils are used to successfully control RA symptoms. Non-steroidal anti-inflammatory drugs (NSAIDs, which inhibit the production of reactive oxygen species, ROS, and reduce neutrophil adherence), corticosteroids (decrease IL-8 neutrophil production) and disease modifying anti-rheumatic drugs (DMARDs, which includes the reduction of migration and ROS production of neutrophils) (reviewed by Wright, Moots and Edwards, 2014). The high expression levels of adhesion molecules on neutrophils allow rapid binding to activated endothelial cells (see section 1.3.10) (Tsubaki *et al.*, 2005). A range of synovial components have been identified as essential for neutrophil survival, including GM-CSF, type 1 IFN, and more recently lactoferrin, an iron binding protein of the transferrin family (Wong *et al.*, 2009).

1.3.5 B-cells

B cells form a minority of the infiltrates in RA tissue, accumulating in the germinal centers of lymphoid follicles present in ~20% of RA cases (Loetscher and Moser, 2002). Plasma cells differentiate from mature B-cells upon their stimulation by toll like receptors (TLRs) or antigen encounters and can generate autoantibodies such as rheumatoid factor (see table

1.1) which is used as a diagnostic tool for the development of RA. Antigen activated B-cells can also assist in the differentiation of effector T-cells and thus the production of proinflammatory cytokines involved in the destruction of cartilage and bone (Mauri and Ehrenstein, 2007) as well as the generation of degrading enzymes and cytokines. Despite the low representation of B-cells in RA the role they play in disease pathogenesis has been highlighted by the amelioration of symptoms due to B-cell depletion in a range of studies (reviewed by Nakken *et al.*, 2011) including anti CD20 (rituximab) administration (Mauri and Ehrenstein, 2007) which has been successfully used for a number of years

1.3.6 T-cells (reviewed by Imboden, 2009)

T-cells heavily infiltrate the RA synovium. They can be separated into CD4+ and CD8+, with CD4+ T-cells being dominant in RA synovial infiltrates. Activated/memory T-cells are found in the inflamed RA joint. The naive T-cells are activated via antigens presented by HLA molecules of APCs, such as dendritic cells and macrophages. The APC to T-cell contact is augmented and T-cell signalling increased with co-stimulation by CD28. CD28 is expressed on T-cells ligated with CD80/86 on APCs. Cytotoxic T lymphocyte-associated antigen (CTLA) T-cells also binds to CD80/86 on APCs and acts as an ‘off’ switch for the immune system. Thus its presence causes a down-regulation of T-cell signalling (Malmström *et al.*, 2005). A study involving immunising mice with the CTLA4-Ig showed that it prevented collagen-induced arthritis; and if administered after disease onset ameliorated the symptoms (Webb, Walmsley and Feldmann, 1996)

A range of genes in RA have shown to be linked to T-cells such as PTPN22 (protein tyrosine phosphatase non-receptor type 22), which codes Lyp, a tyrosine phosphatase which regulates T-cell receptor signal transduction (Lundy *et al.*, 2007) and MHC class II DR4/DR1.

T-cells can accumulate in the synovium in one of 3 patterns:

1. Diffuse infiltrates throughout the tissue.
2. Clustered with B-cells in follicle organisation with germinal centres.
3. Clustered with B-cells in follicle organisation without germinal centres.

1.3.7 Pannocytes (PCs)

PCs were identified at sites of cartilage damage in RA. They share some phenotypic and functional features seen in both fibroblast-like synoviocytes (FLS) and articular chondrocytes; such as mRNA for inducible nitric oxide synthase (iNOS) and collagenase for both PCs and chondrocytes, and the mRNA for the collagen type-1 gene. However, despite having mRNA for inducible nitric oxide synthase PCs do not generate NO constitutively or when stimulated by cytokines. PCs can also be distinguished morphologically as they have a rhomboid morphology which distinguishes them from articular chondrocytes and FLS (which are spherical and bipolar respectively). Furthermore they exhibit bright VCAM staining compared to chondrocytes and FLS (Zvaifler *et al.*, 1997). Results obtained by Longato *et al.*, (2005) support the reasoning that PCs are part of the primitive embryonic connective tissue-forming cell group and exclude the theory that PCs originate from fibroblasts or monocyte-macrophages.

1.3.8 Chondrocytes

Chondrocytes exclusively form the cell population in human articular cartilage which covers the long bone articulating surfaces. Collagen types II, IX, and XI form part of the interterritorial cartilage matrix which provides the required tensile strength. The other major component is aggrecan, a large aggregating proteoglycan, which provides the cartilage matrix with compressive resistance (reviewed by Otero and Goldring, 2007).

Where there is no vascular supply for nutrient/metabolite transfer chondrocytes rely on diffusion both from subchondral bone and the articular surface.

Proteinases such as cathepsin B, L and D and metalloproteinases such as MMP-10 and MMP-3 (which activate procollagenases), are generated by chondrocytes. This range of cellular responses to inflammation shows that chondrocytes may not only be involved in cartilage matrix destruction in response to synovium generated proinflammatory cytokines, but could also be a source of proinflammatory cytokines/proteins themselves (reviewed by Otero and Goldring, 2007). This was backed up recently by results obtained by Jeong *et al.*, (2009), who showed that in the mouse RA animal model, Pin-1 (a peptidyl prolyl isomerase) and cyclo-oxygenase-2 (COX-2) were over expressed in ankle cartilage, and that cultures of primary human chondrocytes had increased basal expression of the proinflammatory proteins COX-2, TNF-alpha, and IL-1beta.

1.3.9 Osteoclasts (Schett, 2007)

Osteoclasts are essential for bone remodelling throughout life as the primary bone resorbing cells, enabling bone shaping in early life, adulthood bone remodelling and old age bone loss. In RA monocytes/macrophages differentiate into osteoclasts via signals from activated T-cells and FLS. These express RANKL (receptor activator of nuclear factor κ B ligand) and so 'drive osteoclast formation'. Activated T-cells which express IL-17 (Th17 cells) as well as RANKL also support the formation of osteoclasts whereby RANKL binds the monocyte surface receptor RANK leading to their osteoclastogenesis. RANKL and macrophage colony stimulating factor are key factors in osteoclast differentiation with RANKL expression being regulated by TNF- α , IL-1, IL-6 and IL-17 which are abundant in the synovial membrane (reviewed by Schett, 2007).

1.3.10 Endothelial cells (ECs)

Synovial ECs in RA are involved in a wide range of processes such as angiogenesis, leukocyte trafficking from the circulation and presentation/expression of a range of mediators and effectors involved in disease pathology. These include cytokines IL-1, TNF- α and IL-15; chemokines, CXCL8, CCL2, CCL21, CXCL5, CXCL12, CCL3 and CCL19; chemokine receptors, CXCR3 and CXCR4; proteinases, MMP-1, MMP-3, MMP-9, MMP-13, cathepsin B and L; adhesion molecules, E-selectin, P-selectin, ICAM-1, ICAM-2 and PECAM-1 and angiogenesis regulators, VEGF and TGF- β^1 among others (Middleton *et al.*, 2004). EC phenotypes are characterised as activated, angiogenic, apoptotic and leaky and play a major role in the pathophysiology of RA in several ways (Middleton *et al.*, 2004); (table 1.6)

1. Subintimal blood vessel ECs allow leukocyte migration into the synovium and synovial fluid. To do this ECs become activated, expressing adhesion molecules such as E-selectin and ICAM-1 which facilitate leukocyte adhesion to the ECs (reviewed by Middleton *et al.*, 2004)
2. EC permeability increases leading to extravasation of plasma, formation of oedema and joint swelling. The vascular permeability is primarily induced by vasoactive agents such as NO (among other ROS), histamine and bradykinin (Szekanecz and Koch, 2004; Szekanecz and Koch, 2005)
3. The proliferation of ECs in angiogenesis allows nutrition and oxygen requirements of the expanding pannus and synovial tissue to be met.
4. Expression of cytokines/chemokines and their receptors involved in proliferation, angiogenesis and bone and tissue degeneration.

5. Release of inflammatory mediators from vascular ECs such as TGF- β , endothelial cell-derived growth factor, and colony stimulating factor (Szekanecz and Koch, 2008)

It should be noted that the regulation of angiogenesis involves phases of apoptosis since vascular remodeling is an ongoing process. Therefore, a range of apoptosis related genes are also active during angiogenesis, such as TNF- α , HIF-1, Smo, and $\alpha v \beta 3$ (Firestein, 1999; Middleton *et al.*, 2003; Semerano *et al.*, 2011; Zhu *et al.*, 2015)

In the human synovium venular endothelial changes occur very early in RA. These include morphological changes with the ECs developing a cuboidal appearance and gaps appearing between ECs (Middleton *et al.*, 2004).

Table 1.6 Some characteristics of activated, angiogenic, apoptotic and leaky endothelial cells (data adapted from Firestein, 1999; Middleton *et al.*, 2003; Middleton *et al.*, 2003 and references therein; Semerano *et al.*, 2011; Zhu *et al.*, 2015)

Cell Phenotype			
Activated	Angiogenic	Apoptotic	Leaky
Increased adhesion molecule expression (ICAM, Selectins, MECA-79 etc.)	Expression of cell-cycle-associated antigens (PCNA and Ki67), the $\alpha v\beta 3$ integrin (associated with vascular proliferation) and VEGF stimulates EC proliferation	Decreased adhesion molecule expression. Increased ROS	Reduced expression of tight junction proteins
Increased pro-inflammatory/cytokine chemokine presentation and expression	Increased pro-angiogenic chemokine expression and upregulation of Ets-1 expression	Increased ROS. Increased oxidative stress. The Shh signalling pathway is involved in endothelial cell apoptosis in a Smo dependent manner	VEGF generates vascular permeability
Cuboidal appearance. MECA-79 binding on HEVs	'Flat' (normal) appearance. The influx of EC progenitors leads to capillary sprouting which can be observed	Cell blebbing, shrinkage, nuclear fragmentation, chromatin condensation And DNA fragmentation	'Gaps' between cells observed
$\alpha v\beta 3$ integrin is expressed by endothelial cells and considered a marker for activation	$\alpha v\beta 3$ is also a marker for angiogenesis. The angiopoietins and their receptors Tie-1 and Tie-2 play a key role in the development of the vasculature	The HIF-1 gene is associated with apoptosis (as are changes in NO levels and 'stress genes' and angiopoietins among others) however these genes are also involved in angiogenesis	Reductions in junction protein expression are considered markers for 'leaky' ECs

PCNA - Proliferating Cell Nuclear Antigen; MECA-79 - monoclonal antibody to carbohydrate epitope expressed on HEVs; VEGF - vascular endothelial growth factor; HIF - Hypoxia inducible factor; HEV - high endothelial venules; Ets-1 - an angiogenesis regulator; Smo - Smoothed protein; Shh - sonic hedgehog; ROS - reactive oxygen species. ICAM – intra cellular adhesion molecule; NO – nitrous oxide; EC – endothelial cell; DNA – deoxyribo nucleic acid.

1.3.11 Cell populations in acidic environments.

Little data are available on the pH *in vivo* in the rheumatoid joint tissue. This is partly due to it constantly changing in response to environmental cues, and the difficulty of measuring it *in vivo*. Much of the data available refer to cultured cell types in artificially induced pH environments; evidence shows the hypoxic joint to be acidic to various degrees in nature. Various studies exist showing differential gene expression and thus functional differences in reduced pH (Andersson *et al.*, 1999; Lardner, 2001; Murata *et al.*, 2009; Dong *et al.*, 2013).

Under inflammatory conditions hypoxia stimulates lactate production due to anaerobic glycolysis, which leads to the extracellular acidification (Lardner, 2001). pH has been established at around pH 5.2-7.1 in a number of disease states, including RA SF (Farr., 1985) and as between 7.27 and 7.30 in the pannus tissue from antigen induced rat models, while being lower at 5.66-6.91 in joint intracellular fluid (Andersson *et al.*, 1999).

A range of both pro- and anti-inflammatory responses are modulated by acidic environments (reviewed by Okajima, 2013). Macrophages from mice have been shown to have inhibited TNF- α and IL-6 expression (Mogi *et al.*, 2009) and increased IL-10 secretion at between pH 6.2-7.3. Low extracellular pH has also been shown to stimulate macrophage phagocytosis (reviewed by Okajima, 2013). Neutrophils at pH 6.8 showed inhibited O²⁻ production (Murata, *et al.*, 2009) and ECs have been shown to stimulate the adhesion of monocytes and increase VCAM-1 and ICAM-1 expression (Chen *et al.*, 2011). Increases in the expression of a number of genes involved with inflammation such as those for chemokines, cytokines, adhesion molecules, and COX-2 have also been observed in human ECs (Dong *et al.*, 2013).

1.4 Angiogenesis in RA (reviewed by Szekanecz and Koch, 2008; Szekanecz *et al.*, 2009; Szekanecz *et al.*, 2010; Szekanecz, Besenyei, Szentpétery, and Koch, 2010).

Due to the thickening of tissue in RA, the nutrient and oxygen requirements from the circulating blood for the synovium increase. Angiogenesis is the development of new blood vessels from existing vessels and is mediated by a range of both soluble and cell surface bound factors. The mediators activate the vascular ECs, which release MMPs to breakdown the extracellular matrix (ECM) and basement membrane allowing ECs to migrate out. From here ‘capillary sprouts’ form from single ECs which develop into capillary loops as the lumen forms and finally into new capillaries upon basal membrane formation. The increased vascularisation present in some RA is also a contributing factor in the increased infiltration of leukocytes which occurs across the synovial blood vessels. Microparticles (MPs) (small membrane-bound vesicles released by cells undergoing activation or apoptosis) have been indicated as involved in processes ranging from transcellular communication to molecular trafficking as evidenced by their presence on biologically active molecules such as DNA, adhesion molecules and cytokines. Furthermore, they may be involved in angiogenesis in RA due to their induction of chemokines such as CCL5 and cytokines such as TNF- α (reviewed by Dye, Ullal and Pisetsky, 2013).

The ELR motif divides CXC chemokines onto ELR⁺ (angiogenic) and ELR⁻ (angiostatic). It consists of the residues glutamate-leucine-arginine residues and is found near the N-terminus of pro-angiogenic chemokines such as CXCL1, CXCL5, CXCL7 and CXCL8 (Haringman *et al.*, 2004; Koch, 2005; Charo and Ransohoff, 2006; Bonecchi *et al.*, 2009). The ELR motif is involved in binding to receptor CXCR2 on ECs. This results in stimulating EC division and migration which are major components of angiogenesis

(reviewed by Keeley *et al.*, 2008). ELR⁺ CXC chemokines can bind and activate neutrophils. The angiogenic properties of ELR⁺ CXC chemokines, such as CXCL8 and CXCL5 have been stated to be a result of their induction of endothelial cell migration which is not seen in the ELR⁻ CXC chemokines such as CXCL4 (Strieter *et al.*, 1995). The migration of ECs allows for the development of new vessels within the synovium.

1.5. Structure of the synovium

The ultrastructure of the synovium was first described by Key (1932) where, based on the subintimal structure, it was divided into 3 major types; areolar, adipose and fibrous (see figure 1.4). The most highly specialised is areolar (see figure 1.5) which, whilst very rarely having villi, often has folds which upon stretching disappear.

Within the synovium there are two major layers; the intimal (or lining) layer and the sub-intimal (or sub-lining) layer. The intimal layer is marked by a fine fibrillar structure which contains a low number of collagen type I fibres which become denser in the sub-intima. The intimal layer of the areolar type is 1-2 cells thick with capillaries lying below or between these cells in the compact zone. Barland *et al.*, (1962) described the intimal layer as containing two distinct cell types; fibroblast-like and macrophage-like cells. The electron microscopy techniques have been superseded by the advent of cytochemical analysis, which has identified the presence of intimal fibroblasts via identification of specific mRNAs and gene products.

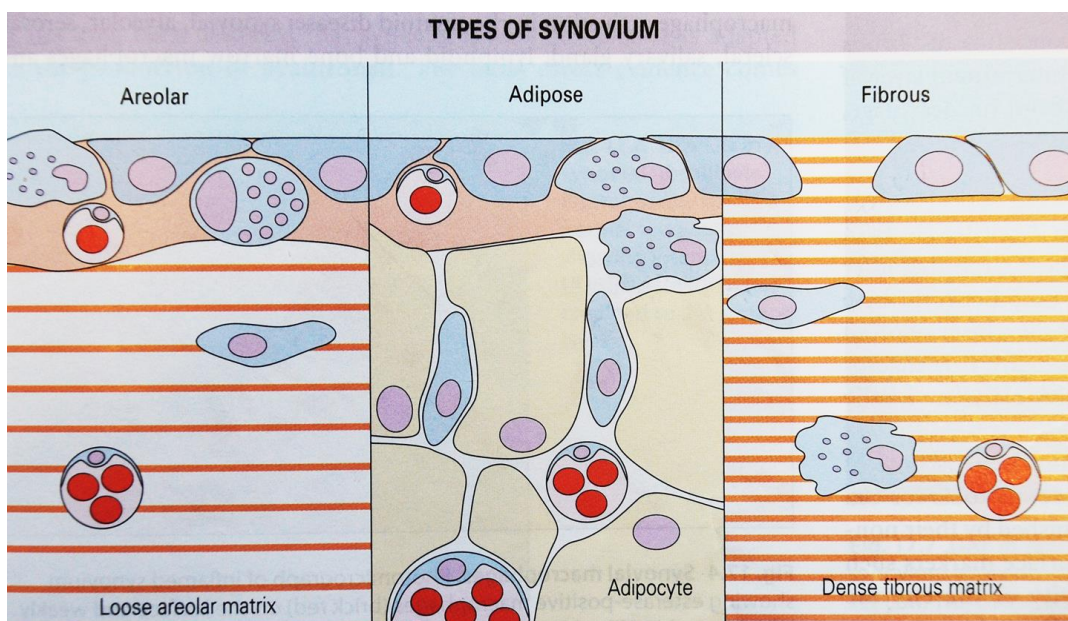


Figure 1.4 Diagrammatic representations of the major synovium types. (Edwards, 1998).

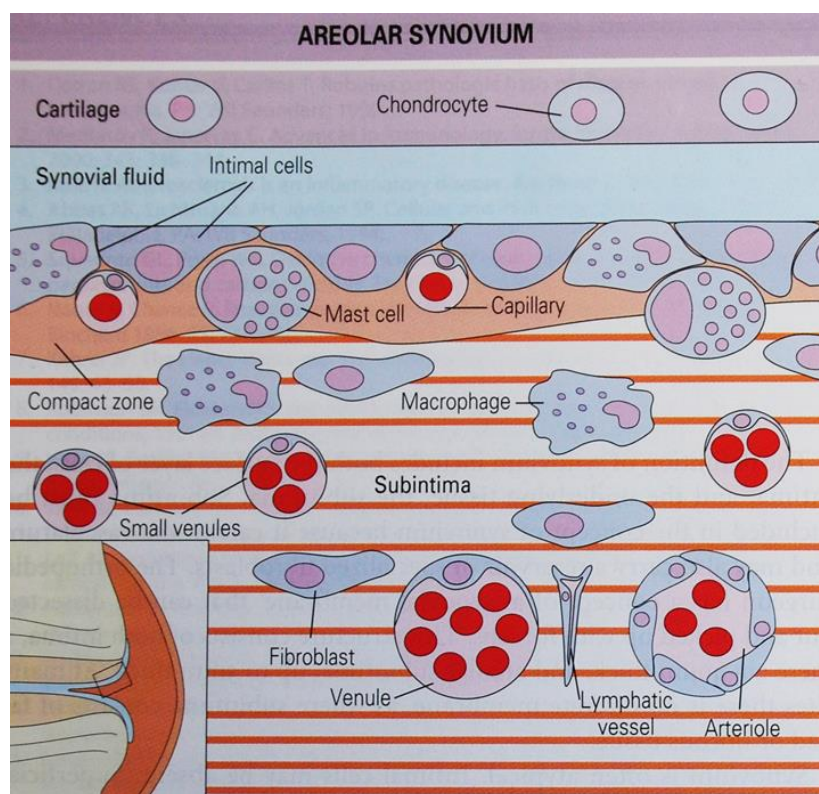


Figure 1.5 Diagrammatic representation of areolar synovium. (Edwards, 1998)

These intimal fibroblasts show a high degree of uridine diphospho-glucose dehydrogenase (UDPGD) enzyme activity (Wilkinson *et al.*, 1992; Pitsillides, 2003) and display high expression of a range of adhesion molecules such as vascular cell adhesion molecule-1 (VCAM-1), (Morales-Ducret *et al.*, 1992; Smith *et al.*, 2003) and intercellular adhesion molecule (ICAM). Decay accelerating factor (DAF) has also been identified in synovial intimal fibroblasts (Hamman *et al.*, 1999). Edwards (1998) has also shown that intimal fibroblasts are capable of interacting with immune response elements as well as showing specialisation in matrix component synthesis and synthesis of synovial fluid.

The subintimal layer is where the accumulation of infiltrating cells (including leukocytes) occurs. Mast cells and associated associated venules and arterioles, some of which are in association with nerve fibers, are also seen. The presence of neutrophils within the joint space is also seen in RA. (Edwards, 1998)

Adipose synovium occurs within villi as 'fat pads'. Whilst the intimal layer usually has a collagen containing layer separating it from the adipocytes it can also lay directly upon them with the lower tissue layers consisting of fat cells. Fibrous synovium consists of dense fibres, such as those found in tendon/ligament and carries a non-continuous layer of cells.

1.6. Function of the synovium

The synovium has several major functions:

1.6.1 Cartilage lubrication

Synovial fluid (SF) is generated by the synovium and is of major importance in lubrication. Jay *et al.*, (2007) identified lubricin as being responsible for the elastic behaviour of SF

and its ability to safely dissipate the ‘strain energy’ generated by motion, making it not only a distinct requirement for ‘boundary lubrication’ but also chondrocyte protection.

Lubricin is a glycosylated protein produced by the gene proteoglycan 4 (PRG4), also known as ‘superficial zone protein’ (SZP) which is expressed by synoviocytes and chondrocytes and in the superficial zone but not by deeper chondrocytes. Lubricin has also been suggested to bind polymorphonuclear granulocytes (PMN) which are recruited to the synovial tissue during inflammation and so ‘may play a role in PMN mediated inflammation’ (Jin *et al.*, 2012). Cartilage does not self-repair so damage due to everyday exertion must be minimised and it is the lubricin containing SF which helps to fulfil this requirement and maintain joint longevity (Rhee *et al.*, 2005). Gene defects on PRG4 have been shown to be involved in several joint defects, including the autosomal recessive disease camptodactyly-arthropathy-coxa vara-pericarditis syndrome (CACP) (Marcelino *et al.*, 1999).

1.6.2 Tissue surface maintenance

A non-adherent synovial surface is a requirement for continued movement. Hyaluronan is generated by intimal fibroblasts and is considered of importance in adhesion prevention (Edwards *et al.*, 2003). Scarring and fibrin formation at the synovium surface can damage synovial function, the intimal fibroblast products plasminogen activator and decay accelerating factor (DAF) are thought to inhibit this. Hyaluronan is a major constituent of the SF which must be retained within the joint to ensure correct surface maintenance. Yu *et al.*, (2005) ascertained that at the surface of the synovium the osmotic pressure of a hyaluronan concentration polarisation layer leads to ‘outflow buffering’ and thus gives a mechanism which retains the synovial fluid in a joint cavity under pressure. The intimal

matrix also aids in synovial fluid retention by being of a specific porosity to prevent fluid/hyaluronan loss whilst readily allowing the exchange of other substances.

1.6.3 Chondrocyte nutrition

It would be expected that the blood vessels within the synovium would provide the most direct route for nutrients and oxygen to reach the cartilage via the SF. This is a source of controversy as the required evidence to support this is not present as the vessels are not structurally adapted to this function (Edwards *et al.*, 2003). Indirect routes such as the subchondral bone have also been considered as a route for nutrient delivery, but were initially discounted as a route of major importance as the subchondral plate is complete in adults and thus would prevent this function. However, Malinin and Ouellette, (2000) ascertained using cartilage autografts in primates that disrupting the contact between vascularised subchondral bone and cartilage resulted in cartilage degeneration. This is supported by work carried out by Amin *et al.*, (2009) whose experiments on *in vitro* bovine tissue showed that removal of subchondral bone led to marked increases in chondrocyte death and that the presence of subchondral bone within the tissue culture medium appeared to protect superficial zone chondrocytes from death. This suggests that the subchondral bone provides mediators essential for chondrocyte and thus articular cartilage survival.

1.6.4 Synovial fluid composition and volume control

SF components are primarily secreted by cells of the synovium. SF is a plasma dialysate with hyaluronan as an added component as well as collagenases, proteinases and lubricin. A wide range of binding proteins, structural proteins, degenerative enzymes, lubricating molecules and signalling molecules have been identified as altered in differentially altered in diseases such as RA, OA, and in response to injury (reviewed by Hui *et al.*, 2012). The

SF glutamate concentration has also been shown to which increase in arthritis with the glutamate receptors having recently been tied to inflammation and identified as a potential therapeutic target (Bonnet *et al.*, 2013). Decreases in synovial fluid lubricin are seen to be associated with increases in inflammatory cytokines (Elsaid *et al.*, 2008), as seen in RA sufferers. Lubricin is a hyaluronan binding protein important in dissipating the energy generated by the strain of everyday wear and tear from normal motion thus acting as a 'chondroprotective' factor distinct from its role in joint lubrication (Jay *et al.*, 2007).

In RA there is a marked increase in the volume of SF as the disease progresses which contributes to the swelling of the joint. Elevated cytokine levels in RA SF are also observed (reviewed by Szekanecz and Koch; 2010). SF from early RA patients has been shown to have a differing composition from later stage RA whereby the cytokine and MMP profiles between the two shows marked differences. The levels of cytokines in patients with early RA has been shown to include increased T-cell related cytokines (Raza *et al.*, 2005) such as IL-2, IL-4, IL-13 and IL-17 as well as EGF, bFGF, IL-1 and IL15. In established RA IL-2, IL-4, IL-13, IL-15, EGF, bFGF were seen to decrease. A range of other cytokines and chemokines including CCL3, CCL4, CCL11, granulocyte-macrophage colony-stimulating factor (GM-CSF) and granulocyte colony-stimulating factor (G-CSF) showed no significant differences between early and late RA (Raza *et al.*, 2005). MMP-1 and MMP-3 are both increased in early RA with MMP-8 and MMP-9 increasing as RA progresses (Yoshihara *et al.*, 2000)

1.7. Leukocyte infiltration into the synovium

Inflammation under normal (non-RA) conditions is a protective mechanism in response to injury and/or tissue damage whereby leukocytes travel to the site of injury to remove infectious agents and facilitate tissue repair. The transendothelial migration of leukocytes

is also a major feature in chronic inflammation in RA as it is the method by which leukocytes from the post capillary venules cross from the circulating blood to the site of 'injury'. This migration across ECs and the basement membrane into the synovial tissue and SF is mediated via a range of processes, including chemokines.

1.7.1 Chemokines and transendothelial migration (TEM)

1.7.1.1 Chemoattraction and Integrin activation

The unidirectional movement of a cell from a region of low to high ligand concentration along a chemical gradient is 'chemoattraction'. Platelet-activating factor (PAF) and leucotriene-B4 (LTB4) are examples of 'classic' chemoattractants. PAF is a mediator of inflammation, and a potent monocyte chemoattractant.

While selectins mediate the leukocyte capture at the ECs (McEver, 2002) selectin bonds alone cannot arrest rolling leukocytes. This process relies almost exclusively on chemokine mediated integrin activation on leukocyte surfaces (Zarbock *et al.*, 2007). Firm adhesion is regulated by the integrins and their EC ligands, including the α_4 integrins, VLA-4 ($\alpha_4\beta_1$) and $\alpha_4\beta_7$ and the β_2 integrins, LFA-1 ($\alpha_L\beta_2$) and MAC-1 ($\alpha_M\beta_2$) (reviewed by Alon and Schulman, 2011). As the leukocytes come into contact with the EC the leukocyte G-protein coupled receptors (GPCRs) are 'triggered' by heterotrimeric G-proteins, activated by the EC surface immobilised chemokines (Alon and Ley, 2008). The chemokine receptor signal causes the α and β subunits of the integrin heterodimer to shift from the inactive to the active formation (Tadokoro *et al.*, 2003). Chemokine activated VLA-4 molecules rearrange to form dispersed microclusters around their VCAM-1 EC ligand and LFA-1 and VLA-1 become mobilised to the leading and trailing edges of lymphocytes in the absence of the ligand (Woolfe *et al.*, 2007). Chemokine activated ICAM-1/ LFA-1 microclusters are localised to the lymphocyte where it makes contact with

the EC and appear to facilitate the shear-resistant crawling of lymphocytes on ECs (Schulman *et al.*, 2009). A series of studies have shown this cascade of events as occurring rapidly, allowing the abrupt arrest of leukocytes to the ECs (Campbell *et al.*, 1998; Shamri *et al.*, 2005)

1.7.1.2 Activation

For leukocytes to effectively extravasate they must first firmly adhere to the venule ECs. For many years it was believed that soluble chemoattractants were responsible for leukocyte-EC adhesion (Middleton *et al.*, 1997 and references therein; Middleton *et al.*, 2002). However, it was recognised that due to blood flow the chemoattractant gradient could not be maintained at the EC-blood interface. This led to the suggestion that chemokines were bound to the EC surface (Middleton *et al.*, 1997 and references therein; Middleton *et al.*, 2002) from where they effectively enabled leukocyte activation and transmigration from circulating blood. Middleton *et al.*, (1997) showed using CXCL8 (IL-8) injections into rabbit skin that the chemokine was not only internalised abluminally into caveolae by postcapillary and small vein ECs but was also transcytosed and presented on the EC luminal surface, predominantly in association with EC microvilli. Mediators involved in this process include glycosaminoglycans (GAGs) and the Duffy antigen receptor complex (DARC) (reviewed by Middleton *et al.*, 2002; Pruenster *et al.*, 2009) which are discussed further below. It is likely that chemokines generated from within the ECs themselves are presented in the same fashion but without transcytosis occurring (figure 1.6) (Middleton *et al.*, 2002).

The chemokines are immobilised and presented on EC microvilli (figure 1.6) by GAGs which exhibit electrostatic interactions with the largely basic chemokines. However the interaction is not entirely electrostatic, as best shown by the fact that acidic chemokines

such as CCL3 and CCL4 also bind GAGs (Kuschert *et al.*, 1999). Electrostatic chemokine-GAG interactions are selective with chemokine immobilisation occurring via the chemokine C-terminus α -helix for some chemokines (i.e CXCL8), and at sites distinct from the C-terminus for chemokines such as CCL5. The heparin binding motifs XBBXB, XBBBXXB and BBXB, where B is a basic amino acid residue, are common for a number of proteins, as exemplified by chemokines such as CCL5 and CCL3 having the BBXB motif. Binding occurs between the chemokine and carbohydrate structures (e.g sulphate groups) of GAGs such as heparan sulphate and chondroitin sulphate are found (reviewed by Middleton *et al.*, 2002).

DARC was first described on the surface of erythrocytes and was later found on postcapillary venule ECs where it was shown to bind both CC and CXC chemokines (Nibbs *et al.*, 2003; Neote *et al.*, 1993; Gardener *et al.*, 2004). Further studies indicated that DARC mediates chemokine-EC interactions (Middleton *et al.*, 1997; Rot, 2005) and Pruenster *et al.*, (2009) has shown that DARC mediates chemokine transcytosis, increasing leukocyte transmigration across DARC expressing venules.

As well as the chemokines and chemokine receptors, adhesion molecules such as the selectins, integrins and VCAM are present at the EC surface. Each of these can be localised on microvilli projections of the ECs (figure 1.6), and a range of work indicating the importance of microvilli localised adhesion molecule distribution in leukocyte migration has been carried out (reviewed by Middleton *et al.*, 2002).

As well as microvilli providing a greater surface area allowing the presentation of more chemokines and receptors, they have been seen to elongate in response to specific molecules such as ICAM-1. This was observed by Oh *et al.*, (2007) where ICAM was seen to regulate *de novo* microvilli elongation allowing its clustering at the most apical region of the EC.

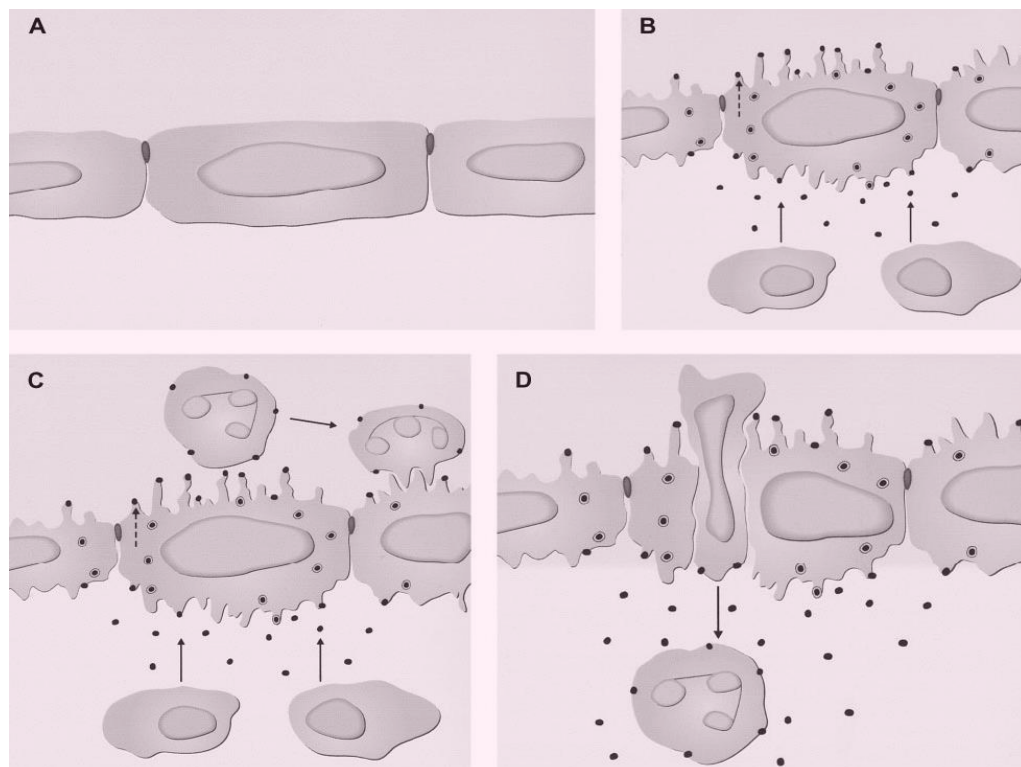


Figure 1.6 Subcellular events in the endothelium during chemokine-directed leukocyte extravasation. (A) Noninflamed tissue. (B) Inflamed tissue. Release of chemokines from extravascular cells in the tissue occurs (\rightarrow), and there is wrinkling of the endothelial cell surface. Chemokines are taken up at the abluminal surface of the endothelium and transcytosed in caveolae. This process involves binding to glycosaminoglycans (GAGs) and/or the Duffy receptor. At the luminal surface, chemokines are released and bound preferentially on the tips of projections. These mediators may also be produced and released directly by endothelial cells, in which case they are also bound at the luminal surface but not transcytosed ($--\blacktriangleright$). (C) Chemokines bound at the luminal endothelial cell surface build up in concentration. They do this sufficiently to bind to and activate the signaling receptors on the leukocyte cell surface, leading to activation of integrins and firm attachment. (D) Leukocyte migration occurs either transcellularly through a pore in the endothelial cell or through the intercellular junction, following a chemokine gradient bound to GAGs and/or the Duffy receptor. The cell then enters the basement membrane and continues migration along a chemokine gradient that is soluble or immobilized to the extracellular. (Figure taken from Middleton *et al.*, 2002).

1.7.1.3 Leukocyte capture and rolling.

Site specific inflammation starts with the capture and rolling of leukocytes along ECs of the post capillary venule walls. The capture and rolling are mediated by type-1 transmembrane glycoproteins (Barreiro and Sanchez-Madrid, 2009) which are members of the selectin family. The most important of these here are: L-selectin (CD62L), expressed on the leukocyte outer membrane, P-selectin, (CD62P), expressed on ECs and platelet surface and E-selectin (CD62E), expressed on activated EC surface and specifically up-regulated on synovial ECs under inflammatory conditions. These interact with carbohydrate structures on P-selectin glycoprotein ligand-1 (PSGL1) and other glycosylated ligands. PSGL1 binding to L-selectin ‘nucleates leukocyte-leukocyte interactions by which leukocyte derived fragments and adherent leukocytes facilitate secondary leukocyte capture’ (Ley *et al.*, 2007). Serine phosphorylation of L-selectin has also been shown to affect the positioning of the receptor on the cell surface (Wedepohl *et al.*, 2012).

Selectin-ligand interactions have a very high on/off rate (rate at which the bonds are formed and broken) and so facilitate leukocyte adherence to the ECs in blood flow conditions and create rolling (Li *et al.*, 2007). The L-selectin function is strengthened by interactions between lymphocyte function associated antigen-1 (LFA-1) and intercellular adhesion molecule (ICAM) which reduces the velocity of rolling leukocytes by stabilising the initial transient contact between the leukocytes and the EC (Barreiro and Sanchez-Madrid, 2009). Once firmly adhered leukocytes change morphology from round to ‘polarised’ (see figure 1.7).

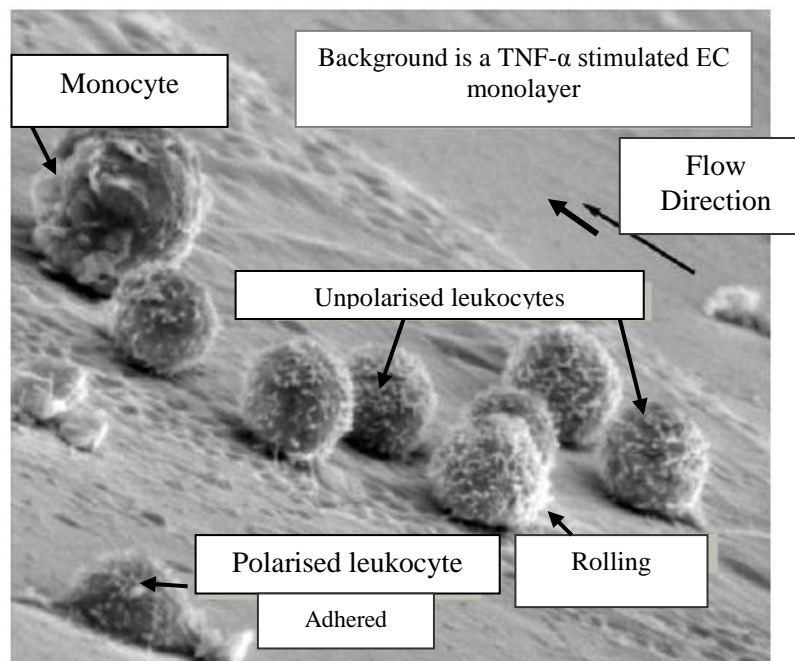


Figure 1.7 Scanning electron microscope image of leukocyte rolling and adhesion to an EC monolayer. A human endothelial monolayer (treated with pro-inflammatory stimuli and exposed to human peripheral blood lymphocytes and monocytes under flow). A number of unpolarised leukocytes have been captured during the rolling process. Also shown is a firmly adhered lymphocyte which has changed morphology from rounded to polarised. (Taken and adapted from Barreiro and Sanchez-Madrid, 2009).

Integrins are of great importance in the initial stages of leukocyte transmigration for controlling the cell-cell interactions. The activation of leukocyte integrins is chemokine mediated. Other than integrins and selectins, mucosal vascular addressin cell adhesion molecule, (MAdCAM-1) participates in capture by collaborating with L-selectin function to stabilise the initial capture and reduce rolling velocity (Barreiro and Sanchez-Madrid, 2009). In particular, they can change their adherent activity by maintaining an inactive surface conformation until the site of inflammation is reached where rapid integrin activation allowing initial adherence occurs (Campbell *et al.*, 1998). The conformational

changes in the integrins are induced by chemokine receptor initiated signalling pathways causing an increase in the integrin-ligand affinities (Hyduck and Cybulsky, 2009).

1.7.1.4 Arrest and firm adhesion

As capture of leukocytes on the vascular endothelium is achieved and the rolling rate slows, leukocytes are activated by contact with the EC luminal surface bound chemokines and integrin ligands enable leukocyte arrest in normal blood flow conditions (termed 'activation-dependent stable arrest') (Tarrent and Patel, 2006; Barreiero and Sanchez-Madrid, 2009). Once firmly adhered the leukocytes change morphology from round to 'polarised' (see figures 1.7 and 1.8). The integrin-ligand interaction is key to firm adhesion. Each integrin is composed of an α -subunit and a β -subunit, which undergo conformational changes, as well as integrin redistribution on the leukocyte cell surface. Three conformational states have been proposed; bent conformation with low affinity, extended conformation with intermediate affinity and lastly, extended conformation with high affinity (Beglova *et al.*, 2002; Nishida *et al.*, 2006). The most important integrins for leukocyte firm adhesion to ECs are $\beta 2$ subfamily members, particularly LFA-1 (CD11a/CD18 or $\alpha L\beta 2$) and myeloid-specific integrin Mac-1 (CD11b/CD18 or $\alpha M\beta 2$), as well as $\alpha 4$ integrins VLA-4 ($\alpha 4\beta 1$) and $\alpha 4\beta 7$. LFA-1 binds to a range of intercellular adhesion molecules (ICAM-1 to ICAM-5), the most important being ICAM-1 and ICAM-3 (Barreiero and Sanchez-Madrid, 2009).

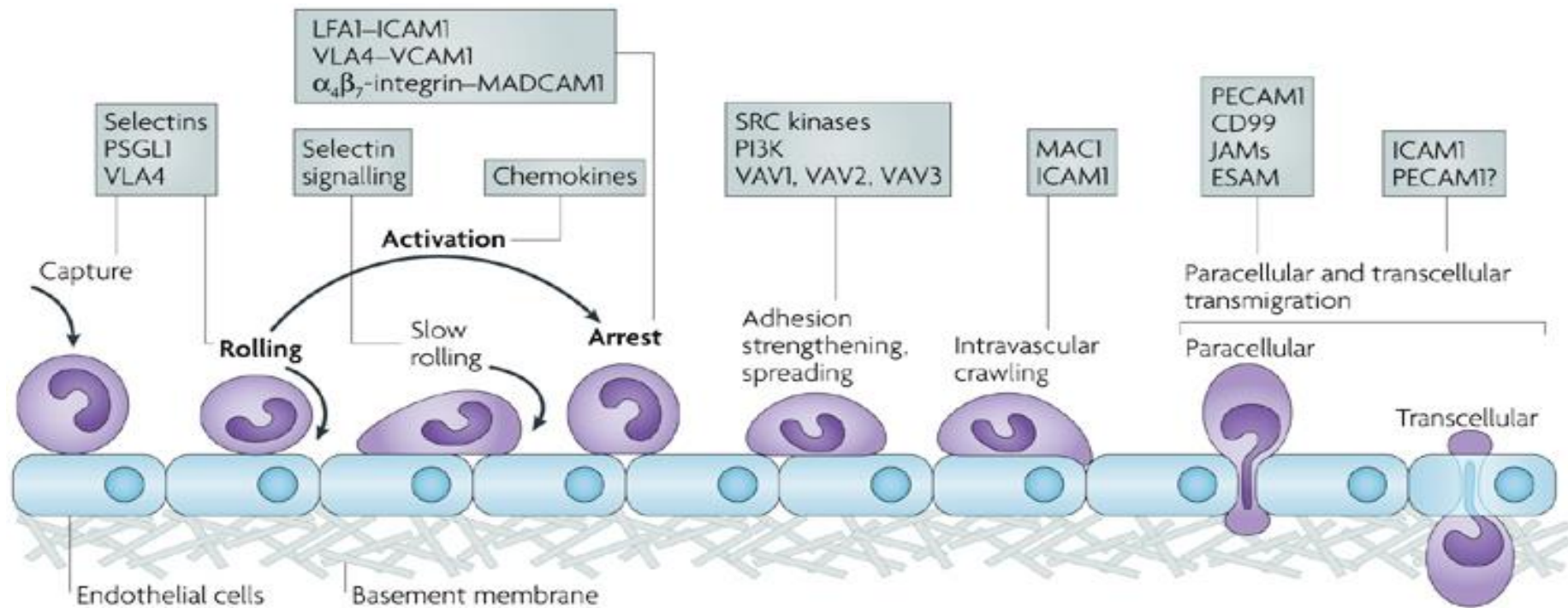


Figure 1.8 Leukocyte adhesion cascade. The original three steps in TEM were; rolling (selectin mediated), activation (chemokine-triggered) and arrest (integrin dependent). Additional steps have now been added, slow rolling, adhesion strengthening and spreading, intravascular crawling and paracellular/transcellular migration. Boxes indicate the main molecules involved in the marked step. **ESAM**, endothelial cell-selective adhesion molecule; **ICAM1**, intercellular adhesion molecule 1; **JAM**, junctional adhesion molecule; **LFA1**, lymphocyte function-associated antigen 1 (also known as $\alpha_L\beta_2$ -integrin); **MAC1**, macrophage antigen 1; **MADCAM1**, mucosal vascular addressin cell-adhesion molecule 1; **PSGL1**, P-selectin glycoprotein ligand 1; **PECAM1**, platelet/endothelial-cell adhesion molecule 1; **PI3K**, phosphoinositide 3-kinase; **VCAM1**, vascular cell-adhesion molecule 1; **VLA4**, very late antigen 4 (also known as $\alpha_4\beta_1$ -integrin). **VAVs**, Rho family guanine nucleotide exchange factors that become tyrosine phosphorylated in response to adhesion. (Taken from Ley *et al.*, 2007).

1.7.1.5 Crawling (figure 1.9 A)

Prior to transmigration across the post capillary ECs leukocytes ‘crawl’ on the luminal EC surface in a ‘MAC-1 and ICAM-1 dependent manner’ (Ley *et al.*, 2007) actively seeking out a suitable transmigration site. This crawling is mediated by chemokines.

1.7.1.6 Podosome formation and conformational changes

It is believed that the extracellular matrix degradation and cell motility that facilitates cell migration are coordinated by podosomes, most probably dependent on cell matrix and cell type (Murphy and Courtneidge, 2012). A range of podosome initiation mechanisms have been elucidated, including integrin signalling, microRNA control and ROS signalling (reviewed by Murphy and Courtneidge, 2012). Concomitantly with integrin activation and clustering a series of actin remodelling events are triggered by chemokines, which cause leukocyte microvilli to collapse and formation of the polarised shape (anterior-posterior axis) (Brown *et al.*, 2003). Both lymphocytes and neutrophils use invasive podosomes to probe ECs during the migration process (Cinamon *et al.*, 2004; Schulman *et al.*, 2009). During paracellular migration lymphocyte podosomes probe subendothelial chemokines (Lee *et al.*, 2009). Studies have suggested that these podosomes are seldom found at lymphocyte-EC contact points when chemokine signals are limited and shear force is not applied (Schreiber *et al.*, 2007; Schulman *et al.*, 2009). As transmigration rarely occurs under these conditions podosome frequency appears to correlate with successful migration (Schreiber *et al.*, 2007; Schulman *et al.*, 2009). Podosome analysis suggests lymphocyte contacts with the apical EC surface are composed of LFA-1 rings that surround the base of the podosome (Schulman *et al.*, 2009). These may act as signalling moieties and nucleating assemblies for chemokine triggered cytoskeletal remodeling on both the leukocyte and the endothelial sides.

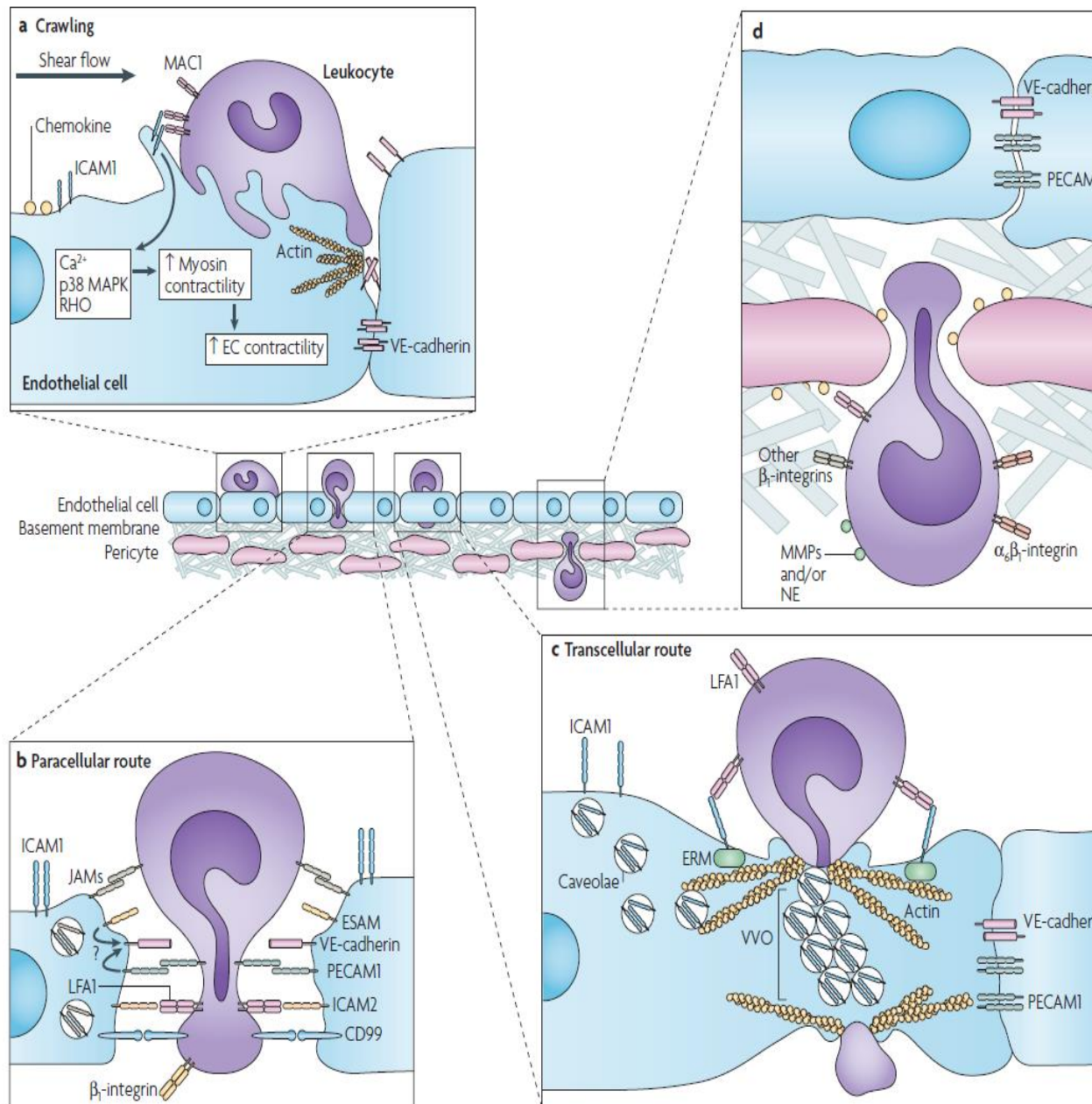


Figure 1.9 Leukocyte crawling and transmigration. **A** Leukocyte membrane protrusion extension into the endothelial-cell body and endothelial-cell junctions is initiated by ligation of intercellular adhesion molecule 1 (ICAM1) by macrophage antigen 1 (MAC1). Ligation of ICAM1 is associated with increased intracellular Ca²⁺ and activation of p38 mitogen-activated protein kinase (MAPK) and RAS homologue (RHO) GTPase, which together may activate myosin light-chain kinase enhancing endothelial-cell contraction and thus opening interendothelial contacts. Transmigration through ECs can also induce cell-surface expression of members of the β₁-integrin family and proteases on neutrophils and other leukocytes that may facilitate the progression of the leukocyte through the vessel wall. **B** Paracellular migration involves the release of endothelial-expressed vascular endothelial cadherin (VE-cadherin) and is facilitated by intracellular membrane compartments containing a pool of platelet/endothelial-cell adhesion molecule 1 (PECAM1) and possibly other endothelial-cell junctional molecules, such as junctional adhesion molecule A (JAM-A). Other molecules involved in paracellular transmigration are endothelial cell-selective adhesion molecule (ESAM), ICAM2 and CD99. **C** Transcellular migration occurs in narrow endothelium regions, ICAM1 ligation leads to translocation of ICAM1 to actin- and caveolae-rich regions. ICAM1-containing caveolae come together as vesiculo-vacuolar organelles (VVOs) which develop an intracellular channel enabling leukocyte migration. Ezrin, radixin and moesin (ERM) proteins may link ICAM1 and cytoskeletal proteins such as actin and vimentin causing their localization around the channel. **D** Migration through the endothelial basement membrane and pericyte layer occurs through gaps between adjacent pericytes and areas of low protein deposition within the extracellular matrix. This response can be facilitated by α₆β₁-integrin and possibly proteases, such as matrix metalloproteinases (MMPs) and neutrophil elastase (NE), ERM, ezrin, radixin and moesin; LFA1, lymphocyte function-associated antigen 1. (Figure taken from Ley *et al.*, 2007)

1.7.1.7 Transmigration

Transmigration of leukocytes from blood to tissues across the EC barrier occurs by two routes, the transcellular (through individual ECs) route and/or the paracellular (between adjacent ECs) route (Ley *et al.*, 2007; Carmen and Spinger, 2008; Wittchen, 2009).

1.7.1.8 Transcellular migration (figure 1.9 C)

Transcellular migration occurs preferentially in several regions including HEVs of secondary lymphoid organs and the blood brain barrier where migration occurs without disturbing interendothelial junctions. As mentioned in section 1.7.1.6. this is dependent on the generation of protrusions known as ‘podosomes’ (~500nm in depth and diameter), which are dependent on actin and Src kinase as well as being Wiskott–Aldrich syndrome protein (WASP) activity dependent (Vijayakumar *et al.*, 2015; Carmen and Spinger, 2008; Wittchen, 2009; reviewed by Carmen *et al.*, 2007;). The podosomes (feet-like structures) palpate the EC surface searching for a site of low EC resistance where an invasive podosome of >1000nm can begin penetration. When a suitable site is located the EC surface is locally disrupted, initially by forcing a ‘podo-print’ into the surface membrane disrupting the cytoskeletal arrangement, cytoplasm and other organelles, then by driving pore formation in the EC membrane.

Also reported (Barreiero and Sanchez-Madrid, 2009 and references therein), is that vimentin (a filament protein) plays a role in transcellular migration. In addition there is translocation of ICAM-1 to caveolae following the adhesion of leukocytes and subsequent formation of ICAM-1 and cavaolin-1 containing vesicular channels around the podosomes penetrating the cell. Further to this dome-shaped endothelial structures have been shown *in vivo* encapsulating the leukocyte indicating the possibility that the docking structures may develop into encapsulating domes allowing the podosomes to penetrate not only the EC

membrane and pass through the cytoplasm, but also to allow the basal membrane to be penetrated without disrupting EC barrier function.

1.7.1.9 Paracellular migration (figure 1.9 B)

Paracellular migration requires the transient disruption of EC tight junctions. Woodfin *et al.*, (2009) recently ascertained that EC junctional molecules (such as ICAM-2, JAM-A, and PECAM-1) act sequentially and in distinct steps to facilitate/mediate neutrophil transmigration, which is likely to hold true for all leukocytes. ECs interact with adjacent T-cells via tight junction and adherens junctions which are comprised of a range of proteins important in facilitating paracellular transmigration (see table 1.7). Occludin is one such protein and was the first transmembrane protein to be positively identified in tight junction

Table 1.7 Proteins seen at tight and adherens junctions involved in paracellular transmigration. (Ley *et al.*, 2007; Wittchen, 2009; Barreiro and Sanchez-Madrid, 2009)

Junction type	Protein	
Tight	Occludin	Involved in cytoskeleton rearrangement, postulated that the homophilic binding of leukocyte to EC occludin may preserve EC barrier function during transmigration
	Claudin-5	A member of the claudin family. Vascular EC-specific transmembrane (TM) protein
	JAM	Junction adhesion molecule. A TM protein concentrated at the apical region of EC tight junctions. Engages in homophilic interactions between adjacent T-cells
	ESAM	Endothelial specific adhesion molecule Another TM protein. Can interact homophilically and heterophilically to maintain the junction
	ZO-1 and ZO-2	Zonula occludin. Intracellular proteins forming a complex on the cytoplasmic side of the plasma membrane immediately beneath the tight junction
Adherens	VE-cadherin	A TM protein forming contacts between adjacent EC cells and interacts with the cytoskeleton of the cell to maintain EC barrier function. During transmigration VE-cadherin is displaced from the junction and rapid relocates once transmigration has occurred
	Catenins	α -, β -, and p120-catenin form a complex with VE-cadherin on the cytoplasmic side of the junction allowing VE-cadherin to interact with the cytoskeleton
	PECAM-1 (CD31)	Platelet endothelial cell adhesion molecule-1. A TM protein expressed on ECs, platelets, and some leukocytes. The PECAM pool at the junction is critical in cell-cell adhesion for adjacent ECs
	CD99	A highly glycosylated protein expressed by most ECs and leukocytes. Many can interact both homophilically and heterophilically to maintain the junction

1.8. Chemokines and chemokine receptors

1.8.1 Chemokines

Chemotactic cytokines or ‘chemokines’ are small heparin binding proteins produced by a range of both tissue cells and leukocytes. They are essential factors in immune defence being involved in the generation, localisation, recruitment and activation of leukocytes as a response to inflammatory stimuli (Pease and Williams, 2006). There are currently over 40 chemokines (table 1.8) grouped according to structural criteria. Each is a single polypeptide chain of 70-100 amino acid residues which share 20-95% sequence homology, including a number of conserved cysteine residues. The cysteine residues have been utilised in the nomenclature system for chemokines (see table 1.8) and give four distinct chemokine subgroups (Pease and Williams, 2006; Iwamoto *et al.*, 2008; Bonecchi *et al.*, 2009)

- 1) **CC chemokines**. The first two of four cysteine residues are adjacent to each other. The largest of the chemokines groups whose major target is monocytes.
- 2) **CXC chemokines**. The first two of the four cysteine residues are separated by a single amino acid. The genes for these are mostly clustered on two chromosomes, 4q12-q13 (the major cellular target being neutrophils) and 4q21.21 (the major cellular target being lymphocytes).
- 3) **C (or XC) chemokines**. Contain only two cysteine residues. Represented by only two chemokines which are specifically active on T-lymphocytes.
- 4) **CX3C chemokines**. Only one chemokine currently resides in this subgroup. The two cysteine residues here are separated by three other amino acid residues. Structurally different to the other subgroups by having a transmembrane domain.

As chemokines are designated as being ligands in the new (2000) nomenclature system, namely CCL, CXCL, XCL and CX3CL with their corresponding receptors being designated as CCR, CXCR, XCR and CX3CR respectively (reviewed by Szekanecz *et al.*, 2003; Iwamoto *et al.*, 2008; Bonnechi *et al.*, 2009). Chemokines can be broadly grouped into two categories depending on their function: inflammatory (inducible), and constitutive (homeostatic). A less represented sub-type are the dual function chemokines.

1.8.2 Chemokine receptors

There are currently 19 identified chemokine receptors (Bonecchi *et al.*, 2009; Bachelierie *et al.*, 2014), all of which belong to the G-protein coupled receptor family subset with 7-transmembrane domains (Pease and Williams, 2006; Bonecchi *et al.*, 2009; Bachelierie *et al.*, 2014).

Many of the receptors bind multiple ligands (table 1.8) and are expressed on a range of leukocyte cell types. Whilst most CC and CXC chemokine receptors will bind only CC and CXC chemokines respectively, the Duffy antigen receptor for chemokines (DARC) bind both CC and CXC chemokines (Neote *et al.*, 1993; Nibbs *et al.*, 2003), but has also been shown to bind inflammatory rather than constitutive/homeostatic chemokines (Gardner *et al.*, 2004). DARC and the receptor D6 are termed ‘atypical receptors’ as neither generate a signalling cascade involving G-proteins typical of all other chemokine receptors (Nibbs *et al.*, 2003) and are involved in internalisation and transport. A further atypical receptor is chemocentryx chemokine receptor (CCX-CRK), which along with D6 binds CC chemokines, targeting them for degradation and thus acting as ‘decoy receptors’ (Pruenster *et al.*, 2009).

Signal transduction is achieved by two interactions, the first being an interaction whereby the basic chemokine ligand is tethered by the acidic extracellular N-terminus domain of the

receptor. The first interaction enables the second (lower affinity) interaction whereby the ligand is moved to the body of the receptor, activating the G-protein subunits initiating the signalling cascade (Pease and Williams, 2006).

All chemokine receptors share a number of common features (Murphy., 1994)

1. 340-380 amino acid residues in length.
2. An Asp-Arg-Tyr (DRY) motif in the second intracellular domain loop. This motif is not present on the atypical chemokine receptors (Pruenster *et al.*, 2009).
3. N-terminal segment containing a tyrosine sulphation motif.
4. A disulphide bond formed from two conserved cysteine residues which stabilise the binding pocket.

Table 1.8 Human chemokines and chemokine receptors (Adapted from Filer *et al.*, 2008; Bonocchi *et al.*, 2009)

Chemokine (Ch)			Receptor(s)	Functional expression
Nomenclature		Chromosome		
Old	New			
GRO α	CXCL1	4q21	CXCR2	Inflammatory
GRO β	CXCL2	4q21	CXCR2	Inflammatory
GRO γ	CXCL3	4q21	CXCR2	Inflammatory
PF4	CXCL4	4q21	CXCR3 splice variant	
ENA-78	CXCL5	4q12-q13	CXCR2	Inflammatory
GCP-2/CTAP-III	CXCL6	4q21	CXCR1, 2	Inflammatory
NAP-2	CXCL7	4q12-q13	CXCR2	Inflammatory
IL-8	CXCL8	4q13-q21	CXCR1, 2	Inflammatory
Mig	CXCL9	4q21	CXCR3	Inflammatory
IP-10	CXCL10	4q21	CXCR3	Inflammatory
I-TAC	CXCL11	4q21.2	CXCR3	Inflammatory
SDF-1	CXCL12	10q11.1	CXCR4	Constitutive
BLC/BCA-1	CXCL13	4q21	CXCR5	Constitutive
BRAK	CXCL14	5q31	Unknown	Unknown
SR-PSOX	CXCL16	17p13	CXCR6	Heterogeneous
Lymphotactin	XCL1	1q23	XCR1	
SCM-1 β	XCL2	1Q23	CXR1	
Fractalkine	CX3CL1	16q13	CX3CR1	Heterogeneous
I-309	CCL1	17q12	CCR8	Inflammatory
MCP-1	CCL2	17q11.2	CCR2	Inflammatory
MIP-1 α	CCL3	17q11	CCR1, 5	Inflammatory
MIP-1 β	CCL4	17q12	CCR5, 8	Inflammatory
RANTES	CCL5	17q11.2	CCR1, 3, 5	Inflammatory
MCP-3	CCL7	17q11.2	CCR1, 2, 3	Inflammatory
MCP-2	CCL8	17q11.2	CCR3, 5	Inflammatory
MIP-1 γ	CCL9		CCR1	Inflammatory
MIP-1 γ	CCL10		CCR1	Inflammatory
Eotaxin	CCL11	17q21.1	CCR3	Inflammatory
MCP-5	CCL12		CCR2	
MCP-4	CCL13	17q11.2	CCR2, 3	Inflammatory
HCC-1	CCL14	17q11.2	CCR1	Heterogeneous
HCC-2/Lkn-1	CCL15	17q11.2	CCR1, 3	
HCC-4/LEC	CCL16	17q11.2	CCR1, 2	
TARC	CCL17	16q13	CCR4, 8	Heterogeneous
DC-CK-1	CCL18	17q11.2	Unknown	Constitutive
ELC/MIP-3 β	CCL19	9p13	CCR7	Constitutive
LARC/MIP-3 α	CCL20	2q33-q37	CCR6	Inflammatory
SCL/6CKine	CCL21	9p13	CCR7	Constitutive
MDC	CCL22	16q13	CCR4, 8	Heterogeneous
MPIF-1	CCL23	17q12	CCR1	Heterogeneous
Eotaxin-2	CCL24	7q11.23	CCR3	Inflammatory
TECK	CCL25	19p13.2	CCR9	Constitutive
Eotaxin-3	CCL26	7q11.23	CCR3	Inflammatory
CTACK	CCL27	9p13	CCR10	Constitutive
MEC	CCL28	5p12 *	CCR3, 10	Heterogeneous

* gene number supplied by NCBI Entrez gene (<http://www.ncbi.nlm.nih.gov/sites/entrez>)

1.8.3 Chemokine involvement in rheumatoid arthritis

1.8.3.1 Inflammatory chemokines (figure 1.10)

Inflammatory chemokines (table 1.8, and figure 1.10) such as CXCL8 and CCL1 are usually only expressed under inflammatory conditions, and as such are found in high levels in the RA joint (table 1.9). They are expressed by a wide range of cell types and frequently bind non-selectively, with multiple receptors accommodating multiple chemokine ligands (Baggiolini, 2001; Haringman *et al.*, 2004; Loetscher, 2005; Filer *et al.*, 2008). Inflammatory chemokine production can be induced in response to stimulation by pro-inflammatory cytokines such as IL-1 and TNF α (Haringman *et al.*, 2004) and as such they are important mediators in the recruitment of effector cells of both the innate and adaptive immune system. Inflammatory chemokines in RA include CXCL1, CXCL5, CXCL6, CXCL8, CXCL9, CXCL10, CCL2, CCL3, CCL5, CCL13 and CCL20 (table 1.8 and table 1.9).

Table 1.9 Chemokines considered important in RA/expressed in RA joints. (Szekanecz *et al.*, 2003; Szekanecz *et al.*, 2006; Iwamoto *et al.*, 2008)

Subgroup	Name
CXC	CXCL1, CXCL4, CXCL5, CXCL6, CXCL8, CXCL9, CXCL10, CXCL12
CC	CCL2, CCL3, CCL5, CCL13, CCL17, CCL18, CCL20
C	CXL1
CX3C	CX3CL1

Many of these chemokines have not been specifically investigated to assess their presence at RA ECs and so a range of important data in this field which may contribute to the chemokine address code for RA has not been ascertained.

1.8.3.2 Constitutive chemokines (figure 1.10)

Constitutive chemokines (table 1.8 and figure 1.10) are expressed continuously and direct essential physiological processes such as haematopoiesis (Filer *et al.*, 2008) and lymphocyte and dendritic cell homing (Baggiolini, 2001; Loetscher, 2005) and the normal immune surveillance of body tissues. Unlike inflammatory chemokines they usually bind to specific single receptors (Filer *et al.*, 2008). Their presence in the bone marrow, thymus and lymph nodes indicates a role in the regulation of normal leukocyte production and distribution (Bonecchi *et al.*, 2009).

RA synovium bears resemblance to lymphoid tissue due to the generation of LFs in RA synovium (discussed in section 1). Constitutive chemokines, particularly CXCL13 and CCL21, have been implicated in the development of LFs in RA (Loetscher, 2005; Filer, 2008). Other constitutive chemokines in RA include CXCL12, CCL18 and CCL19 (table 1.8 and table 1.9).

1.8.3.3 Dual function chemokines (figure 1.10)

Dual function chemokines have features representative of both inflammatory and constitutive chemokines, being involved in normal immune defence and being up-regulated in inflammatory conditions. This group include CXCL9, CXCL10, CXCL11, CCL1, CCL20 and CCL25 (Moser and Willmann, 2004; Loetscher, 2005), however, these same chemokines are also designated as inflammatory or constitutive in other texts (Filer *et al.*, 2008).

1.8.3.4 The CCL chemokines and their receptors in RA

As stated in section 1.8.3.1 the chemokines CCL2, CCL3, CCL5, CCL13 and CCL20 have been shown to be important in RA with their role in RA being well established.

As prolific mononuclear cell recruiters, the following text will focus on CCL2 and CCL3. CCL2 (previously known as monocyte chemoattractant protein-1/MCP-1) is the CCR2 ligand. It is expressed in both synovial tissue and fluid where macrophages are its main source (Koch *et al.*, 1992) and has chemoattractive abilities in a range of cells including inducing the transmigration of monocytes, T-cells and NK cells (Loetscher *et al.*, 1994; Iikuni *et al.*, 2006; Wang *et al.*, 2009; Lebre *et al.*, 2011; Melado *et al.*, 2015) and is known to induce angiogenesis (Niu *et al.*, 2008). CCR2 has also recently been linked to neutrophil transmigration whereby high CCR2 expression and CCL2 responsiveness were seen in the peripheral blood neutrophils from early RA patients (Talbot *et al.*, 2015). Furthermore, monocyte chemoattractant protein-1 induced protein (MCP-1) has been indicated to be involved in RA associated endothelial dysfunction via decreasing the generation of nitric-oxide (NO) synthase-derived NO (He *et al.*, 2013). Normal vascular ECs exist at low levels of oxidative stress by the release of mediators such as NO (among others) (Napoli *et al.*, 2001).

CCL3 is a ligand of both CCR1 and CCR5 (Iwamoto *et al.*, 2008) and shows chemotactic activity for T-cells and monocytes (Stanford and Isseuts, 2003). The CCL3 mRNA is found within RA joints (Robinson *et al.*, 1995). Furthermore, CCL3 shows a two-fold increase in RA SF compared to control SF (Patel *et al.*, 2001). It has also been shown to stimulate neutrophil migration via CCR1, and to induce TNF generation in a mouse model of inflammation (Ramos *et al.*, 2005).

Further chemokines and their receptors are extensively discussed in a number review articles (Middleton *et al.*, 2004; Szekanecz and Koch, 2007; Szekanecz, Besenyei, Szentpétery, and Koch, 2010; Alon and Schulman, 2011; Dye, Ullal and Pisetsky, 2013; Wright, Moots and Edwards, 2014). Further details from these, and other reviews and references therein, are discussed in later chapters.

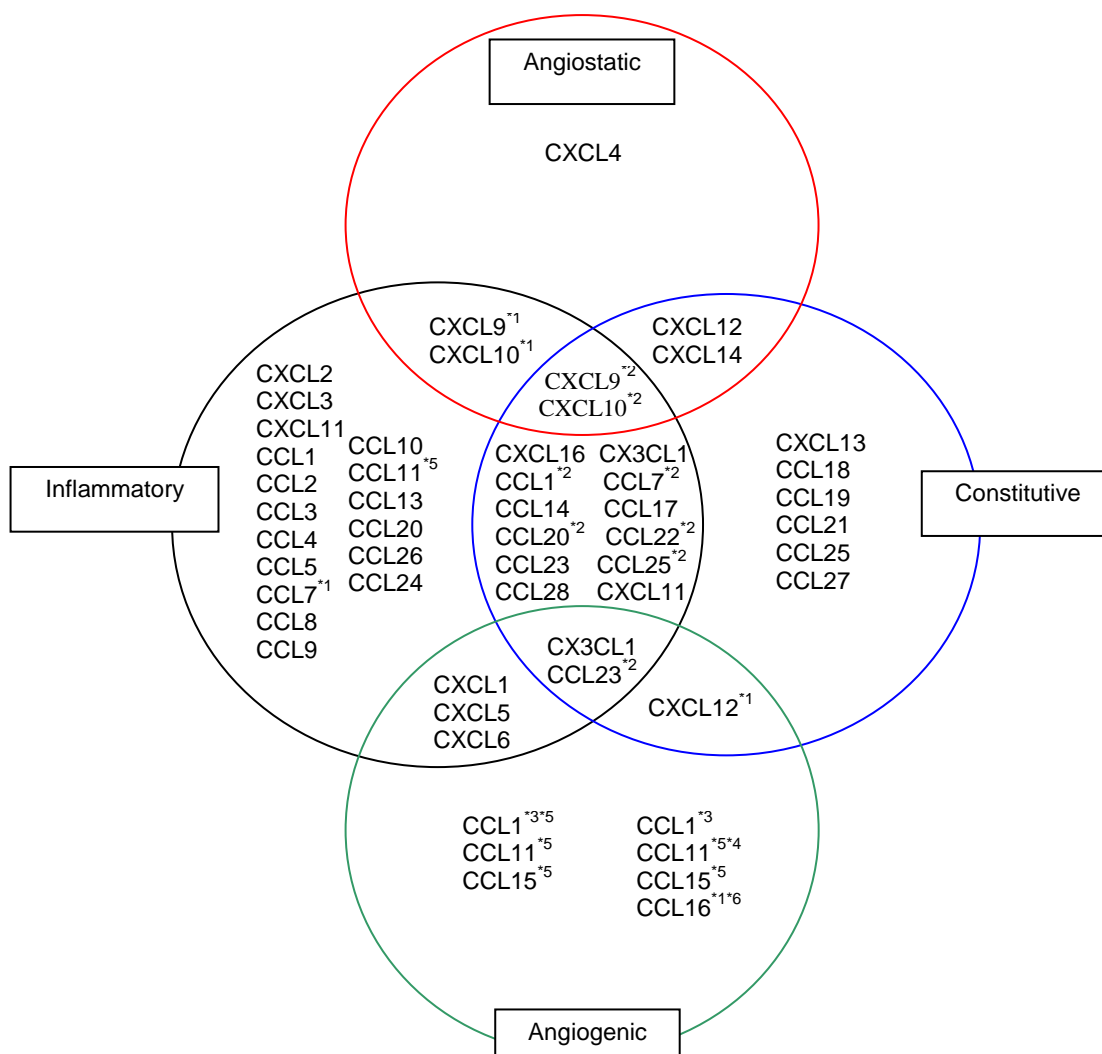


Figure 1.10 Schematic showing some inflammatory, constitutive, angiogenic and angiostatic chemokines designated to various different groups. (Adapted from Salcedo *et al.*, 2001; Strasly *et al.*, 2004 Hwang *et al.*, 2004; Loetscher., 2005; Filer., 2008;; Szekanecz and Koch., 2008; Szekanecz *et al.*, 2009). *1 indicates Filer, 2008, *2 indicates Loetscher, 2005, *3 indicates Bernardini *et al.*, 2001. *4 indicates Salcedo *et al.*, 2001, *5 indicates Hwang, 2009, *6 indicates Strasly *et al.*, 2004.

Whilst the chemokines in table 1.9 are the ones considered to be of importance in RA, a range of other chemokines have been established as being present in the RA joint (see table 1.10). The EC barrier where extravasation occurs offers a valuable source of therapeutic targets for leukocyte entry into the synovial tissue and thus invites more thorough investigation into the chemokines expressed specifically in this area.

Table 1.10 Human chemokines present at RA microvascular ECs

Chemokine	Present at RA ECs	Present in control	Control tissue	Upregulated in RA	Technique	Reference
CXCL5	Y	Y	OA/non RA	Y	Imf	Koch <i>et al.</i> , (1994a)
CXCL9	Y	N	Isotype matched negative control	–	Imh	Tsubaki <i>et al.</i> , (2005)
CXCL12	Y	Y (OA) N (he)	OA/healthy	Y (compared to he)	PImh NB	Pablos <i>et al.</i> , (2003)
	Y	Y	OA	Y	PImh	Santiago <i>et al.</i> , (2006)
	Y	~Y	Salivary glands in Sjogren's syndrome	Y	Imf	Burman <i>et al.</i> , (2005)
CXCL13	Y	Y	Non GC LF in RA	–	Imh	Takemura <i>et al.</i> , (2001)
CXCL16	Y	N	Non RA ST	Y	Imh	Van Der Voort <i>et al.</i> , (2005)
CX3CL1	Y	N	Control IgM antibody	–	Imh	Ruth <i>et al.</i> , (2001)
	Y	~Y	OA/ normal ST	Y	Imh	Blaschke <i>et al.</i> , (2003)
CCL2	Y	N	Isotype-matched negative controls	–	Imf	Burman <i>et al.</i> , (2005)
CCL3	Y	Y (OA) ~Y (he)	OA/healthy	Y	Imh	Koch <i>et al.</i> , (1994b)
CCL4	Y	Y	HUVEC/ normal PB	*	Imh. Adhesion assay	Tanaka <i>et al.</i> , (1998)
CCL8	Y	~Y	OA	Y	Imh	Pierer <i>et al.</i> , (2004)
CCL19	Y	~Y	Salivary glands in Sjogren's syndrome.	Y	Imh	Burman <i>et al.</i> , (2005)
	Y	Y	Tonsil/ non-GC RA	–	Imf	Page <i>et al.</i> , (2002)
CCL21	Y	Y	Tonsil	–	Imf	Page <i>et al.</i> , (2002)
	Y	~Y	Psoriasis	Y	Imf & mRNA hybridisation	Weninger <i>et al.</i> , (2003)

Imf – Immunofluorescence; **Imh**- Immunohistochemistry.; **NB** – northern blot; **PImh** – peroxidise immunohistochemistry; **GC LF** – germinal centres in lymphoid follicles; **PB** – peripheral blood; **he** – healthy; **~Y** – very little observed; **HUVEC** – human umbilical vein ECs; * indicates that while Tanaka *et al* (1998) showed CCL4 to be present on ECs its up-regulation was not established, however increases in T-cell adhesion in the presence of CCL4 were seen (also applies to CCL3, data not in table); **ST** – synovial tissue.

1.9. The Lymphatic System

In normal conditions lymphatic (or lymph) vessels are valved EC lined vessels which carry lymph from the tissues (figure 1.11). APCs are also carried to the lymph nodes via the afferent lymph vessels as part of normal essential maintenance and immune responses. The lymph is formed when lymphatic capillaries collect interstitial fluid for transport to lymph nodes via the lymphatic vessels to the subclavian vein where it is mixed back in with the blood. The lymph is pushed through the lymph vessels in a passive manner by contraction of body muscles during normal movement. The valves within lymph vessels prevent backflow of lymph fluid.

Lymphatic vessels can be distinguished from arterioles in a number of ways, such as the lack of a continuous basal membrane and the presence of ‘gaps’ between LECs, and the absence of desmosomes between LEC cell membranes (Rovenská and Rovenský, 2012). Histologically both LECs and arteriole ECs will stain with pan-endothelial markers such as CD31. However, LECs can be distinguished by staining for Lymphatic vessel endothelial HA receptor-1 (LYVE-) 1 and podoplanin.

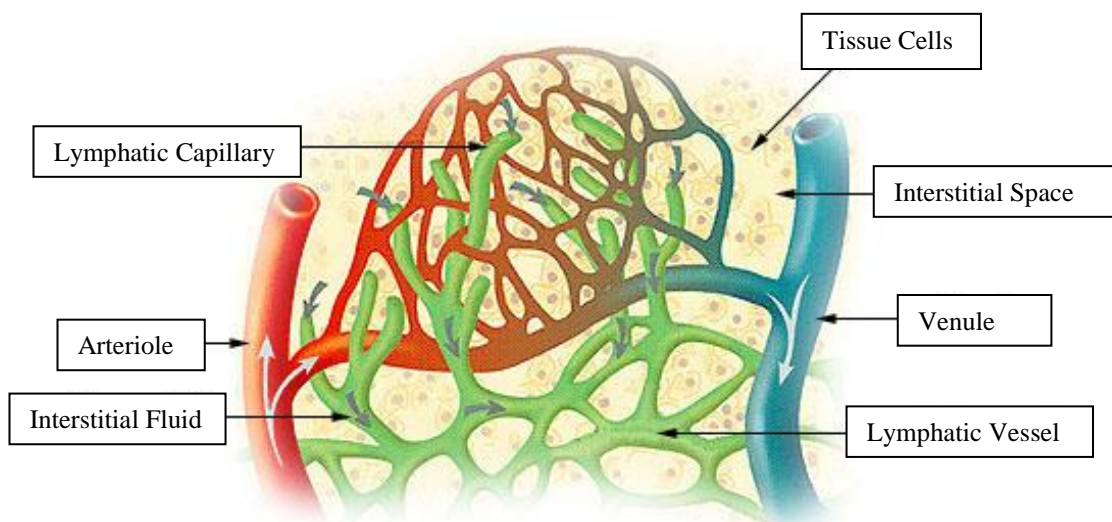


Figure 1.11 Diagram showing basic blood-tissue-lymphatic exchange. The process of transport from the blood to the tissue and the tissue to the lymphatic system (Taken and adapted (http://training.seer.cancer.gov/module_anatomy/images/illu_lymph_capillary.jpg.)

1.9.1 The Lymphatic vessels of the synovium

It has been shown that lymphatic vessel formation increases in RA (Xu *et al.*, 2003) and should act as a compensatory mechanism for the removal of the interstitial fluid containing the invading lymphocytes and pro-inflammatory chemokines and cytokines (Olszewski *et al.*, 2001). However, Zhou *et al.*, 2010 showed that despite an increase in lymphatic flow during the acute phase of arthritic inflammation there is a decrease in lymphatic flow as new lymphatic vessels form during the chronic phase. This has also been seen in the human TNF transgenic mouse (hTNF α) model where lymphatic vessels increased in number through the initial stages of inflammation but underwent no further significant increases as synovitis progressed (Polzer *et al.*, 2008). This would lead to reduction in removal of the ever increasing joint interstitial fluid and is further exacerbated by the reduction in muscular contractions around the damaged joint that encourage flow through the lymph vessels.

1.9.2 Chemokines and lymphatic vessels

It has been shown that the TNF- α activated dermal lymphatic endothelial cells (DLECs) show >100 fold increases in production of a range of chemokines including CCL2, CCL5 and CCL20 which attract T-cells and monocytes (Johnson *et al.*, 2006). This indicates that in inflammatory conditions lymphatic vessels would be required to upregulate the expression of chemokines chemoactive for the effective removal of the leukocytes in the synovium. This would be particularly pertinent in the later stages of RA where lymphangiogenesis has reduced and normal lymphatic drainage is declining. However, Burman *et al.*, (2005) has shown ‘inappropriately high’ levels of the same chemokine on both vascular and lymphatic vessels indicating that the chemokine gradient is corrupted within the RA synovium. Further studies to elucidate if there are correlations between the presence and/or absence of specific chemokines on the both vascular and lymphatic vessels of the synovium would be beneficial. This would further indicate the possibility that targeting the lymphatic system as a therapy for RA is feasible.

1.10. Hypoxia in RA (figure 1.12)

As discussed in section 1.4 angiogenesis allows for the increase in the blood supply to the synovium as it expands and its metabolic activity increases. Hypoxia due to increased oxygen requirements has been shown to upregulate angiogenesis in the RA synovium (Akhavani *et al.*, 2009). Despite this the increasing need for oxygen by the tissue is not met and the tissue oxygen pressure (tPO) decreases. tPO in the synovial tissue of RA patients has been measured to be as low as a mean of 19.35 mm Hg, an ambient oxygen tension of 2.5% (Biniecka *et al.*, 2010), compared to 74mm Hg, or 10% ambient oxygen tension in non RA synovium (Akhavani *et al.*, 2009). Hypoxia is also associated with increased levels of lipid peroxidation (Biniecka *et al.*, 2010) whereby membrane lipids undergo

oxidative degradation by the hydroxyl radical (OH•) leading to cell damage due to the generation of toxic aldehydes (reviewed by Mapp, Grootveld and Blake, 1995). The aldehyde 4-hydroxynonenal (4-HNE) which is an aldehyde product of membrane lipid peroxidation has been shown to generate a range of inflammatory responses including increased levels of IL-1 β , IL-6, TNF- α transcriptions and the expression of COX-2. It has also been shown that 4-HNE induces NF- κ B activation and nuclear translocations resulting in cell apoptosis (Yin *et al.*, 2015). Further to this cytokine-stimulated chondrocyte breakdown of the cartilage matrix has been shown to be primarily caused by lipid peroxidation (Tiku, Shar and Allison, 2000). It has also been reported that increased hypoxia in RA tissue can significantly delay neutrophil apoptosis (Cross *et al.*, 2006), reduce vessel stability, increase damage to DNA and upregulate hypoxia-inducible factor 1 (HIF-1) (see figure 1.12). HIF-1 is an important transcription factor in the hypoxic cell response as well as having involvement in angiogenesis, migration, cell survival pathways and reactive oxygen species (ROS) (figure 1.12) (Kennedy *et al.*, 2010). ROS are by-products of normal cellular metabolism and normally have defensive properties in that they are generated by activated neutrophils (among others) in an attempt to kill invading pathogens (Hitchon and El-Gabalawy, 2004). Hypoxia has been shown to significantly correlate with differing macro/microscopic inflammation sites, which affects cytokine production and may be part of the initial events in inflammation (Ng *et al.*, 2010).

In RA, as with tumours, hypoxia plays a major role in gene regulation in relation to FLS migration (Akhavani *et al.*, 2009). HIF-1 α is the major transcription factor by which hypoxia exerts its effects and is expressed in rheumatoid synovial tissue and synoviocytes (Zhao *et al.*, 2013). While little work has been done on hypoxia induced chemokine receptor expression, CXC chemokine receptor 4 (CXCR4) has been shown as a key gene upregulated by HIF-1 α . Furthermore, increased CXCR4 expression has been shown in RA

synovial fibroblasts (Li *et al.*, 2013). Hypoxia has also been shown to increase chemokine receptor expression such as in ovarian tumours where the expression of CCR1 was increased 5-fold by hypoxia (Scotton *et al.*, 2001). This indicates that regions of differing hypoxic microenvironments within the macro-environment of an RA joint may have different chemokine and chemokine/receptor profiles.

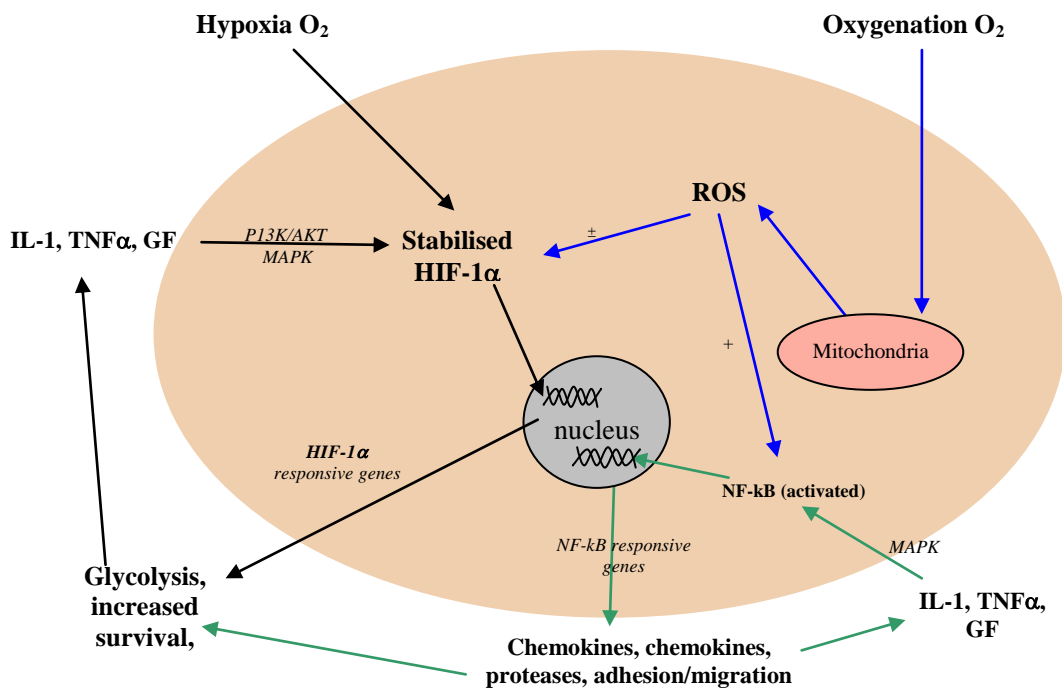


Figure 1.12 Diagram showing regulation of HIF-1 and nuclear factor- κ B (NF- κ B) pathways by reactive oxygen species and cytokine stimulation. Occurrences such as angiogenesis, leukocyte transmigration, endothelial cell activation and infiltrating cell survival beyond the norm in synovial inflammation in RA is perpetuated by the HIF-1 α and NF- κ B activation and actions. (Diagram altered from Hitchon and El-Gabalawy, 2004)

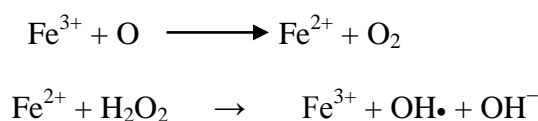
1.10.1 Oxidative stress in RA

Oxidative phosphorylation is the process by which adenosine-tri-phosphate (ATP) is generated by mitochondria where oxygen acts as the final electron acceptor in the process. By-products of this process are partly reduced oxygen metabolites which leave the mitochondria and react with other molecules generating a range of other ROS. The term 'oxidative stress' is used when the ROS generated by an organism increases beyond its ability to neutralise them. If levels of ROS are unregulated they cause damage to matrix components, proteins, nucleic acids and lipids (Hitchon and El-Gabalawy, 2004). A range of studies have provided evidence for oxidative stress in RA including studies which correlate poor prognosis for RA with increased oxidant levels, and good prognosis with increased antioxidant levels, as well as evidence of oxidative damage to cartilage, hyaluronic acid and proteins (reviewed by Hitchon and El-Gabalawy, 2004). Thioredoxin is a 'cellular catalyst' which is induced by oxidative stress and has pro-inflammatory effects. It has been shown to be overexpressed in RA synovial tissue where mutations to the regulatory genes due to oxidative stress in RA, such as p53 (Yamashishi *et al.*, 2002), have also been shown, and may negatively affect the countermeasures in place to prevent oxidative damage (reviewed by Schett *et al.*, 2001).

1.10.2 The involvement of iron in oxidative stress and RA (see figure 1.13)

As previously mentioned, in oxidative stress ROS are generated. An example of a ROS is the hydroxyl radical which is the most toxic of the ROS (Mapp, Grootveld and Blake, 1995) and can react with the vast majority of molecules within any living cell (Morris *et al.*, 1995; Mapp, Grootveld and Blake, 1995; Hitchon and El-Gabalawy, 2004). Free iron catalyses the formation of hydroxyl radicals from superoxide and hydrogen peroxide via

the Fenton reaction, whereby ferrous iron (Fe^{2+}) reacts with hydrogen peroxide (H_2O_2) forming the hydroxyl radical ($\text{OH}\cdot$)



This shows that the main force for the toxicity of ROS is due to the presence of free iron. Free iron is usually immobilised as ferritin or sequestered by iron binding proteins and is thus prevented from participating in the above reaction. The acidity of the environments can lead to iron metabolism dysfunction whereby iron is released from reticuloendothelial (RE) cells (also known as the mononuclear phagocyte system or the macrophage system). This may serve as a primary source of free iron in the synovium, however ‘microbleeding’ within the inflamed joint further exacerbates the iron levels in the synovium (Biernacki *et al.*, 1986; reviewed by Dabbagh *et al.*, 1993; reviewed by Morris *et al.*, 1995) (figure 1.13) with this ‘iron overload’ resulting in inadequate removal by the iron binding protein. There is an accepted correlation between iron concentration and arthritis, and in RA increased levels of free iron are found in SF and ST (Mowat *et al.*, 1968; Biernacki *et al.*, 1986). The iron levels in RA synovium have been measured as three times greater than in normal synovium, at $36\mu\text{g/g}$ and $12\mu\text{g/g}$ dry mass, respectively (Senator and Muirden., 1968) Furthermore, it has been established by Telfer and Brock (2004) that the presence of pro-inflammatory cytokines leads to further increases in the iron burden of the RA synovium.

Lactotransferrin is an iron binding protein found in SF which is capable of remaining bound to iron in the acidic environment of the inflamed synovium (Guillén *et al.*, 1998), has antibacterial action (Baker and Lindley, 1992) and may also have a protective function by collecting/holding the iron which would be released by transferrin in the same

conditions (Morris *et al.*, 1995). However, lactoferrin not bound to iron has also been shown to prolong neutrophil survival in established RA (Wong *et al.*, 2009).

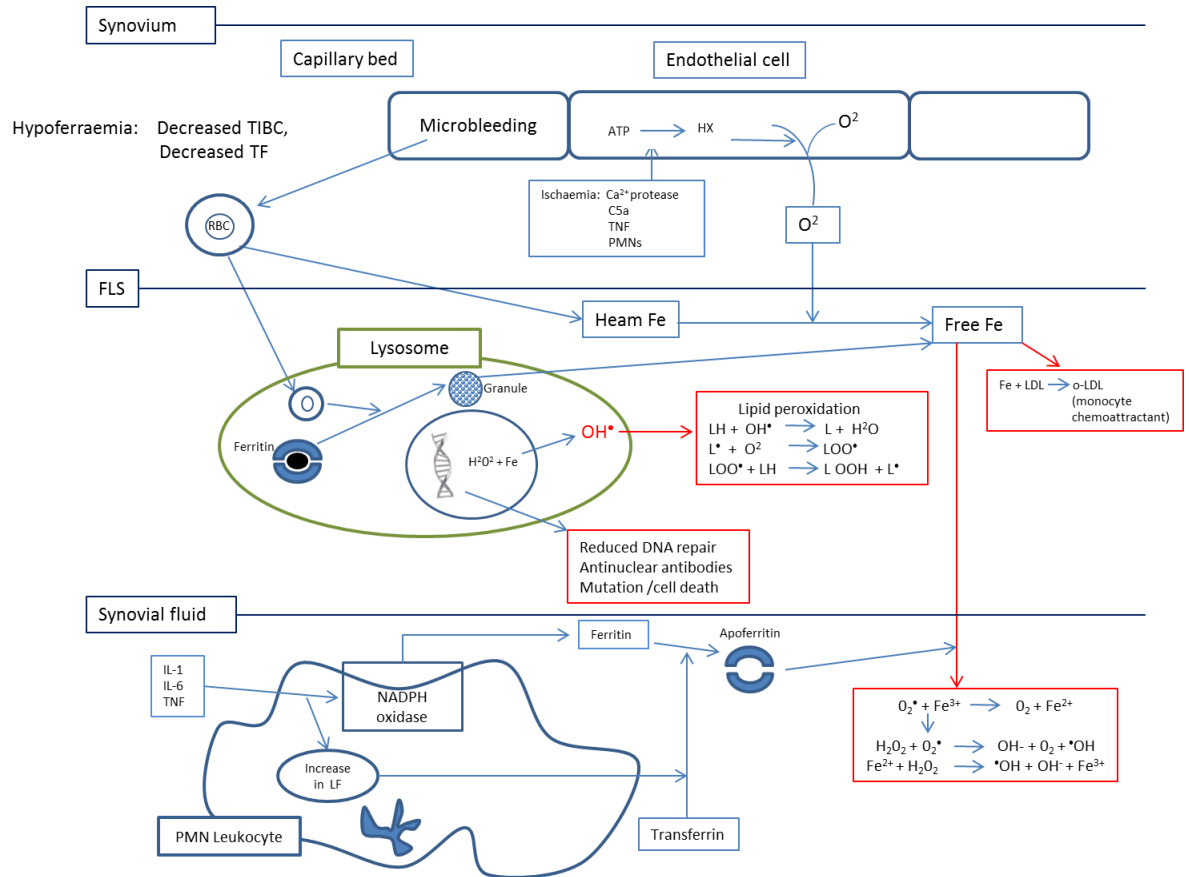


Figure 1.13 Schematic showing the source of iron and ROS and the cell damaging effects of ROS in the synovium. TIBC - total iron binding capacity; TF - transferrin; TNF - tumour necrosis factor; PMNs - polymorphonuclear leucocytes; IL-I - interleukin I; Fe – Iron; FLS – fibroblast like synoviosite; RBC - red blood cells; o-LDL - oxidised low density lipoprotein. ATP - Adenosine-tri-phosphate; H_2O_2 - hydrogen peroxide; NADPH – Nicotinamide adenine dinucleotide phosphate; H_2O – water; DNA – deoxyribo nucleic acid; (image adapted from Dabbagh *et al.*, 1993)

1.10.3 The involvement of Aluminium in oxidative stress.

Aluminium has been found throughout the body in the same way as the metals essential to our survival are, yet it has no known biological functions (Exley, 2003; Perez *et al.*, 2004). Aluminium toxicity is due to a range of mechanisms including inositol signalling, the adenylate cyclase cascade, peroxidation and iron uptake (reviewed by Abreo and Glass, 1993) to name only four. It has been shown to bind to both transferrin and lactoferrin (Congiu-Castellano *et al.*, 1997; Rondau *et al.*, 2006) and is an effective competitor for iron binding sites in biological systems (Mostaghi and Skillen, 1990).

1.11 Conclusion, hypothesis and objectives

In conclusion, it appears that a small number of chemokines such as CXCL12 and CXCL16 have been shown to be present at RA ECs where their presentation may play a vital role in leukocyte extravasation. However, a large number of chemokines in table 1.10 were not studied specifically to assess their EC presentation/expression in RA, and if established as present they were not necessarily assessed for degrees of up/down-regulation in RA or the chemotactic effects exerted. There is still therefore a need to gain further information on the presence/absence of such chemokines, particularly the CCL family chemokines which are less studied than the CXC chemokines in RA. Investigation of the role of chemokines currently not studied at RA ECs may add to our understanding of RA pathogenesis and potentially offer, as yet unexplored, therapeutic opportunities.

The hypothesis for this study is synovial ECs express and/or present selected CCL chemokines, and may facilitate the migration of leukocytes into the synovium. The main aims were to:

1. Elucidate which members of the CCL chemokine family are present at RA ECs and quantify the presence of the most highly represented in comparison to non-RA synovial ECs.
2. Establish if there are differences in the presence of these chemokines at RA blood and lymphatic ECs.
3. Investigate the potential for newly identified RA EC presented chemokines to be chemoactive within the RA joint.
4. Investigate if these RA EC presented chemokines are also present in a range of sera and SF from a range of arthritis types.

Chapter 2

Materials and methods

2.1 Ethical approvals

Full ethical approval for the study was granted by the Birmingham, East, North and Solihull Research Ethics Committee (study ID 11/WM/0035).

2.2 Data presentation and approach to statistical analysis

The data were checked for normal distribution at each stage of the analysis. Factors including n number, possible repetition number, numbers of field of view available for analyses and distribution of the data were factored into the methods finally used for both analysis and presentation. For example, where data were parametric mean \pm SEM and for multiple comparison ANOVA was used, or for single comparisons T-tests. For non-parametric data median and interquartile range and Kruskal-Wallis ANOVA was used to assess significant difference or Wilcoxon signed rank test for comparisons. Fisher's exact test was used to obtain P values following odds ratio calculations. Appropriate statistical analyses for each data set are described fully in the quantitation of results sections.

2.3 Materials and methods used in chapter 3

2.3.1 Synovial tissue samples

For all tissues used, RA (n=8) synovial tissue was obtained from patients (see table 2.1) who fulfilled the American College of Rheumatology (ACR) criteria for RA (see table 1.2) and were undergoing joint replacement surgery. Disease control (DC) tissue (n=6) was obtained by needle biopsy during outpatient exploratory procedures at the Robert Jones and Agnes Hunt Orthopaedic Hospital (see table 2.2). RA and non-RA tissue samples from the suprapatellar pouch and the medial gutter were stored in HBSS for transport to the laboratory where they were snap frozen in liquid nitrogen cooled in iso-pentane and then stored in liquid nitrogen until cryosectioning. 5-6 μ m thick serial cryostat sections of the tissue were cut then dried at room temperature before being stored at -80°C.

Table 2.1 showing patient details for the RA tissue samples used

Patient	Sex	Age	Age of Onset	Disease Duration (years)	RF (titre)	ESR*	CRP*	Medication
RA1	F	77	62	16	N/A	62	N/A	Piroxicam, Paracetamol, Omeprazole, Diclofenac, Methylprednisolone 40mg, Methotrexate 10mg, Pepsid (famotidine).
RA2	F	48	33	15	N/A	86	203	Diclofenac
RA3	M	54	37	17	RF+ (1/640)	N/A	8	Sulphasalazine, Methotrexate, Gold, Chloroquine
RA4	F	64	35	29	RF+	60	109	Leflunomide 10mg, Co-codamol, Omeprazole, Naproxen prednisolone 5mg, Lisinopril (Enalapril), Actonel (Risedronate), Calcichew D3 (calcium plus vitamin D)
RA5	F	72	N/A	>23	N/A	42	28	N/A
RA6	F	61	41	20	N/A	33-54	N/A	Sulphasalazine, Azathioprine, Methotrexate, Gold
RA7	F	83	48	35	RF+ (1/320)	74	111	Sulphasalazine, Oruvail (ketoprofen), Co-codamol, Dihydrocodeine
RA 8	F	74	39	35	N/A	38	20	Didronel (Etidronate), Methotrexate 2.5mg, Prednisolone 5mg, Co-dydramol

* Historical values taken during routine appointments prior to surgery. N/A – not available. Where patient medical notes do not list medication non-proprietary name, the non-proprietary name is entered in brackets.

Table 2.2 showing patient details for the non-RA tissue samples used

Patient	Sex	Age	Diagnosis
DC1	F	47	Tear to lateral meniscus
DC2	M	41	Patella tendon decompression.
DC3	F	45	Probable tear to lateral meniscus
DC4	M	45	Probable tear to right medial meniscus
DC5	F	41	Thickened medial plica, rest of meniscus normal.
DC6	M	41	Partial medial meniscectomy. Rest of meniscus normal.

DC – Day case. All samples were removed during exploratory arthroscopy. No patients had any signs of inflammatory illness. Patients were not taking medication other than over counter painkillers at time of procedure.

2.3.2 Immunofluorescent staining

2.3.2.1 von-Willebrand and Duffy Antigen Receptor for Chemokines (DARC) immunofluorescent staining to establish the endothelial cell marker for following experiments.

Six 5-6 μ m thick cryostat sections from two RA patients were air dried and fixed in ice-cold acetone for 10 minutes. Following rehydration in PBS (Invitrogen) for 5 minutes, sections were blocked using 2% BSA in PBS for 30 minutes, then washed for 5 minutes in PBS. Sections were incubated for one hour with the primary antibody of mouse monoclonal DARC or rabbit polyclonal VWF (R & D Systems) and with the secondary antibody, goat anti-mouse Alexa Fluor 594 IgG₁ (2 μ g/ml, Invitrogen) and goat anti-rabbit Alexa Fluor 488 IgG (2 μ g/ml, Invitrogen) respectively (see tables 2.3 and 2.4) for 45 minutes. Sections were washed for 5 minutes in PBS three times between each step and counterstained in 4',6-Diamidino-2-Phenylindole (DAPI) (at 1:5 with PBS from a 1:5000 working solution, Sigma Aldrich) before mounting using Hydromount (Fisher Scientific). Negative control slides were prepared using Isotype matched immunoglobulins instead of the primary antibodies. The control antibodies used in this work were: for mouse anti-human IgG₁ antibodies - mouse IgG₁ (Dako); for rabbit anti-human antibodies - rabbit IgG (Dako); for mouse anti-human IgG_{2b} antibodies - mouse IgG_{2b} (Dako); goat anti-human antibodies - goat IgG (R&D Systems); for mouse anti-human IgM - mouse IgM antibodies (Dako). All control antibodies were used at the same concentration as the primary antibody.

Table 2.3 showing the primary antibodies used for immunofluorescence

Primary Antibody	Description	Code	Company
CCL1	Mouse monoclonal IgM. Anti-human	LS-C4342	LifeSpan Biosciences
CCL2	Mouse monoclonal IgG _{2b} . Anti-human	MAB2791	R&D Systems
CCL3	Mouse monoclonal IgG ₁ . Anti-human	MAB270	R&D Systems
CCL4	Goat polyclonal IgG. Anti-human	AF-271- NA	R&D Systems
CCL5	Goat polyclonal IgG. Anti-human	AF-278- NA	R&D Systems
CCL7	Rabbit polyclonal IgG. Anti-human	LS-B930	LifeSpan Biosciences
CCL8	Goat polyclonal IgG. Anti-human	Sc-1307	Santa Cruz Biotechnology Inc.
CCL10	Rabbit polyclonal IgG. Anti-human	Orb13568	Biorbyte
CCL11	Mouse monoclonal IgG ₁ . Anti-human	MAB320	R&D Systems
CCL12	Rabbit polyclonal IgG. Anti-human	Orb13284	Biorbyte
CCL13	Goat polyclonal IgG. Anti-human	Sc-9655	Santa Cruz Biotechnology Inc.
CCL14	Mouse monoclonal IgG _{2b} . Anti-human	Sc-28388	Santa Cruz Biotechnology Inc.
CCL15	Rabbit IgG. Anti-human	Orb13287	Biorbyte
CCL16	Goat polyclonal IgG. Anti-human	AF802	R&D Systems
CCL17	Goat polyclonal IgG. Anti-human	AF364	R&D Systems
CCL18	Goat polyclonal IgG. Anti-human	Sc-9781	Santa Cruz Biotechnology Inc.

Table 2.3 continued

Primary Antibody	Description	Code	Company
CCL19	Mouse monoclonal IgG _{2b} . Anti-human	MAB361	R&D Systems
CCL20	Goat polyclonal IgG. Anti-human	AF360	R&D Systems
CCL21	Goat polyclonal IgG. Anti-human	AF366	R&D Systems
CCL22	Goat polyclonal IgG. Anti-human	Sc-12285	Santa Cruz Biotechnology Inc.
CCL23	Goat polyclonal IgG. Anti-human	Sc-12263	Santa Cruz Biotechnology Inc.
CCL24	Goat polyclonal IgG. Anti-human	AF343	R&D Systems
CCL25	Goat polyclonal IgG. Anti-human	Sc-12277	Santa Cruz Biotechnology Inc.
CCL26	Goat polyclonal IgG. Anti-human	AF653	R&D Systems
CCL27	Mouse monoclonal IgG ₁ . Anti-human	MAB376	R&D Systems
CCL28	Goat polyclonal IgG. Anti-human	Sc-27339	Santa Cruz Biotechnology Inc.
VWF	Rabbit polyclonal IgG ₁ . Anti-human	A0082	DakoCytomation,
VWF	Mouse monoclonal IgG ₁ . Anti-human	M0616	DakoCytomation
LYVE-1	Goat IgG. Anti-human	AF2089	R&D Systems
LYVE-1	Rabbit polyclonal IgG. Anti-human.	Sc-28190	Santa Cruz Biotechnology Inc.
DARC	Mouse monoclonal anti-human clone	NAM185-2C3	R&D Systems
CD68	Mouse anti-human C68	IR609/IS609	DakoCytomation

Table 2.3 shows the details of where the anti-human chemokine antibodies used in this work were obtained. DARC = Duffy Antigen Receptor for Chemokines

Table 2.4 showing the Secondary antibodies used for immunofluorescenc

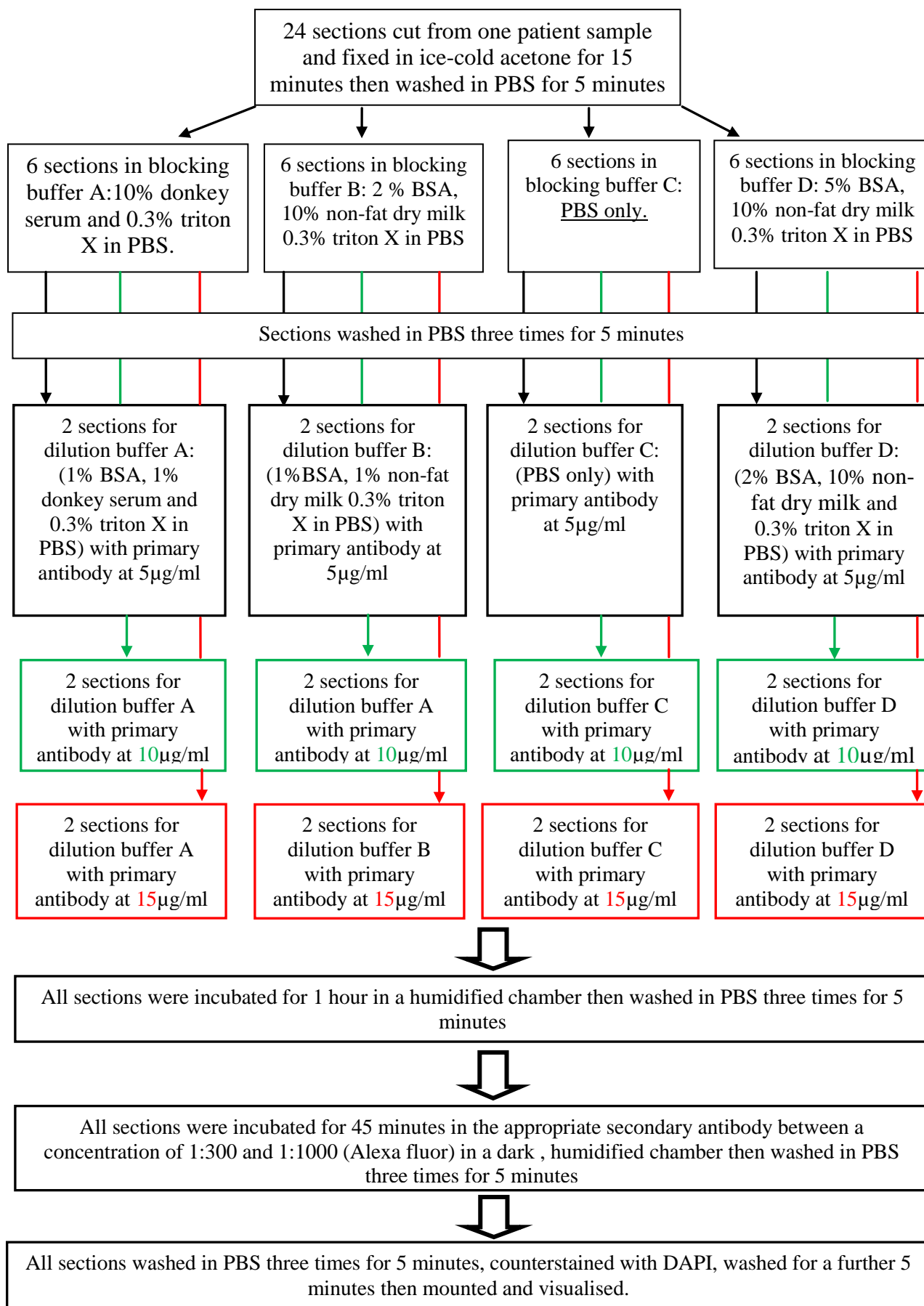
Secondary Antibody	Code
Goat anti-mouse Alexa Fluor IgG 488	A11001
Donkey anti-mouse Alexa Fluor IgG 488	A21202
Goat anti- rabbit Alexa Fluor IgG 488	A21042
Donkey anti-rabbit Alexa Fluor IgG 488	A21206
Goat anti-mouse Alexa Fluor IgG 594 IgG _{2b}	A21121
Goat anti-mouse Alexa Fluor IgG 594 IgG ₁	A21145
Goat anti- rabbit Alexa Fluor IgG 594	A11037
Donkey anti-mouse Alexa Fluor IgG 594	A21203
Donkey anti-rabbit Alexa Fluor IgG 594	A21207
Donkey anti-goat Alexa Fluor IgG 594	A11058

Table 2.4 shows the codes for where the secondary antibodies used in this work. All were from Molecular probes, Invitrogen.

2.3.2.2 Optimisation of immunofluorescent staining

For each antibody used in this project it was required to optimise the antibody concentration, the blocking buffer and the dilution buffers to reduce non-specific and background staining. Isotype matched controls were utilised throughout and the procedure was repeated twice with 2 different samples to minimise the number of sections used. The basic guide followed for optimisation of the different primary antibodies is outlined in figure 2.1. The final blocking and dilution buffers for each antibody are listed as A, B, C or D in figure 2.1, table 2.5 and table 2.6. The control antibodies used in this work were as stated in section 2.3.2.1.

Figure 2.1 Schematic showing initial optimisation carried out for primary antibodies



If the combinations in figure 2.1 did not produce viable images for analysis the procedure was repeated with the blocking and dilution buffers interchanged (such as blocking buffer A with dilution buffer B for example). Further optimisation at different antibody concentrations was performed as required. This was done until a combination which provided optimal primary antibody staining with minimal background staining was identified.

2.3.2.3 Double immunofluorescent staining of synovial tissue using for VWF and CCL family antibodies.

Six 5-6 μ m thick cryostat sections from 8 RA patients were air dried and fixed in ice-cold acetone for 10 minutes. Following rehydration in PBS (Invitrogen) for 5 minutes the sections were blocked using blocking buffer A, B, C or D (as in table 2.5) for 30 minutes, then washed for 5 minutes in PBS. Sections were incubated for one hour with the fully optimised primary antibody pairings shown in table 2.5 and for 45 minutes in the corresponding optimised secondary antibodies also shown in table 2.5. A full schematic is shown in figure 2.2. Given the fact that each of the 27 anti-human CCL antibodies tested with VWF in RA tissue generates the need to individually list 2 different buffer solutions and a total of 4 different antibodies (each of two primary antibodies and two secondary antibodies) the author decided to leave them properly categorised in a table separate to this text to prevent confusion. For full details please refer to table 2.5. The control antibodies used in this work were as stated in section 2.3.2.1.

2.3.2.4 Double immunofluorescent staining for lymphatic endothelial vessels and CCL chemokines in RA and non-RA synovial tissue.

Lymphatic EC staining was performed to assess if there were differences in CCL family chemokine presentation on blood and lymphatic endothelial cells. As VWF is a pan-endothelial marker and will therefore stain both blood and lymphatic ECs, the lymphatic specific EC marker LYVE-1 was optimised as described in figure 2.1 and double staining performed as set out in figure 2.2 with goat anti-human LYVE-1 antibody or rabbit anti-human antibody (dependant on the anti-human CCL antibody being used, see table 2.5) in place of the anti-human VWF antibody.

As with section 2.3.2.1 the numbers of solutions used made listing each solution in a table the most feasible option. As such, please refer to table 2.5 and 2.6 for the full list of anti-human antibodies, their concentration and the blocking and dilution buffers used (following the optimisation procedure described in figure 2.1) and each of their working concentrations. A full schematic is shown in figure 2.2. The control antibodies used in this work were as stated in section 2.3.2.1

Table 2.5 Showing solutions used for immunofluorescence (continued on next 2 pages)

Chemokine under investigation	RA/DC Tissue	Blocking buffer	*Dilution buffer	Primary antibodies and concentrations used	Secondary antibodies and concentrations used
CCL1	RA	A	A	Rabbit anti-human VWF, 3µg/ml Mouse anti-human CCL1, 2.5µg/ml	Donkey anti-rabbit 594, 1µg/ml Goat anti-mouse 488 IgM, 3.3µg/ml
CCL2	RA	C	C	Rabbit anti-human VWF, 3µg/ml Mouse anti-human CCL2, 10µg/ml	Donkey anti-rabbit 488 IgG, 3.3µg/ml Goat anti-mouse 594 IgG _{2b} , 6.6µg/ml
CCL3	RA	C	C	Rabbit anti-human VWF, 3µg/ml Mouse anti-human CCL3, 10µg/ml	Goat anti-rabbit 488, 10µg/ml Goat anti-mouse 594 IgG ₁ , 10µg/ml
CCL4	RA/DC	D	B	Rabbit anti-human VWF, 3µg/ml Goat anti-human CCL4, 10µg/ml	Donkey anti-rabbit 488 IgG, 3.3µg/ml Donkey anti-goat 594, 6.6µg/ml
CCL5	RA	D	B	Rabbit anti-human VWF, 3µg/ml Goat anti-human CCL5, 15µg/ml	Donkey anti-rabbit 488 IgG, 3.3µg/ml Donkey anti-goat 594, 6.6µg/ml
CCL7	RA/DC	A	A	Mouse anti-human VWF, 4µg/ml Rabbit anti-human CCL7, 2.5µg/ml	Donkey anti-mouse 594 IgG ₁ , 3.3µg/ml Donkey anti-rabbit 488 IgG, 3.3µg/ml
	RA/DC	A	A	Rabbit anti-human CCL7, 2.5µg/ml Goat anti-human LYVE-1, 7.5µg/ml	Donkey anti-rabbit 488 IgG, 3.3µg/ml Donkey anti-goat 594, 3.3µg/ml
CCL8	RA/DC	A	A	Rabbit anti-human VWF, 3µg/ml Goat anti-human CCL8, 2µg/ml	Donkey anti-goat 594, 6.6µg/ml Donkey anti-rabbit 488 IgG, 3.3µg/ml
CCL10	RA	A	A	Mouse anti-human VWF, 4µg/ml Rabbit anti-human CCL10, 4µg/ml	Goat anti-mouse 488, 3.3µg/ml Donkey anti-rabbit 594, 6.6µg/ml
CCL11	RA	B	B	Rabbit anti-human VWF, 3µg/ml Mouse anti-human CCL11, 15µg/ml	Donkey anti-rabbit 488 IgG, 3.3µg/ml Donkey anti-mouse 594 IgG ₁ , 6.6µg/ml
CCL12	RA	A	A	Mouse anti-human VWF, 4µg/ml Rabbit anti-human CCL12, 2µg/ml	Goat anti-mouse 488, 3.3µg/ml Donkey anti-rabbit 594, 6.6µg/ml

Table 2.5 continued

Chemokine under investigation	RA/DC Tissue	Blocking buffer	*Dilution buffer	Primary antibodies and concentrations used	Secondary antibodies and concentrations used
CCL13	RA	A	A	Rabbit anti-human VWF, 3µg/ml Goat anti-human CCL13, 4µg/ml	Donkey anti-goat 594, 6.6µg/ml Donkey anti-rabbit 488 IgG, 3.3µg/ml
CCL14	RA/DC	C	C	Rabbit anti-human VWF, 3µg/ml Mouse anti-human CCL14, 2µg/ml	Donkey anti-rabbit 488 IgG, 3.3µg/ml Goat anti-mouse 594, 2.5 µg/ml
	RA/DC	C	C	Mouse anti-human CCL14, 2µg/ml Goat anti-human LYVE-1, 15µg/ml	Donkey anti-mouse 594, 6.6µg/ml Donkey anti-rabbit 488 IgG, 3.3µg/ml
CCL15	RA	A	A	Mouse anti-human VWF, 4µg/ml Rabbit anti-human CCL15, 4µg/ml	Goat anti-mouse 488, 3.3µg/ml Donkey anti-rabbit 594, 6.6µg/ml
CCL16	RA/DC	C	C	Rabbit anti-human VWF, 3µg/ml Goat anti-human CCL16, 15µg/ml	Donkey anti-goat 488, 3.3µg/ml Donkey anti-rabbit 594, 6.6µg/ml
	RA/DC	C	C	Goat anti-human CCL16, 15µg/ml Rabbit anti-human LYVE-1, 4µg/ml	Donkey anti-goat 488, 3.3µg/ml Donkey anti-rabbit 594, 3.3µg/ml
CCL17	RA	B	B	Rabbit anti-human VWF, 3µg/ml Goat anti-human CCL17, 10µg/ml	Donkey anti-rabbit 488 IgG, 3.3µg/ml Donkey anti-goat 594, 6.6µg/ml
CCL18	RA	A	A	Rabbit anti-human VWF, 3µg/ml Goat anti-human CCL18, 4µg/ml	Donkey anti-rabbit 488 IgG, 3.3µg/ml Donkey anti-goat 594, 6.6µg/ml
CCL19	RA/DC	C	C	Rabbit anti-human VWF, 3µg/ml Mouse anti-human CCL19, 20µg/ml	Donkey anti-rabbit 488 IgG, 3.3µg/ml Goat anti-mouse 594, 6.6µg/ml
CCL20	RA	B	B	Rabbit anti-human VWF, 3µg/ml Goat anti-human CCL20, 100µg/ml	Donkey anti-rabbit 488 IgG, 3.3µg/ml Donkey anti-goat 594, 6.6µg/ml
CCL21	RA	A	A	Rabbit anti-human VWF, 3µg/ml Goat anti-human CCL21, 15µg/ml	Donkey anti-rabbit 488 IgG, 3.3µg/ml Donkey anti-goat 594, 6.6µg/ml

Table 2.5 continued

Chemokine under investigation	RA/DC Tissue	Blocking buffer	*Dilution buffer	Primary antibodies and concentrations used	Secondary antibodies and concentrations used
CCL22	RA/DC	A	A	Rabbit anti-human VWF, 3µg/ml Goat anti-human CCL22, 4µg/ml	Donkey anti-rabbit 488 IgG, 3.3µg/ml Donkey anti-goat 594, 6.6µg/ml
	RA/DC	A	A	Goat anti-human CCL22, 4µg/ml Rabbit anti-human LYVE-1, 4µg/ml	Donkey anti-goat 594 IgG, 3.3µg/ml Donkey anti-rabbit 488, 6.6µg/ml
CCL23	RA	A	A	Rabbit anti-human VWF, 3µg/ml Goat anti-human CCL23, 4µg/ml	Donkey anti-rabbit 488 IgG, 3.3µg/ml Donkey anti-goat 594, 6.6µg/ml
CCL24	RA	B	B	Rabbit anti-human VWF, 3µg/ml Goat anti-human CCL24, 15µg/ml	Donkey anti-rabbit 488 IgG, 3.3µg/ml Donkey anti-goat 594, 6.6µg/ml
CCL25	RA	A	A	Rabbit anti-human VWF, 3µg/ml Goat anti-human CCL25, 2µg/ml	Donkey anti-rabbit 488 IgG, 3.3µg/ml Donkey anti-goat 594, 6.6µg/ml
CCL26	RA	A	A	Rabbit anti-human VWF, 3µg/ml Goat anti-human CCL26, 15µg/ml	Donkey anti-rabbit 488 IgG, 3.3µg/ml Donkey anti-goat 594, 6.6µg/ml
CCL27	RA	A	A	Rabbit anti-human VWF, 3µg/ml Mouse anti-human CCL27, 20µg/ml	Donkey anti-rabbit 488 IgG, 2.8µg/ml Goat anti-mouse 594, 5µg/ml
CCL28	RA	A	A	Rabbit anti-human VWF, 3µg/ml Goat anti-human CCL28, 4µg/ml	Donkey anti-rabbit 488 IgG, 3.3µg/ml Donkey anti-goat 594, 6.6µg/ml

This table shows the primary and secondary antibody solutions used following the optimisation procedures.

*Dilution buffer - for secondary antibody solutions, 10% human serum was also included. All of the above experiments were carried out with isotype matched negative controls. The details of the buffers used were:

Blocking buffer A – 10% donkey serum and 0.3% triton X in PBS.

Blocking buffer B – 2% BSA, 10% non-fat dry milk 0.3% triton X in PBS.

Blocking buffer C – PBS only.

Blocking buffer D – 5% BSA, 10% non-fat dry milk 0.3% triton X in PBS

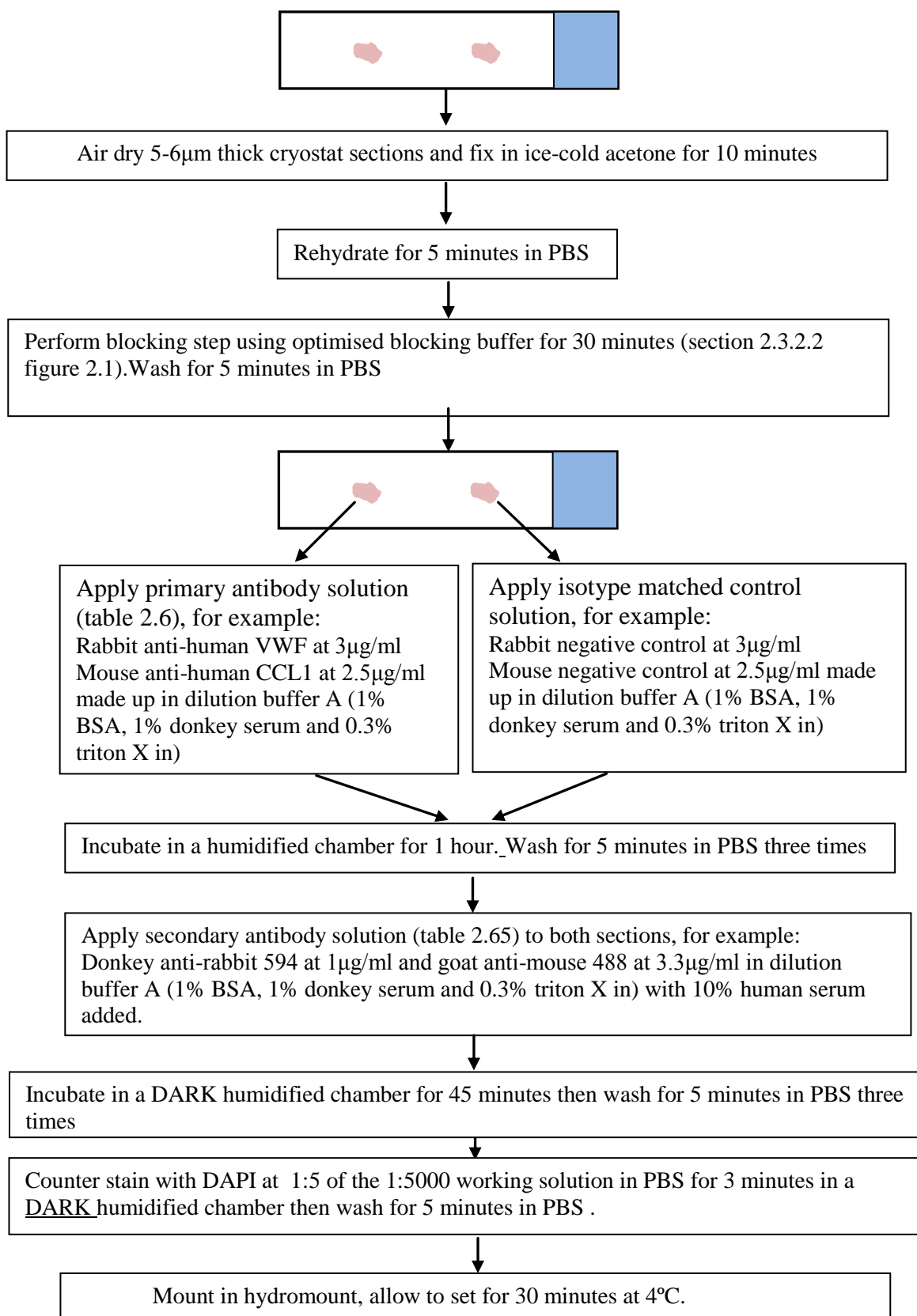
Dilution buffer A – 1% BSA, 1% donkey serum and 0.3% triton X in PBS

Dilution buffer B – 1% BSA, 1% non-fat dry milk 0.3% triton X in PBS

Dilution buffer C – PBS only

Dilution buffer D – 2% BSA, 10% non-fat dry milk 0.3% triton X in PBS

Figure 2.2 Schematic showing double immunofluorescent staining process.



Negative control slides were prepared using isotype matched IgGs instead of the primary antibody. For a full list of the antibodies and concentrations used refer to table 2.5 and 2.6

Table 2.6 showing solutions for the Duffy antigen receptor for chemokines (DARC) and VWF and CD68 with LYVE-1 staining

Antibody	Tissue	Primary antibody solution and Concentration used	Secondary antibody solution and concentration used
DARC and VWF	RA	PBS Rabbit anti-human VWF, 4 μ g/ml Mouse anti-human CCL24, 15 μ g/ml	PBS with 10% human serum Goat anti-rabbit 488 IgG, 3.3 μ g/ml Goat anti-goat 594, 6.6 μ g/ml
CD68 and LYVE-1	RA	PBS Rabbit anti-human VWF, 3 μ g/ml Goat anti-human LYVE-1, 2 μ g/ml	PBS with 10% human serum Donkey anti-rabbit 488 IgG, 3.3 μ g/ml Donkey anti-goat 594, 6.6 μ g/ml

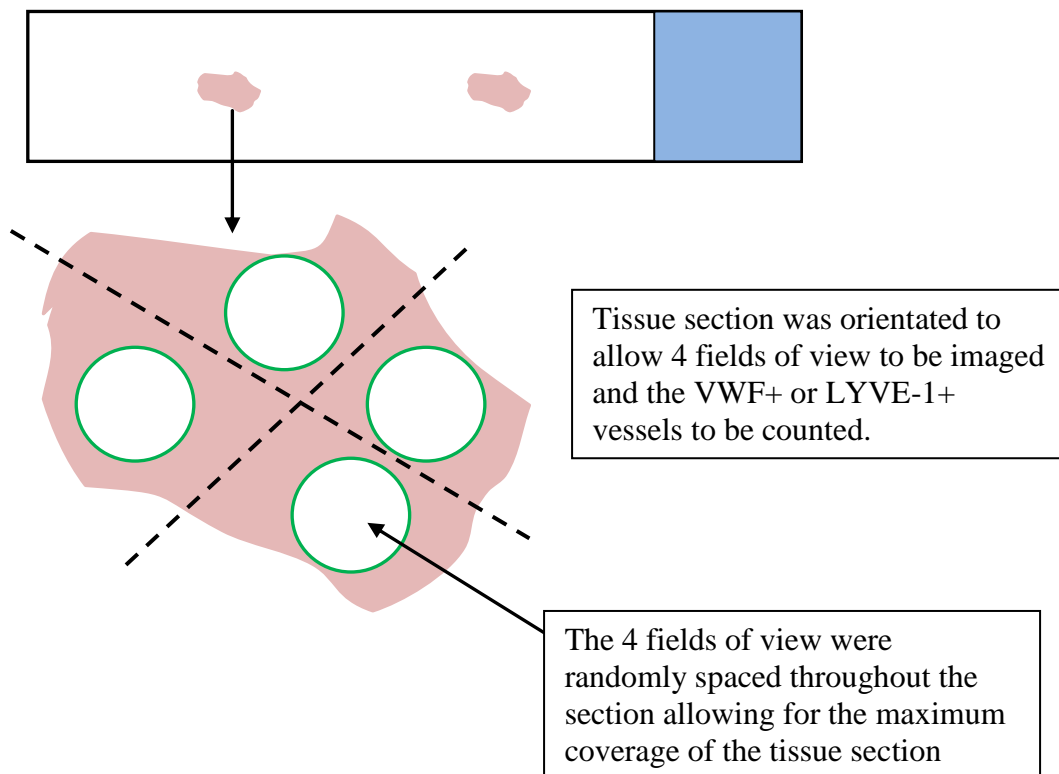
Negative control slides were prepared using isotype matched IgGs instead of the primary antibodies. For a full list of the antibodies and concentrations used refer to table 2.5.

2.3.2.5 Quantitation of immunofluorescence

For accurate quantitation a range of parameters were taken into consideration including the number of patient samples used, the number of fields of view and the number of blood vessels. The first 15 blood vessels positive VWF in 4 fields of view per section (figure 2.3) were counted (magnification X20), any of those vessels also positive for the chemokine under investigation were then counted. The mean number of vessels was then calculated as a percentage of VWF positive vessels also stained with the chemokine. Standard errors were also calculated for each result.

Immunofluorescence was visualised on a light microscope (Olympus IX51) and analysis was performed using CellF software (Olympus UK Ltd, Southend-on-Sea, UK). Intensity of staining was done by recording the intensity of a random point per cell ($n = 12$ cells) in three separate images for a single experiment. All experiments were carried out in triplicate giving 108 points ($n=3$).

Figure 2.3 Diagram showing field of view layout for immunofluorescent quantification.



The first 15 blood vessels positive for von-Willebrand Factor (VWF) or LYVE-1 in each of the 4 fields of view per section were counted (magnification X20). Any of those vessels also positive for the chemokine under investigation were then counted. The mean number of vessels was then calculated as a percentage of VWF+ or LYVE-1+ vessels also stained with the chemokine. Standard errors were also calculated for each result. It should be noted that given the nature of the tissue samples available the sections were not of equal size and so the total coverage of the 4 fields of view per sections ranged from approximately 40-90% of the section as a whole.

2.3.3 Microwave Synovial tissue digestion for Transverse Heated-Graphite Furnace Atomic Absorption Spectrometry (T H-GFAAS)

Digest tubes, lids and plugs were rinsed x2 in ultrapure water, left immersed in ultrapure water overnight, then left to dry at 37°C. This process reduced the chances of Fe and Al contamination of the tubes. The tissue samples were removed from the freezer and left to defrost without removing the cryotube lid. Once fully dry the digest tubes were labelled and their individual weights recorded. The defrosted tissue samples were removed from the cryotubes and placed into the dried and weighed digest tubes. Following re-weighing to measure the wet weight of the samples they were placed back into the incubator (at 37°C) with the lids loosely attached and the plugs absent and left until the tissue samples were totally dry (~48 hours).

Following tissue drying the samples were again weighed to measure the tissue final dry mass. Following this 1ml of concentrated nitric acid was added, followed by 1ml of hydrogen peroxide to each tube (30% weight to volume solution). The plug and cap were put on the tube and it was placed in the digester carousel for 1.5 hours. Control tubes of acid and hydrogen peroxide only were also made. Each tube was completed before moving onto the next to standardise all times the tissue spent in the reagents.

Following digestion the tubes were allowed to cool before 3ml of ultrapure water was added to the first tube and very gently mixed. The solution was then transferred to a 5ml bijou and stored at room temperature until used.

2.3.3.1 TH-GFAAS determination of Iron and Aluminium content

Total iron (Fe) and aluminium (Al) were measured as described by House *et al.*, (2012) using an Analyst 600 atomic absorption spectrometer with a transversely heated graphite atomizer (THGA) and longitudinal Zeeman-effect background corrector and an AS-800

autosampler with WinLab32 software (Perkin Elmer, UK). Standard THGA pyrolytically-coated graphite tubes with integrated L'Vov platform (Perkin Elmer, UK) were used. The Zeeman background-corrected peak area of the atomic absorption signal was used for the determinations.

The samples stored from 2.3.3 were diluted 20 fold by adding 9.5ml of ultrapure water to 0.5ml of the sample in a volumetric flask (pre-washed twice with ultrapure water) giving a final acid concentration of 1%. This solution was gently mixed before 2ml of it poured into a 2ml sample cup which was then placed into the autosampler (Perkin Elmer Precisely A5 500 autosampler) of the spectrometer (Atomic Absorption Spectrometer AAnalyst 600) and the position of each sample recorded.

The TH-GFAAS was calibrated by automated serial dilution of 40, 60 and 100 mg L⁻¹ solutions of Fe and 10, 20, 40, and 60 mg L⁻¹ solutions of Al with 1% HNO₃.

Iron and aluminium content was expressed as µg/ml.

2.4 Materials and methods used in chapter 4

2.4.1 Cell culture, Growth and freezing

2.4.1.1 Culturing human bone marrow endothelial cells (HBMECs)

Medium was prepared as follows: 5ml of fungizone (amphotericin B at 250 μ g/ml) (Lonza, Wokingham, UK): 5ml penicillin (5000 I.U./ml), streptomycin (5000 μ g/ml) (Lonza) and 50ml heat inactivated foetal bovine serum (FBS; Invitrogen, Paisley, UK) were mixed with 500ml DMEM-F12 medium (1:1 mixture with 15mM Hepes, 0.365g/L L-glutamine and 3.151g/L glucose) (Lonza, Wokingham, UK) and warmed to 37°C (herein this solution is known as DMEM-F12 medium solution). Once warmed 12ml of the culture medium was added to two T75 Iwaki tissue culture flasks (Scientific Laboratory Supplies, Nottingham, UK). The cells were removed from liquid nitrogen and defrosted at room temperature before adding to 2ml of the DMEM-F12 medium solution and gently mixed. 1ml of the cell suspension was added to each of the flasks and placed in an incubator at 37°C. All of the above was carried out in aseptic conditions. Cells were fed with the same DMEM-F12 medium solution and passaged at 80-90% confluent.

Fungizone, Penicillin and FBS were stored at -20°C prior to use and the culture medium was stored at 4°C. 5% CO₂ was present in the incubators during cell cultures.

2.4.1.2 Passaging HBMECs

Cells were passaged at 80-90% confluence. 5ml of trypsin-EDTA (200mg/L versene, 170000 u trypsin/L) per flask were warmed to 37°C along with 10ml PBS per T75 culture flask and the DMEM-F12 medium solution. The old medium was removed from the flasks and the cells were washed twice with 10 ml of the warmed PBS. 5ml trypsin- EDTA was added to each flask and the flasks were returned to the incubator for approximately 3 minutes until the HBMECs were lifting from the surface of the flask. The trypsin-EDTA was neutralised by adding 15ml of the DMEM-F12 medium solution (3 times the volume of trypsin used). The resulting cell suspension was centrifuged at 1700rcf for 6 minutes. After centrifugation the supernatant was poured off and the pellet was resuspended in 2-3 ml of fresh medium. The cells were then counted and the required number of cells transferred to new flasks (or wells for transmigration assays) containing the required volume of fresh medium. All of the above was carried out in aseptic conditions using sterile pipettes.

2.4.1.3 Culturing HDLECs.

EBM-2 medium, with the microvascular cell bullet kit (Lonza) added, was used for HDLEC culture and growth (herein referred to as EBM-2-MV medium). 5ml of the culture medium (warmed to 37°C) was added to two T25 Iwaki tissue culture flasks (Scientific Laboratory Supplies, Nottingham, UK). HDLECs were removed from liquid nitrogen and defrosted in a water bath at 37°C for no more than 2 minutes as per the Lonza protocol. Once defrosted the cells were added to 2ml of EBM-2-MV and very gently mixed to separate any clumps of cells. 1ml of the cell suspension was added to each of the flasks and placed in an incubator at 37°C. Cells were fed with the same EBM-2-MV medium

solution and passaged at 75-80% confluence. 5% CO₂ was present in the incubators during cell cultures.

2.4.1.4 Passaging HDLECs,

Cells were passaged at 75-80% confluence. 2ml of trypsin-EDTA (200mg/L versene, 170000 u trypsin/L) per flask and the EBM-2-MV medium was warmed to 37°C. The cells were washed in 5ml of PBS (X 2) and 2ml trypsin-EDTA was added to each flask for approximately 3 minutes. Once cells had lifted, 15ml of the EBM-2-MV (3x the volume of trypsin used) was added to each of the flasks and the solution was then transferred to 50ml tube(s) (Scientific Laboratory Supplies) and centrifuged at 1100rcf for 3 minutes. After centrifugation the supernatant was poured off and the pellet was resuspended in 2-3 ml of fresh medium. The cells were then counted and the required number of cells transferred to new flasks (or wells for transmigration assays) containing the required volume of fresh medium

2.4.1.5 Freezing cells in liquid nitrogen

Cells at 75-80% confluence were detached from the tissue culture flask(s) by removing medium, washing twice with PBS and adding 5ml of trypsin-EDTA. The flasks were incubated at 37°C for approximately 3 minutes until the cells were lifting. The trypsin-EDTA was neutralised by adding 3 times the volume of trypsin-EDTA to the flasks. The resulting cell suspension was then centrifuged at 1700rcf for 6 minutes at room temperature (or at 1100rcf for 3 minutes for HDLECs). Following this the cell pellet was resuspended in filtered FBS containing 10% dimethyl sulfoxide (DMSO; Sigma-Aldrich Company Ltd, Dorset, UK) at a density of 1×10^6 cells/ml. Cells were dispensed into a pre-cooled Nalgene cryo 1°C freezing container (Fischer Scientific LTD, Leicestershire, UK)

containing 250ml isopentane alcohol (IPA; Fischer Scientific) prior to overnight storage at -80°C before transfer to liquid nitrogen for long term storage.

2.4.1.6 Endothelial cell lines used in this study

The cell line HBMECs were donated by BB Weksler (Weill-Cornell University, New York); this immortalised, microvascular endothelial cell line is involved in haematopoietic progenitor cell homing to the bone marrow and their differentiation and proliferation. The transformed cell line needed significantly less serum concentrations and did not require additional growth factors for proliferation. These cells were used as a model for synovial endothelial cells, which were not directly available.

HDLECs were supplied by PromoCell (Sickingenstraße, Heidelberg, Germany) number C-12217. The HDLECs were used as a model for synovial lymphatic endothelial cells (LECs) which were not commercially available at the time of the study.

2.4.1.7 Cell viability

To assess the numbers of live cells for use in experiments Trypan blue solution, 0.4% (Sigma-Aldrich) was used during cell counting. Cells were removed from flasks and pelleted as described in section 2.4.1.2 and 2.4.1.4. The cells were resuspended in approximately 3ml of growth medium and 10µl of the cell suspension was added to 10µl of Trypan blue solution. 10µl of this was then placed onto a haemocytometer and cells were visualised using phase-contrast microscopy at x100 magnification. Densely stained cells were designated dead/dying and not counted.

2.4.1.8 Seeding and stimulating inflammatory conditions in ECs to assess ICAM staining

For HBMECs 50,000 cells per well in 250 μ l of DMEM-F12 medium solution were placed in each well of a chamber slide (Fisher Scientific) and were returned to the incubator at 37°C (with 5% CO₂) for 24 hours until the cells were approximately 60% confluent.

The medium was removed from the wells and control wells had 250 μ l of DMEM-F12 medium solution added to them. The wells being activated had either: A, 250 μ l total of TNF- α at 100ng/ml in DMEM-F12 medium solution; B, 250 μ l total of TNF- α at 100ng/ml and IFN- γ at 100ng/ml in DMEM-F12 medium solution added to each well dependent upon the specific experiment being performed. 100ng/ml of TNF- α was found to be optimal for activating HBMECs.

For HDLECs 100,000 cells per well in 250 μ l of EBM-2-MV medium were placed in each well of a chamber slide) and the chamber slides were returned to the incubator at 37°C (with 5% CO₂) for 24 hours until approximately 60% confluent. The medium was removed from the wells and control wells had 250 μ l of EBM-2-MV medium added to them. The wells being activated had either: A, 250 μ l total of TNF- α at 100ng/ml in EBM-2-MV medium; B, 250 μ l total of TNF- α at 100ng/ml and IFN- γ at 100ng/ml in EBM-2-MV medium added to each well dependent upon the specific experiment being performed. 100ng/ml of TNF- α and IFN- γ was found to be optimal for activating HDLECs.

Optomisation for transmigration analysis was performed in 24 well plates (see figure 2.4)

For both HBMECs and HDLECs the chamber slides were then returned to the incubator for between 1 and 24 hours depending on the experiment being performed.

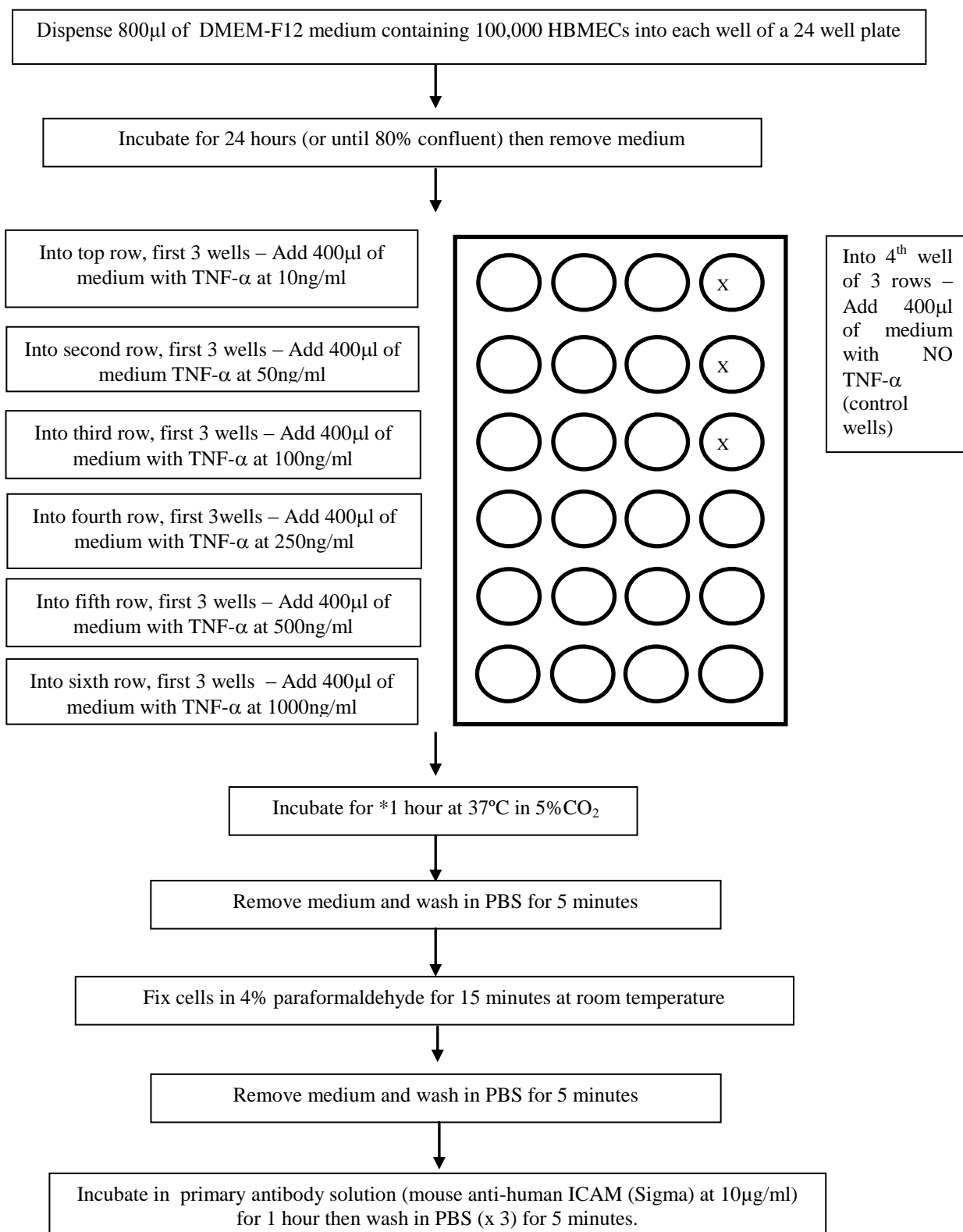
2.4.1.9 Optimisation of simulated inflammatory conditions using TNF- α and/or IFN- γ for transmigration analysis (figure 2.4)

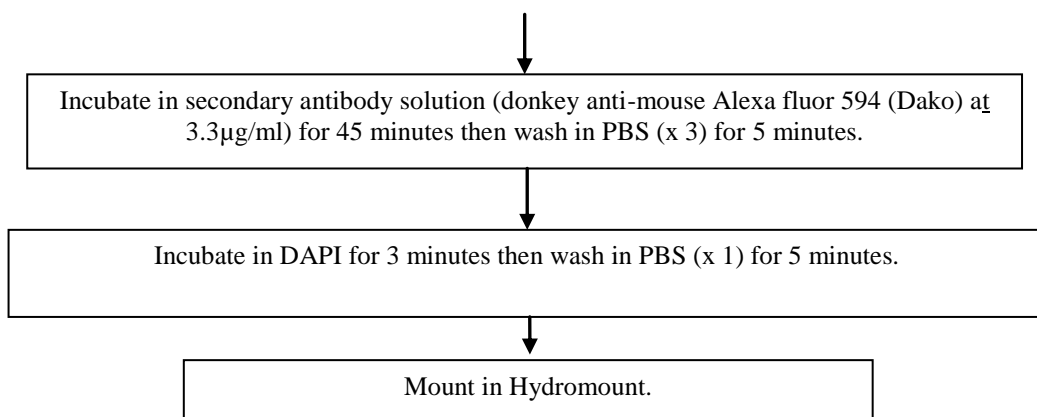
It was required to optimise the concentration to be used for the HBMECs and HDLECs prior to transmigration analysis. This was achieved by activating a monolayer of the cells as described in section 2.4.1.8 and performing immunofluorescent staining to assess the degree of ICAM staining. The solution which provided the greatest increase in ICAM intensity was used for transmigration analysis as the model for inflammation. Control wells containing no TNF- α and/or IFN- γ were also assessed.

For optimisation for transmigration analysis (figure 2.4) 800 μ l of DMEM-F12 medium containing 100,000 HBMECs was dispensed into each well of a 24 well plate (Scientific Laboratory Supplies). Once the ECs were confluent the medium was replaced with fresh medium containing 400 μ l total of TNF- α and/or IFN- γ at 10ng/ml, 50ng/ml, 100ng/ml, 250ng/ml, 500ng/ml and 1000ng/ml (see figure 2.4). Experiments were carried out in triplicate. The experiments were repeated whereby the cells were incubated in the activation solution for 1, 2, 4, 8, 16 and 24 hours prior to fixing in 4% paraformaldehyde and staining with the primary antibody, mouse anti-human ICAM (Sigma) at 10 μ g/ml in PBS for 1 hour. This was followed by 3x 5 minute washes in PBS, then an incubation of 45 minutes in the secondary antibody, donkey anti-mouse Alexa Fluor 594 (Dako) at 3.3 μ g/ml. Once washed (3x 5 minutes PBS) then counterstained using DAPI at 1:5 with PBS (from a 1:5000 working stock, Sigma) for three minutes the cells were mounted in Hydromount.

Solutions ascertained as optimal for activation and for ICAM staining are shown in table 2.7 on page 97.

Figure 2.4 Schematic showing optimisation process for the activation solutions; TNF- α ; IFN- γ and TNF- α + IFN- γ prior to transmigration analysis using HBMECs and HDLECs





*This experiment was repeated 6 times as shown above, but the activation solution was left on for 1, 2, 4, 6, 8, 18 and 24 hours respectively prior to adding the primary antibody.

The experiment was repeated in full using IFN- γ in place of TNF- α , and repeated again using both TNF- α + IFN- γ . The process was performed for both HBMECs and HDLECs.

Solutions ascertained as optimal are shown in table 2.7.

2.4.2 Protein synthesis arrest

Cells were cultured and optimised as described in section 2.4.1.1 and 2.4.1.9 (also see figure 2.4). Following optimisation cells were cultured in the activation solution with 10µg/ml cycloheximide added as a protein synthesis inhibitor (Sigma-Aldrich) for 0 (base line), 2, 3, 4, 5 and 6 hours. Following protein synthesis arrest the cells were fixed in ice cold 1:1 methanol: acetone then blocked for 15 minutes in PBS with 10% donkey serum and 2% BSA. After this cells were stained using rabbit anti-human CCL7 at 2.5µg/ml (Lifespan Biosciences); mouse anti-human CCL14 at 2µg/ml (Santa Cruz); goat anti-human CCL16 at 15µg/ml (R&D Systems) or goat anti-human CCL22 at 4µg/ml (Santa Cruz) for one hour. As background staining was less evident than on human tissue sections all solutions were made up in 1% BSA, 1% donkey serum and 0.3% triton X in PBS. Following washing three times in PBS for 5 minutes the cells were incubated in the secondary antibody solution for 45 minutes (in a darkened humidified chamber). The secondary antibody solutions were donkey anti-mouse Alexa Fluor 594, donkey anti-rabbit Alexa Fluor 594, and donkey anti-goat Alexa Fluor 594 respectively, all at 6.6µg/ml (all from Invitrogen) and made up in 1% BSA, 1% donkey serum and 0.3% triton X in PBS. Following washing (as above) cells were counterstained using DAPI at 1:5 with PBS (from a 1:5000 working stock, Sigma) before mounting using Hydromount (Fisher Scientific). The control antibodies used in this work were as stated in section 2.3.2.1.

These experiments were performed to assess if each of the chemokines were present following the activation of cultured HBMECs giving a stimulated inflammatory environment. This would indicate that the chemokines may be generated by the ECs themselves in response to inflammatory conditions rather than present in tissue due to other cellular sources. The addition of cycloheximide would indicate if the chemokines were present as pre-existing proteins and released in response to inflammatory conditions

(as the levels in the cells would decrease); or if they were generated in an ongoing manner, and thus were actively produced by the HBMECs themselves by protein synthesis.

Table 2.7 Solutions for TNF- α , IFN- γ , (and combination) activation and staining of cultured cell monolayers.

Solution	Cell Type	Activation solution	Primary antibody solution and concentration	Secondary antibody solution And concentration
TNF-α	HBMEC HDLEC	Human TNF- α (Peprotech) at 100ng/ml in appropriate medium	Dilution buffer A Mouse anti human ICAM, 10 μ g/ml (Peprotech)	Dilution buffer A with 10% human serum Donkey anti-mouse 594 IgG, 2.5 μ g/ml
IFN-γ	HBMEC HDLEC	Human IFN- γ (Peprotech) at 100ng/ml in appropriate medium	Dilution buffer A Mouse anti human ICAM, 10 μ g/ml	Dilution buffer A with 10% human serum Donkey anti-mouse 594 IgG, 2.5 μ g/ml
Combination	HBMEC HDLEC	Human TNF- α at 100ng/ml and IFN- γ at 100ng/ml in appropriate medium	Dilution buffer A Mouse anti human ICAM, 10 μ g/ml	Dilution buffer A with 10% human serum Donkey anti-mouse 594 IgG, 2.5 μ g/ml

Dilution buffer A – 1% BSA, 1% donkey serum and 0.3% triton X in PBS. Blocking Buffer – 2% BSA and 0.3% triton X in PBS.

All of the above experiments were carried out with isotype matched negative controls.

Where cell surface only staining was carried out Triton X was not used in the primary antibody dilution buffer and the cells were fixed at room temperature with 3.7 % paraformaldehyde.

TNF- α , IFN- γ and anti- ICAM were supplied by Peprotech

Where whole cell staining was carried out dilution buffer A was used as stated and the cells were fixed in 1:1 ice cold acetone: methanol at 4°C

2.4.3 Immunofluorescent staining of cultured HBMECs and HDLECs

2.4.3.1 Whole cell staining in chamber slides

The conditioned medium from each well was aspirated and stored at -20°C until ready for ELISA testing. Cells were grown to 85-90% confluence in chamber slides at 37°C (with 5% CO₂) in the appropriate media as described in section 2.4.1.1 and 2.4.1.3. Following washing each well with 500µl of room temperature PBS the cells were fixed in ice cold 1:1 acetone: methanol for 15 minutes. Cells were incubated for one hour with the primary antibody as follows: mouse anti-human ICAM, 10µg/ml (R&D Systems), (the concentration of ICAM used was ascertained following the optimisation procedure for concentrations shown in figure 2.1); rabbit anti-human CCL7 at 2.5µg/ml (Lifespan Biosciences); mouse anti-human CCL14 at 2µg/ml (Santa Cruz); goat anti-human CCL16 at 15µg/ml (R&D Systems) or goat anti-human CCL22 at 4µg/ml (Santa Cruz) for one hour. As background staining was less evident than on human tissue sections all solutions were made up in 1% BSA, 1% donkey serum and 0.3% triton X in PBS. Following washing three times in PBS for 5 minutes the cells were incubated in the secondary antibody solution for 45 minutes (in a darkened humidified chamber). The secondary antibody solutions were donkey anti-mouse Alexa Fluor 594, donkey anti-rabbit Alexa Fluor 594 or donkey anti-goat Alexa Fluor 594, all at 6.6µg/ml (all from Invitrogen) and made up in 1% BSA, 1% donkey serum and 0.3% triton X in PBS. Following washing (as above) cells were counterstained using DAPI at 1:5 with PBS (from a 1:5000 working stock, Sigma) before mounting using Hydromount (Fisher Scientific). The control antibodies used in this work were as stated in section 2.3.2.1.

2.4.3.2 Cell surface staining in chamber slides

Cells were grown to 85-90% confluence in chamber slides at 37°C (with 5% CO₂) in the appropriate media as described in section 2.4.1.1 and 2.4.1.3. Following washing each well using 500µl of PBS per well the cells were fixed for 15 minutes in freshly made 3.7% paraformaldehyde. Cells were incubated for one hour with the primary antibody as follows: rabbit anti-human CCL7 at 2.5µg/ml (Lifespan Biosciences), mouse anti-human CCL14 at 2µg/ml (Santa Cruz), goat anti-human CCL16 at 15µg/ml (R&D Systems) or goat anti-human CCL22 at 4µg/ml (Santa Cruz) for one hour. As background staining was less evident than on human tissue sections all solutions were made up in 1% BSA and 1% donkey serum in PBS. Following washing three times in PBS for 5 minutes the cells were incubated in the secondary antibody solution for 45 minutes (in a darkened humidified chamber). The secondary antibody solutions were donkey anti-mouse Alexa Fluor 594, donkey anti-rabbit Alexa Fluor 594 or donkey anti-goat Alexa Fluor 594, all at 6.6µg/ml (all from Invitrogen) and made up in 1% BSA, 1% donkey serum and 0.3% triton X in PBS. Following washing (as above) cells were counterstained using DAPI at 1:5 with PBS (from a 1:5000 working stock, Sigma) before mounting using Hydromount (Fisher Scientific). The control antibodies used in this work were as stated in section 2.3.2.1.

2.4.4 Quantitation of Immunofluorescence

Quantitation was performed as described in section 2.3.2.5 with the random fields of view being within the wells as opposed to spread over a tissue section.

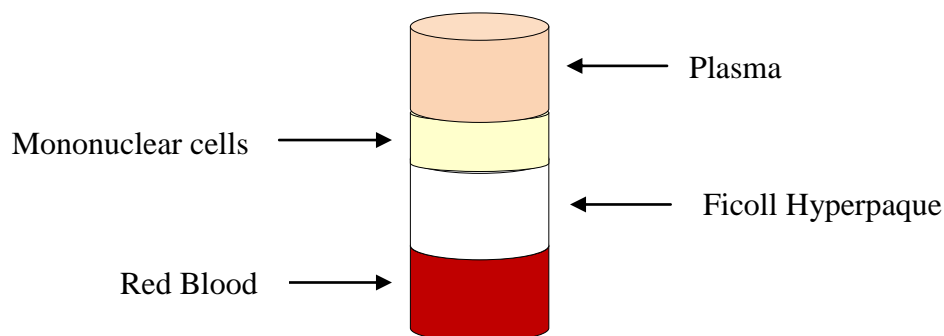
2.5 Materials and methods used in chapter 5

2.5.1 Isolation of cells from human blood

2.5.1.1 Peripheral Blood Mononuclear Cell (PBMC) isolation

Mononuclear cells (monocytes and lymphocytes) were isolated using the density gradient centrifugation method. Approximately 5ml of fresh peripheral whole blood was collected in heparin coated vacutainers. The blood was then diluted with an equal volume of RPMI-1640 medium with 5ml penicillin streptomycin (5000u penicillin/ml, 500u streptomycin/ml) (Lonza) and 5ml of fungizone (amphotericin B at 250µg/ml) (Lonza, Wokingham, UK) and warmed to room temperature (herein referred to as complete PBMC medium) in a 50ml falcon tube (Fischer Scientific). This was carefully layered over 13ml of Ficoll Hyperpaque at room temperature and was centrifuged at room temperature for 30 minutes at 1600rcf. The brake on the centrifuge was switched off for this stage, allowing the centrifuge to slowly come to a rest at the end of the 30 minute cycle. The PBMCs were slowly aspirated from the interface (see figure 2.5) into a falcon tube containing 20ml of the complete PBMC medium. The cells were then washed twice, first by centrifuging at 1500rcf for 10 minutes (centrifuge brake switched on from this stage) followed by the supernatant being removed and the pellet being resuspended in a further 20ml of the complete PBMC medium and centrifuged for 8minutes at 1600rcf to complete the second wash. The pellet was then resuspended in 2ml fresh DMEM-F12 medium with 0.5% fraction V FBS (Sigma-Aldrich, UK) until ready for use.

Figure 2.5. Schematic showing mononuclear cell isolation from whole blood.



The schematic shows the Ficoll Hyperpaque gradient and the mononuclear cell layer following centrifugation. The plasma and red blood cell layers are also indicated.

2.5.2 Transmigration

2.5.2.1 Stimulation of inflammatory conditions in transwell systems for transmigration analysis across cultured cell monolayers

The transwell system was set up by dispensing 800 μ l EBM-2-MV medium for HDLECs or (DMEM-F12 medium solution for HBMECs) into each well of a 24 well plate (Scientific Laboratory Supplies) and a 5 μ M pore hanging filter (Merck Chemicals, Nottingham, UK) was then placed into each well. Following this 400 μ l of the DMEM-F12 medium solution containing 100,000 HBMECs was placed into each hanging filter and left overnight until confluent.

Once the cells ECs were >95% confluent the medium in the hanging filters was replaced with fresh medium containing either;

- A. 400 μ l total of TNF- α at 100ng/ml. (for HBMECs)
- B. 400 μ l total of TNF- α at 100ng/ml and IFN- γ at 100ng/ml. (for HDLECs)

(concentrations of TNF- α and TNF- α / IFN- γ ascertained as described in section 2.4.1.8 and detailed in table 2.7). A minimum of three filters were activated using each solution and left for two hours.(see figure 2.4).

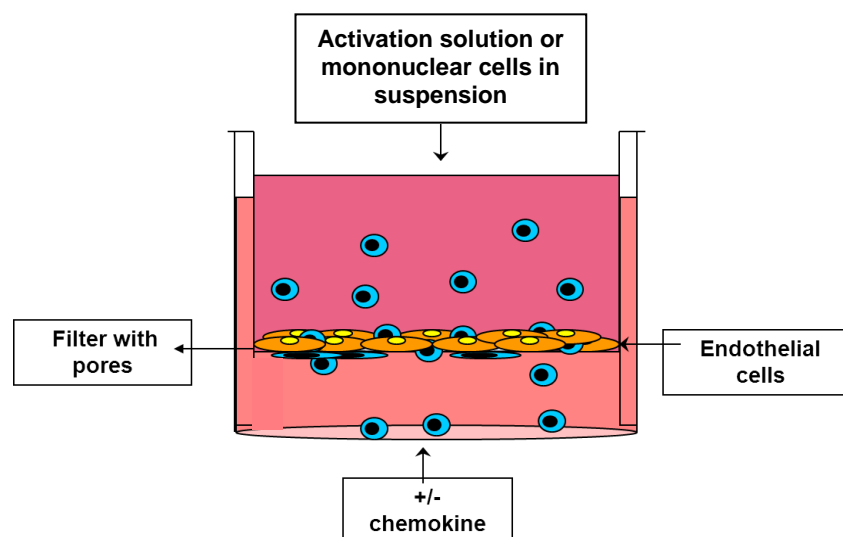
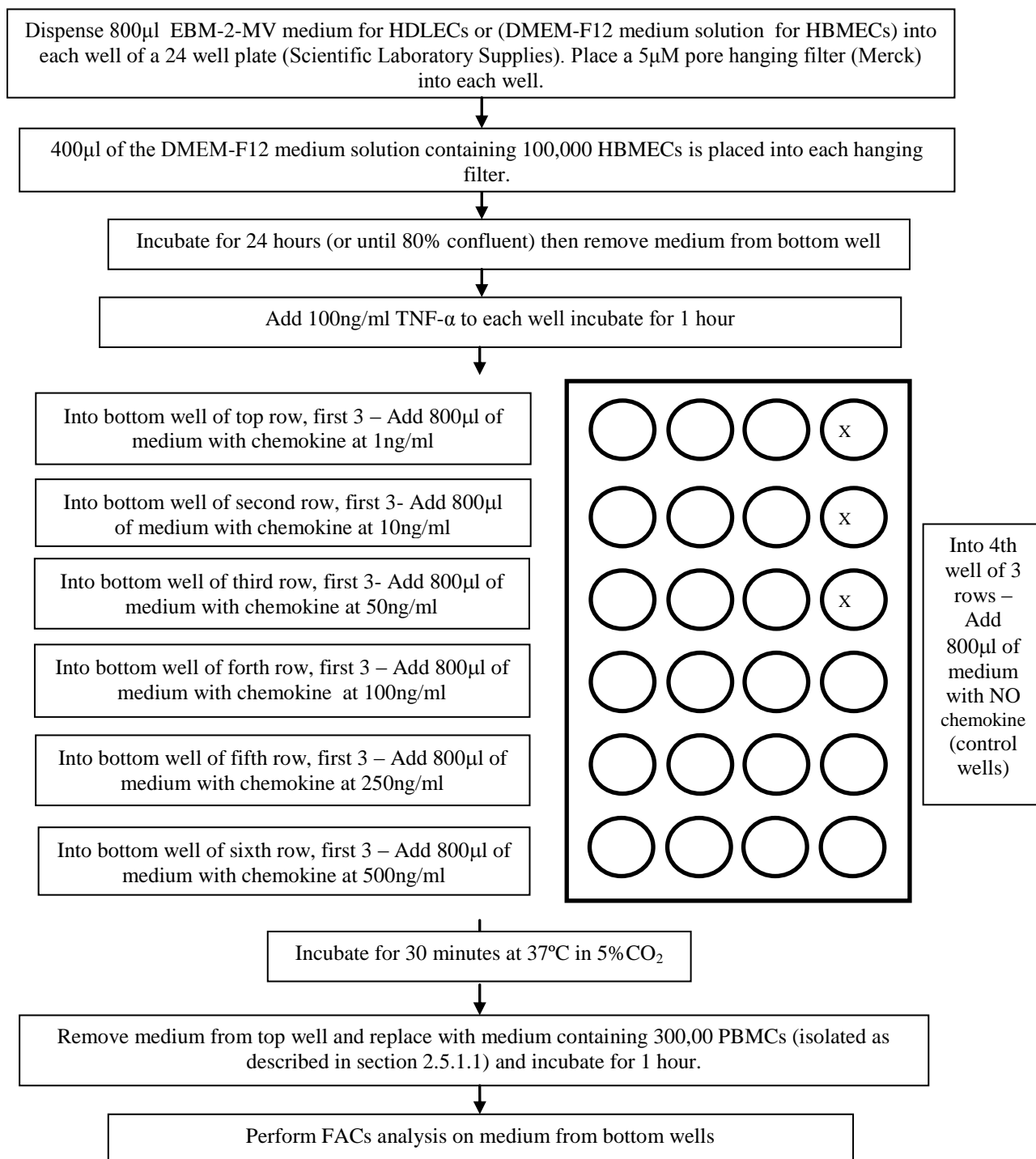


Figure 2.6: Schematic diagram showing transwell system used to study leukocyte migration. ECs are shown cultured onto the filter apical surface through which the leukocytes migrate in response the EC activation and chemokines. (Schematic reproduced with the kind consent of Dr Catherine Whittall).

2.5.2.2 Optimisation of chemokine concentrations for transmigration analysis.

Prior to transmigration analysis the optimal concentrations of the chemokines CCL7, CCL14, CCL16 and CCL22 for mononuclear cell chemotaxis were elucidated. The optimisation process is outlined in figure 2.7. Following the optimisation process 100ng/ml of the chemokine was shown to give optimal results in terms of numbers of migrated mononuclear cells and were used for all other transmigration work in this study.

Figure 2.7 Schematic showing optimisation process for chemokines CCL7, CCL14, CCL16 and CCL22 prior to transmigration analysis using HBMECs and HDLECs



2.5.2.3 Transmigration of mononuclear cells across HBMEC monolayers in response to human CCL7, CCL14, CCL16 and CCL22.

The transwells were set up as in as in section 2.5.2.1. Following addition of the activation medium, cells were incubated for 1.5 hours, and the medium in the bottom well was replaced with 800 μ l of the chemokine medium. The chemokine medium was made using RPMI-1640 medium containing 0.5% fraction V BSA with human chemokines CCL7, CCL14, CCL16 and CCL22 (Peprotech. Table 2.8) added, giving final chemokine concentration of 100ng/ml and left for 30 minutes to allow the chemokine to be presented on the EC apical surface. Two negative controls were the chemokine only in the absence of activation. Following this, the medium from the hanging filter well was removed and immediately replaced with 400 μ l of RPMI-1640 medium (with 0.5% fraction V BSA) containing 100,000-300,000 leukocytes (freshly separated from human peripheral blood as previously described in section 2.5.1.1) and left for 1 hour to allow migration to occur. The negative control was performed using 0ng/ml chemokine over an un-activated (non-inflammatory) HBMEC monolayer. This was carried out in triplicate for each assay, total number of assays; RA n = 3, non-RA n = 3.

Following migration the medium was removed from the bottom wells and placed into a 5ml FACS tube. The tubes were then centrifuged at 1000rcf for 10 minutes at 4°C. The supernatant was taken off and the cells resuspended in either PBS containing 2% fraction V BSA (Invitrogen) and kept on ice for immediate FACS analysis, or resuspended in PBS with 10% cell fix and stored at ~4°C for later FACS analysis.

Table 2.8 Recombinant proteins used in transmigration analysis (section 2.5.2.3).

Protein	Code	Company
Human CCL7	300-7	PeperoTech
Human CCL14	300-38	PeperoTech
Human CCL16	300-44	PeperoTech
Human CCL22	300-36A	PeperoTech

This table shows the details for where the recombinant proteins used in this work were from.

2.5.3 Sample preparation for transmission electron microscopy (EM).

2.5.3.1 Buffers:

A) 0.1M sodium cacodylate (NaCac) + 2mM calcium chloride (CaCl₂)

10.7015g NaCac (Sigma-Aldrich) and 0.11g CaCl₂ (Sigma-Aldrich) were added to 500ml of distilled water and the pH then adjusted to pH7.4. This was stored at 4°C until use.

B) 2.5% Glutaraldehyde (GTA)

1ml GTA stock solution (25% solution, Sigma-Aldrich) was added to 9ml NaCac/CaCl₂ solution immediately before use.

C) 0.1% GTA

1ml of the 2.5% GTA solution was made up to 25ml NaCac/NaCl₂ immediately before use.

2.5.3.2 Preparation of filters for EM.

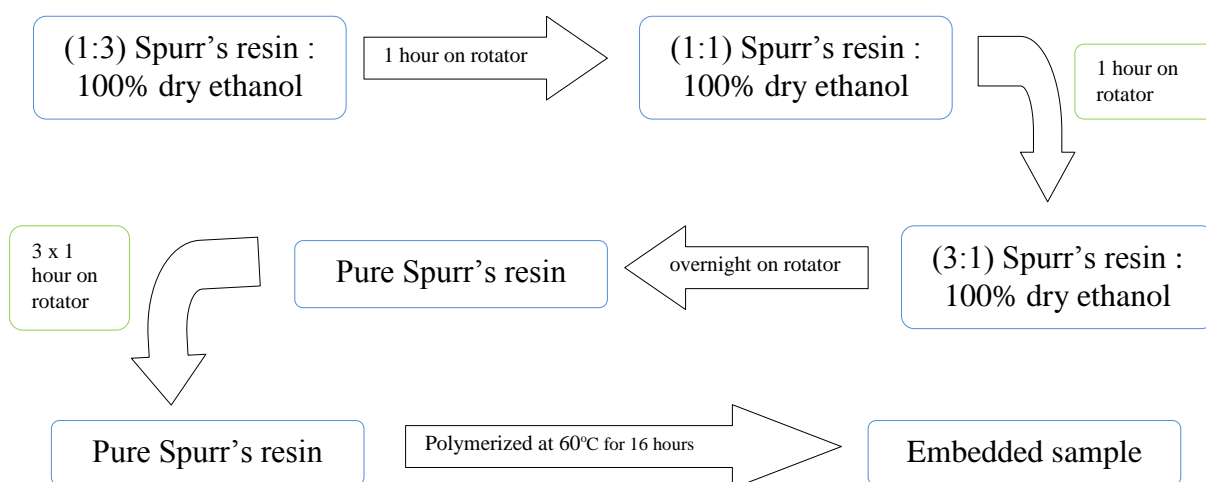
HBMECS were grown to ~80% confluence on 5µm pore filters (as described in section 2.5.2.2). The medium was aspirated and the filters washed with PBS after which they were incubated with 2.5% GTA (as in 2.5.3.1B above) for 2 hours at room temperature.

Following incubation the filters stored in 0.1% GTA and kept at 4°C prior to being sent to Keele University for EM processing and imaging.

2.5.3.3 Post fixation and Spurr embedding of cells on filters.

EM was performed in collaboration with Karen Walker, Electron Microscopy Unit, Keele University.

The samples were washed three times, for five minutes in 0.1M sodium cacodylate (NaCac) + 2mM calcium chloride (CaCl₂). They were post fixed in 0.1% osmium tetroxide (in NaCac.CaCl₂) for 1 hour. Following washing (as above) the samples were stored in 70% ethanol overnight. The samples were dehydrated in 80% ethanol for 15 minutes, 100% ethanol for 15 minutes and 100% dry ethanol for 15 minutes. Infiltration embedding in Spurr's resin and dry ethanol was then performed. Spurr's resin allows specimens which are normally difficult to embed to be successfully embedded as it is a low viscosity embedding medium. Infiltration and polymerisation were as follows



90-100nm thick sections were cut from the embedded sample with a diamond knife using a Leica Ultracut microtome. The cut sections were floated on water and then placed onto copper grids ready for staining.

2.5.3.4 Staining of ultrathin sections for EM

A) 2% Lead Citrate

1.33g of lead nitrate ($\text{Pb}(\text{NO}_3)_2$), 1.76g of (tri) sodium citrate ($\text{NA}_3[(\text{C}_6\text{H}_5)_7]\cdot 2\text{H}_2\text{O}$) and 30ml of CO_2 free, distilled water were added to a 50ml flask and ultrasonicated for 30 minutes. 8ml of 1M sodium hydroxide (NaOH) was then added and the solution diluted to 50ml with distilled water and well mixed. The buffer was then stored at 4°C.

B) 2% Uranyl Acetate

0.04g uranyl acetate was dissolved in 2ml of 70% ethanol using a sonicator then centrifuged at high speed for 5 minutes and used immediately.

Materials

- A) Dental wax in petri dish
- B) Petrie dish containing potassium hydroxide pellets with a piece of dental wax on top.
- C) Double (grade 50) filter papers.
- D) Rinse 1. 100ml of 30% ethanol
- E) Rinses 2-6. 5 x 100ml of distilled water.

One spot of uranyl acetate per copper grid was placed onto the dental wax in the petri dish (A). The grids were fully immersed in the spots and left for 20 minutes. The grids were then dipped into rinse 1 20 times, then into rinses 2 and 3 5 times. The grids were then washed by directing distilled water down the forceps (rather than directly onto the grids) from a wash bottle and excess water was carefully blotted away using the filter paper.

Small spots of lead citrate (1 spot per copper grid) were placed onto the petri dish B and again the grids were carefully fully immersed into the spots with forceps and left for 5 minutes. The grids were then dipped 10 times each into rinses 4-6 and then washed and blotted as earlier described. The stained samples were then ready to be visualised using a JEOL 1230 electron microscope and analysed using AnalySIS software.

2.6 Materials and methods used in chapter 6

Cultured cell stimulation was performed as previously described in section 2.4.1.8.

Transmigration across HBMECs was performed as described in section 2.5.2.3.

2.6.1 RA and non-RA blood samples.

Peripheral blood was obtained from 24 patients with longstanding RA fulfilling the American College of Rheumatology (ACR) criteria for RA. 16 age matched non-RA peripheral blood samples were obtained from a database of previous donors who had expressed their willingness to be contacted for future blood samples. Full informed consent was obtained in all cases.

2.6.2 Transmigration of mononuclear cells across HDLEC monolayers in response to human CCL7

Following the optimisation process 100ng/ml of the chemokine was shown to give optimal results and was used for all other transmigration work in this study.

Two negative controls was again performed; one in the absence of TNF- α / IFN- γ and chemokine, and one in the absence of CCL7 only. The transwells were set up as in section 2.5.2.1 for HBMECs only.

Following addition of the activation medium (serum free EBM-2mv with TNF- α at 100ng/ml and IFN- γ at 100ng/ml), for 1.5 hours, the medium in the bottom well was replaced with 800 μ l of the 100ng/ml CCL7 medium. The chemokine medium was made using EBM-2mv (Lonza) containing 0.5% fraction V BSA. This was left for 30 minutes to allow the chemokine to be presented on the EC apical surface. Following this, the medium from the hanging filter well was removed and immediately replaced with 400 μ l EBM-2mv (Lonza) (with 0.5% fraction V BSA) containing 100,000-300,000 mononuclear cells dependent on the numbers obtained from individual blood donors freshly separated from peripheral blood as previously described in section 2.5.1.1. It was left for 1 hour to allow migration to occur. The negative control was performed using 0ng/ml chemokine over an un-activated (non-inflammatory) HDLEC monolayer. This was carried out in triplicate for each assay, total number of assays: RA n = 3, non-RA n = 3.

Following migration the medium was removed from the bottom wells and placed into 5ml FACS tubes. The tubes were then centrifuged at 1000rcf for 10 minutes at 4°C. The supernatant was shaken off and the cells resuspended in either PBS containing 2% fraction V BSA (Invitrogen) and kept on ice for immediate FACS analysis, or resuspended in PBS with 10% cell fix and store at ~4°C for later FACS analysis.

2.6.3 Flow Cytometry

2.6.3.1 Chemokine receptor staining of leukocytes from human blood.

PBMCs were isolated as described in section 2.5.1.1 and the total number of cells calculated. 300,000 PBMCs per well were dispensed into a 96 round bottom well flexiplate (Scientific Laboratory Supplies) and centrifuged for 4 minutes at 1400rcf and at 4°C. Following supernatant removal the cells were washed by adding 50µl of 10% flebogamma diluted 1:10 in PBS (Invitrogen) to each well and carefully vortexed to mix. This was then left to incubate on ice for 30 minutes, centrifuged as before and the supernatant removed. The cells were then washed with 100µl 2% BSA in PBS, vortexed briefly to mix, centrifuged as before and the supernatant removed. 50µl of the unconjugated primary antibodies, mouse anti-human CCR1, CCR2, CCR4 and CCR5 (all from Immunotools, Germany, table 2.9) diluted in 2% BSA in PBS, was added to each well, vortexed and left for 30 minutes to incubate on ice. The plate was then centrifuged, washed, and the supernatant removed. 50µl per well of the secondary antibody, goat anti-mouse IgG^{2b} PE conjugated (Immunotools) was then added (1:100 in 2% BSA PBS), vortexed and left to incubate on ice for 30 minutes. The plate was then centrifuged, washed and the supernatant removed as before and the cells were resuspended in 50µl 2% BSA PBS and added to 200µl 2% BSA PBS in 5 ml Falcon tubes and stored on ice prior to flow cytometry on the FACS machine (BD FACScan; Becton Dickinson).

2.6.3.2 CD marker staining of leukocytes from human blood

PBMCs were isolated as described in section 2.5.1.1 and the total number of cells calculated. 300,000 PBMCs per well were dispensed into a 96 round bottom well flexiplate (Scientific Laboratory Supplies) and centrifuged for 4 minutes at 1400rcf and 4°C.

Following supernatant removal the cells were washed by adding 50 μ l of 10% flebogamma diluted 1:10 in PBS (Invitrogen) to each well and carefully vortexed to mix. This was then left to incubate on ice for 30 minutes, centrifuged as before and the supernatant removed. The cells were then washed with 100 μ l 2% BSA in PBS, vortexed briefly to mix, centrifuged as before and the supernatant removed. 50 μ l of PE conjugated CD antibodies: mouse anti human IgG¹ CD3 PE conjugated; mouse anti human IgG¹ CD14 PE conjugated and mouse anti human IgG^{2a} CD14 PE conjugated (Immunotools) and controls (Immunotools) were added to the cells, giving a final concentration of 5 μ l antibody per 100,000 cells (see table 2.9), prepared with 2% BSA in PBS and vortexed briefly to mix.

Table 2.9 showing reagents used for CD marker and chemokine receptor staining for FACS analysis

Marker	Primary antibodies and volumes used	Secondary antibodies and concentrations used
CD3	5µl mouse anti human IgG ¹ CD3 PE conjugated per 100,000cells (500µg/ml)	n/a
CD14	5µl mouse anti human IgG ¹ CD14 PE conjugated per 100,000cells (500 µg/ml)	n/a
CD20	5µl mouse anti human IgG ^{2a} CD14 PE conjugated per 100,000cells (500 µg/ml)	n/a
CCR1	Mouse anti-human CCR1 (500 µg/ml) (50µl per well)	5µl goat anti-mouse IgG ^{2b} PE conjugated (500 µg/ml)
CCR2	Mouse anti-human CCR2 (500 µg/ml) (50µl per well)	5µl goat anti-mouse IgG ^{2b} PE conjugated (500µg/ml)
CCR4	Mouse anti-human CCR4 (500µg/ml) (50µl per well)	5µl goat anti-mouse IgG ^{2b} PE conjugated (500 µg/ml)
CCR5	Mouse anti-human CCR5 (500µg/ml) (50µl per well)	5µl goat anti-mouse IgG ^{2b} PE conjugated (500µg/ml)

All of the above experiments were carried out with isotype matched negative controls.

2.7 Materials and methods used in chapter 7

2.7.1 Matched blood and synovial fluid for ELISA analysis.

Matched serum and synovial fluid samples from 17 RA patients, 7 OA patients, 14 reactive arthritis (ReA) patients and 7 psoriatic arthritis (PsA) patients (exact numbers per-experiment stated in figure legends) were kindly donated by Dr Derek Matthey (Keele University, Guy Hilton Research Centre, Stoke-on-Trent, UK). These samples were used for the analysis of the chemokines CCL7, CCL14, CCL16 and CCL22 in chapter 7. The synovial fluid was centrifuged at 2500rcf for 10 minutes at 4°C. and stored at -80 °c following flocculate removal.

2.7.2 ELISA of matched synovial fluid and serum samples

DuoSet ELISA kits were used for CCL7 (DY282), CCL14 (DY1578), CCL16 (DY802) and CCL22 (DY336), all from R&D Systems, Abingdon, UK. Wash buffer (WA126), substrate solution (DY999) stop solution (DY994) (all R&D Systems) were used throughout. The individual reagent diluents and blocking buffers were as recommended by the individual product datasheets.

Titration were performed to establish the optimal working concentrations for both the serum and synovial fluid samples. Sample standards were run for each experiment.

2.7.3 Plate Preparation

The capture antibody was diluted to 1 µg/ml with PBS and 100 µl were added to each well of a 96 well plate (Scientific Laboratory Supplies) which was then sealed and incubated at room temperature overnight. The following day, each well was washed by aspirating with 400 µl of wash buffer 3 times. After the last wash the plate was inverted and tapped over paper towels to ensure removal of the wash buffer.

The plates were blocked by incubating for 1 hour with the wash buffer at room temperature before being washed as previously stated.

2.7.4 Assay procedure

100 µl of the sample (diluted to working concentration with reagent diluent) was pipetted into each well (in duplicate) then sealed and left to incubate at room temperature for 2 hours. The wash step was repeated as previously stated. 100 µl of the detection antibody (diluted with the reagent diluent to the working concentration of 30 ng/ml) was added to each well and again sealed and left at room temperature for 2 hours to incubate. After washing (as earlier stated) 100 µl of the Streptavidin-HRP (at working concentration) was

added to each well and incubated in the dark at room temperature for 20 minutes, after which 50 μ l of the stop solution was added to each well and the plate was gently tapped to ensure thorough mixing.

Additional information for experimental procedures whose results are not used in this thesis and principles of TH-GFAAS can be found in the appendix.

Chapter 3

Immunofluorescent analysis of synovial tissue

3.1 Introduction and Aims

Chemokines are important mediators of transmigration via the activation of leukocyte surface integrins which are important in the early stages of leukocyte transmigration for controlling cell-cell interactions. As this initial interaction occurs at the EC : blood interface of the microvasculature the elucidation of the chemokines present at this interface may offer further insight into the pathology of RA. While there has been a plethora of work looking at the expression of both CXCL and specific CCL (beta) chemokines in RA, a literature review established that there has been little definitive work to demonstrate the presence of chemokines at the ECs. This is important to understand which chemokines are stimulating leukocyte recruitment and which to target for therapy. During initial work on this study the CXCL and CCL chemokines were both to be assessed to attempt to find a 'chemokine address code at ECs for RA'. However, it became apparent within the first six months that to perform the required levels of optimisation and analysis with fluorescent immunohistochemistry for both types of chemokine would not be feasible in the time allowable. A further literature review showed that the CCL chemokines were less well elucidated at the ECs than the CXCL chemokines so it was decided to focus on the former for the remainder of the work. CCL chemokines are known to stimulate a wide range of leukocytes, including monocytes and lymphocytes (Mellado *et al.*, 2015)

While performing the analysis of the chemokines using VWF as the EC marker a paper by Burman *et al.*, (2005) was identified which suggested that the dysregulation of chemokines

at synovial ECs led to altered leukocyte migration into the synovium. This led me to the hypothesis that differential expression/presentation of the same chemokine at blood vessel ECs and lymphatic ECs may be involved in the persistence of leukocytes within the inflamed joint. It was decided by the author to look at the expression of the most highly presented chemokines found in this study at both blood vessel ECs and lymphatic ECs to further analyse the dysregulation hypothesis. The tissue samples used had been previously categorised (Schmutz *et al.*,2006) for the degree of infiltration/hyperplasia and the presence of lymphoid aggregates by staining for T-cells and B-cells. Much of the following work was performed on the remaining sections of these tissue samples.

A range of anti-human chemokine antibodies are available from a range of sources. The choices of the antibodies in this study were based on their previous use in published work (where possible) to prove their reliability. Lesser known antibodies were purchased where other sources were not available in order to assess the greatest complement of CCL chemokines possible. The use of the antibodies for other markers, such as VWF for blood ECs and LYVE-1 for lymphatic ECs as these are markers expressed by the relevant EC cell type and are cited extensively as such.

The aims were to:

- Establish which CCL chemokines are highly presented at RA synovial ECs and then compare the presence of the most highly represented chemokines (present on

≥60% of RA vessels) with their presence in non-RA synovial tissue to establish which specific chemokines are increased in RA.

- Examine whether differences exist in blood and lymphatic vessel EC presentation of the most highly represented chemokines in both RA and non-RA synovial tissue to establish whether particular chemokines are dysregulated in RA. Such dysregulation could potentially lead to leukocyte persistence in the inflamed joint.

3.2 Materials and Methods

Synovial tissue was obtained as described in section 2.3.1 Immunofluorescence was performed and quantified as described in section 2.3.2. The counted fields cover between 40-80% of the tissue sections.

3.2.1 Quantitation of results

Statistical analysis was performed using Graphpad (La Jolla California USA, www.graphpad.com).

For chemokines present at less than 60% of VWF+ vessels the percentage of VWF and/or LYVE-1 vessels which were positive for the chemokine was calculated and is shown as mean ± SE. Where chemokines were present at greater than 60% of VWF+ vessels in RA synovium they were also investigated in non-RA synovial tissue and significant differences between the two assessed by Student's t-test ($p < 0.05$).

3.3 Results

3.3.1 Beta chemokines on synovial ECs.

Each of the chemokines which had anti-human immunofluorescence antibodies commercially available were initially assessed on 8 RA tissue samples. A range of staining for each of the chemokines was elucidated whereby differing degrees of EC staining was observed. A high degree of heterogeneity between individual patients was also observed (appendix, table 1). This may be due to variations in the level of inflammation within the joints of different patients. Such variations may be caused by fluctuations in the disease course and/or differences in medication between patients. Both DMARDS and biologic agents have an effect on the chemokines seen in tissues, and reductions in TNF (for example) reduce chemokine levels within the inflamed joint (Szekanecz et al., 2010; Eriksson C., Rantapää-Dahlqvist and Sundqvist, 2013). Each of the samples chosen were previously designated as being areolar in morphology, apart from a number of later sections from RA sample 8 which had fibrous regions, (Schmutz, unpublished work). The sections analysed were not serial but were from the same tissue blocks. Serial cryosections were not technically possible.

3.3.1.1 CCL1 in RA synovial tissue

CCL1 was shown to be present on both ECs and infiltrate within the RA joint (figures 3.1A and 3.1B). 11.9% (± 4.0) of VWF+ RA vessels were CCL1+ (figure 3.1B and table 3.1). Colocalised staining was apparent but as the CCL1 staining was quite weak merged images were not shown in these data.

3.3.1.2 CCL2 in RA synovial tissue

CCL2 was present in both infiltrate and ECs (figure 3.2A). Particularly intense EC staining was observed in regions of more diffuse infiltration (figure 3.2A) with weaker EC staining seen in regions of lymphoid follicles and more dense infiltration (figure 3.2B). Colocalisation of VWF and CCL2 was seen throughout the synovial tissue (figure 3.2A) and was present on 51.5% (± 6.9) of VWF+ vessels (table 3.1). The negative control (figure 3.2C) showed no background staining.

3.3.1.3 CCL3 in RA synovial tissue

A combination of weakly CCL3+ vessel ECs and infiltrate was seen (figure 3.3A and 3.3B). It appears that CCL3 was predominantly seen on the basement membrane of the RA vessel ECs. CCL3 was shown to be present on 27.4% (± 6.1) of VWF+ RA vessels (table 3.1). The negative control (figure 3.3C) showed no background staining.

3.3.1.4 CCL4 in RA and non-RA synovial tissue.

CCL4 was shown to be highly represented on RA ECs. It was identified at 62.3% (± 11.0) of VWF+ RA vessels (figure 3.4A and 3.4B). CCL4+ infiltrate was also observed (figure 3.4A). The negative control (figure 3.4A inset) showed no background staining. CCL4 staining was seen within vessel walls in non-RA synovial tissue, but to a lesser degree than in RA tissue at only 49.2% (± 16.0) of VWF+ vessels (figure 3.4C) although the difference was not significant ($p = 0.49$). See table 3.2.

3.3.1.5 CCL5 in RA synovial tissue.

CCL5 staining was evident throughout the synovium, including EC basement membrane (figure 3.5A), luminal EC surface and on infiltrating cells and within lymphoid aggregates (figure 3.5B and 3.5C). CCL5 was shown to be present on 44.9% (± 7.6) of VWF+ RA vessels. See table 3.1.

Table 3.1 Chemokine present at $\leq 59.9\%$ of VWF+ vessels in RA synovial tissue.

Chemokine	RA
CCL1*	11.9 % (± 4.0)
CCL2	51.5% (± 6.9)
CCL3	27.4% (± 6.1)
CCL5	44.9% (± 7.6)
CCL10*	52.6% (± 10.0)
CCL11*	15.8% (± 6.3)
CCL12*	9.6% (± 3.2)
CCL13*	56.6% (± 7.0)
CCL15*	47.3% (± 6.3)
CCL17*	17.4% (± 10.6)
CCL18*	38.0% (± 6.4)
CCL20*	18.5% (± 2.7)
CCL21	36.1% (± 10.4)
CCL23*	37.7% (± 4.5)
CCL24*	28.8% (± 4.6)
CCL25*	28.2% (± 4.5)
CCL26*	63.6%* (± 7.5)
CCL27*	8.3% (± 1.2)
CCL28*	40.9% (± 6.8)

The percentage of VWF+ vessels for each RA sample (n=8) that was also chemokine+ and present on $< 59.9\%$ of the VWF+ vessels. * indicates novel identification on synovial ECs at the time of writing. Data are shown with mean \pm SE. * early analysis showed this value to be 59.2% and so further study was not performed.

Table 3.2 Chemokine present at $\geq 60\%$ of VWF+ vessels in RA synovial tissue assessed on non-RA synovial tissue.

Chemokine	RA	Non-RA	<i>p</i> =
CCL4	62.3% (± 11.0)	49.2% (± 16.0) \blacksquare	<i>p</i> = 0.49
CCL7 \bullet	69.3% (± 6.1)	61.9% (± 14.8) \blacksquare	<i>p</i> = 0.54
CCL8	64.1% (± 7.4)	25.6% (± 17.0) \blacklozenge	<i>p</i> = 0.04
CCL14 \bullet	73.0% (± 7.0)	28.4% (± 8.2) \blacksquare	<i>p</i> = 0.0041
CCL16 \bullet	74.1% (± 7.2)	75.3% (± 7.0) \blacksquare	<i>p</i> = 0.89
CCL19	80.0% (± 4.5)	10.3% (± 2.6) \blacklozenge	<i>p</i> = < 0.0001
CCL22 \bullet	60.1% (± 8.1)	18.7% (± 5.7) \blacksquare	<i>p</i> = 0.014

This table shows the percentage of VWF+ vessels in RA patients (n=8) that were also chemokine+ and were present on $\geq 60\%$ of vessels. These were compared with the percentage of VWF+/chemokine+ vessels in non-RA samples (\blacklozenge n=6, \blacksquare n = 5). \bullet indicates novel identification on synovial ECs in RA at the time of writing. Data is shown as mean percentage of VWF+ vessels also chemokine+ (n = 8), \pm SE. Significant differences as assessed by t-test ($p = < 0.05$) are shown.

Table 3.3 Chemokine with VWF, and chemokine with LYVE-1 in RA and non-RA tissue.

chemokine	VWF and chemokine			LYVE-1 and chemokine		
	RA	non-RA	<i>p</i> =	RA	non-RA	<i>p</i> =
CCL7	69.3% (±6.1)	61.9% (±14.8)	<i>p</i> = 0.54	32.3% (±10.1)	83.3% (±10.1)	<i>p</i> = 0.011
CCL14	73.0% (±7.0)	28.4% (±8.2)	<i>p</i> = 0.0041	45.7% (±11.5)	40.0% (±23.3)	<i>p</i> = 0.83
CCL16	74.1% (±7.2)	75.3% (±7.0)	<i>p</i> = 0.89	65.4% (±8.0)	60.0% (±23.2)	<i>p</i> = 0.80
CCL22	60.1% (±8.1)	18.7% (±5.7)	<i>p</i> = 0.014	75.1% (±6.0)	10.0% (±9.5)	<i>p</i> = 0.0001

Shows the percentage of VWF+ vessels for each RA and non-RA sample that was also positive for the chemokine. The percentage of LYVE-1+ vessels for each RA (n=8) and non-RA for CCL7 (n=6), CCL14, CCL16 and CCL22 (n=5) sample that was also positive for the chemokine is also shown (±SE). Significant differences as assessed by t-test ($p < 0.05$) are shown.

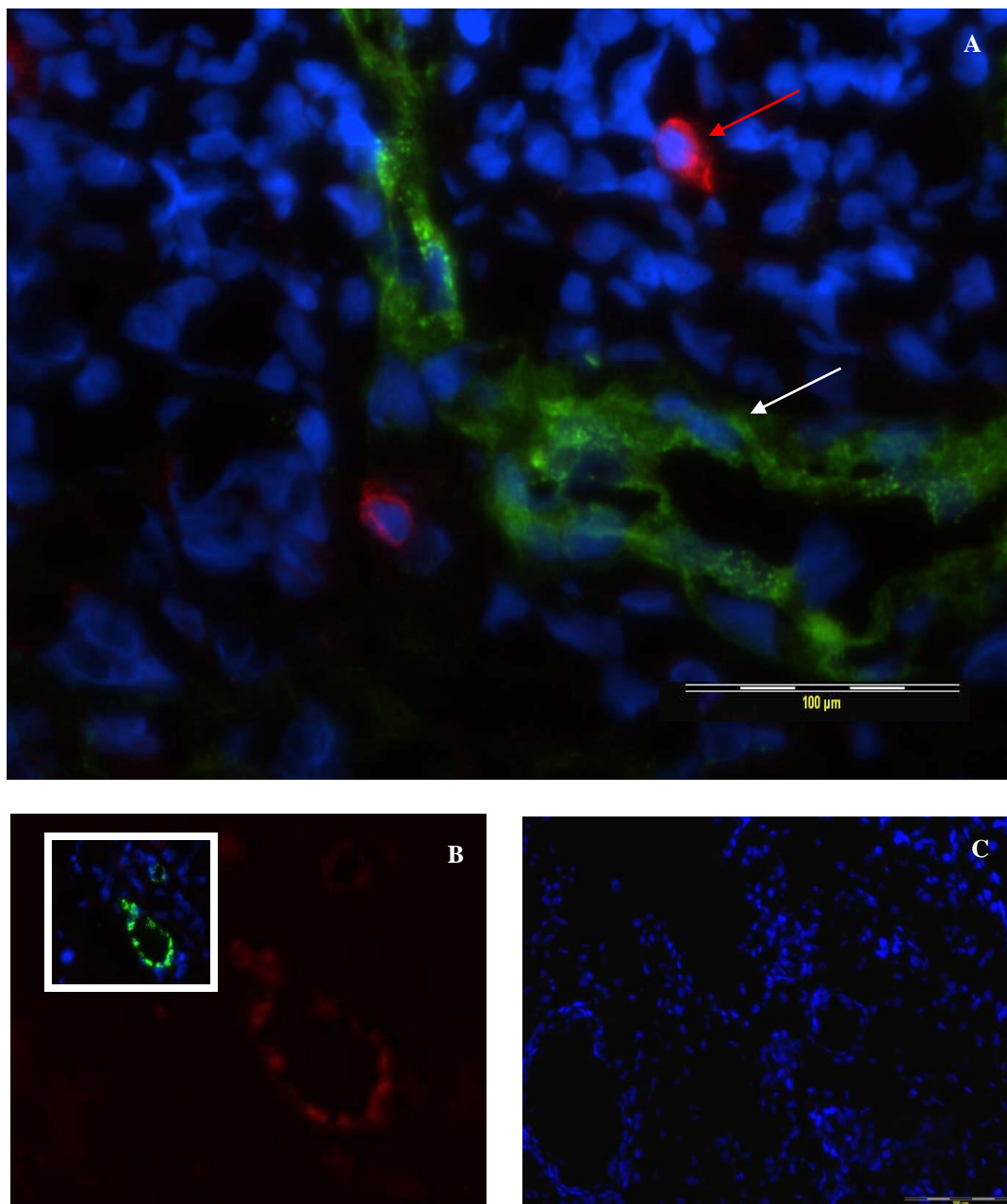


Figure 3.1 CCL1 and VWF staining in RA synovium. **3.1A** shows a merged image of staining for CCL1 (red), VWF (green) and DAPI (blue). The white arrow indicates a CCL1 negative vessel. The red arrow indicates an example of CCL1+ infiltrate. **3.1B** shows an enlarged image of a CCL1+ vessel, the inset image shows the merged image for the same vessel. **3.1C** show the isotype matched negative control (scale bar shows 100μm in all images). RA sample 1 is shown as a representative example.

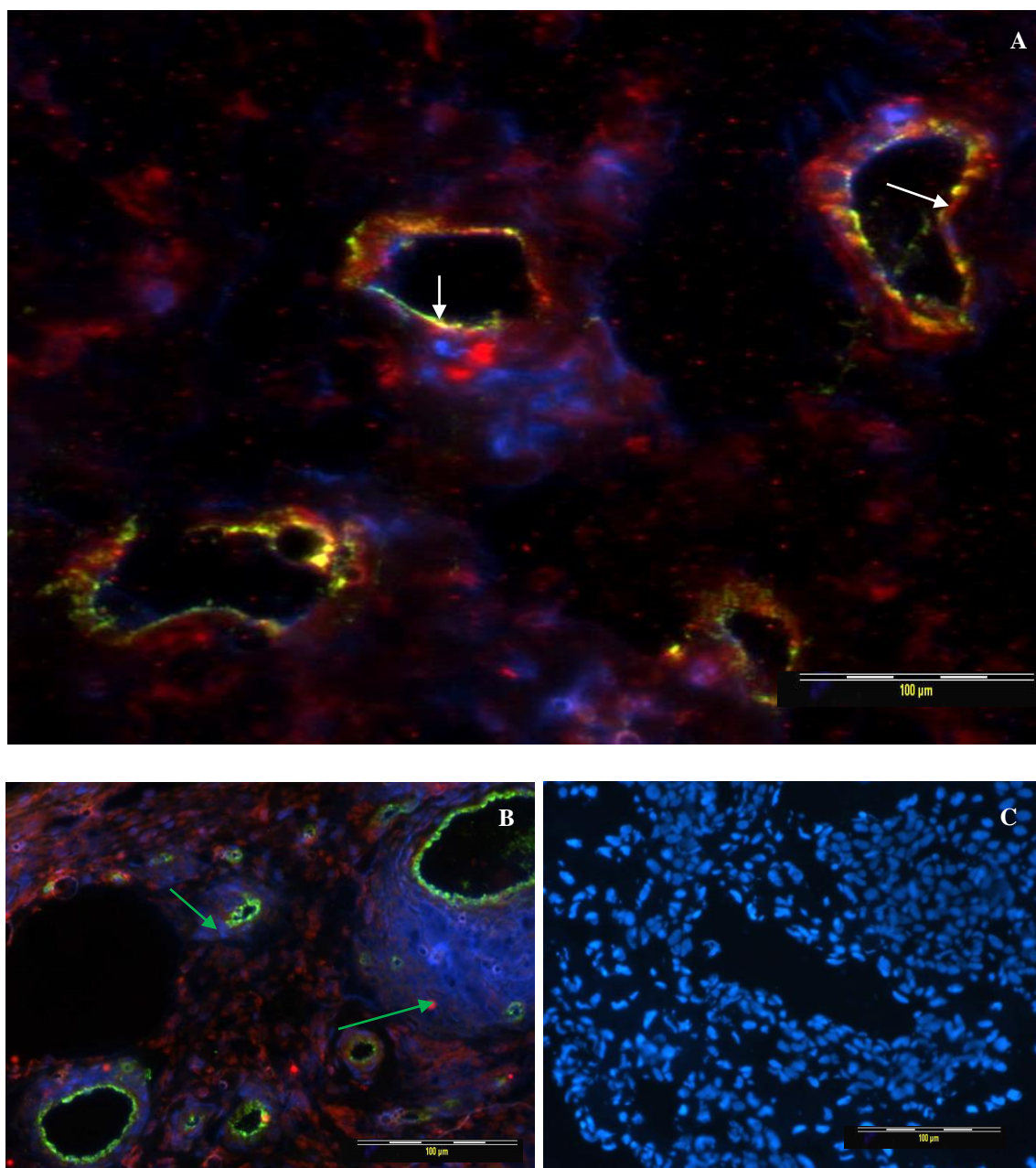


Figure 3.2 CCL2 and VWF staining in RA synovium. 3.2A and 3.2B show merged images of staining for CCL2 (red), VWF (green) and DAPI (blue). CCL2+ vessels are indicated with white arrows in 3.2A with yellow staining indicating strong colocalisation between VWF and CCL2. 3.2B shows what appear to be lymphoid follicles, indicated with green arrows. 3.2C shows a show the isotype matched negative control merged image (scale bar shows 100μm in all images). RA sample 6 is shown as a representative example.

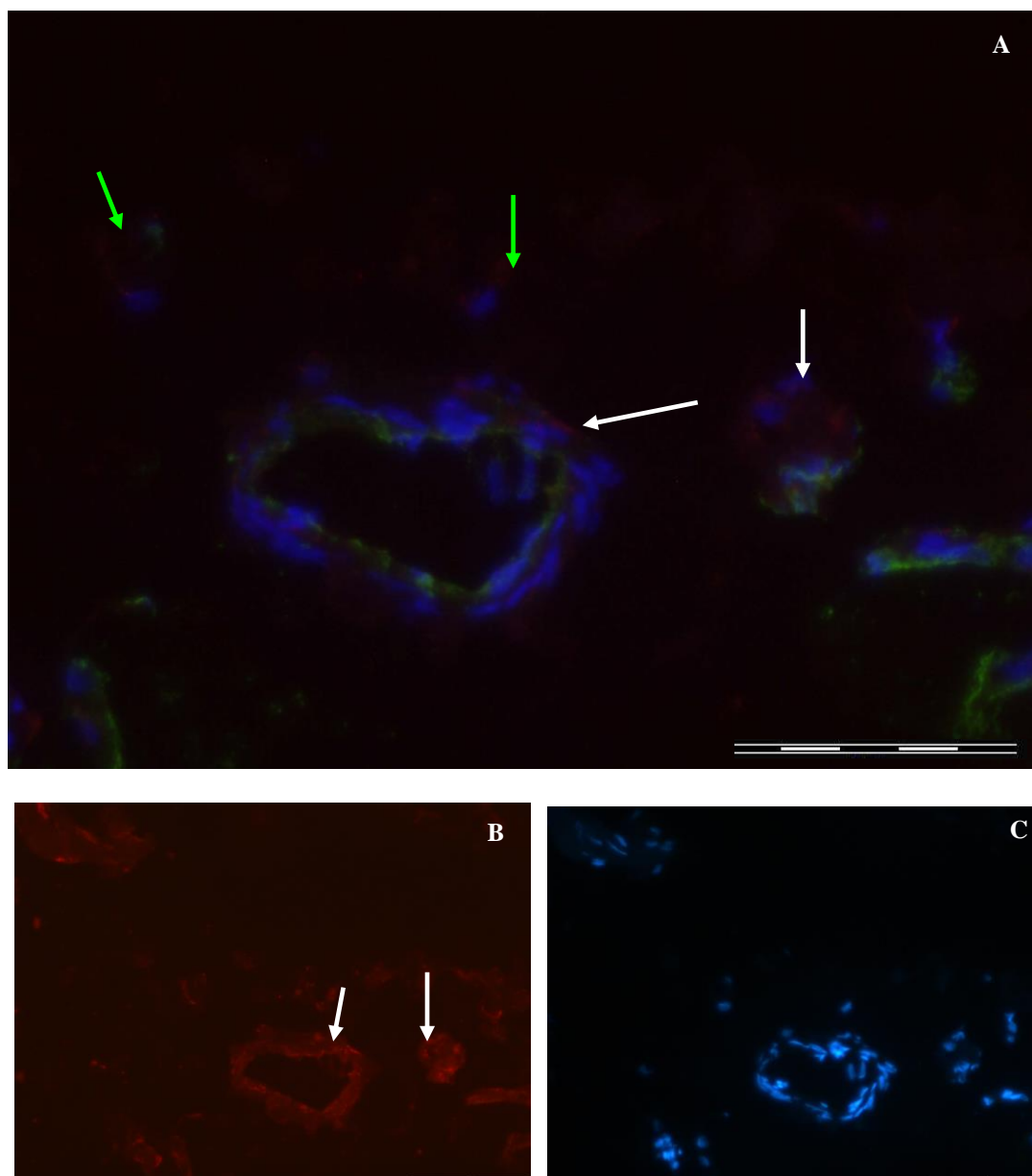


Figure 3.3 CCL3 and VWF staining in RA synovium. 3.3A shows a merged image of staining for CCL3 (red), VWF (green) and DAPI (blue) on RA sample 7 as a representative example. The white arrow indicates a weak CCL3+ vessel, the green arrows indicate weak CCL3+ infiltrate. 3.3B shows the CCL3 staining only to confirm its presence as it is overpowered by the more intense VWF staining in 3.3A. 3.3C shows the isotype matched negative control merged image of a serial section at the same magnification (X20 objective), scale bars show 100 μ m.

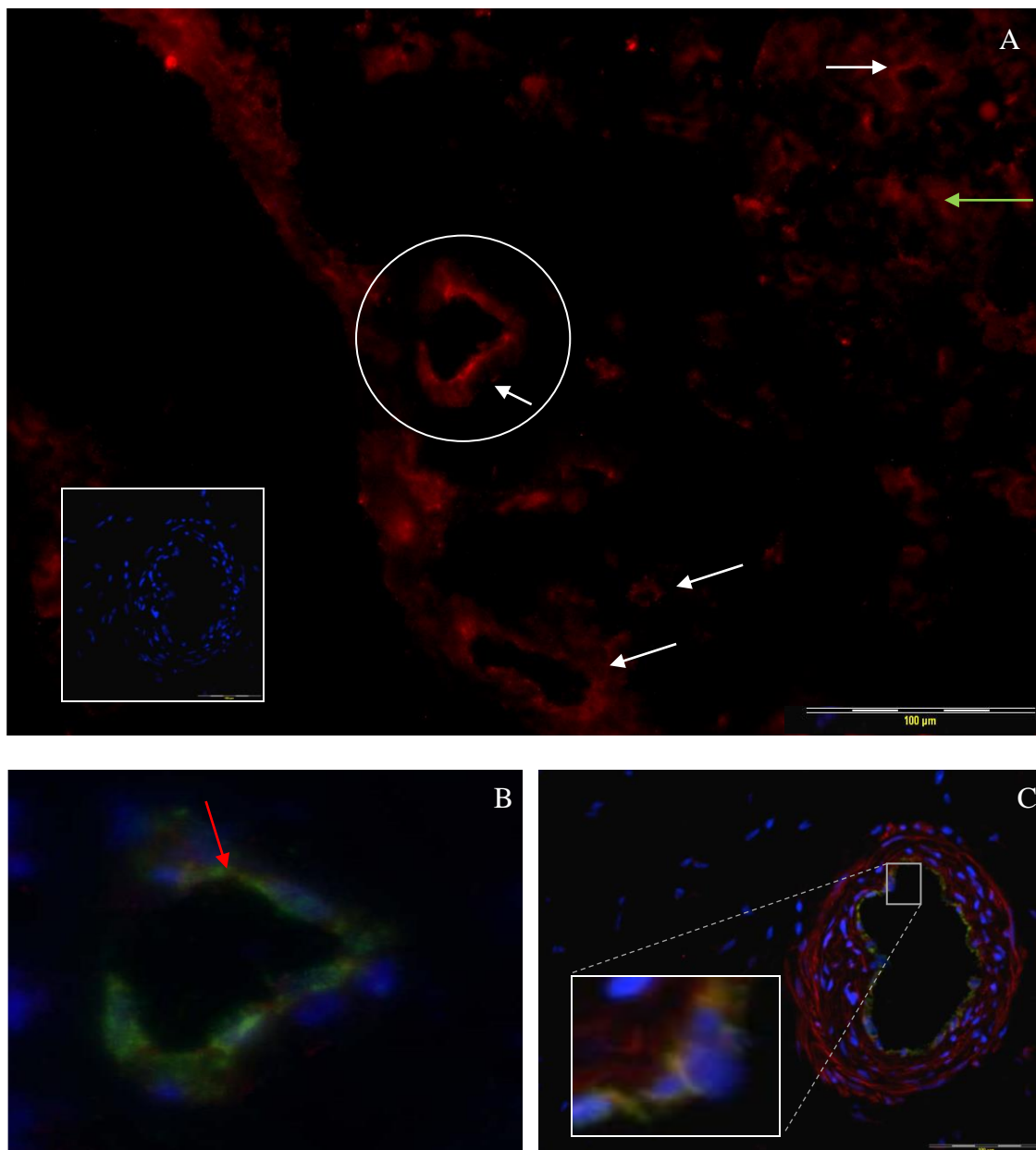


Figure 3.4 CCL4 and VWF staining in RA synovium. **3.4A** shows CCL4+ vessel ECs indicated with white arrows, the green arrow shows CCL4+ infiltrates. Inset image shows the isotype matched negative control. **3.4B** is a merged image of the region in the white circle with DAPI (blue) and VWF (green). The red arrow indicates colocalisation. **3.4C.** shows CCL4 and VWF staining in the non-RA synovium, orange colouration in inset shows colocalisation. Scale bars show 100 μ m (original magnification X20 objective). RA sample 2, and non-RA sample 5 are shown as representative examples.

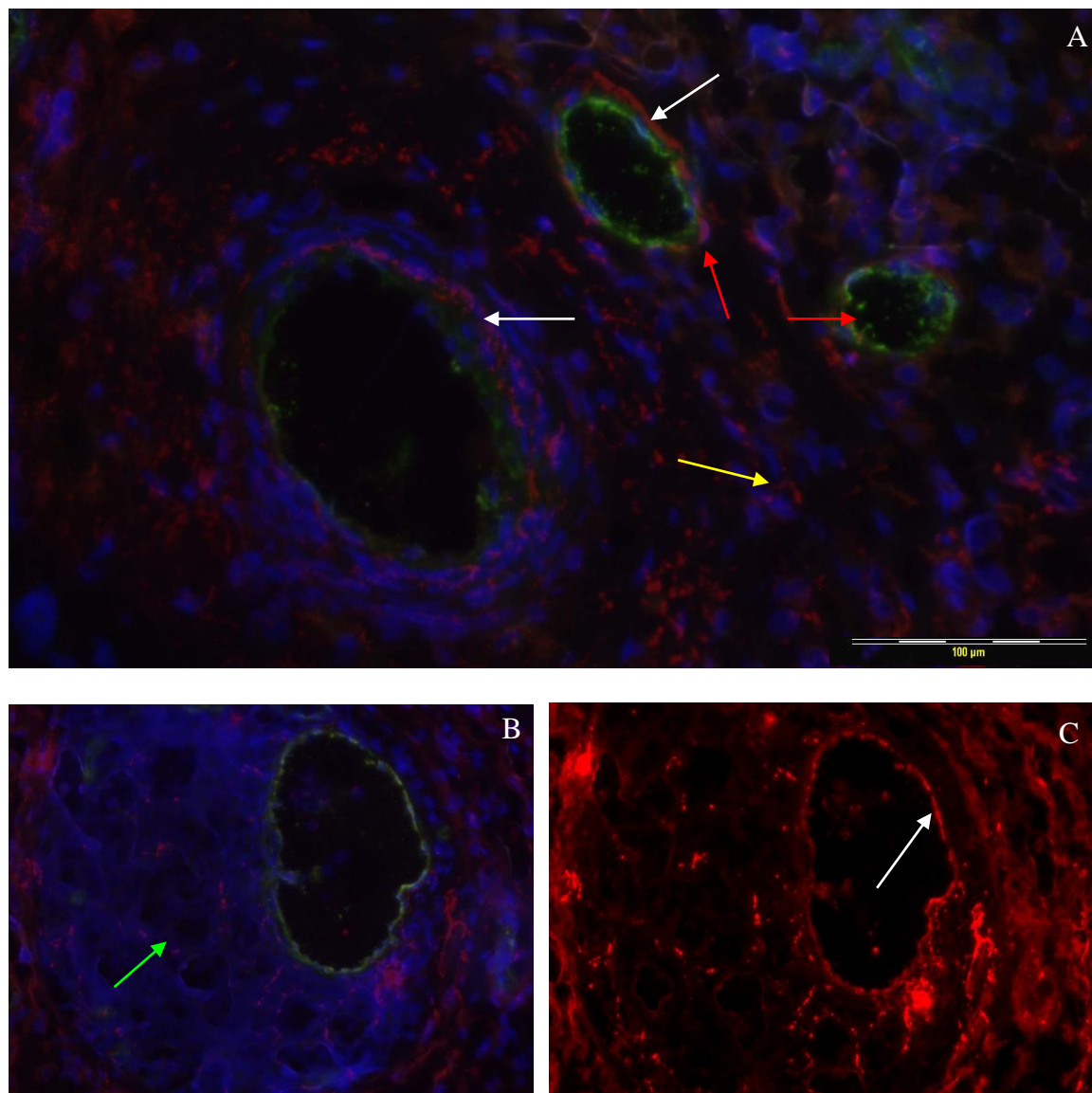


Figure 3.5 CCL5 and VWF staining in RA synovium. 3.5A shows a merged image of staining for CCL5 (red), VWF (green) and DAPI (blue) on RA sample 6 as a representative example. In 3.5A the red arrow indicates colocalisation. White arrows indicate CCL5 at the basement membrane. The yellow arrow indicates CCL5 on infiltrating cells. 3.5B shows a merged image where some CCL5 cells are in close association with what appears to be a large lymphoid aggregate (green arrow). 3.5C shows the same image as 3.5B with CCL5 staining only. The white arrows indicate CCL5 at the luminal EC surface of the vessel. (X20 objective throughout) Scale bars show 100 μ m in 3.5A. Figures 3.5B and 3.5C were enlarged from an original magnification X20 objective.

3.3.1.6 CCL7 and VWF in RA and non-RA synovial tissue.

CCL7 was observed throughout the RA synovium on vessel ECs as indicated by white arrows (figure 3.6A and 3.6B) and on a number of sub-intimal and infiltrating cells (figure 3.6A) which appeared in many cases to be cells resembling fibroblasts (figure 3.6C). A high degree of colocalisation between CCL7 and VWF on vessel ECs was observed. Overall, CCL7 was shown to be present on 69.3% (± 6.1) of VWF+ RA vessels. The negative control (figure 3.6B inset) showed no background staining. In the non-RA synovium, CCL7 staining was less evident on infiltrating cells (figure 3.7) but staining remained high on VWF+ ECs at 61.9% (± 14.8) (figure 3.7A and 3.7B). The difference in the percentage of VWF+ vessels stained for CCL7 in RA and non-RA tissue was not significant ($p = 0.54$), see table 3.2. The negative control (figure 3.7C) showed no background staining.

3.3.1.7 CCL7 and LYVE-1 in RA and non-RA synovial tissue.

CCL7 was present on 32.3% (± 10.1) of RA lymphatic vessels (figures 3.8 and 3.9A, table 3.3). Colocalisation was identified (figure 3.8) primarily on the larger lymphatic vessels and intimal cells (figure 3.9A and 3.9B). CCL7 and LYVE-1 colocalisation was seen on a number of infiltrating cells (figure 3.8, 3.9C and 3.9D). Staining using CD68 as a marker showed these to be macrophages (figure 3.9C and 3.9D). In the non-RA synovium, CCL7 was shown to be present on 80.0% (± 11.6) of LYVE-1+ vessels (figure 3.10A and 3.10B, table 3.3). Whilst LECs were strongly CCL7 positive on larger lymphatic vessels, small lymphatic vessels were also weakly positive (figure 3.10B). The negative control (figure 3.10C) showed no background staining. The difference in the percentage of lymphatic vessels stained for CCL7 in RA and non-RA tissue was significant ($p = 0.011$), see table 3.3.

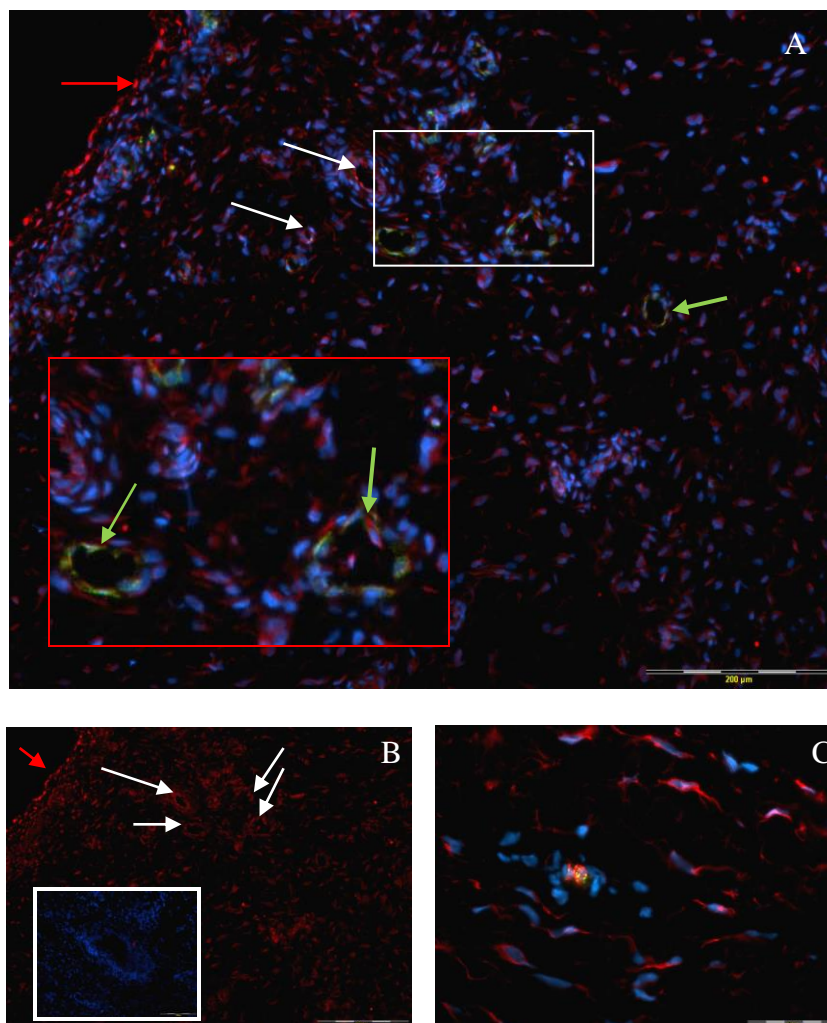


Figure 3.6 CCL7 and VWF staining in RA synovium. **3.6A** shows the merged image for CCL7 (red), VWF (green) and DAPI (blue) on RA sample 1 as a representative example. White arrows indicate CCL7+ vessels, red arrows indicate CCL7+ intimal cells. The inset image (red box) is an enlargement of the area in the white box. A number of CCL7 and VWF+ vessels where co-localisation is evident are indicated by the green arrows. **3.6B** shows the staining for CCL7 (red) only, indicated by white arrows. The inset image shows the merged negative control. Scale bars show 200 μ m. **3.6C** shows CCL7+ cells, which appear to be fibroblasts, and co-localisation of CCL7 and VWF at a single cell. The inset image shows a merged isotype matched negative control image. Scale bars in 3.6A and 3.6B show 200 μ m. Scale bar in 3.6C shows 50 μ m.

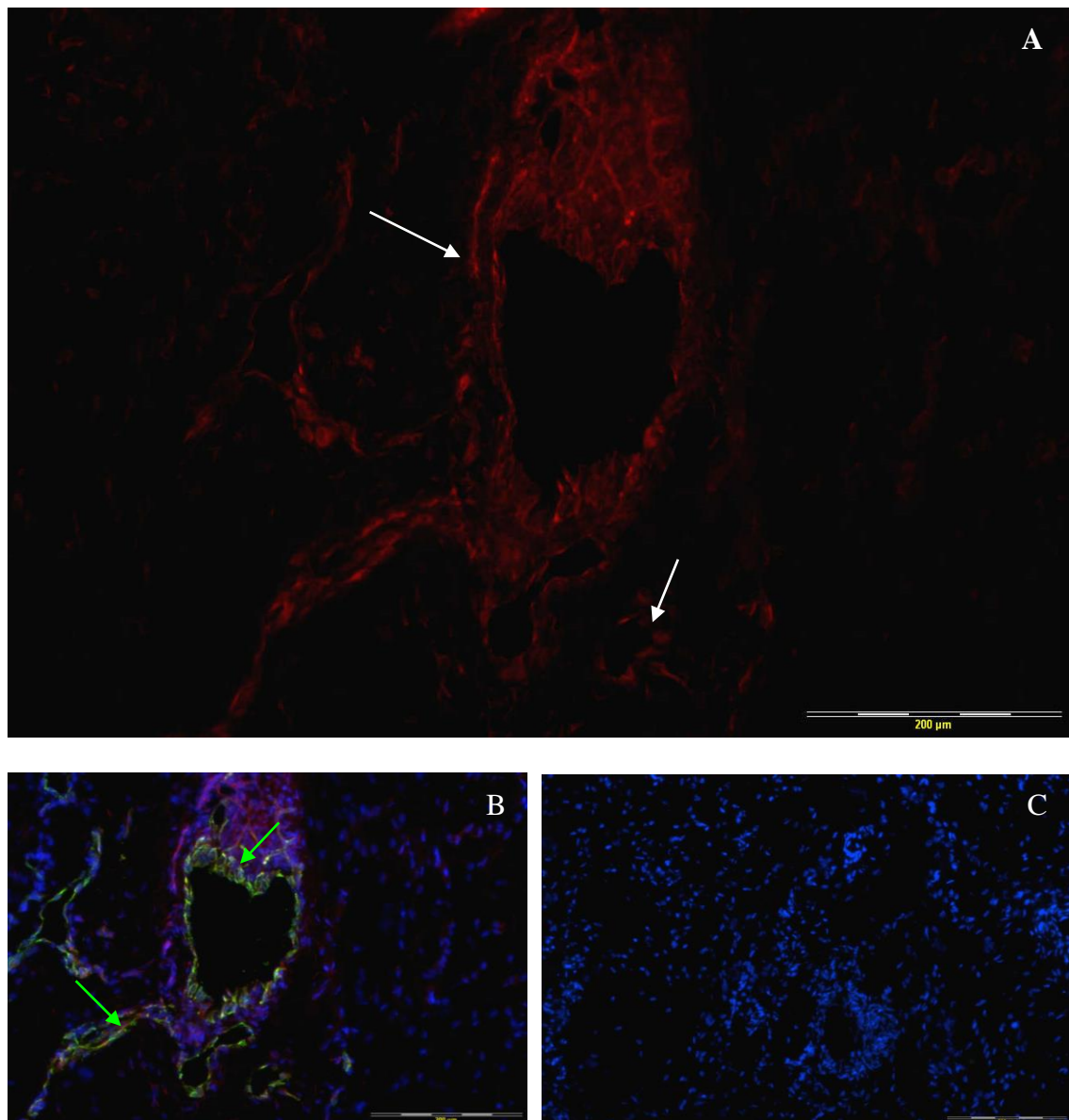


Figure 3.7 CCL7 and VWF staining in non-RA synovium. **3.7A** shows the staining for CCL7 (red) only from non-RA sample 3 as a representative example. White arrows indicate CCL7+ vessels. **3.7B** shows the merge image for CCL7 (red), VWF (green) and DAPI (blue). Colocalisation of CCL7 and VWF is indicated by the green arrows. **3.7C** shows a merged isotype matched negative control image. Scale bars show 200μm.

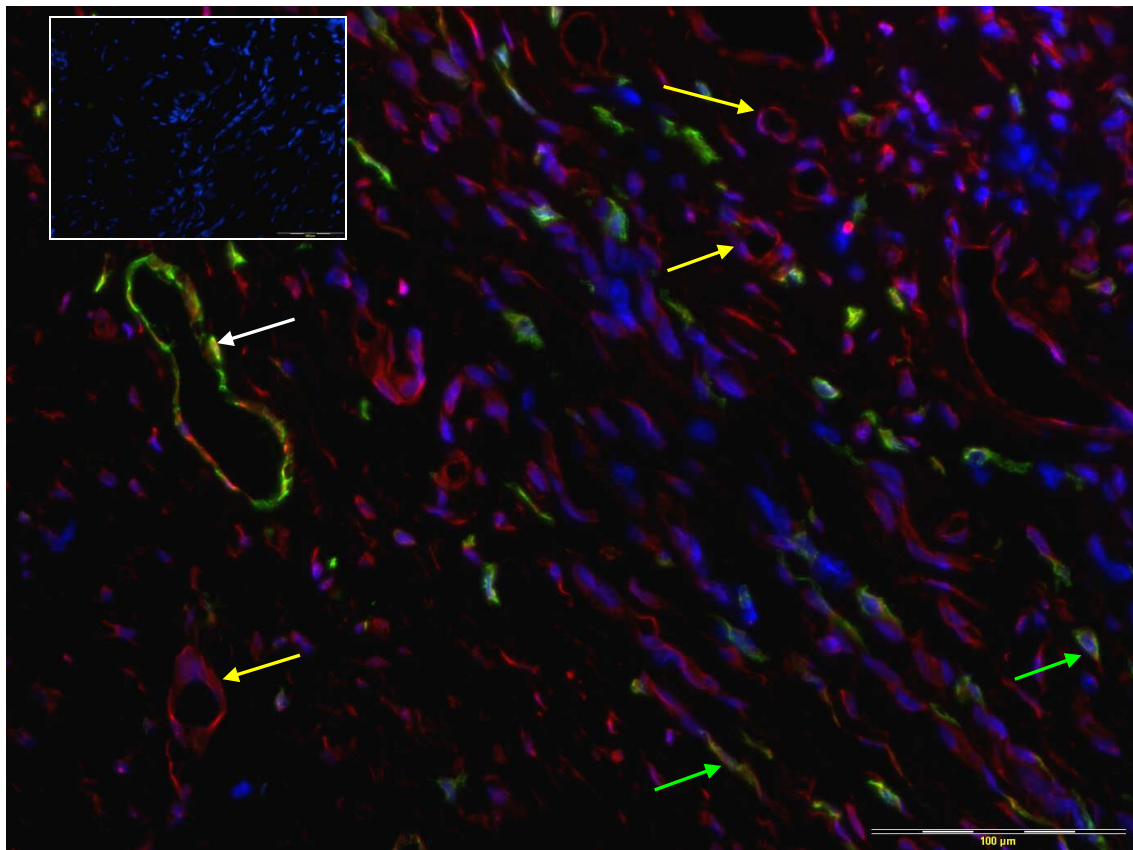


Figure 3.8 CCL7 and LYVE-1 staining in RA synovium. 3.8 shows the merged image of staining for CCL7 (green), LYVE-1 (red), DAPI (blue) from RA sample 1 as a representative example. White arrow indicates CCL7 and LYVE-1 colocalisation. Yellow arrows indicate CCL7 negative vessels. The green arrows indicate CCL7 and LYVE-1 (weakly) on infiltrating cells. The inset image shows the merged isotype matched negative control image. Scale bars show 100 μ m

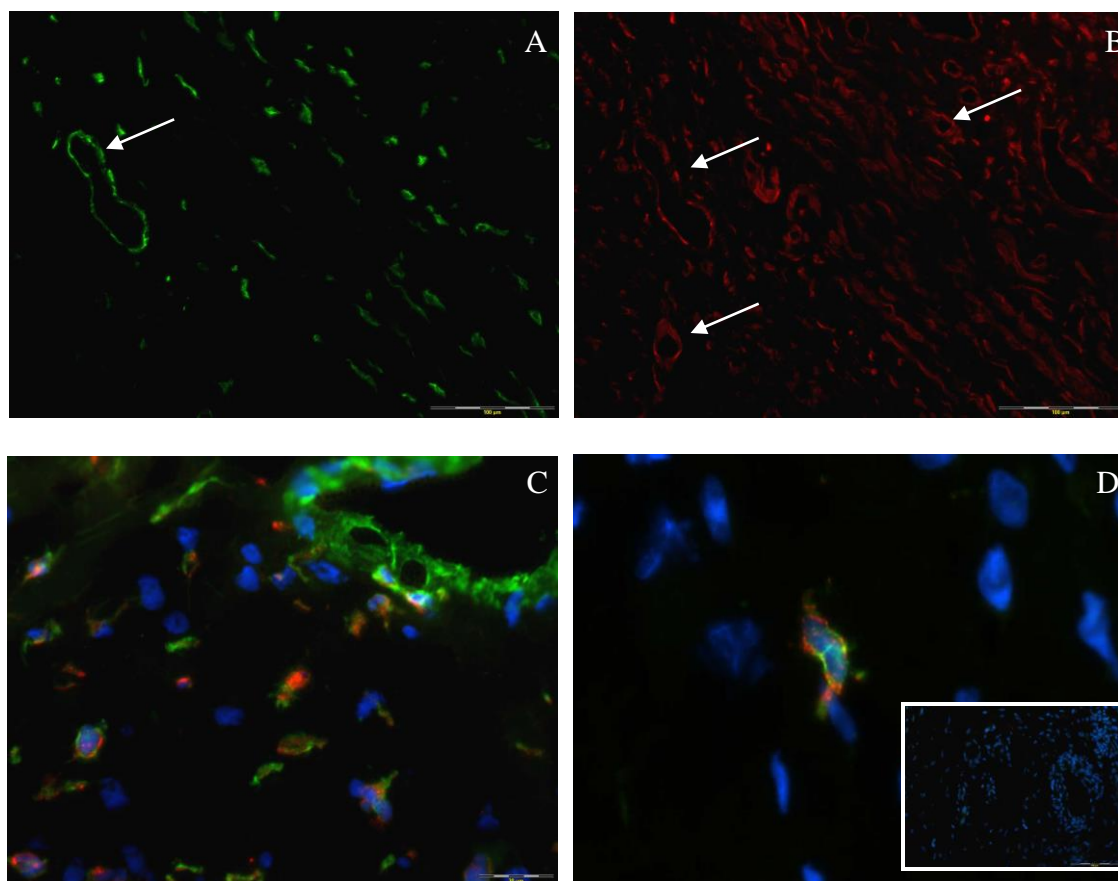


Figure 3.9 CCL7 and LYVE-1 staining in RA synovium . 3.9A shows the CCL7 (green) staining only with white arrow indicating the larger vessel. 3.9B shows the same image for LYVE-1 only (red) with both large and smaller vessels indicated by white arrows. 3.9C and 3.9D show LYVE-1 (green), CD68 (red), and DAPI (blue). 3.9D is an enlarged image (original not shown) at an original magnification of X40 (objective), scale bar shows 20µm. The inset in 3.9D shows the merged negative control image for CD68 staining (X40 objective). All images are from RA sample 1 as representative examples.

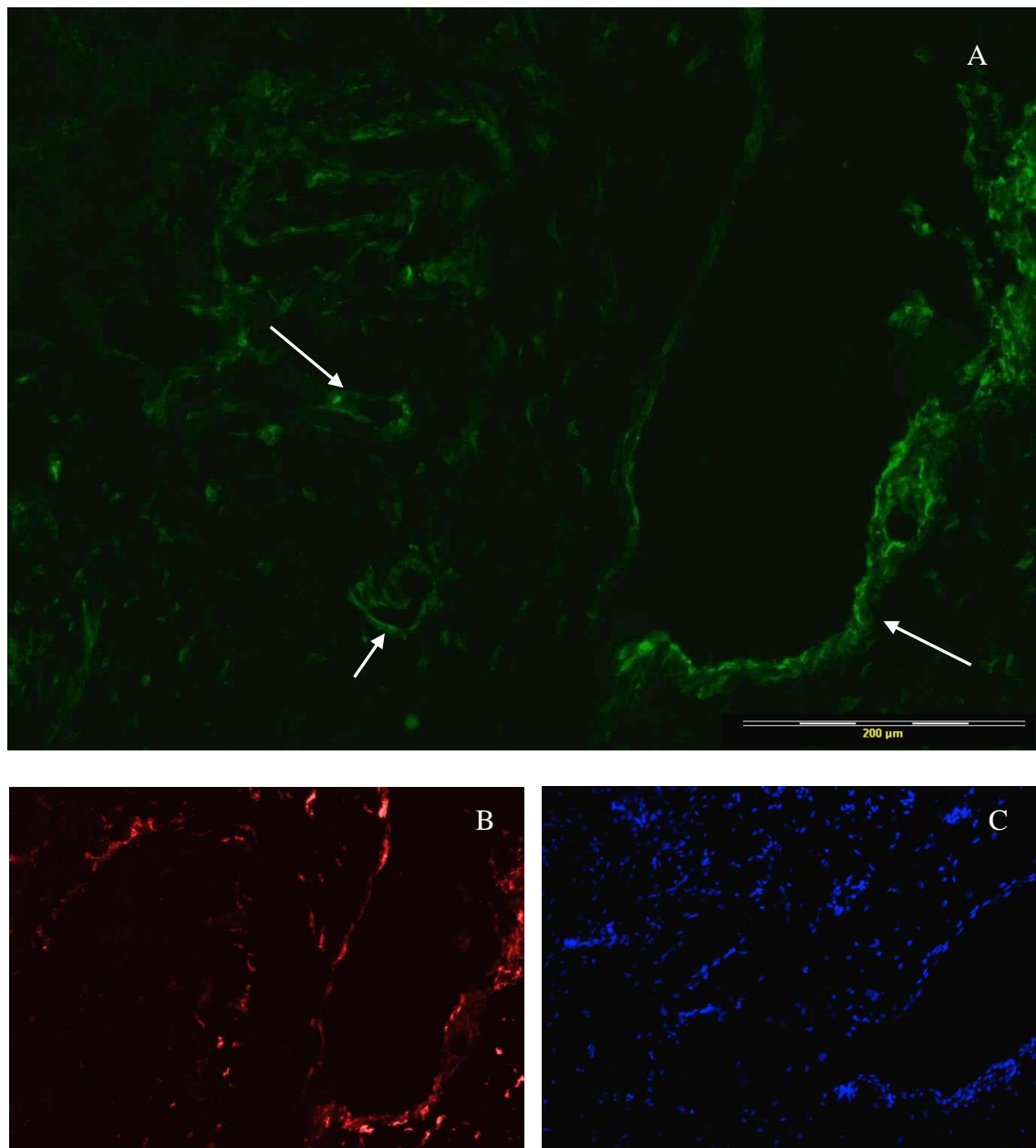


Figure 3.10 CCL7 and LYVE-1 staining in non-RA synovium. **3.10A** shows the staining for CCL7 (green). **3.10B** shows the staining for LYVE-1 only from the same field of view **3.10C** shows the merged isotype matched negative control image. The white arrows indicate CCL7+ vessels (X10 objective). Non-RA sample 4 is shown as a representative example.

3.3.1.8 CCL8 and VWF staining in RA synovial tissue.

CCL8 was present throughout the RA synovium. Strong colocalisation as seen in VWF+ vessels with CCL8+ staining of other cells was also indicated (figure 3.11A) which appeared to be primarily on fibroblasts (3.11B). The percentage of VWF+ vessels stained for CCL8 was shown to be significantly increased in RA (64.1% \pm 7.4) (table 3.2) compared to non-RA (26.6% \pm 17.0) ($p = 0.04$). There was very little visible infiltrate staining (figure 3.12A). The negative control showed no background staining in RA (figure 3.11C) and non-RA tissue (figure 3.12B).

3.3.1.9 CCL10 and VWF staining in RA synovial tissue.

CCL10 was shown to be colocalised on VWF+ vessels and also present on infiltrating cells (figure 3.13A). There was particularly intense staining at the intima (figure 3.13B). Overall, CCL10 was present on 52.6% (\pm 10.0) of VWF+ RA vessels (table 3.1). The negative control (figure 3.13C) showed no background staining.

3.3.1.10 CCL11 and VWF staining in RA synovial tissue.

A number of small VWF+ vessels showed weak staining for CCL11 (figure 3.14A). However, the staining was more intense at larger vessels where infiltrate staining was also present (figure 3.14B). CCL11 was shown to be present on 15.8% (\pm 6.3) of VWF+ RA vessels (table 3.1). The negative control (figure 3.14C) showed no background staining.

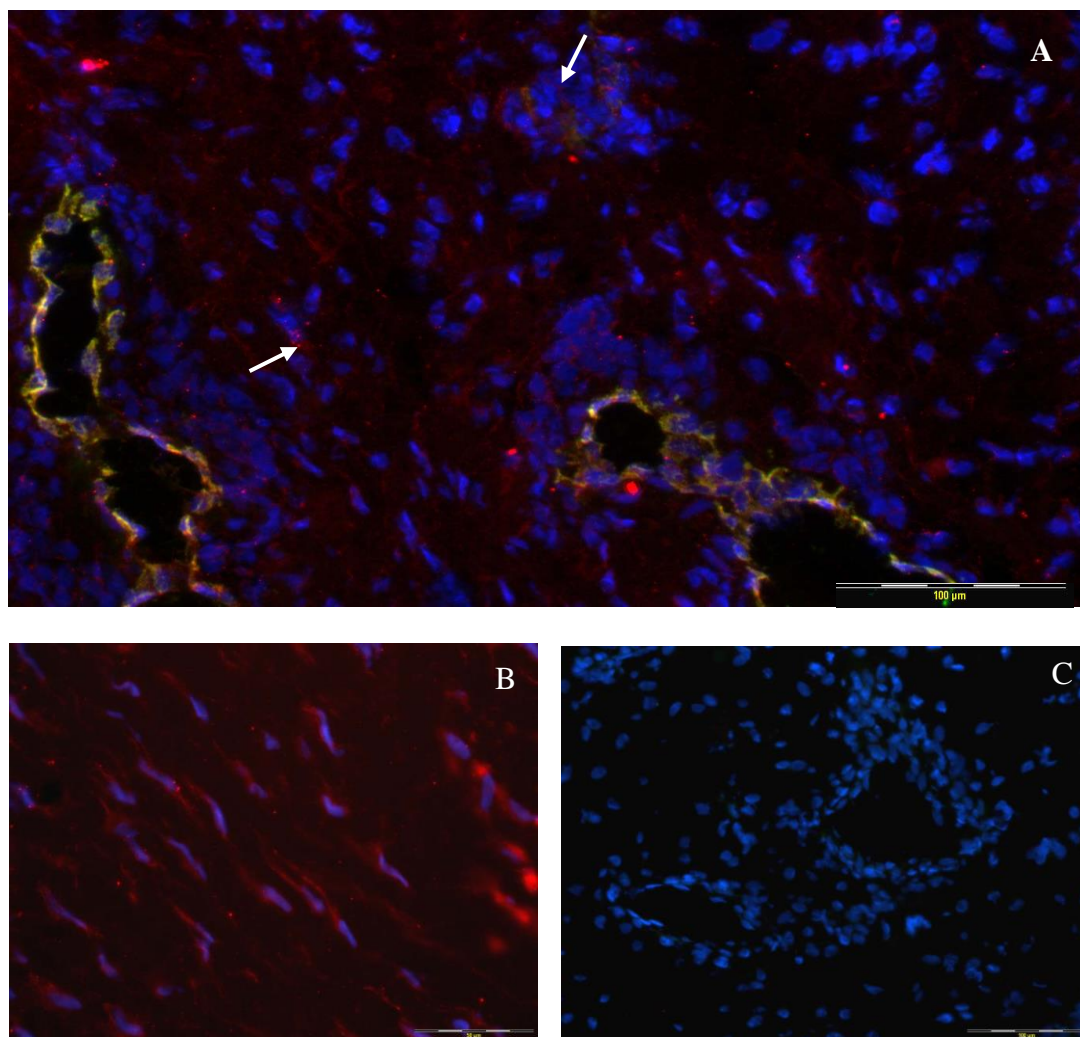


Figure 3.11 CCL8 and VWF staining in RA synovium. 3.11A shows the merged image for staining for CCL8 (red), VWF (green) and DAPI (blue). RA sample 4 is shown as a representative example. Strong colocalisation of CCL8 and VWF at vessels is evident as yellow colouration in 3.11A with CCL8+ infiltrate also being seen, examples of which are highlighted with white arrows 3.11B shows CCL8+ cells which appear to be fibroblast like. 3.11C shows a merged isotype matched negative control image. Scale bars show 100μm throughout.

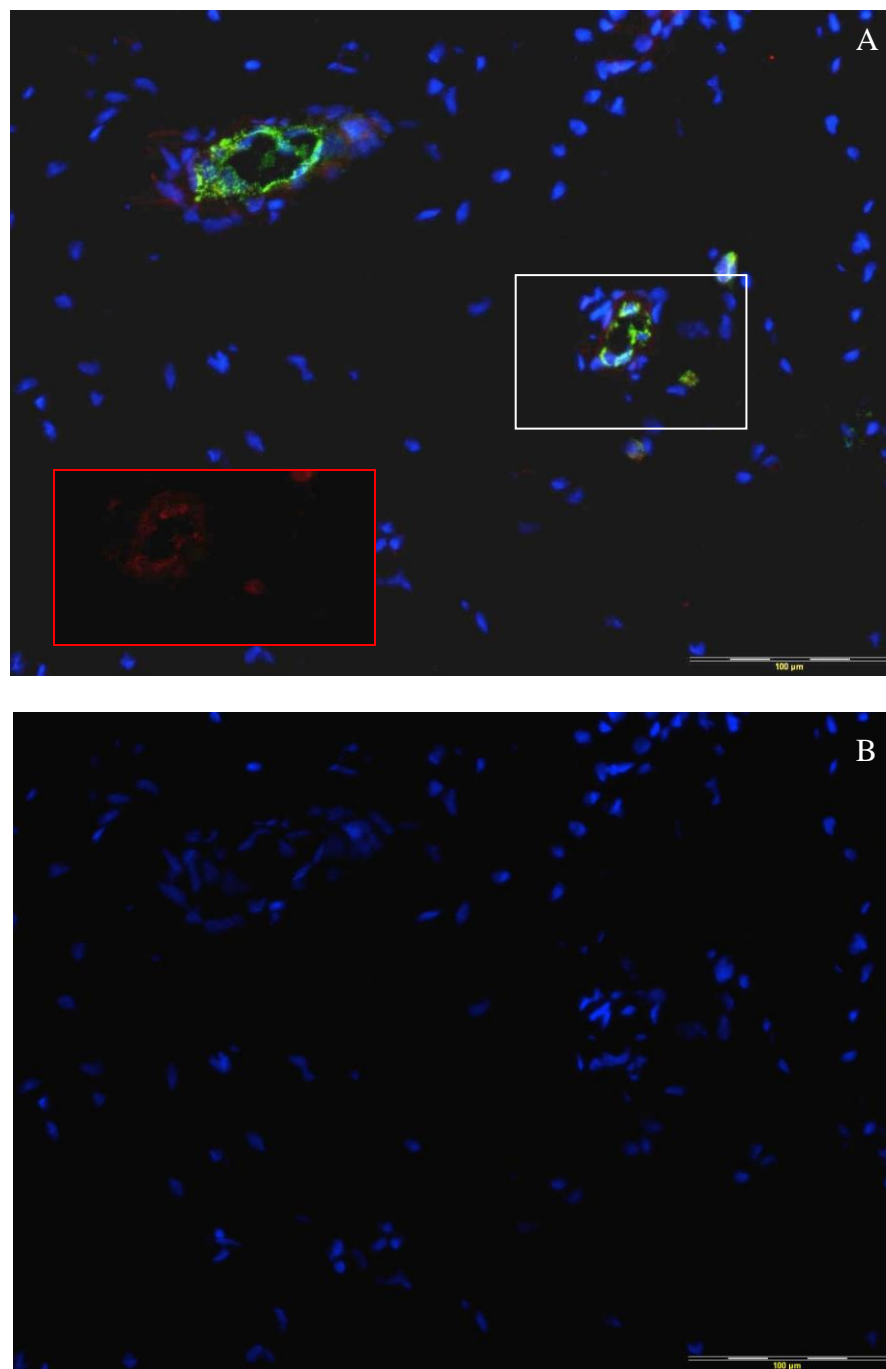


Figure 3.12 CCL8 and VWF staining in non-RA synovium. 3.12A shows the merged image for CCL8 (red), VWF (green) and DAPI (blue) from non-RA sample 3 as a representative example. The inset image (red box) in 3.12A shows CCL8 only from the region in the white box. 3.12B shows a merged isotype matched negative control image. Scale bars show 100μm throughout.

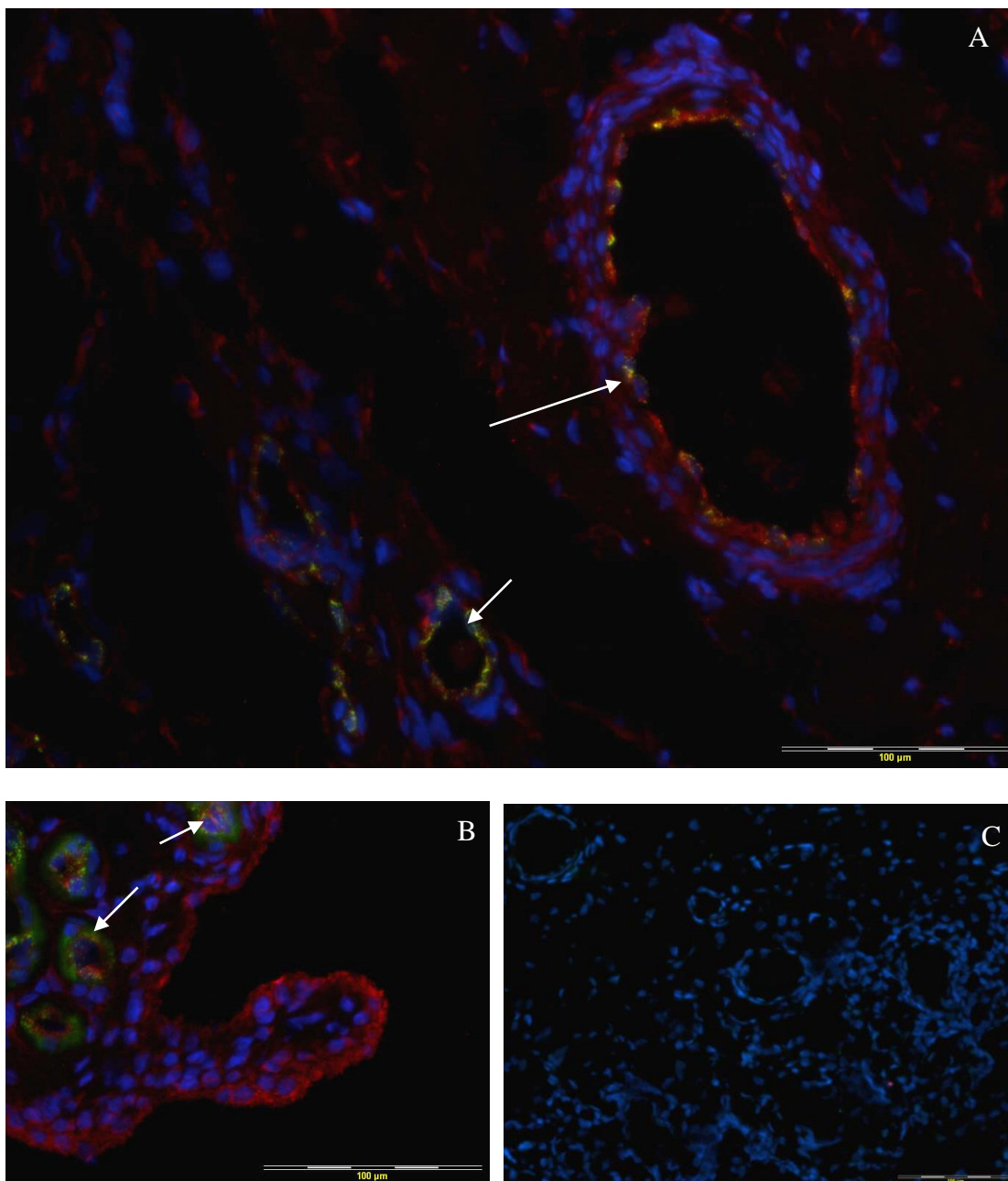


Figure 3.13 CCL10 and VWF staining in RA synovium. 3.13A shows the merged image for staining for CCL10 (red), VWF (green) and DAPI (blue) from RA sample 4 as a representative example. 3.13B shows CCL10+ cells intensely stained at the intima. 3.13C is the merged isotype matched negative control image. The white arrows indicate CCL10+ vessels. Scale bars show 100µm throughout.

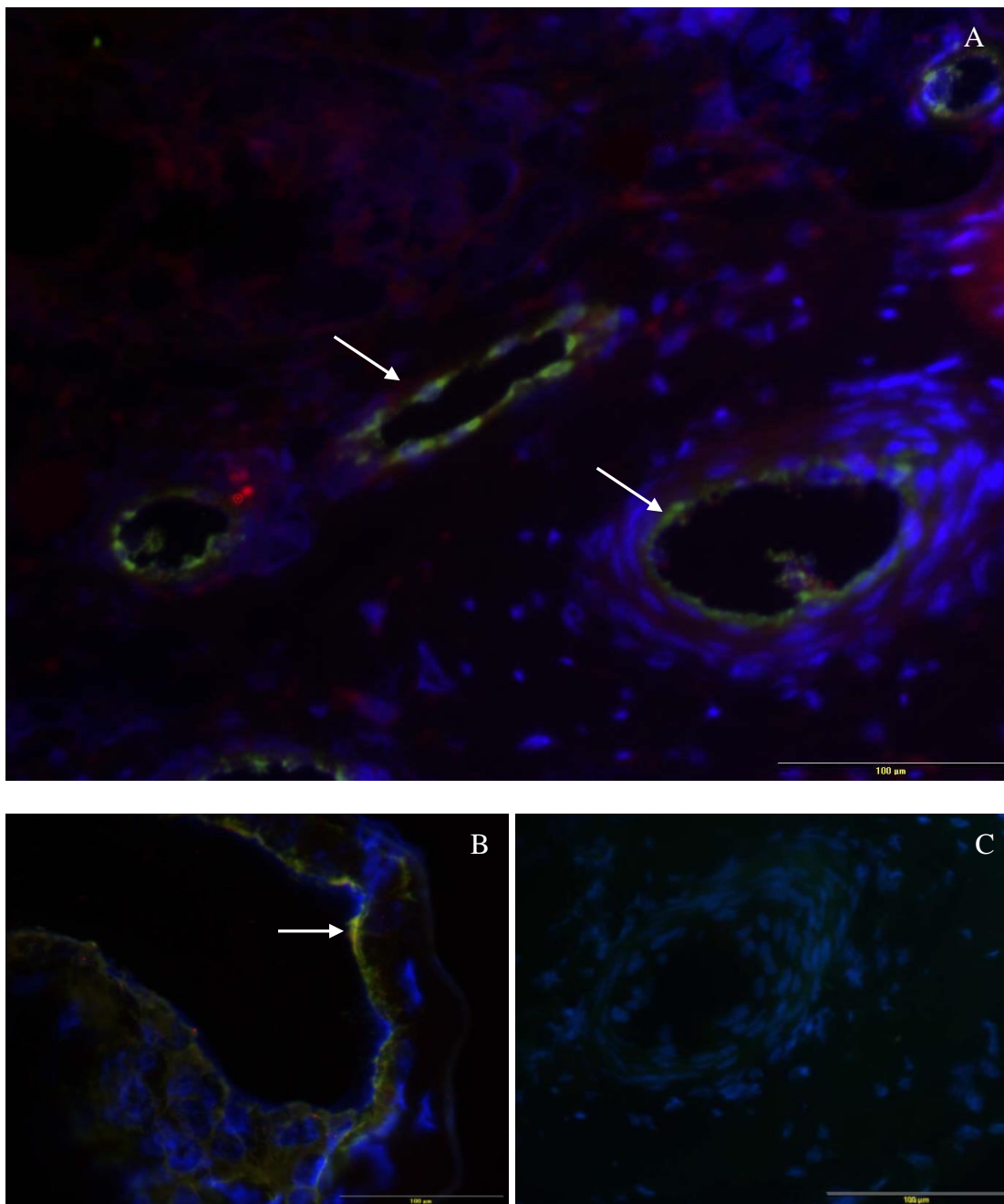


Figure 3.14 CCL11 and VWF staining in RA synovium **3.14A** shows the merged image for staining for CCL11 (red), VWF (green) and DAPI (blue) from RA sample 2 as a representative example, with weakly CCL11+ vessels indicated by white arrows. **3.14B** shows much more intense CCL11 staining on a large vessel with infiltrate staining in the same region. **3.14C** shows a merged isotype matched negative control image. Scale bars show 100 μ m throughout.

3.3.1.11 CCL12 and VWF staining in RA synovial tissue.

CCL12 stained sparsely and very weakly in VWF+ vessels (figure 3.15A, 3.15B) with a small degree of infiltrate staining also seen. CCL12 was shown to be present on 9.6% (± 3.2) of VWF + RA vessels (table 3.1). The negative control (figure 3.15C) showed no background staining.

3.3.1.12 CCL13 and VWF staining in RA synovial tissue.

Colocalisation between CCL13 and VWF was observed (figure 3.16A) in 56.6% (± 7.1) of VWF+ RA vessels (table 3.1). Numerous infiltrating cells were also CCL13+. The negative control (figure 3.16B) showed no background staining.

3.3.1.13 CCL14 and VWF staining in RA and non-RA synovial tissue.

Very strong staining for colocalisation of CCL14 and VWF was seen in RA vessels and on infiltrating cells (figure 3.17A). CCL14 was shown to be present on 73.0% (± 7.0) of VWF+ RA vessels. The negative control (figure 3.17B) showed no background staining. In the non-RA synovium CCL14 staining was present but was markedly weaker (figure 3.18). Overall, CCL14 was present on 28.4% (± 8.2) of VWF+ non-RA vessels (table 3.2). The negative control (3.18B) showed no background staining. The percentage of VWF+ vessels stained for CCL14 was shown to be significantly increased in RA compared to non-RA tissue ($p = 0.0041$), (table 3.2)

3.3.1.14 CCL14 and LYVE-1 staining in RA and non-RA synovial tissue.

Weakly positive CCL14 staining was observed on LYVE-1+ vessels with colocalisation being evident (figure 3.19A, 3.19B). CCL14+ infiltrate was also seen (figures 3.19A, 3.19B). CCL14 was shown to be present on 45.7% (± 11.5) of LYVE-1+ RA vessels (table 3.3). The negative control (figure 3.19C) showed no background staining.

In the non-RA synovium CCL14 was present (figures 3.20A, 3.20B), but to a lesser degree at 40.0% (± 23.2) of LYVE-1+ non-RA vessels. The percentage of LYVE-1+ vessels stained for CCL14 was not significantly different between RA and non-RA tissue ($p = 0.83$), (table 3.3). The negative control (figure 3.14C) showed no background staining.

3.3.1.15 CCL15 and VWF staining in RA synovial tissue.

CCL15 staining was seen in numerous VWF+ vessels (figure 3.21A) with strong staining in the cells of the intima (figure 3.21 B). Infiltrate staining was seen to be primarily at cells near the vessels or intima. CCL15 was shown to be present on 47.3% (± 6.3) of VWF+ RA vessels (table 3.2). The negative control (figure 3.21C) showed no background staining.

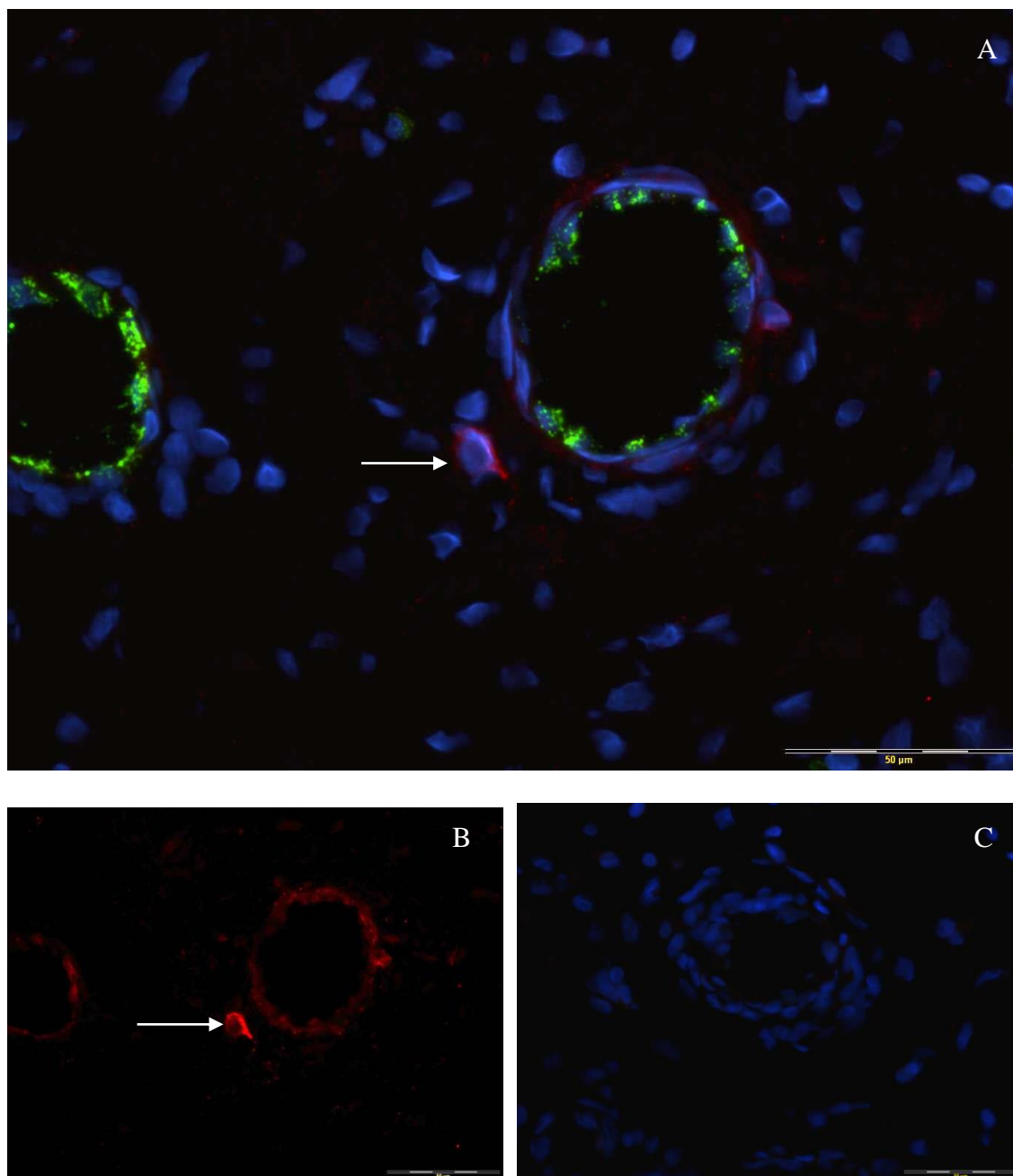


Figure 3.15 CCL12 and VWF staining in RA synovium. 3.15A shows the merged image for staining for CCL12 (red), VWF (green) and DAPI (blue) from RA sample 1 as a representative example, with a weak CCL12+ vessel and a CCL12+ infiltrated cell indicated with a white arrow. 3.15B shows the CCL12 staining only and 3.15C shows a merged isotype matched negative control image. Scale bars show 50μm throughout.

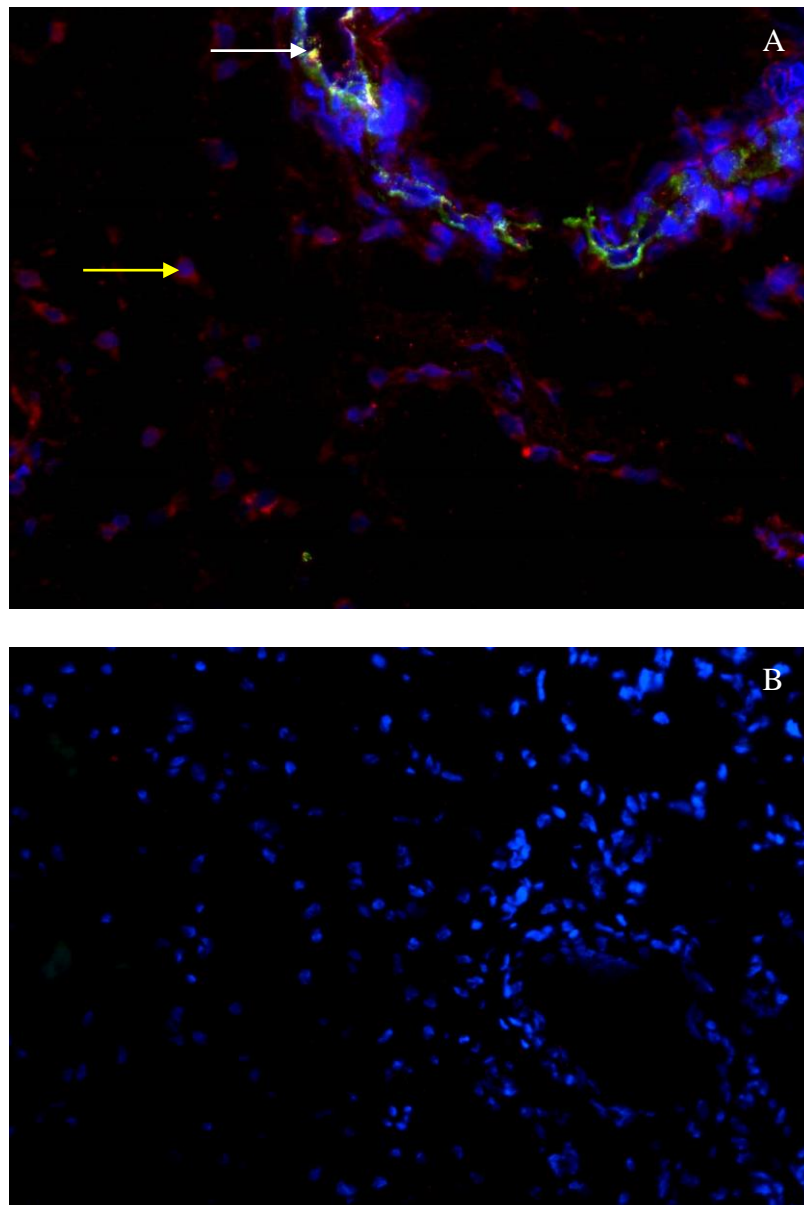


Figure 3.16 CCL13 and VWF staining in RA synovium. **3.16A** shows the merged image for staining for CCL13 (red), VWF (green) and DAPI (blue) from RA sample 3 as a representative example with colocalisation for a VWF+ and CCL13+ vessel indicated with a white arrow. Examples of CCL13+ infiltrate cells indicated with a yellow arrow (original magnification X40 objective). **3.16B** shows a merged isotype matched negative control image (magnification X20 objective).

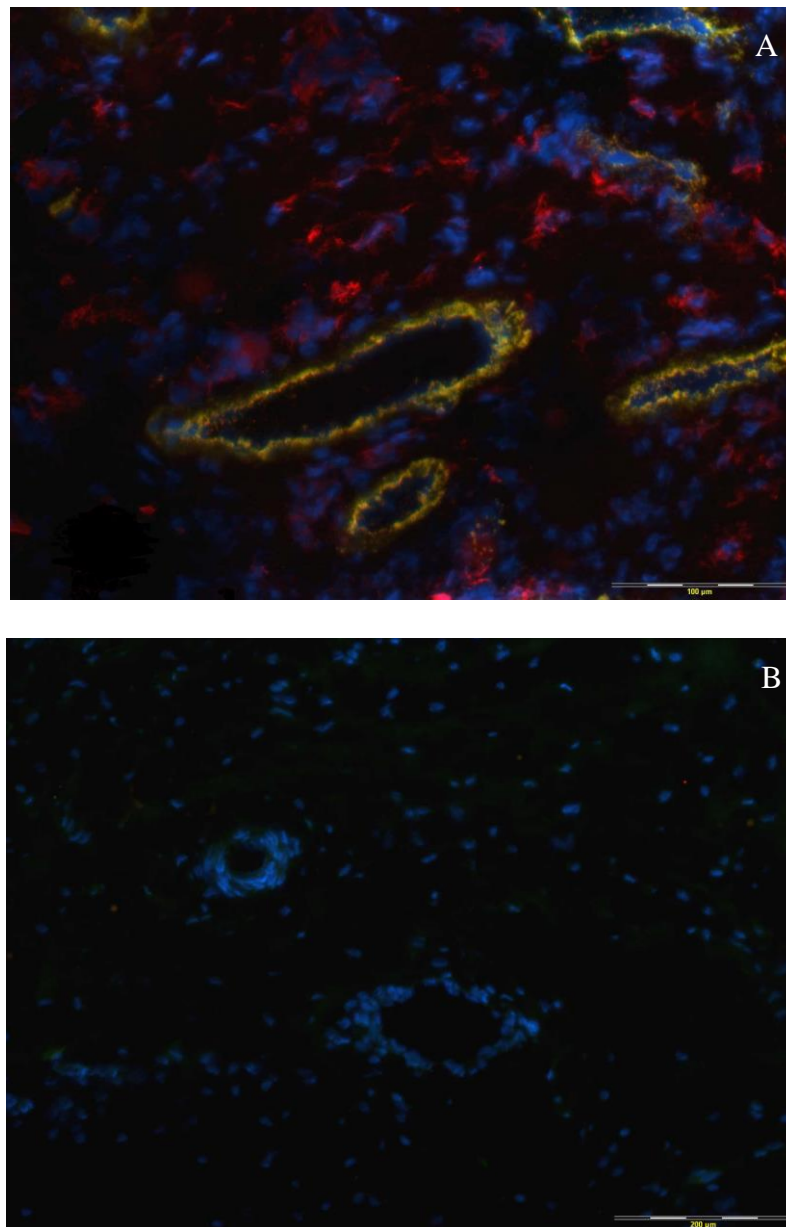


Figure 3.17 CCL14 and VWF staining in RA synovium. 3.17A shows the merged image for staining for CCL14 (red), VWF (green) and DAPI (blue) from RA sample 7 as a representative example. Strong colocalisation is seen where the vessels appear to be yellow and CCL14+ infiltrating cells are also seen. **3.17B** shows a merged isotype matched negative control. Scale bars show 100μm in 3.17A and 200μm in 3.17B.

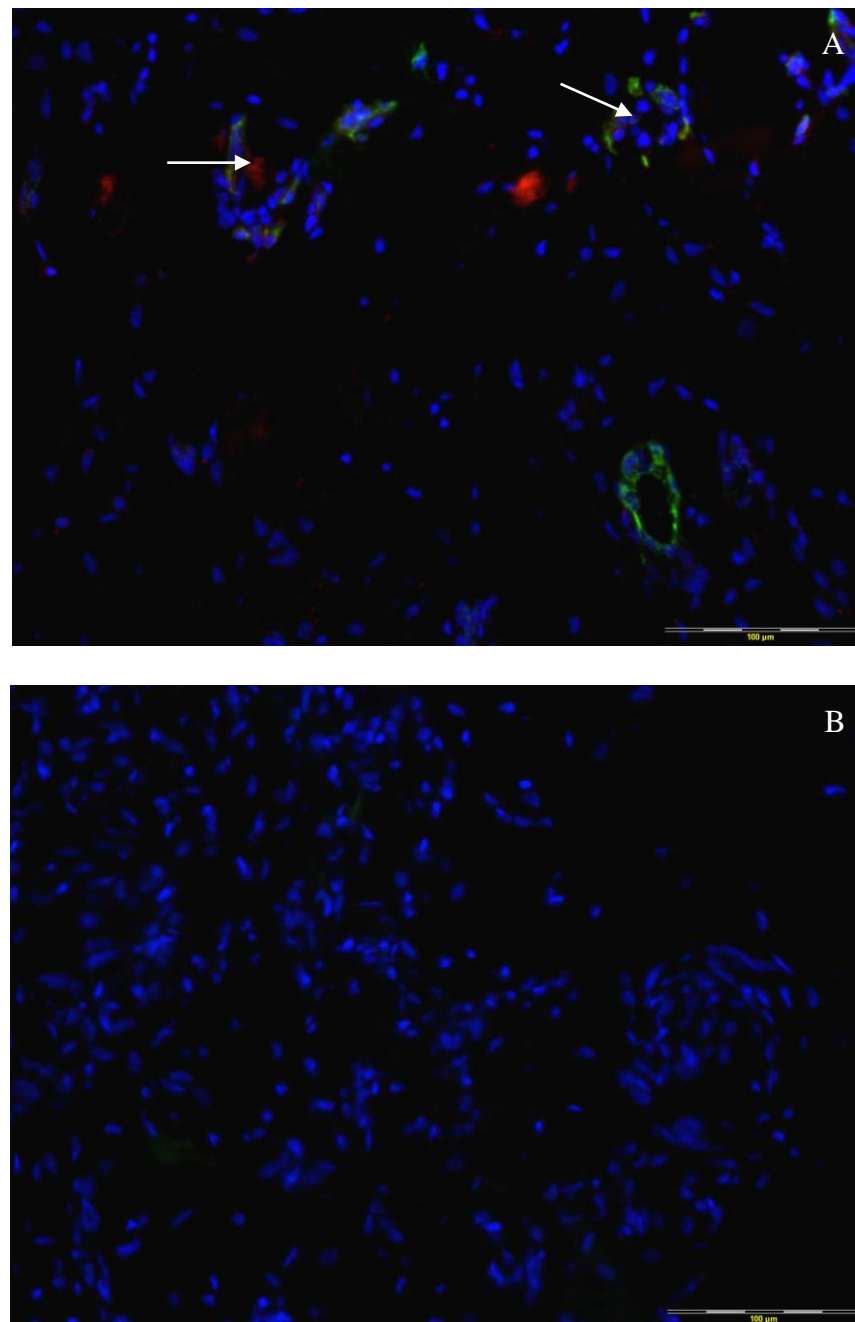


Figure 3.18 CCL14 and VWF staining in non-RA synovium. 3.18A shows the merged image for staining for CCL14 (red), VWF (green) and DAPI (blue) in non-RA sample 3 as a representative example. Weak CCL14 staining is indicated with a white arrow. 3.18B shows a merged isotype matched negative control. Magnification X20 objective, scale bars show 100 μ m.

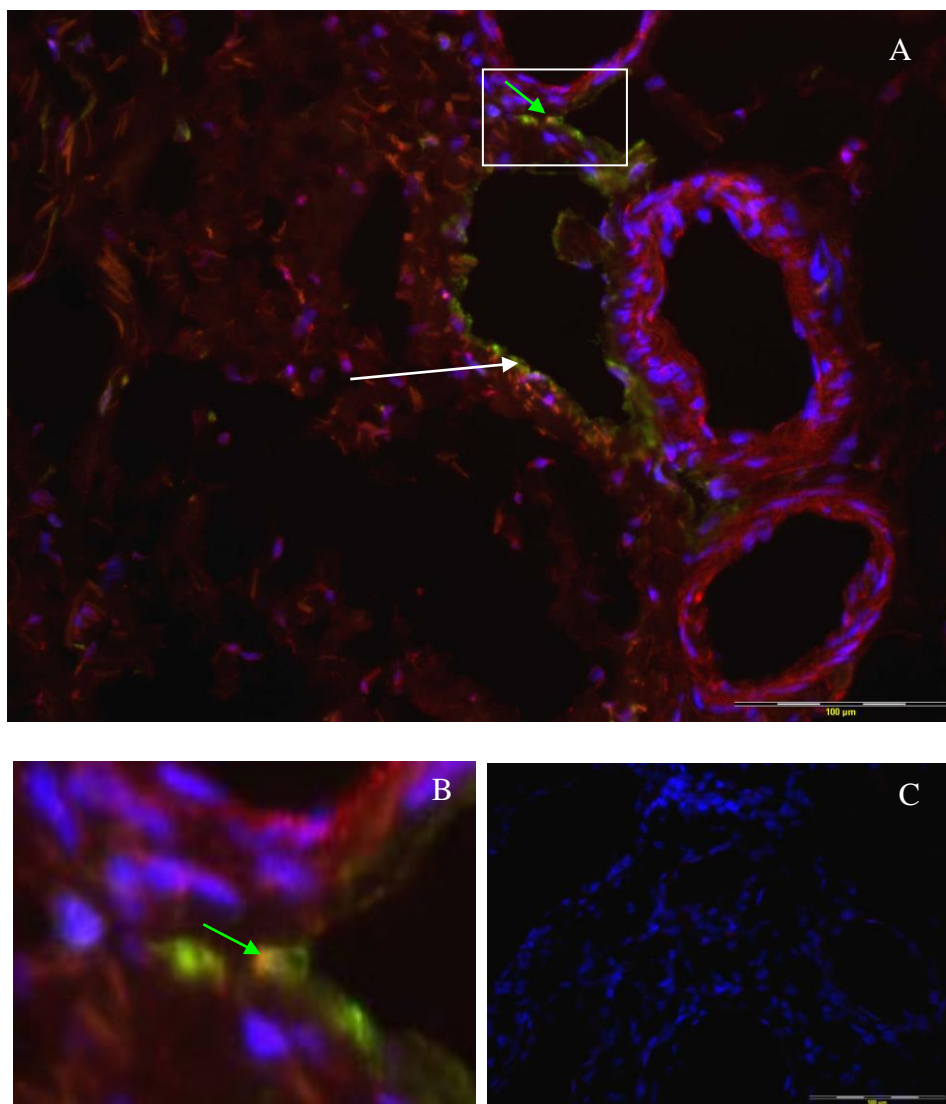


Figure 3.19 CCL14 and LYVE-1 staining in RA synovium. **3.19A** shows the merged image for staining for CCL14 (red), LYVE-1 (green) and DAPI (blue) in RA sample 8 as a representative example. Weak LYVE-1 staining on a lymphatic vessel is indicated with a white arrow. **3.19B** shows the area in the white box of 3.18A close up where colocalisation is evident as orange colouration marked with the green arrow (original magnification X20 objective). **3.19C** shows the merged isotype matched negative control image. Magnification, X20 objective. Scale bars show 100µm.

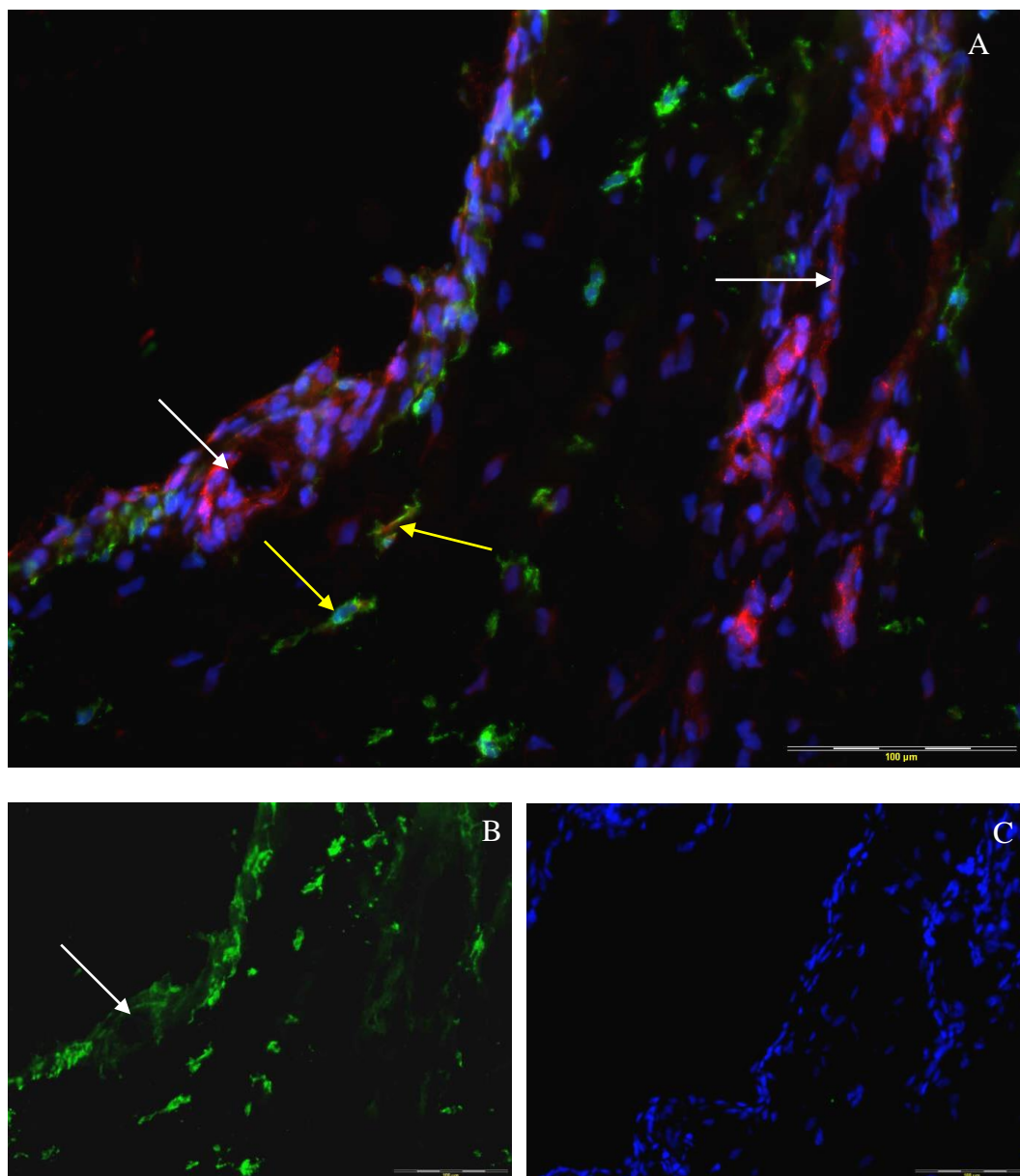


Figure 3.20 CCL14 and LYVE-1 staining in non-RA synovium. **3.20A** shows the merged image for staining for CCL14 (red), LYVE-1 (green) and DAPI (blue) from non-RA sample 3 as a representative example. White arrows indicate CCL14+ vessels. Weakly positive CCL14 and LYVE-1+ stromal cells are indicated with yellow arrows. **3.20B** shows weak LYVE-1 staining on a lymphatic vessel (white arrow). **3.20C** shows the merged isotype matched negative control image. Scale bars show 100µm.

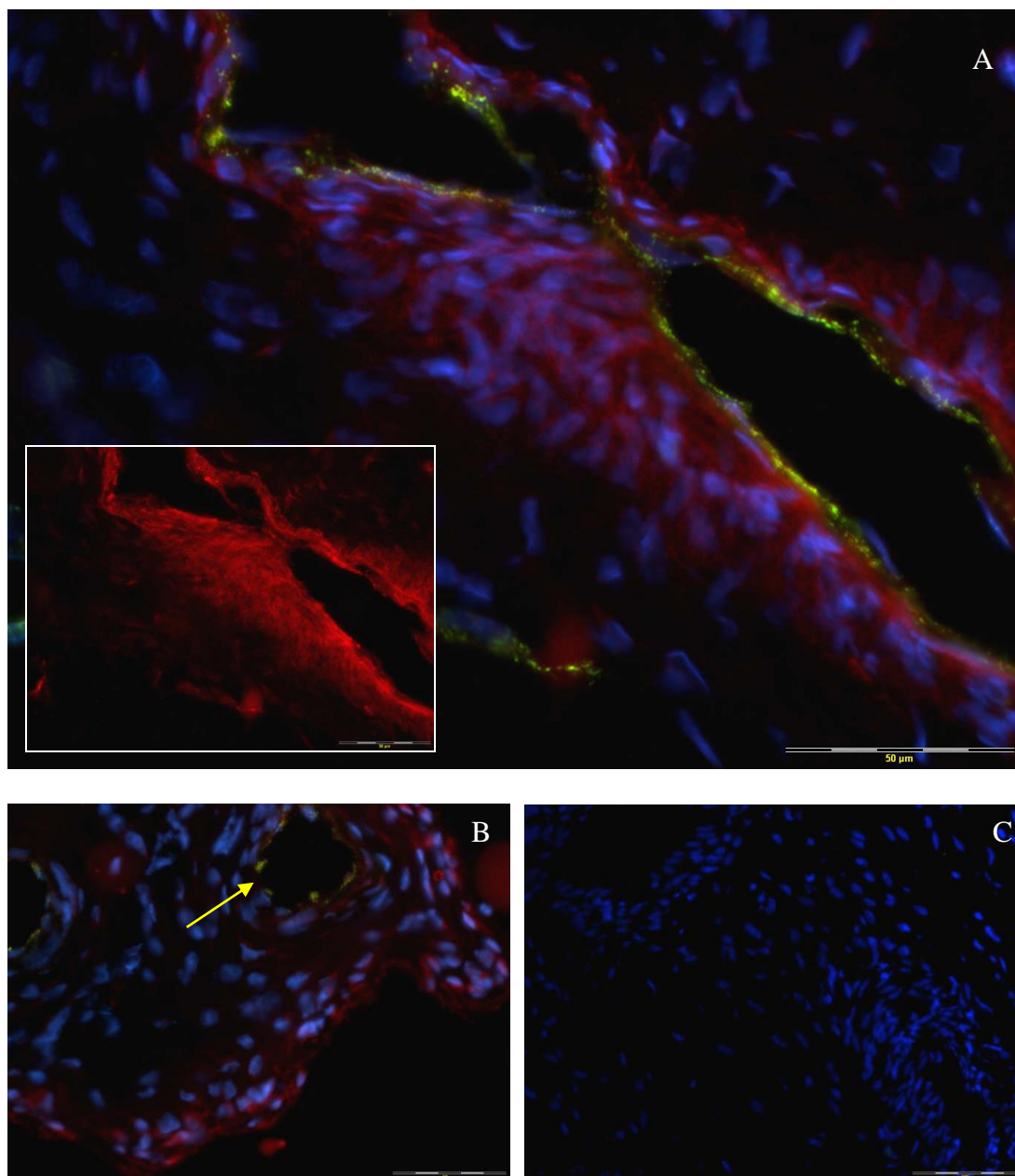


Figure 3.21 CCL15 and VWF staining in RA synovium. **3.21A** shows the merged image for staining for CCL15 (red), VWF (green) and DAPI (blue) from RA sample 2 as a representative example. Inset image shows the CCL15 staining only. **3.21B** shows strong staining for CCL15 in the intima with a weakly positive vessel indicated by the yellow arrow. **3.21C** shows the merged isotype matched negative control image. Scale bars show 50 μ m in 3.21A and 3.21B. Scale bar shows 100 μ m in 3.21C.

3.3.1.16 CCL16 and VWF staining in RA and non-RA synovial tissue.

In RA synovium a high degree of CCL16 staining was seen in vessels (figure 3.22A and 3.22B) with minimal infiltrate staining. CCL16 was shown to be present on 74.1% (± 7.2) of VWF+ RA vessels. CCL16 and VWF colocalisation was evident throughout the synovium (figure 3.22A). The negative control (figure 3.22C) showed no background staining. CCL16 was present in the non-RA synovium at 75.3% (± 7.0) of VWF+ vessels (figure 3.23A, 3.23B). The percentage of vessels stained for CCL16 was not significantly different when RA and non-RA tissue was compared ($p = 0.089$), (table 3.3). The negative control (figure 3.23C) showed no background staining.

3.3.1.17 CCL16 and LYVE-1 staining in RA and non-RA synovial tissue.

CCL16 was highly represented in the RA synovium at 65.4% (± 8.0) of LYVE-1+ RA vessels (figure 3.24A) where some infiltrate staining for LYVE-1 was also observed (table 3.3). The negative control (3.24B) showed no background staining.

In the non-RA synovium CCL16 and LYVE-1 colocalisation was also apparent (figure 3.25A, 3.25B) and CCL16 was present on 60.0% (± 23.2) of LYVE-1+ non-RA vessels which was not significantly different ($p = 0.80$) (table 3.3) to the percentage in RA tissue. The negative control (figure 3.25C) showed no background staining.

3.3.1.18 CCL17 and VWF staining in RA synovial tissue.

Only minute amounts of CCL17 could be found on a very small number of vessel ECs (figure 3.26) with infiltrating cells also being CCL17+. CCL17 was shown to be present on 17.4% (± 10.6) of VWF+ RA vessels (table 3.1).

3.3.1.19 CCL18 and VWF staining in RA synovial tissue.

CCL18 was shown to be present on 38.0% (± 6.2) of VWF+ RA vessels (table 3.1). Infiltrate staining was primarily seen to be on cells in close association with CCL18+ vessels (figure 3.27).

3.3.1.20 CCL19 and VWF staining in RA and non-RA synovial tissue.

Colocalisation between CCL19 and VWF was observed at RA vessels. Overall, CCL19 was shown to be present on 80.0% (± 4.5) of VWF+ RA vessels (figure 3.28A). Infiltrating cells were also positive for CCL19. It was also observed that more intense CCL19 staining appeared to be present in the regions of lymphoid follicle development. The negative control (figure 3.28B) showed no background staining. In the non-RA synovium CCL19 was only present on a small number of VWF+ vessels; primarily the larger vessels (figure 3.29A, 3.29B). CCL19 was shown to be present on 10.3% (± 2.6) of VWF+ non-RA vessels (table 3.2). The difference in the percentage of VWF+ vessels stained for CCL19 in RA and non-RA was highly significant ($p = <0.0001$). The negative control (figure 3.29C) showed no background staining.

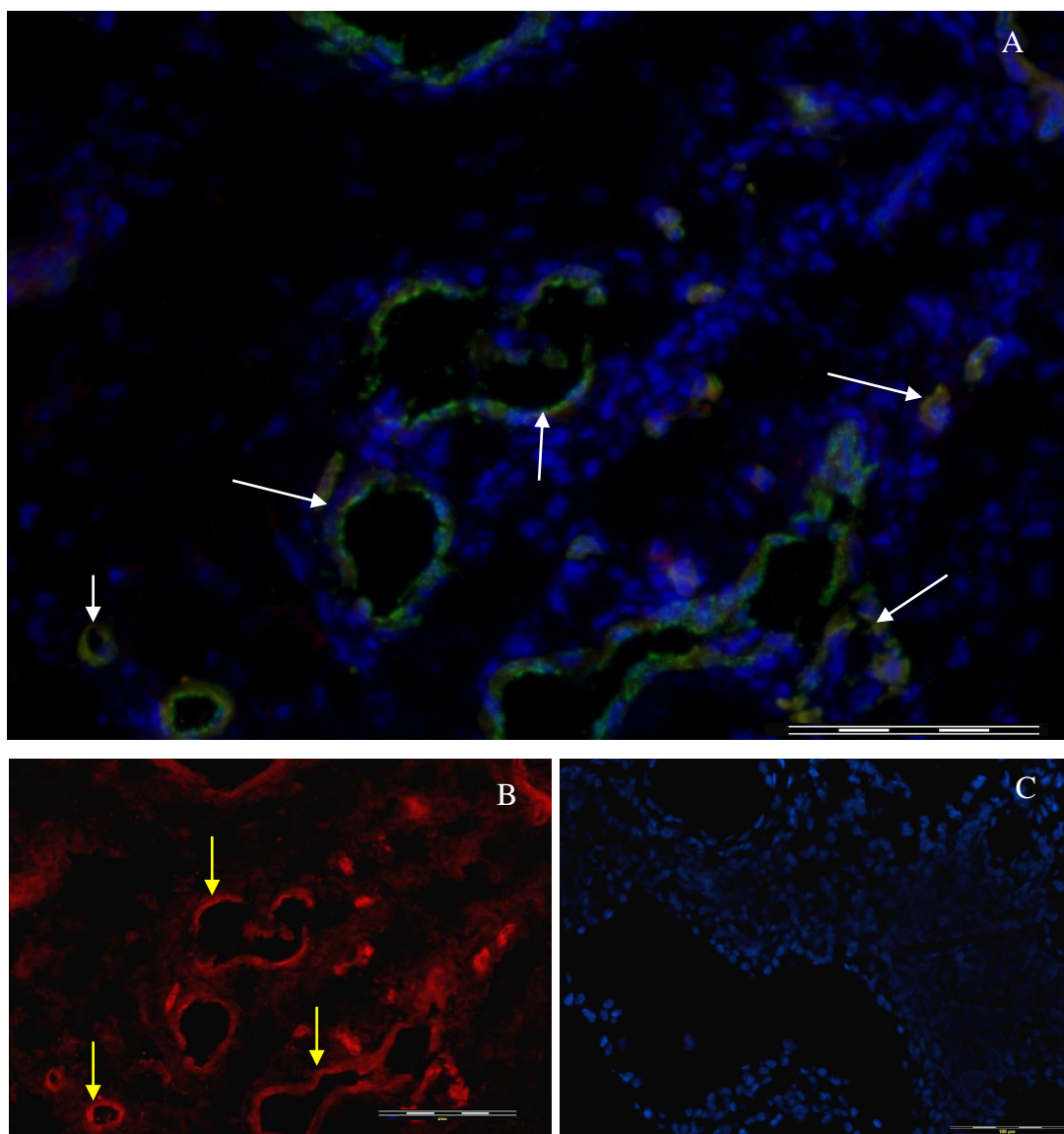


Figure 3.22 CCL16 and VWF staining RA synovium. **3.22A** shows a merged image of CCL16 (red), VWF (green) and DAPI (blue) stain on RA sample 4 as a representative example, where white arrows indicate regions of CCL16 and VWF colocalisation which appear more yellow in colour. **3.22B** shows the result of staining for CCL16 (red). The yellow arrows indicate CCL16+ vessels. **3.22C** shows the merged isotype matched negative control. Scale bars show 100 μ m.

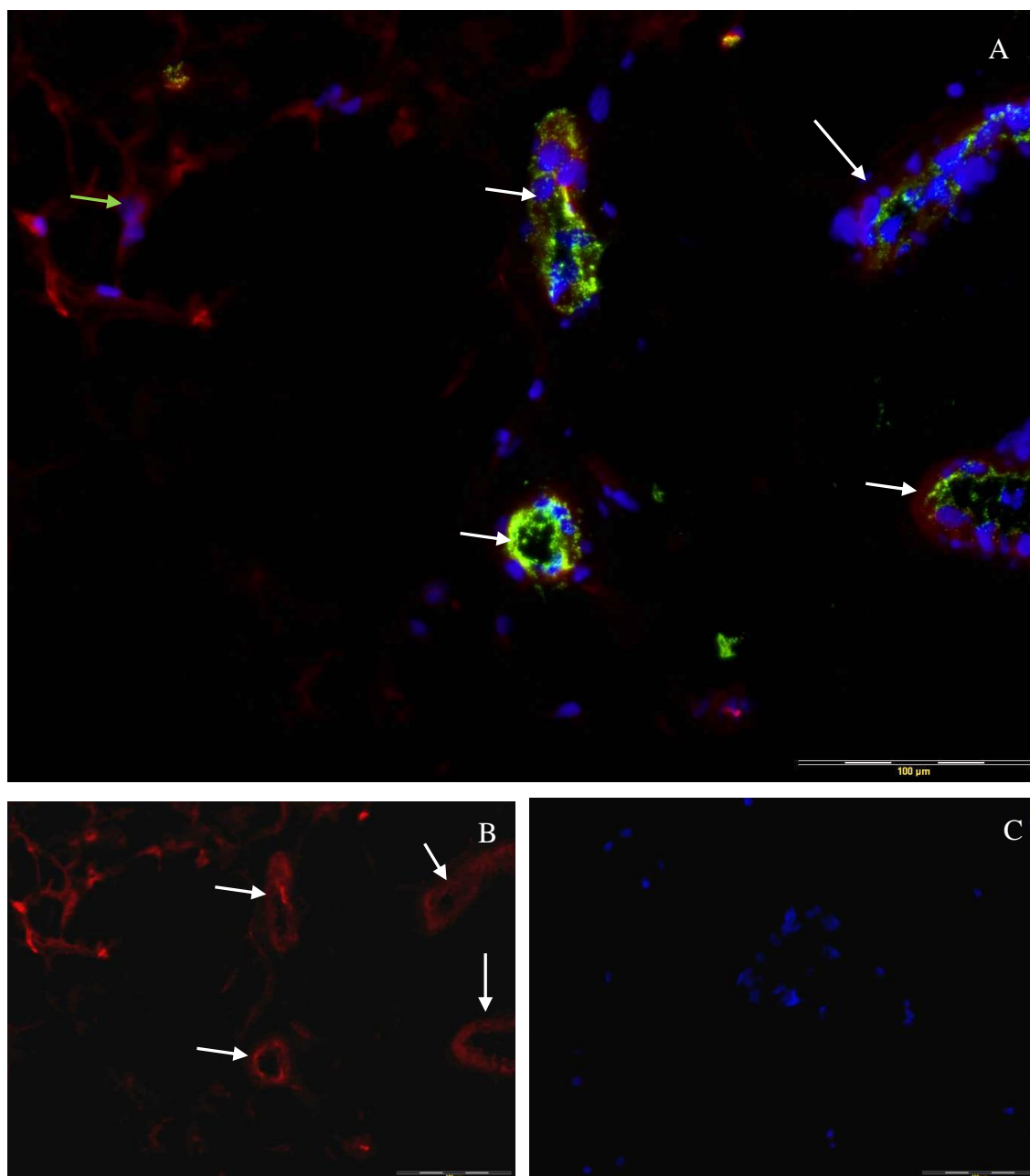


Figure 3.23 CCL16 and VWF staining in non-RA synovium. **3.23A** shows a merged image of CCL16 (red), VWF (green) and DAPI (blue) from RA sample 7 as a representative example. An example of a CCL16+ stromal cell is indicated by a green arrow. **3.23B** shows staining for CCL16 only. The vessels which are CCL16+ and VWF+ are indicated by white arrows in 3.23A and 3.23B. **3.23C** is a merged isotype matched negative control image. Scale bars show 100µm.

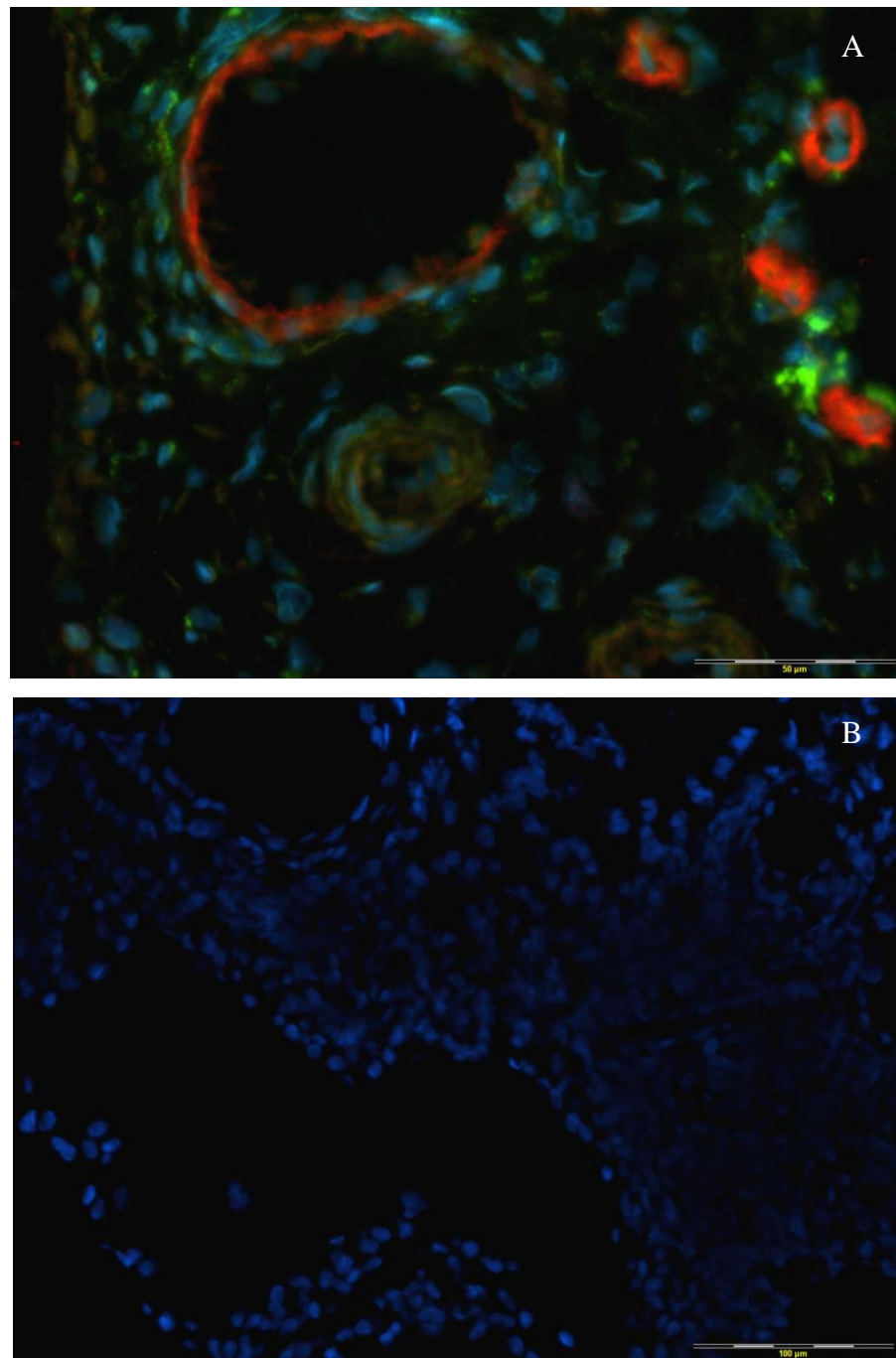


Figure 3.24 CCL16 and LYVE-1 staining in RA synovium. 3.24A shows a merged image of CCL16 (red), LYVE-1 (green) and DAPI (blue) from RA sample 5 as a representative example. A number of infiltrating cells are seen to be LYVE-1+. Scale bar shows 50μm. 3.24B shows a merged isotype matched negative control image. Scale bar shows 100μm.

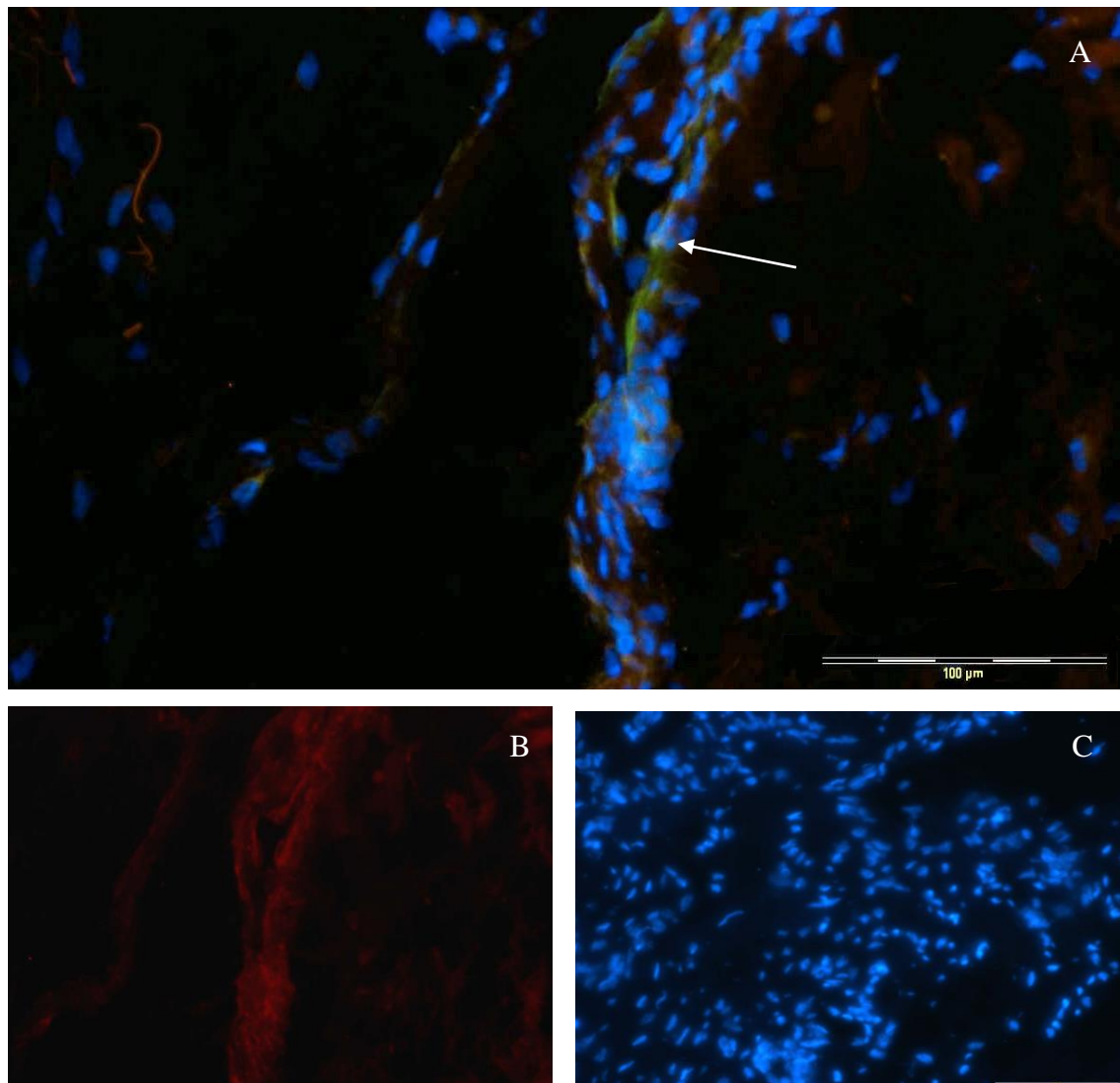


Figure 3.25 CCL16 and LYVE-1 staining in non-RA synovium. 3.25A is a merged image of CCL16 (red), LYVE-1 (green) and DAPI (blue) from non-RA sample 2 as a representative example. A CCL16 and LYVE-1+ vessel is indicated by the white arrow. 3.25B shows the same image with only the CCL16 staining. 3.25C shows a merged isotype matched negative control image. Scale bars shows 100μm.

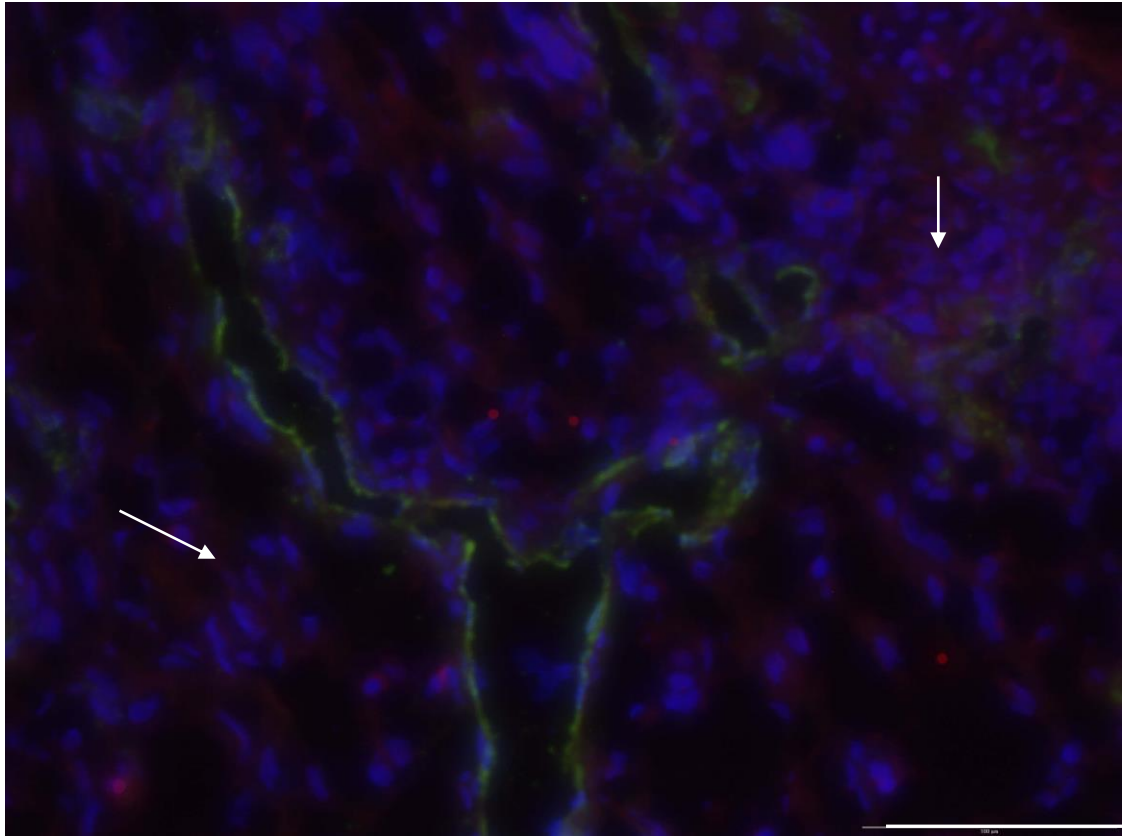


Figure 3.26 CCL17 and VWF staining in RA synovium. 3.26 shows a merged image of staining for CCL17 (red), VWF (green) and DAPI (blue) from RA sample 1 as a representative example. Regions of CCL17+ infiltrate are indicated by the white arrows. Scale bar shows 100 μ m.

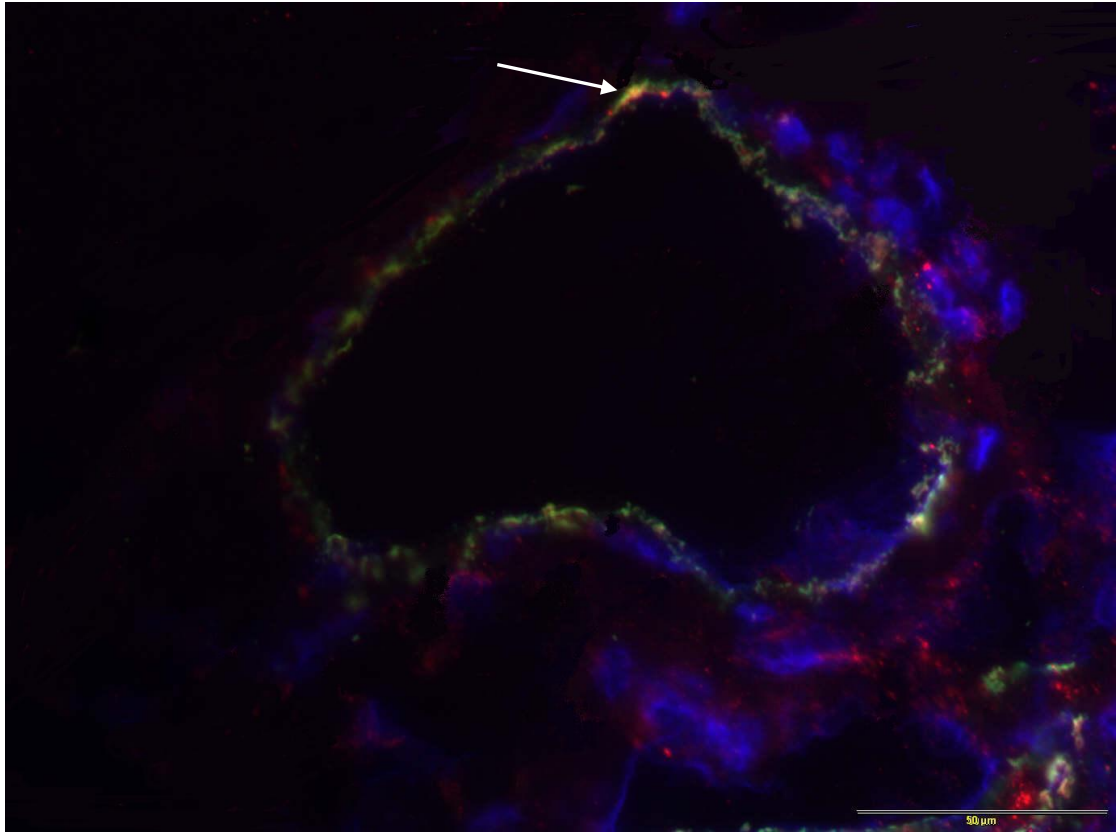


Figure 3.27 CCL18 and VWF staining in RA synovium. 3.27 shows a merged image of staining for CCL18 (red), VWF (green) and DAPI (blue) from RA sample 1 as a representative example. A point of colocalisation which appears orange/yellow in colour is indicated by the white arrow. Scale bar shows 50 μ m.

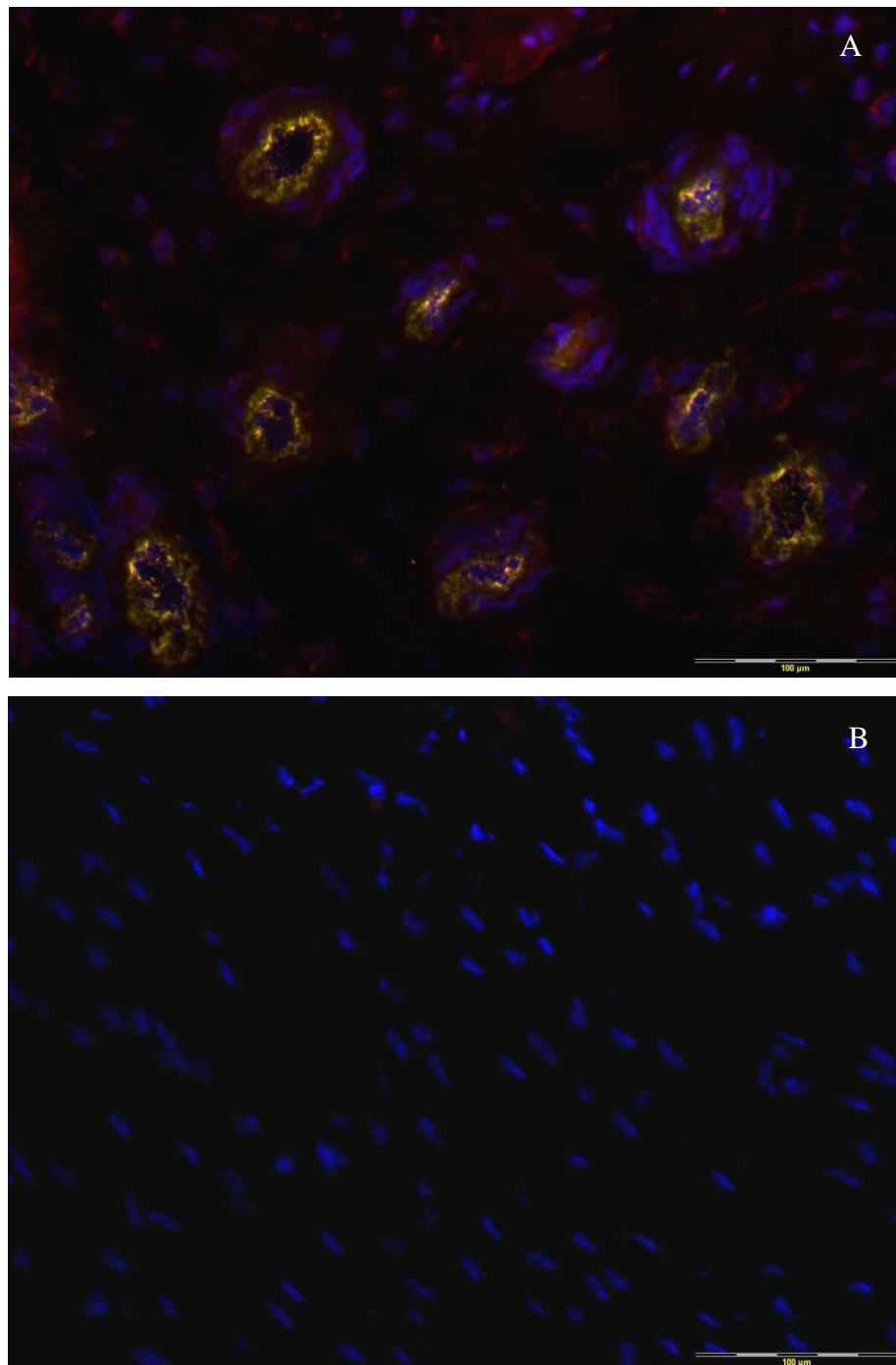


Figure 3.28 CCL19 and VWF staining in RA synovium. 3.28A shows strong staining for CCL19 (red), VWF (green) and DAPI (blue) from RA sample 3 as a representative example. Colocalisation for CCL19 and VWF is seen as yellow colouration on the numerous vessels. **3.28B** shows the merged negative control. Scale bars show 100μm.

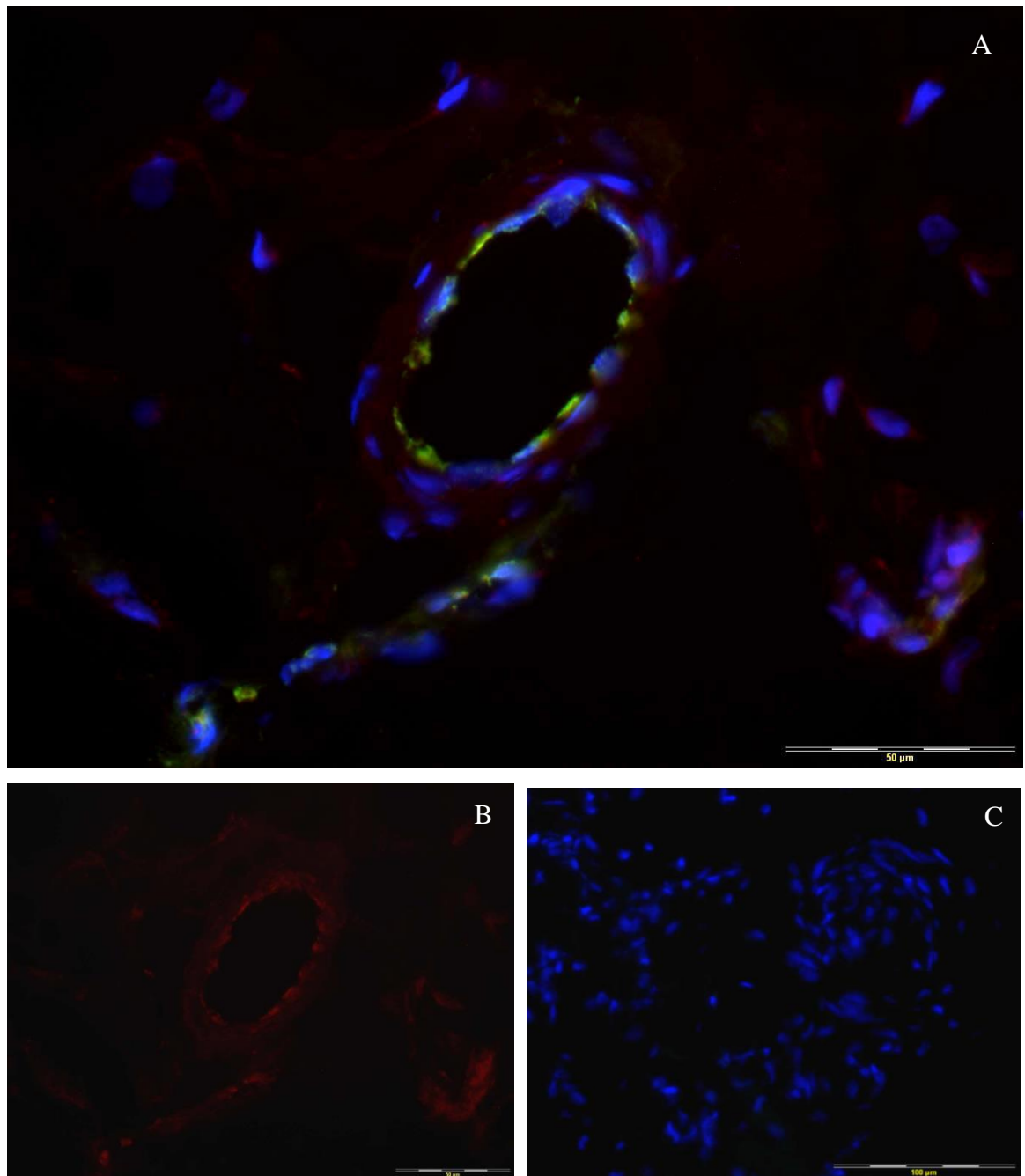


Figure 3.29 CCL19 and VWF staining in the non-RA synovium. 3.29A shows staining for CCL19 (red), VWF (green) and DAPI (blue) from non-RA sample 3 as a representative example. 3.29B shows the same tissue section with only the CCL19 stain. 3.29C shows a merged isotype matched negative control image. Scale bars in 3.29A and 3.29B show 50μm. Scale bar in 3.29C shows 100μm.

3.3.1.21 CCL20 and VWF staining in RA synovial tissue.

Very little CCL20 could be found on the vessel ECs but was identifiable in the intimal layer (figure 3.30). CCL20 was shown to be present on 18.5% (± 2.7) of VWF+ RA vessels. See table 3.1.

3.3.1.22 CCL21 and VWF staining in RA synovial tissue.

CCL21 was observed throughout the synovium (figure 3.31A and 3.31B) and was particularly noticeable in the nuclei of infiltrating cells (figure 3.31B). CCL21 was shown to be present on 36.1% (± 10.4) of VWF+ RA vessels (table 3.1). The negative control (figure 3.31C) showed no staining.

3.3.1.23 CCL22 and VWF staining in RA and non-RA synovial tissue.

In the RA synovium CCL22 colocalisation with VWF + vessels was strongly evident (figure 3.32A, 3.32B). Overall, CCL22 was shown to be present on 60.1% (± 8.1) of VWF+ RA vessels (table 3.3). The negative control (figure 3.32C) showed minimal background staining. In the non-RA synovium (figure 3.33) CCL22 was observed in VWF+ vessels to a lesser degree than in RA synovium. The majority of the staining in the non-RA synovium was observed on small infiltrates in close proximity to large vessels. The negative control (figure 3.33C) showed no background staining. CCL22 was shown to be present on 18.7% (± 5.7) of VWF+ non-RA vessels. The percentage of VWF+ vessels stained for CCL22 was significantly increased in RA compared to non-RA tissue ($p = 0.014$), see table 3.3.

3.3.1.24 CCL22 and LYVE-1 staining in RA and non-RA synovial tissue.

A high degree of colocalisation between CCL22 and LYVE-1 was observed in the RA synovium (figure 3.34A) where CCL22 was shown to be present on 75.1% (± 6.0) of LYVE-1+ RA vessels (table 3.3). The negative control (figure 3.34B) showed no staining. In the non-RA synovium (figure 3.35A) CCL22 was weakly present on 10.4% (± 9.5) of LYVE-1+ non-RA vessels (table 3.3). The percentage of lymphatic vessels stained for CCL22 was shown to be significantly increased in RA compared to non-RA tissue ($p = 0.0001$). The negative control (figure 3.35B) showed no staining.

3.3.1.25 CCL23 and VWF staining in RA synovial tissue.

A combination of both strongly and weakly CCL23+ vessels was observed in the RA synovium (figure 3.36A). CCL23+ infiltrating cells were also observed which were localised within aggregates (3.36B). CCL23 was shown to be present on 37.7% (± 4.5) of VWF+ RA vessels (table 3.1). The negative control (figure 3.36C) showed no staining.

3.3.1.26 CCL24 and VWF staining in RA synovial tissue.

CCL24 was observed to localise to both large and small vessels (figure 3.37). However, more intense staining was seen on small vessels. CCL24 was calculated to be present on 28.8% (± 4.6) of VWF+ RA vessels (table 3.1).

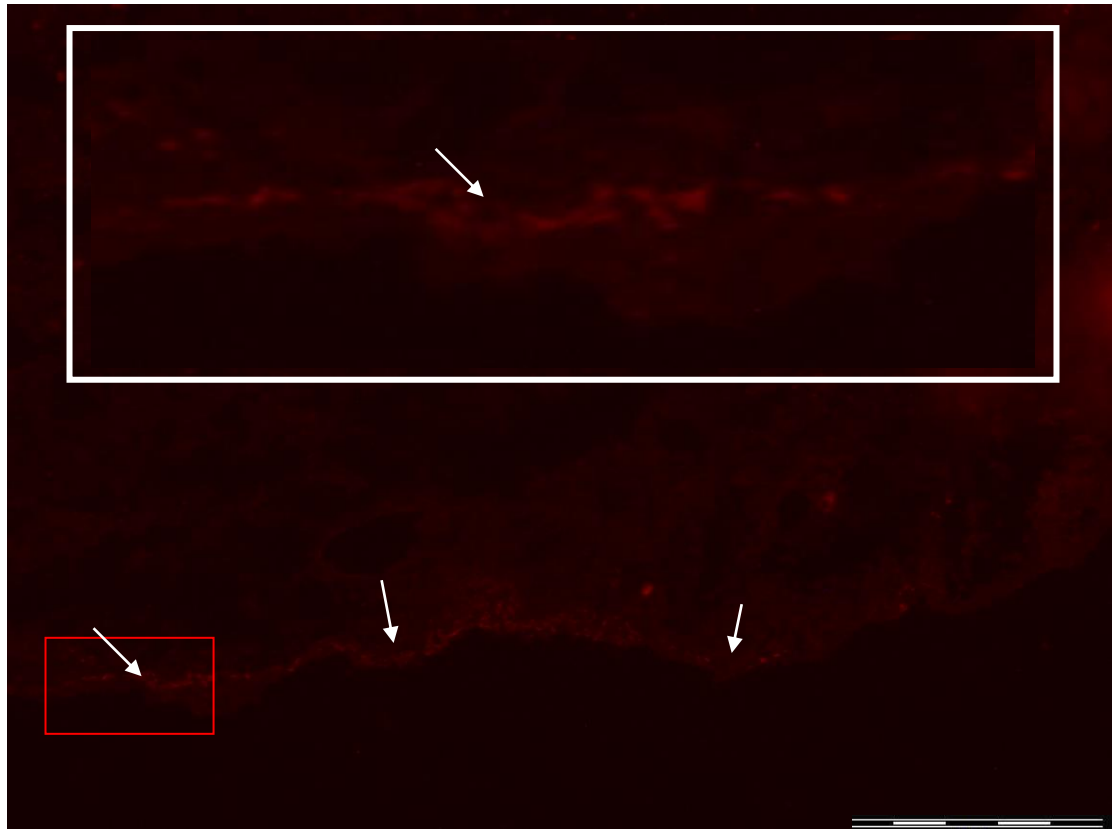


Figure 3.30 CCL20 staining in RA synovium. 3.30 shows staining for CCL20 (red) on RA sample 5 as a representative example. Positive staining is indicated by the white arrows. The inset image (white box) shows a close up of the area highlighted by the red box (original magnification X10 objective) where CCL20 is clearly stained in the intima/sub intima region. The scale bar shows 100 μ m.

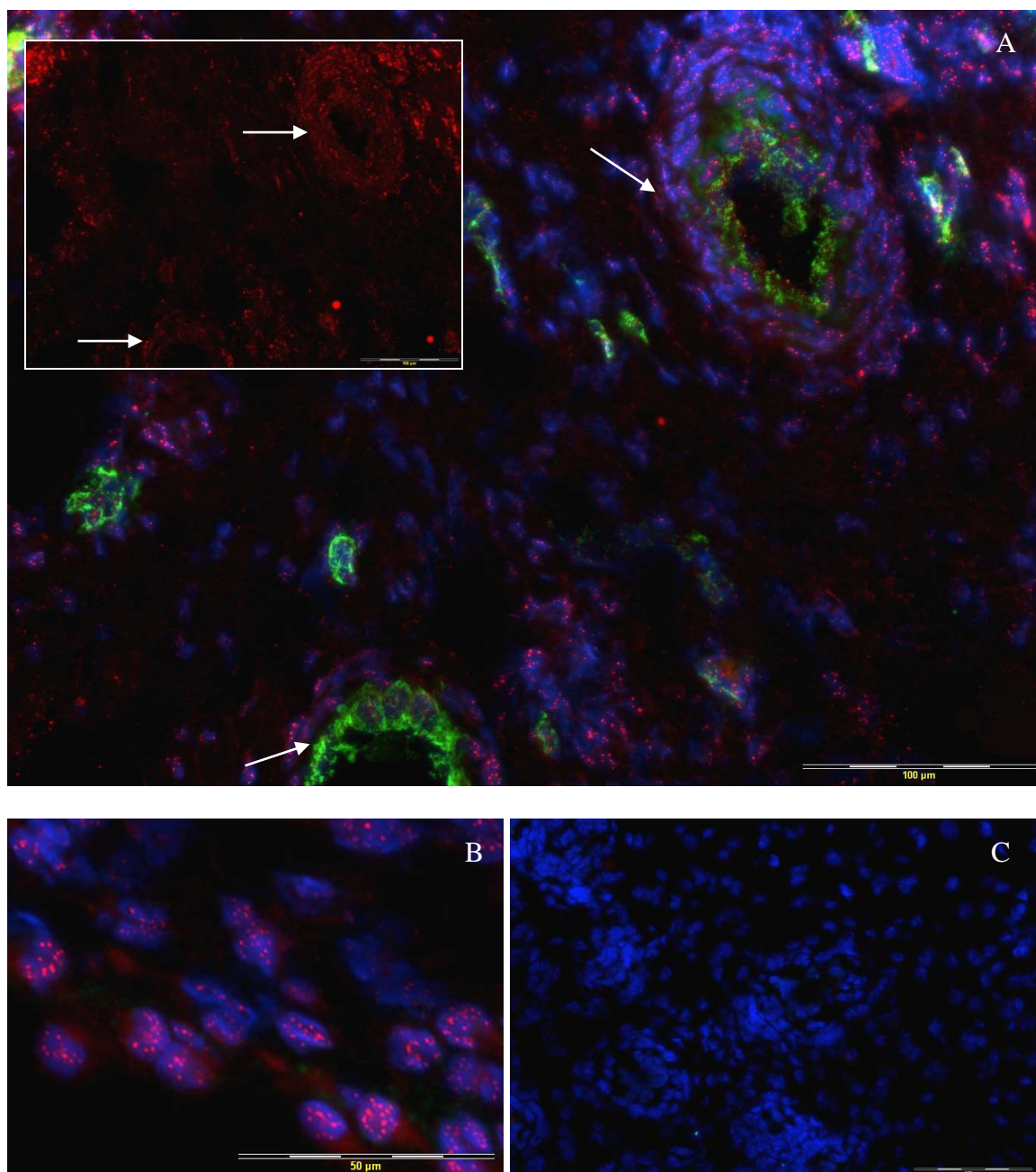


Figure 3.31 CCL21 and VWF staining in RA synovium. 3.31A shows staining for CCL21 (red), VWF (green) and DAPI (blue) from RA sample 7 as a representative example.. Weak CCL21+ staining is indicated by the white arrows in both 3.31A and the inset image showing CCL21 only. 3.31B shows CCL21+ cell nuclei. 3.31C is the isotype matched negative control merged image. Scale bars for 3.31A and 3.31C are 100μm, scale bar for 3.31B is 50μm.

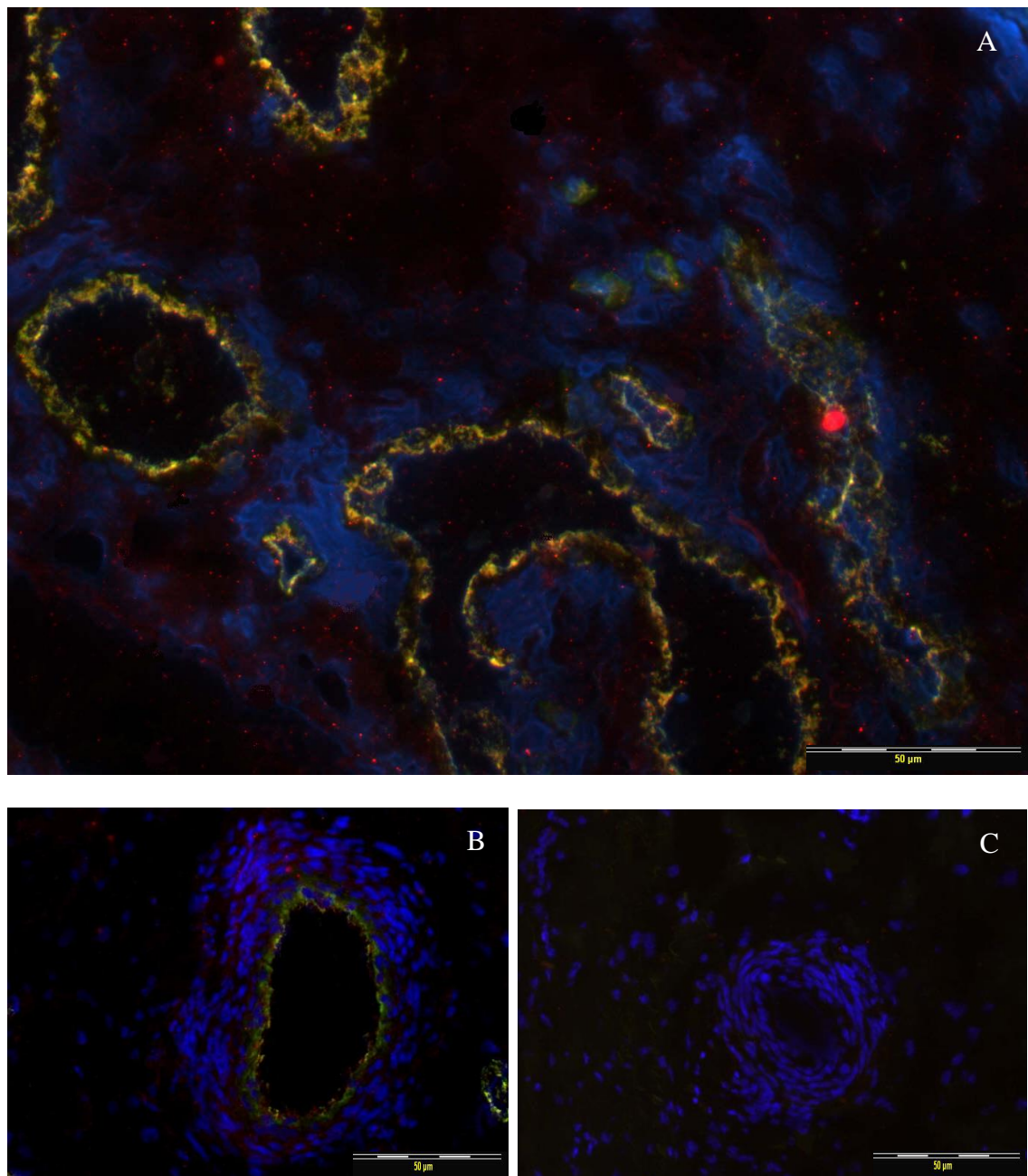


Figure 3.32 CCL22 and VWF staining in RA synovium. 3.32A shows staining for CCL22 (red), VWF (green) and DAPI (blue) from RA sample 5 as a representative example. CCL22 and VWF colocalisation is seen as yellow colouration. 3.32B shows another example of staining on a vessel in the same sample. 3.32C shows a merged negative control image. Scale bars show 50μm throughout.

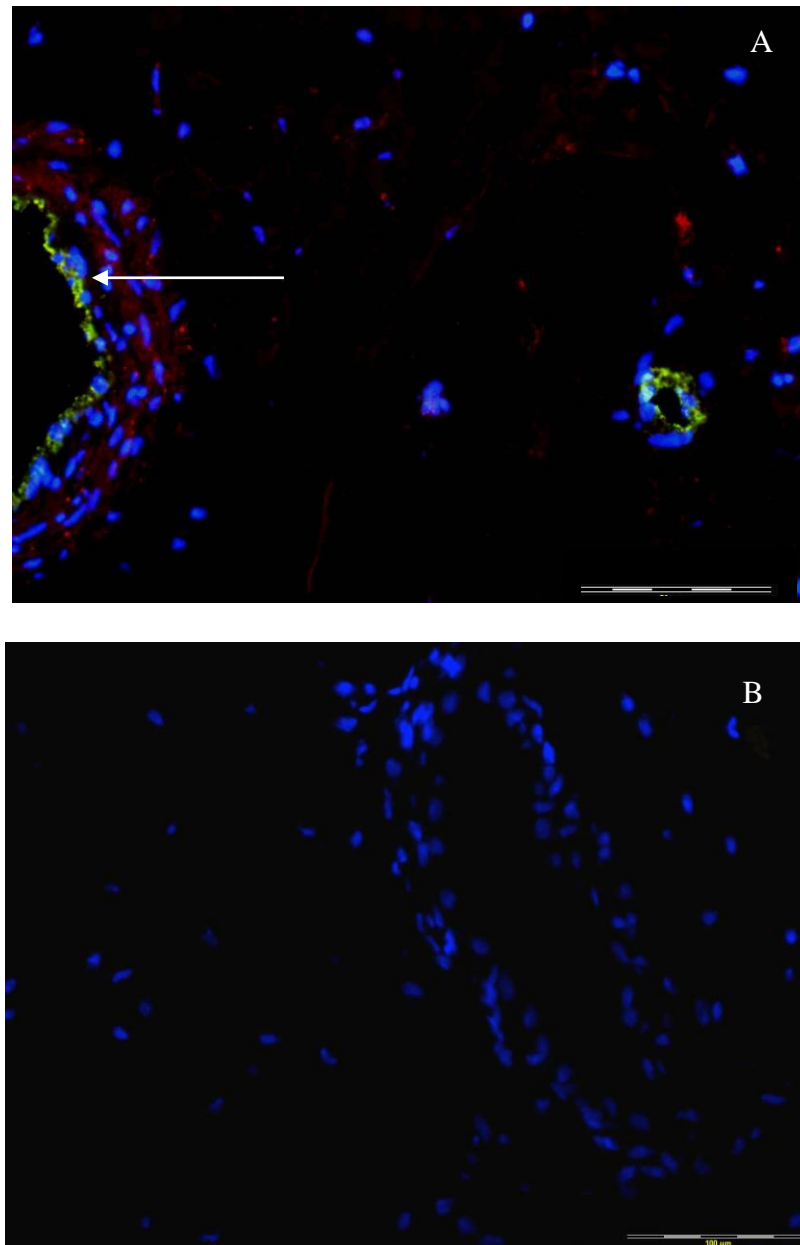


Figure 3.33 CCL22 and VWF staining in non-RA synovium. 3.33A shows staining for CCL22 (red), VWF (green) and DAPI (blue) from non-RA sample 1 as a representative example. Infiltrate stained with CCL22 is seen around the large vessel indicated with a white arrow. 3.33B shows a merged negative control image. Scale bars show 100μm.

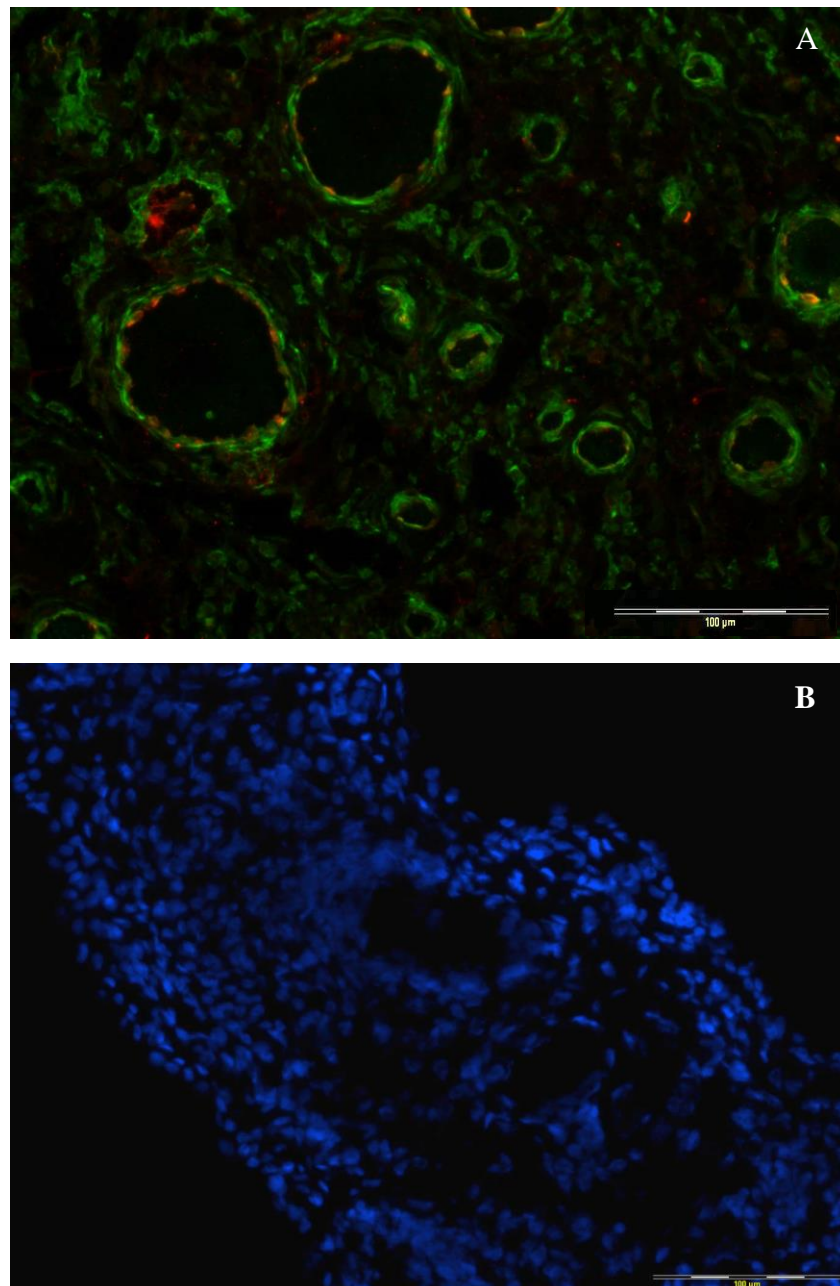


Figure 3.34 CCL22 and LYVE-1 staining in RA synovium. 3.34A shows staining for CCL22 (red) and LYVE-1 (green) on RA sample 5. 3.34B shows the merged isotype matched negative control. Scale bars show 100μm.

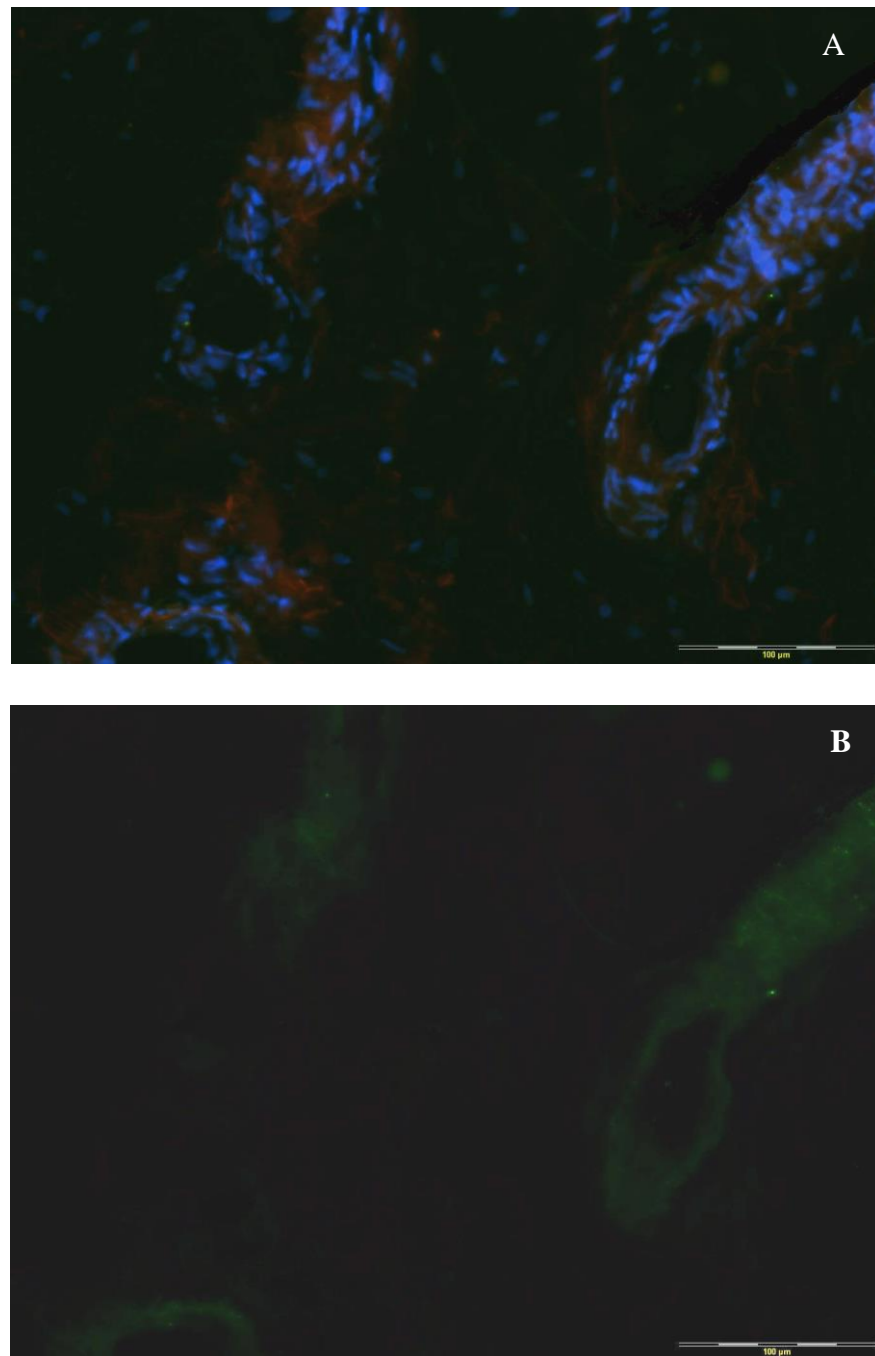


Figure 3.35 CCL22 and LYVE-1 staining in non-RA synovium. 3.35A shows CCL22 (red), LYVE-1 (green) and DAPI (blue) from non-RA sample 3 as a representative example. 3.35B shows LYVE-1 staining only for the same image. Scale bars show 100μm.

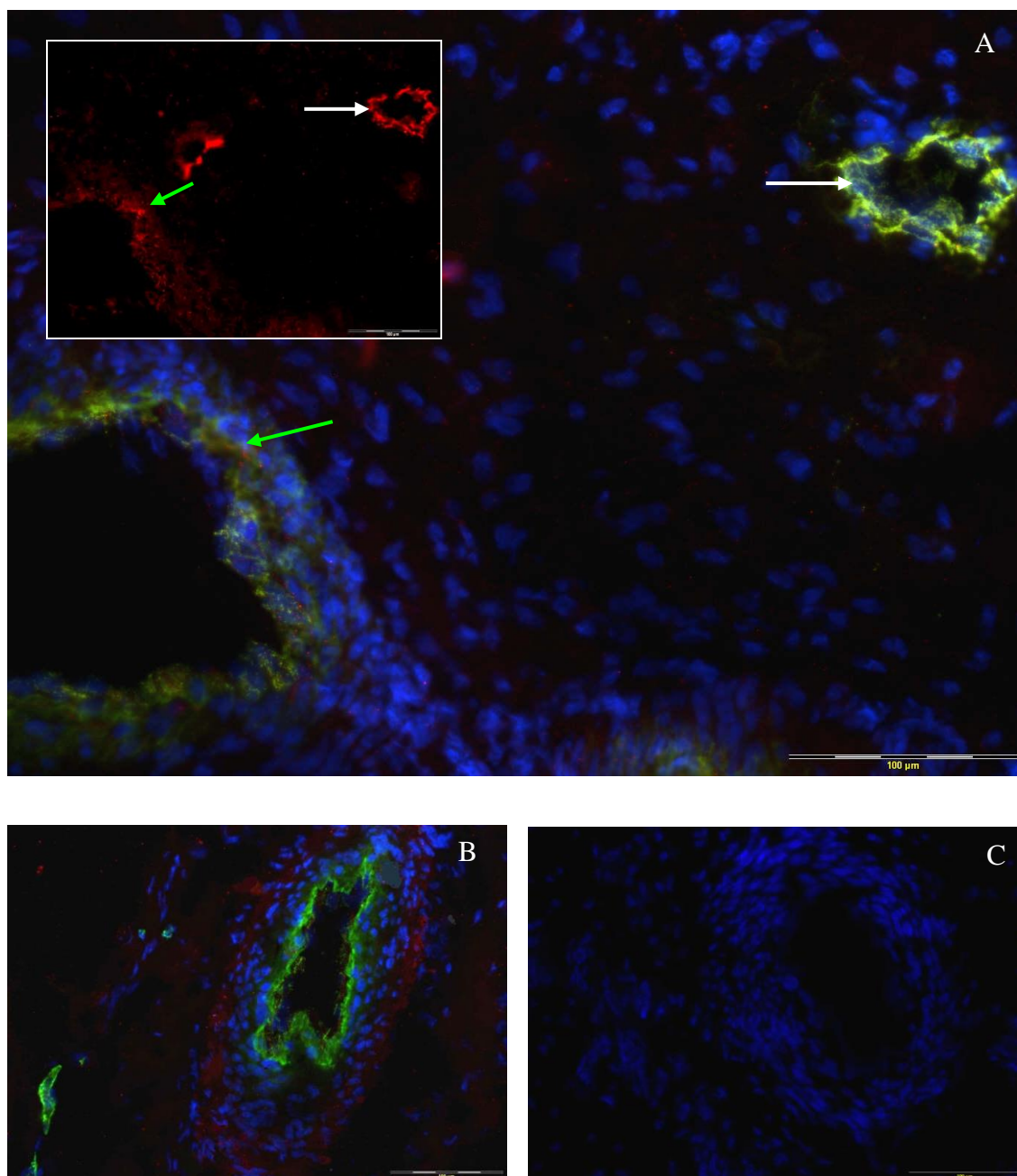


Figure 3.36 CCL23 staining in RA synovium. 3.36A shows staining for CCL23 (red), VWF (green) and DAPI (blue) from RA sample 6 as a representative example. The inset image shows CCL23 staining only from the same section. A strongly CCL23+ vessel is indicated with a white arrow and a weakly CCL23+ vessel is indicated with a green arrow. 3.36B shows CCL23 staining of the infiltrate where aggregates are present. 3.36C is a merged isotype matched negative control image. Scale bars show 100μm.

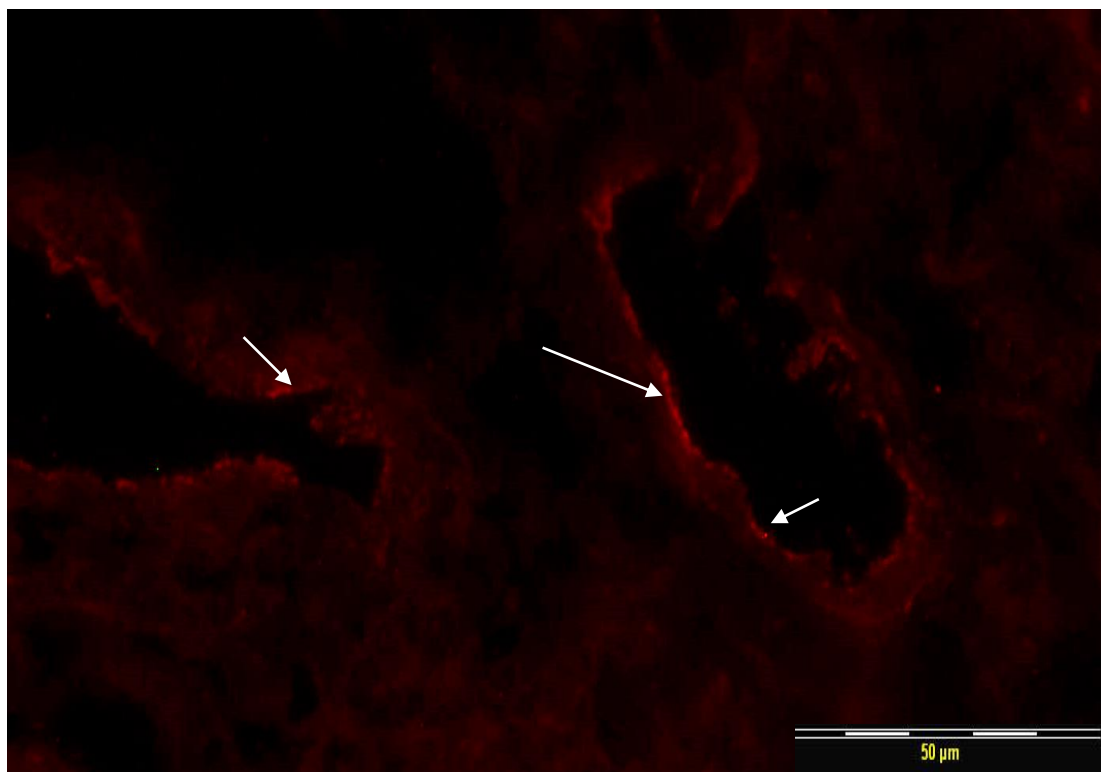


Figure 3.37 CCL24 staining in RA synovium. Intense staining for CCL24 (red) is indicated by the white arrows. RA sample 1 is shown as a representative example.

3.3.1.27 CCL25 and VWF staining in RA synovial tissue.

CCL25 was present primarily on the ECs of larger VWF+ vessels (figure 3.38A, 3.38B). Where staining occurred on smaller vessels it was seen to be much weaker. CCL25 was shown to be present on 28.2% (± 4.5) of VWF+ RA vessels (table 3.1). The negative control (figure 3.38C) showed no background staining.

3.3.1.28 CCL26 and VWF staining in RA synovial tissue.

Colocalisation of CCL26 and VWF was observed (figure 3.39A) and infiltrate staining was also present throughout the samples with some areas being particularly intensely stained. CCL26 was shown to be present on 63.6% (± 7.5) of VWF+ RA vessels (table 3.1). The negative control (figure 3.39B) showed no background staining.

3.3.1.29 CCL27 and VWF staining in RA synovial tissue.

CCL27 was seen to be mostly present in the nuclei of infiltrating cells (figure 3.40A) with very few examples of CCL27 and VWF colocalisation on vessel ECs (figure 3.40B). CCL27 was shown to be present on 8.3% (± 1.2) of VWF+ RA vessels (table 3.1). The negative control (figure 3.40C) showed no background staining.

3.3.1.30 CCL28 and VWF staining in RA synovial tissue.

Colocalisation between CCL28 and VWF was evident as orange colouration (figure 3.41A) and weaker CCL28 staining was observed in smaller vessels. A high degree of intima staining for CCL27 was observed (figure 3.41B). The negative control (figure 3.41C) showed minimal background staining. CCL28 was shown to be present on 40.9% (± 6.8) of VWF+ RA vessels (table 3.1).

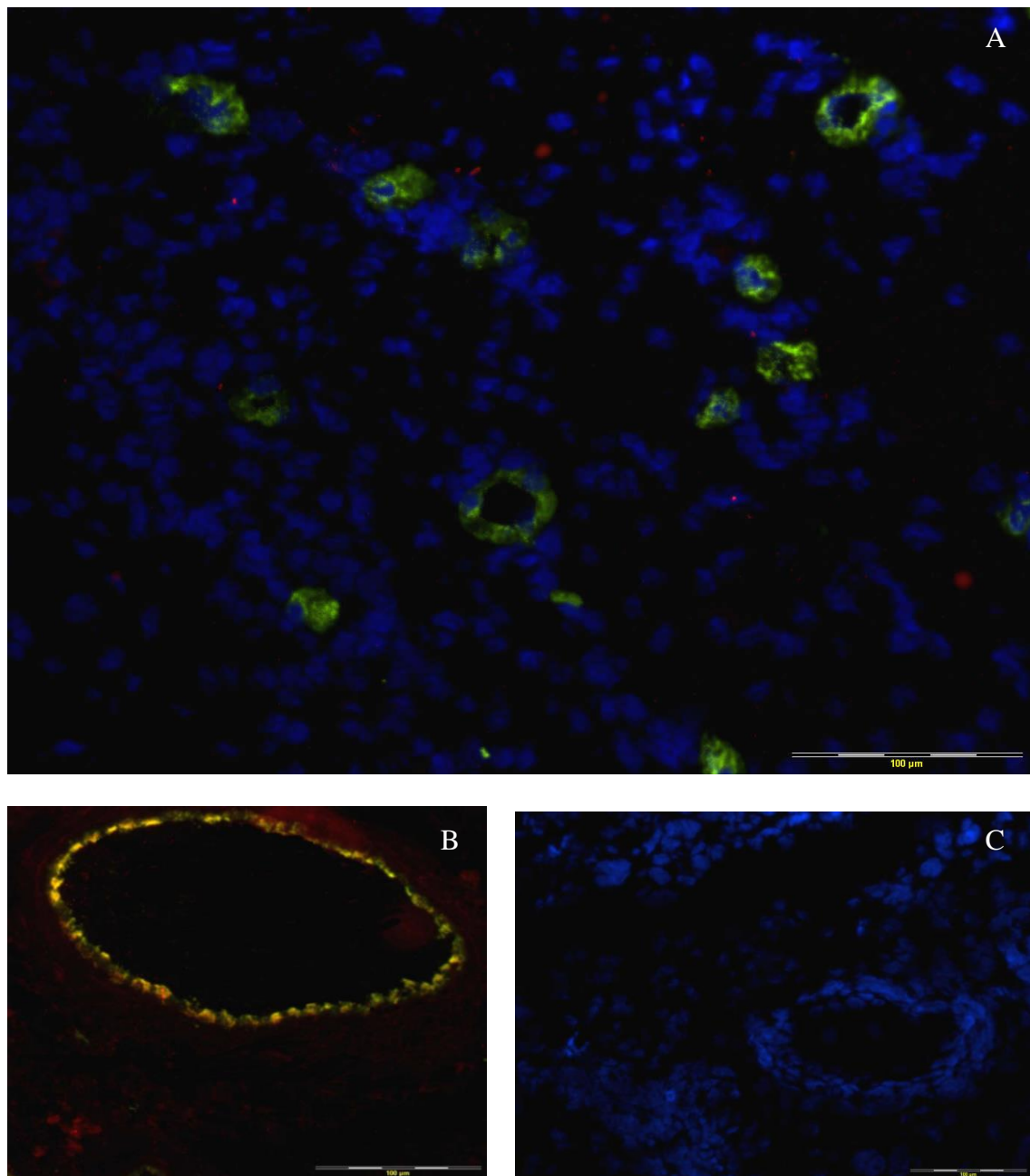


Figure 3.38 CCL25 staining in the RA synovium. **3.38A** shows the merged image for the results of staining for CCL25 (red), VWF (green), and DAPI (blue) from RA sample 4 as a representative example. **3.38B** shows colocalisation of CCL25 and VWF at a large vessel, seen as yellow colouration. **3.38C** is the merged isotype matched negative control image. Scale bars show 100 μ m.

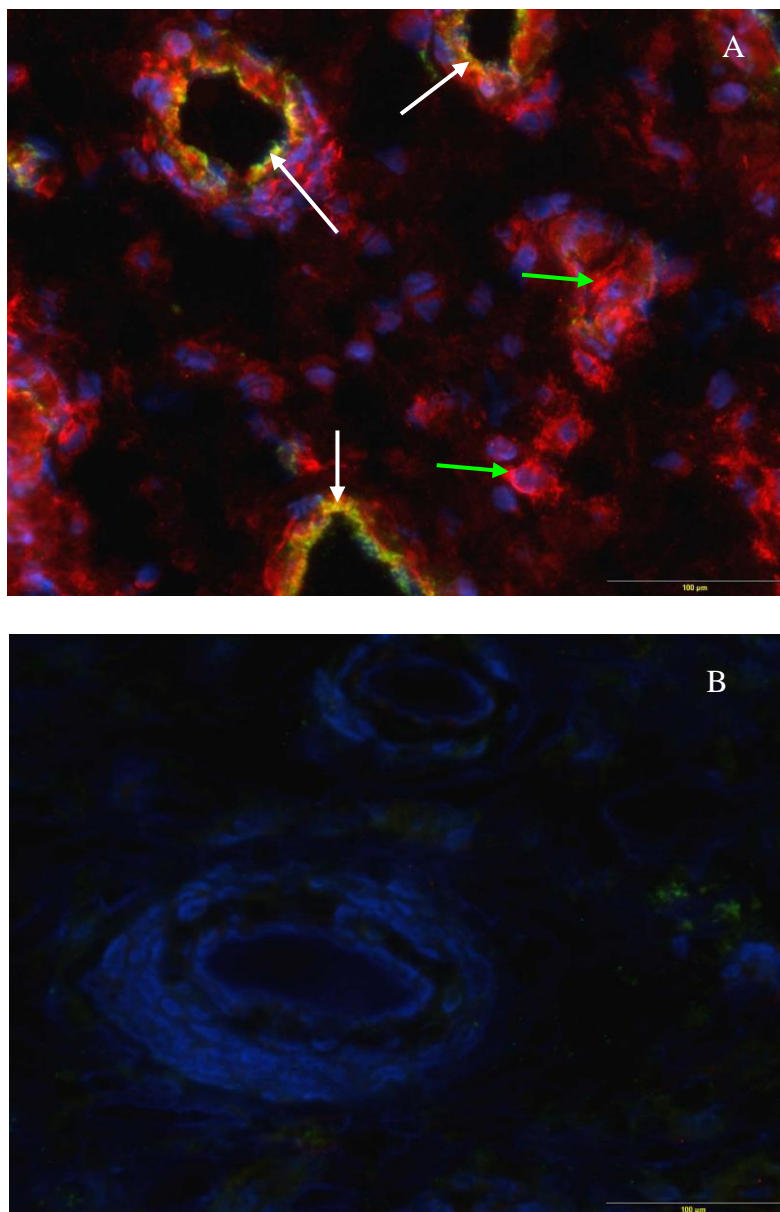


Figure 3.39 CCL26 staining in the RA synovium. **3.39A** shows the merged image for the results of staining for CCL26 (red), VWF (green), DAPI (blue) from RA sample 6 as a representative example. Colocalisation of CCL26 and VWF is indicated with the white arrows. Examples of intensely stained infiltrating cells are indicated with green arrows. **3.39B** shows the merged isotype matched negative control. Scale bars show 100µm.

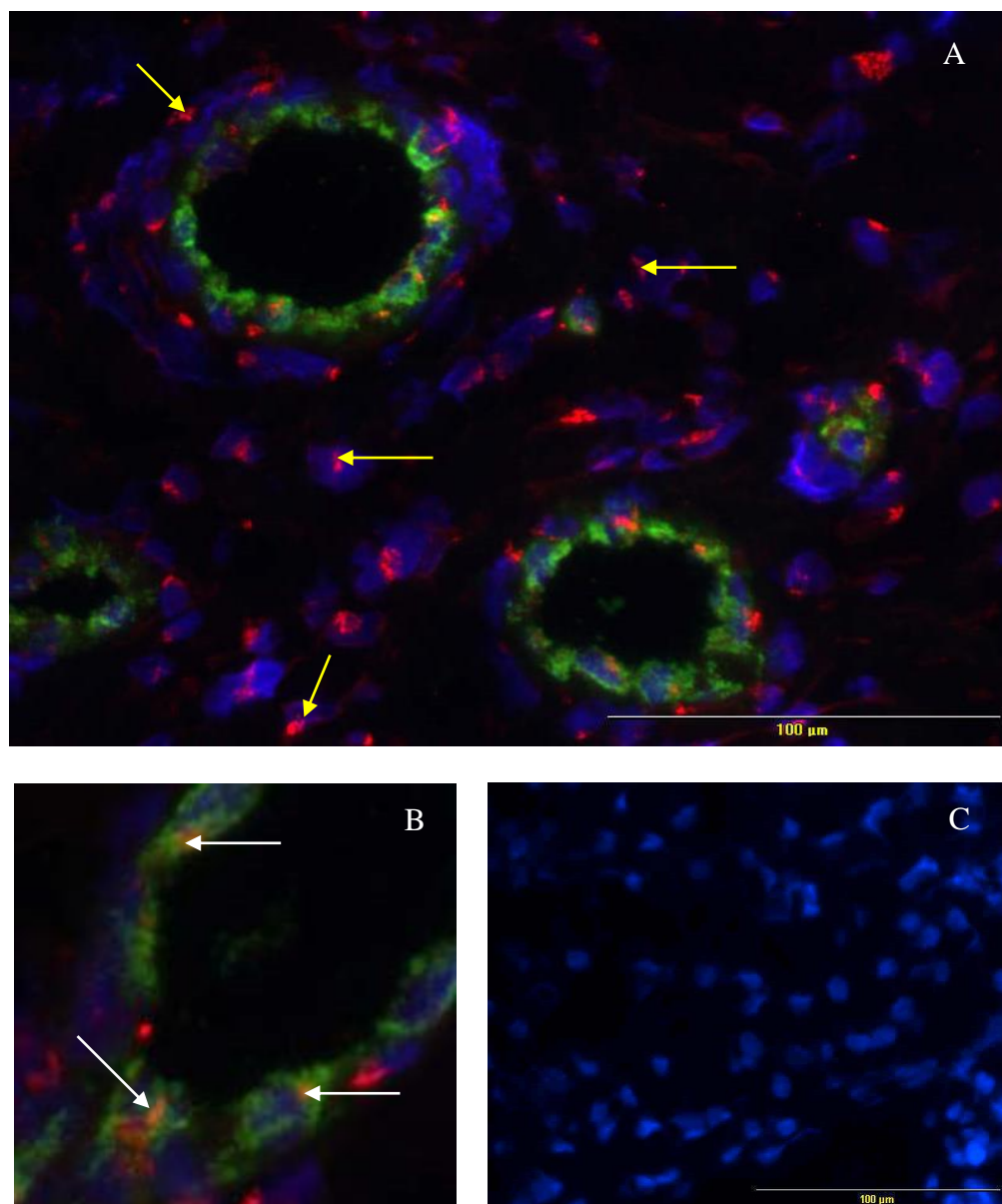


Figure 3.40 CCL27 staining in RA synovium. 3.40A shows the merged image for the results of staining for CCL27 (red), VWF (green), and DAPI (blue) from RA sample 4 as a representative example. CCL27 in the nuclei of infiltrating cells is indicated with yellow arrows (original image X20 objective magnification). 3.40B shows an enlarged image (original not shown) from an original magnification of X40 objective, indicating CCL27 and VWF colocalisation with white arrows. 3.39C shows the merged isotype matched negative control image. Scale bars show 100μm.

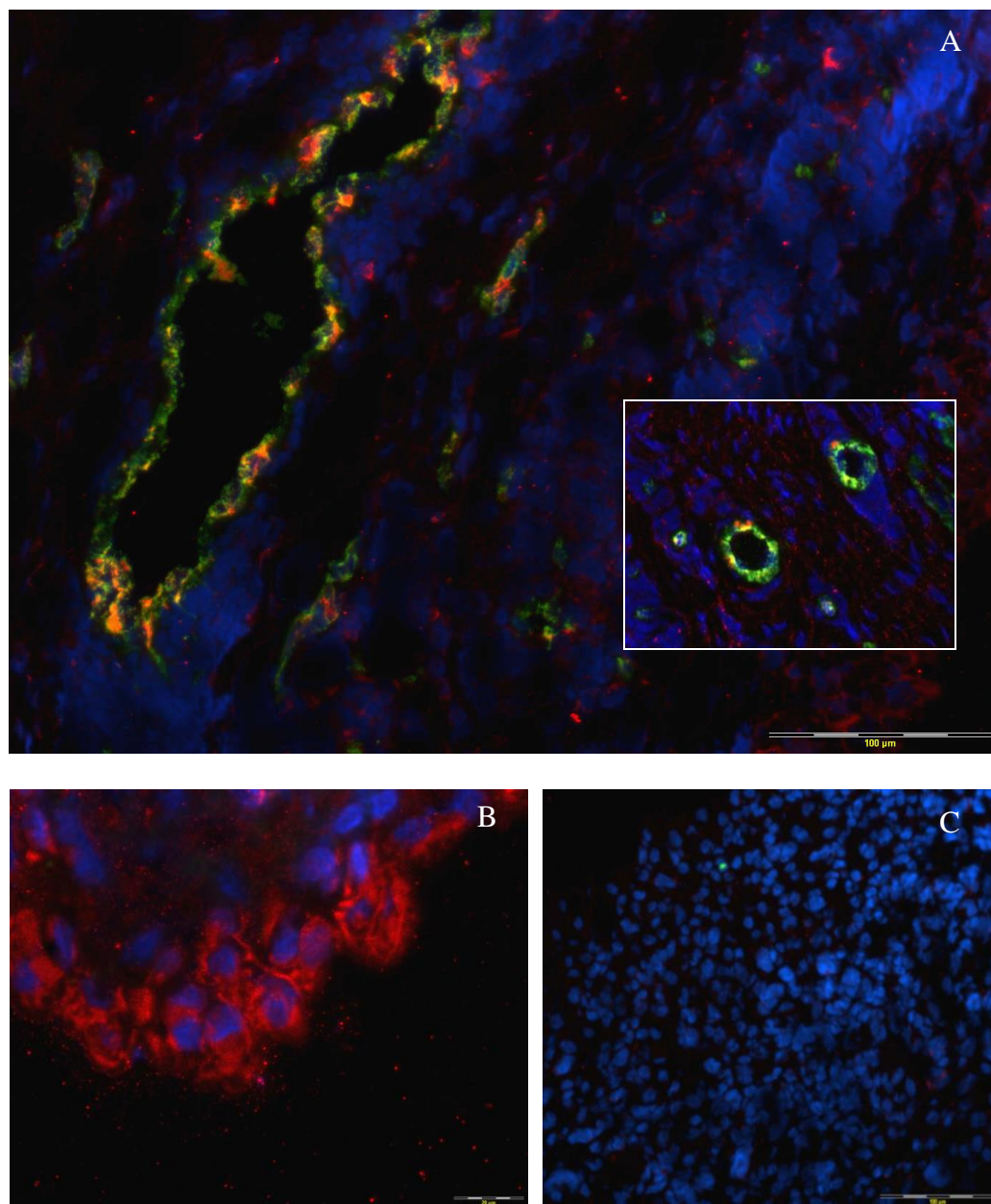


Figure 3.41 CCL28 staining in the RA synovium. Figure 3.41A shows the merged image for the results of staining for CCL28 (red), VWF (green), and DAPI (blue) from RA sample 5 as a representative example. The inset image shows the lesser degree of EC staining at smaller vessels (image at same magnification, X20 objective). 3.41B shows staining for CCL28 at the intima. Scale bar shows 20μm (original magnification X60 objective). 3.41C shows a merged isotype matched negative control image. Scale bars in 3.21A and 3.41C show 100μm.

3.4 Iron and aluminium content of RA tissue.

Due to the degree of heterogeneity between the samples and the chemokines it was hypothesised that different hypoxic macro/microenvironments within the samples were affecting the chemokines presented by the synovium. Due to a lack of high quality tissue from the RA samples previously used, plans were abandoned to stain for HIF-1 (a hypoxia marker) and 8-Oxy-G (a marker for damage due to the generation of ROS, which are known to increase in hypoxic environments (Ng *et al.*, 2010)). Instead the iron content of the tissue samples was measured to provide an approximate guide to the degree of oxidative damage present. Aluminium content was also measured as aluminium is known to compete for iron binding proteins and so can exacerbate oxidative stress within tissues.

No significant correlations between Fe/Al and chemokine presentation could be established which indicated that the aluminium content of the tissues was not related to changes in the iron content. It was however interesting to observe that 4 of the 5 patients who had ≥ 10 of the tested chemokines present in over 60% of vessels had an aluminium content of $>1\mu\text{g/g}^{-1}$ or an iron content of $>60\mu\text{g/g}^{-1}$. Patient 4 had the greatest number of chemokines overall (13 of the 27 tested, see appendix table 1) present at $\geq 60\%$ of vessels with seven chemokines at $\geq 80\%$ of vessels. This patient also had the highest aluminium content within their tissue (see table 3.4).

Table 3.4 Iron (Fe) and aluminium (Al) content of RA samples.

RA sample	Fe ($\mu\text{g/g}^{-1}$)	Al ($\mu\text{g/g}^{-1}$)
2	47.11	6.12
4	28.53	7.55
5	35.10	1.57
6	174.72	7.51
8	65.13	0.23
9	26.58	3.00

Fe and Al content is expressed as μg per gram of the dry mass of the tissue.

3.5 Discussion.

This study is the first to assess the presence of twenty seven of the beta-family chemokines on RA synovial ECs. Novel findings include evidence that each chemokine was present to some degree, the least abundant being CCL27 which was present in 8.3% of RA ECs and the most being CCL19 which was present in 90% of RA ECs. Also, of the twenty seven chemokines investigated, nineteen have not previously been observed at RA ECs. However many of them, such as CCL12 (Schmutz *et al.*, 2004) and CCL13 (Haringman *et al.*, 2006; Hintzen *et al.*, 2009), have been observed as being in the synovial tissue as a whole without analysing their localisation. From the twenty seven chemokines analysed in the present study CCL4, CCL7, CCL8, CCL14, CCL16, CCL19 and CCL22 were shown to be present on $\geq 60\%$ of vessels, of which CCL7, CCL14, CCL16 and CCL22 have not previously been identified as present in RA ECs.

The chemokines CCL4, CCL8 and CCL19 have been observed at ECs by other studies (Tanaka *et al.*, 1998; Pierer *et al.*, 2004; Burman *et al.*, 2005; Page *et al.*, 2002), but their degree of presentation was not quantified. They have been further examined by this study, where it was established that CCL19 was the most highly upregulated at RA ECs, followed by CCL8 then CCL4.

While CCL4 has been previously identified in RA ECs (Koch *et al.*, 1995b; Tanaka *et al.*, 1998) this study is the first to quantify its presentation in comparison to control non-RA tissue, where the control tissue is not from another arthritis type. Koch *et al.*, (1995b) established CCL4 to be down-regulated in RA compared to OA; the present study shows that CCL4 is not significantly upregulated in RA compared to non-RA ECs. While CCL4 acts as a chemoattractant for a variety of leukocytes including T-cells and B-cells

(Krzysiek *et al.*, 1999) as well as monocytes and NK cells (Bystry *et al.*, 2001) the results of this study indicate that it may not be primarily involved in the pathology of RA.

CCL8 activates and chemoattracts a range of cells, including monocytes, T-cells, NK cells and fibroblast like synoviocytes (FLS) (Proost *et al.*, 1996; Gong *et al.*, 1998; Haringman *et al.*, 2006). This study showed that CCL8 is significantly upregulated in RA ECs compared to non-RA ECs, which confirms work by Pierer *et al.*, (2004) who also identified a significant up-regulation of CCL8 in RA ECs compared with OA ECs. The present study also identified CCL8⁺ stromal cells which were fibroblast-like in appearance which concurs with data from Haringman *et al.*, (2006) who also observed CCL8⁺ FLS in tissue samples.

Page *et al.*, (2002) established that CCL19 is present at RA ECs, and Burman *et al.*, (2005) showed that CCL19 is expressed on both lymphatic and vascular ECs in RA. Page *et al.*, (2002) found CCL19 to be expressed in RA tissue where germinal centres were present, and absent where only diffuse infiltrates were found. The present study provides evidence of this as it showed more intense CCL19 staining to be present in the more densely infiltrated lymphoid follicle regions.

Due to time constraints it was decided to assess the four novel, most highly EC presented chemokines identified by this study, (CCL7, CCL14, CCL16 and CCL22), for their presentation by lymphatic ECs as the pan-endothelial marker VWF did not differentiate between the EC types. It was hypothesised that chemokines may be differentially expressed on blood/lymphatic ECs in RA and non-RA tissue, which would affect the leukocytes migration into the RA synovium and/or their removal from the tissue via lymphatics. Future work to test this hypothesis could include performing transmigration analysis over blood and lymphatic EC lines where the chemokines of interest had been neutralised.

Of these four novel chemokines CCL14 showed the most significant upregulation in RA synovial ECs compared to non-RA ECs. This was followed by CCL22, CCL7 and CCL16, with the latter two showing no significant changes.

This study adds to the field as it is the first to show CCL14 to be present in RA ECs, and shows it to be the most significantly upregulated novel chemokine in RA ECs using VWF as the marker ($p = 0.0041$). However, when LYVE-1 was used as the EC marker in RA and non-RA tissue it was shown that there were no significant differences between the two. This suggests that CCL14 may play a role in the recruitment of inflammatory cells into the RA synovium, but not their exit via the lymphatics.

Of the four chemokines chosen, CCL22 was the next most significantly upregulated in RA ECs compared to non-RA ($p = 0.014$). Flylie *et al.*, (2010) identified CCL22 ‘scattered throughout’ RA synovium with CCR4, the CCR22 receptor, localised on ECs but the current study provides further analysis of CCL22 showing there to be a significant CCL22 increases at lymphatic ECs in RA compared to non-RA lymphatic ECs. These novel data indicate that CCL22 may have a role in the recruitment of inflammatory cells to the RA synovium but that the marked increase in CCL22 at RA lymphatic ECs may facilitate the removal of infiltrates.

Haringman *et al.*, (2006), who first identified CCL7 in RA tissue, found it to be ‘abundantly present’ in all arthritis and control groups tested. This study provides further data novel to the field in that CCL7 was shown to be highly presented by RA ECs. While there was no significant difference in CCL7 between RA and non-RA VWF+ ECs, when LYVE-1 and chemokine colocalisation was analysed a significant reduction in the percentage of LYVE-1 lymphatic vessels stained for CCL7 in RA synovium was observed ($p = 0.011$). The results of this study led to the speculation that there may be a novel role for CCL7 in the recruitment of lymphocytes and monocytes in the synovium in both RA

and non-RA, but that the CCL7 reduction at lymphatic ECs may play a role in the persistence of inflammatory cells within the RA synovium which is of greater importance to RA pathology. This is the first study to identify CCL7 in lymphatic ECs in RA. Interestingly, higher CCL7 expression in gastric cancer tissues compared to normal tissues was significantly correlated with both lymph node metastasis and ‘advanced depth of wall invasion’ (Hwang *et al.*, 2012). This provides further evidence for the potential increased cell recruitment in response to CCL7.

While CCL16 has been previously identified in RA tissue (Radstake *et al.*, 2005; Van Lieshout *et al.*, 2005; Haringman *et al.*, 2006), this study is the first to identify its presence in RA ECs. However, the results indicate that there are no significant differences at either VWF+ ECs or LYVE+ ECs in RA and non-RA tissue and so it is unlikely that CCL16 plays a dominant role in the pathology of RA. Further studies to confirm the lack of CCL16 functionality are needed.

When iron and aluminium content of tissue was tested no significant correlations between Fe/Al and chemokine presentation could be established. However, a trend was observed that greater abundance of iron and/or aluminium indicated that the sample would have an increased number of the most highly represented chemokines. The increased presence of iron and its association with increased inflammation is in itself not surprising, and may simply indicate the increased degree of oxidative damage expected in tissue removed at the time of joint replacement. However, there is the potential that increased aluminium and/or other competitors which compete for iron binding proteins (and in doing so increase the levels of free iron and so the oxidative damage in tissue), play a role in chemokine expression and the pathology of RA which remains to be elucidated. The current results allow only for observational, speculative analysis, and a greater number of samples would

need to be analysed for both iron and aluminium to reduce the sample variability seen in the currently available data.

This is the first study to identify LYVE-1+ macrophages in RA. Their presence has been noted in tumours, particularly breast cancers (reviewed by Ran and Montgomery, 2012) where they play a role in tumour lymphangiogenesis. However, lymphangiogenesis in RA decreases as the disease progresses, exacerbating the persistence of inflammatory cells. The results of this study indicate that despite the reduction in lymphangiogenesis at the end stage of the disease there may still be a potential role of the macrophages in the generation of lymphatic vessels.

Conclusions

The first aim of this section of the study was to establish which CCL chemokines are highly presented at RA synovial ECs and to compare the most highly represented chemokines (present on $\geq 60\%$ of RA vessels) with non-RA synovial tissue to establish which chemokines are specifically increased in RA. The chemokines, CCL4, CCL7, CCL8, CCL14, CCL16, CCL19 and CCL22 were shown to be present at $\geq 60\%$ of RA vessels with CCL4, CCL8, CCL14 and CCL22 being significantly upregulated in RA compared to non-RA.

The second aim of this section of the study was to establish whether there are differences in blood and lymphatic vessel EC presentation of the most highly represented chemokines in both RA and non-RA synovial tissue. Such differential expression within the microvasculature of the synovium could potentially lead to leukocyte persistence in the inflamed joint. The study has shown there to be a significant decrease in CCL7 presentation at RA lymphatic vessels compared to non-RA vessels, and a significant increase in CCL22 at RA lymphatic ECs in RA compared to those of non-RA. These

findings provide further novel evidence of differentially expressed chemokines on blood and lymphatic microvasculature. This adds to the evidence that chemokine dysregulation within the microvasculature in inflammatory environments plays a significant role in the recruitment and persistence of inflammatory cells in RA. In addition the study identifies particular chemokines as potential therapeutic targets on ECs.

Chapter 4

Analysis of ICAM-1 and chemokine levels in cultured endothelial cells.

4.1 Introduction and Aims

ECs in RA are involved in angiogenesis, leukocyte trafficking and presentation/expression of a range of mediators and effectors involved in disease pathology. Chemokines CXCL5, CXCL8, CXCL9, CXCL12, CXCL13, CX3CL1, CCL2, CCL3, CCL4, CCL8, CCL19 and CCL21 have already been shown to be present at RA ECs (table 1.8 and references therein). As the role of chemokines is leukocyte integrin activation and migration the presence of these chemokines at ECs may be pivotal in the extravasation process. It was hypothesised that the chemokines CCL7, CCL14, CCL16 and CCL22, which were newly established at present at RA ECs in chapter 3, may be generated by the ECs themselves rather than merely presented by them. If this hypothesis was true, it would indicate whether these EC chemokines played a role in the early stages of leukocyte transmigration and so were potentially functional in RA pathology. As cycloheximide disrupts protein synthesis by blocking the translocation step in elongation (Schneider-Poetsch *et al.*, 2010) it would affect the levels of the chemokine available for staining in a time dependent manner by preventing increases in chemokine intensity. However, a chemokine which was constitutively present should remain at the same intensity level, or reduce if the chemokine was being released by the cell into the medium in the time given.

Xu *et al.*, (2003) showed that increased lymphatic vessel formation occurs in RA, and may provide a compensatory mechanism for the removal of invading leukocytes (Olszewski *et al.*, 2001). Furthermore, Johnson *et al.*, (2006) showed that TNF- α activated dermal lymphatic endothelial cells (DLECs) show >100 fold increases in production of a range of chemokines including CCL2, CCL5 and CCL20 which attract T-cells and monocytes. The author decided that assessing both blood and lymphatic ECs would provide further data to assess EC chemokine dysregulation. In the current study HBMECs provide a model for the presentation/expression of chemokines to leukocytes that cross human vascular ECs into

the synovium; HDLECs were chosen to act as a model for the presentation/expression of chemokines stimulating leukocyte migration from the synovium into the lymphatic system.

The aims of this chapter were:

- Establish if TNF- α , IFN- γ or a combination of the two provides optimal simulated inflammatory conditions for HBMECs and HDLECs.
- Assess if CCL7, CCL14, CCL16 and CCL22 are present in cultured HBMECs and HDLECs in the presence and absence of TNF- α , IFN- γ or a combination of the two.
- Elucidate if there are changes in the intensity of CCL7, CCL14, CCL16 and CCL22 in the presence of a protein synthesis inhibitor.

4.2 Materials and Methods

HBMECs and HDLECs were cultured as described in section 2.4.1.1 and 2.4.1.4 respectively, and inflammatory conditions were stimulated using human TNF- α , IFN- γ or a combination of the two (Peprotech) in DMEM-F12 medium (for HBMECs) or EBM-2-mv medium (for HDLECs) as described in section 2.4.1.8 and section 2.4.1.9. Following optimisation, time dependent stimulation to establish optimal activation times for each cell type was performed (as described in section 2.4.1.9). The generation of chemokines by HBMECs was ascertained by a time dependent analysis of chemokine staining in the absence and presence of TNF- α and the protein synthesis blocker cycloheximide as described in section 4.4. To inhibit protein synthesis cultured HBMECs/HDLECs were

simultaneously stimulated with 100ng/ml TNF- α , with the addition of cycloheximide (at 10 μ g/ml) and left for 2, 3, 4, 5 and 6 hours (as described in section 2.4.2) prior to being fixed and stained for the chemokines (n=3). Negative controls were performed in the absence of TNF- α . (0 hours)

The degree to which cell surface adhesion molecules were upregulated was ascertained by measuring mean cell intensity of ICAM-1 staining over 12 random points within 3 random fields of view for each cell type. Following this analysis, the changes in the chemokines CCL7, CCL14, CCL16 and CCL22 were assessed in the same manner. Minimum measurable intensity, where only background staining in the absence of cells was measured, was shown to be 8au; maximum staining was not ascertained. The conditioned medium was retained for ELISA testing.

Cells were visualised using the Olympus fluorescence microscope and intensity of staining analysed by CellF software (NCSS, Kaysville, UT, USA). Cell surface staining only was achieved by prevention of cell permeabilisation by fixing cells in freshly prepared 3.7% paraformaldehyde at room temperature, in the absence of Triton-X and experiments were performed at room temperature. Whole cell staining was performed by ensuring cell permeabilisation by fixing cells for 15 minutes in 1:1 ice cold acetone:methanol and the addition of 0.3% Triton-X to the dilution and blocking buffer solutions.

4.2.1 Quantitation of results.

Statistical analysis was performed using GraphPad. Normality checks were performed for each dataset which showed all data to have a non-normal distribution, therefore non-parametric tests were used throughout the analysis.

Comparisons of the effect of stimulating cells with TNF α or IFN γ for a single time period were carried out using the Wilcoxon signed rank test. Kruskal-Wallis ANOVA was used to

determine whether there were any significant differences in staining intensity between at least two time points in a time point series. Kruskal-Wallis ANOVA was also used to ascertain if there were differences in the presence and absence of cycloheximide. Multiple comparison post hoc analysis was performed using Dunn's post hoc test to compare differences between unstimulated and stimulated cells at individual time points. Data presented in tables were expressed as median values in arbitrary units with interquartile ranges included. The intensity change was calculated by subtracting median intensity of unstimulated cells from the median intensity following stimulation. Trend analysis was performed using the Jonckheere-Terpstra test.

4.3 Results

4.3.1 Cell surface ICAM-1 intensity following 16 hour stimulation of HBMECs.

4.3.1.1 Stimulation of HBMECs with 100ng/ml TNF- α

There was a significant effect on the generation of ICAM-1 caused by 16 hour stimulation (table 4.1) with TNF- α (figure 4.1).

Under normal conditions (no TNF- α stimulation) ICAM-1 intensity was 23.00au (arbitrary units) which increased by 23.5au to 46.50au following 16 hour stimulation with 100ng/ml TNF- α (p value = <0.0001) giving a ~2 fold increase. Immunofluorescent analysis of ICAM-1 showed a clear increase in ICAM-1 expression once stimulated (figure 4.1A). Unstimulated cells also showed some ICAM expression (Figure 4.1B). An Isotype matched control showed no non-specific staining (inset images).

4.3.1.2 Stimulation of HBMECs with 100ng/ml IFN- γ

There was a significant effect on the generation of ICAM-1 caused by 16 hour stimulation with IFN- γ (see table 4.1). Following 16 hour stimulation with 100ng/ml IFN- γ , ICAM-1

intensity increased from 25.00au under normal conditions to 31.50au (p value = 0.0006). The increase in ICAM-1 expression was clear once stimulated (figure 4.2A), despite some staining being observed on the unstimulated cells (Figure 4.2B). An isotype matched control showed no non-specific staining (inset images).

4.3.1.3 Stimulation of HBMECs with 100ng/ml TNF- α and 100ng/ml IFN- γ

There was a significant effect on the generation of ICAM-1 caused by 16 hour stimulation (see table 4.1) with IFN- γ /TNF- α . Following 16 hour stimulation with 100ng/ml IFN- γ /TNF- α ICAM-1 intensity increased by 9.0au from 28.00au under normal conditions to 37.00au (p value = <0.0001). ICAM-1 showed markedly higher expression on stimulated cells (figure 4.3A) than on unstimulated cells (Figure 4.3B). An isotype matched control showed no non-specific staining (inset images).

Despite the data overlap seen between the different types of stimulation the greatest overall difference between unstimulated and stimulated HBMECs was when 100ng/ml TNF- α was used to activate the HBMECs. Given the significance of the ICAM-1 intensity increase TNF- α was used to stimulate the HBMECS in further studies.

Table 4.1. Intensity of cell surface ICAM-1 staining following HBMEC stimulation with TNF- α , IFN- γ and TNF- α /IFN- γ for 16 hours.

Stimulation solution	Unstimulated (n=108 cells)	Stimulated (n=108 cells)	Difference (p value)
100ng/ml TNF- α	23.00 14.00 – 31.00	46.50 35.00 - 58.75	+23.50 $p = <0.0001$
100ng/ml IFN- γ	25.00 19.00 - 32.75	31.5 23.00 – 40.00	+6.50 $p = 0.0006$
100ng/ml TNF- α /IFN- γ	28.00 18.00 – 37.00	37.00 31.00 – 45.00	+9.00 $p = < 0.0001$

Values for stimulated and unstimulated cells are expressed as median values and given in arbitrary units with interquartile range. Unstimulated analysis was performed in the absence of TNF- α , IFN- γ and TNF- α /IFN- γ as a negative control. Value for difference is stimulated median – unstimulated median. Data were non-parametric so p values are from the Wilcoxon signed rank test. 3 fields of view per chamber slide well were analysed. n=3 wells throughout.

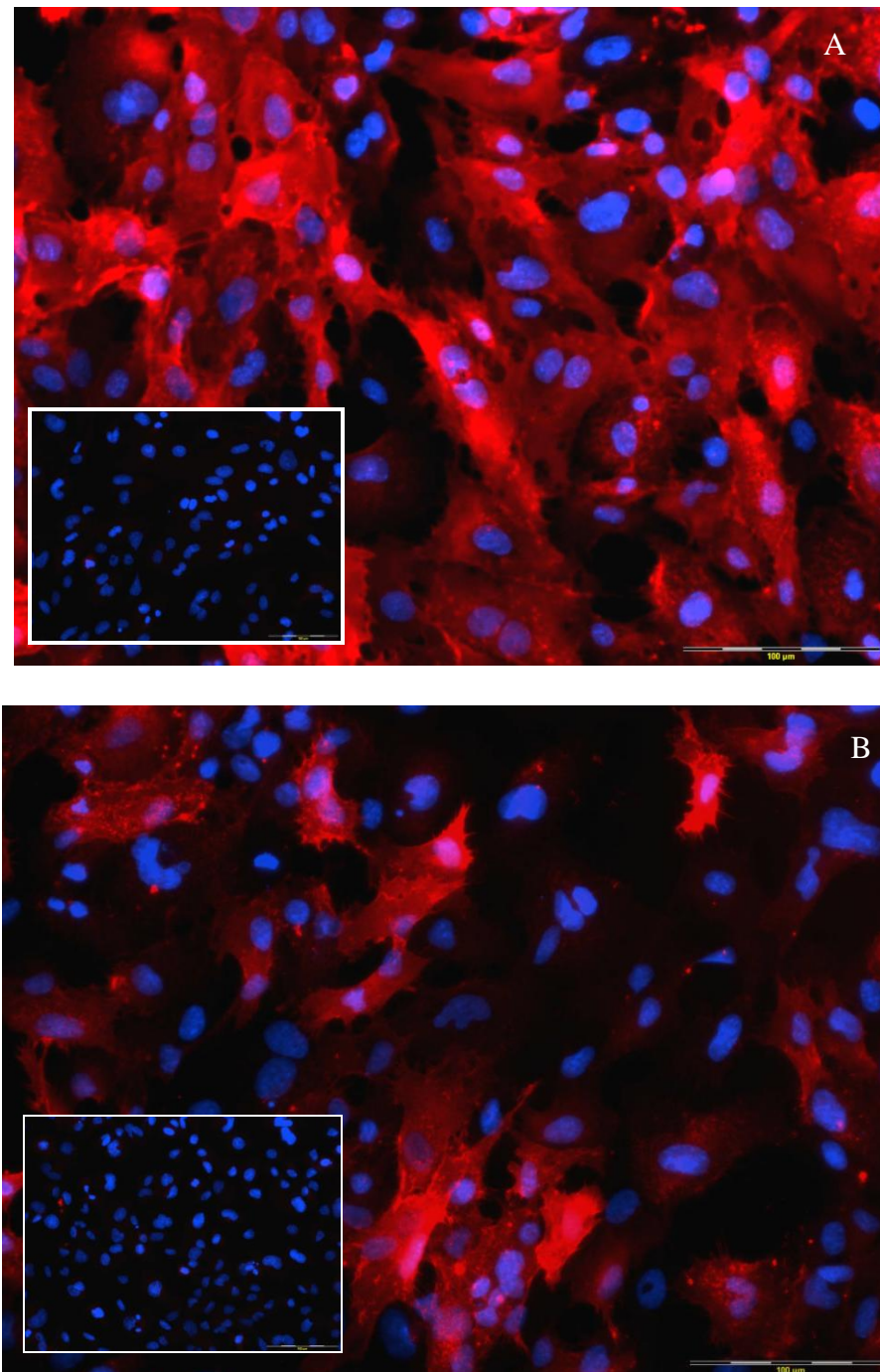


Figure 4.1 ICAM-1 staining of HBMECs stimulated for 16 hours with 100ng/ml TNF- α . **4.1A** shows the merged image for the results of staining for ICAM-1 (red) and DAPI (blue) on stimulated HBMECs. **4.1B.** shows the merged image for the results of staining for ICAM-1 (red) and DAPI (blue) on unstimulated HBMECs. The scale bars show 100 μ m. Inset images show the merged negative control.

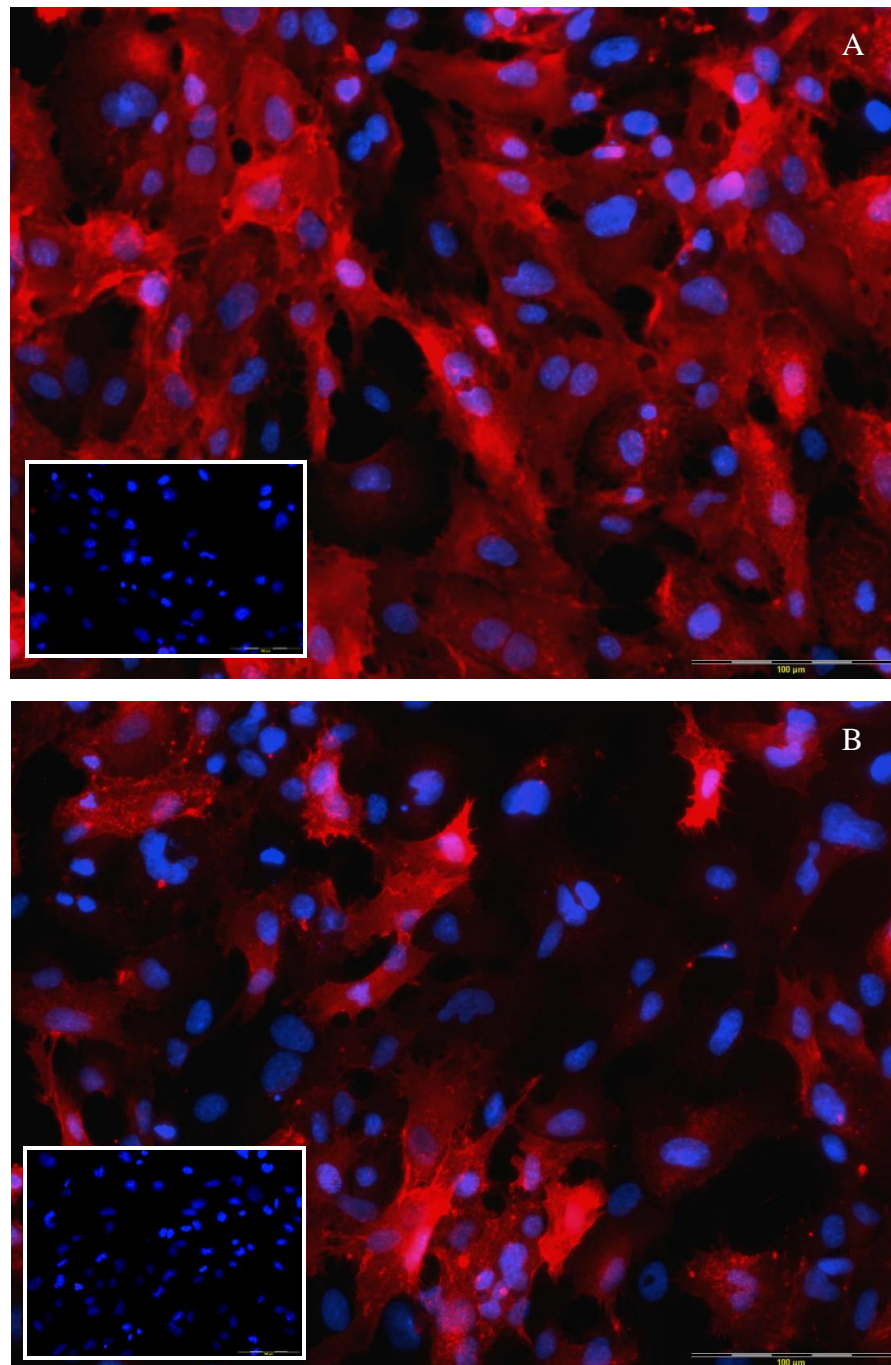


Figure 4.2 ICAM-1 staining of HBMECs stimulated for 16 hours with 100ng/ml IFN- γ . **4.2A** shows the merged image for the results of staining for ICAM-1 (red) and DAPI (blue) on stimulated HBMEC's. **4.2B** shows the merged image for the results of staining for ICAM-1 (red) and DAPI (blue) on unstimulated HBMECs. The scale bars show 100 μ m. Inset images show the merged negative control.

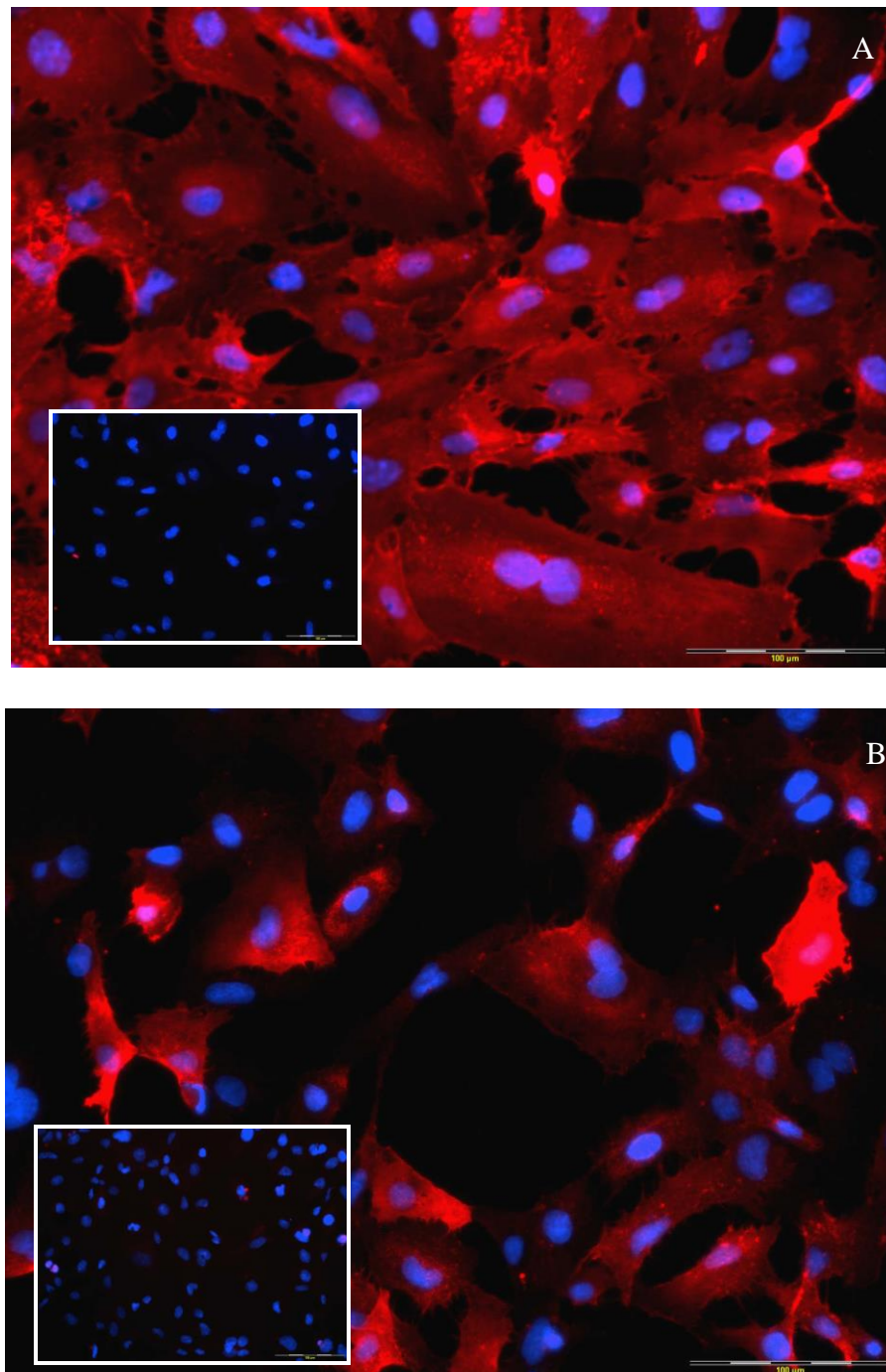


Figure 4.3 ICAM-1 staining of HBMECs stimulated for 16 hours with 100ng/ml $\text{TNF-}\alpha/\text{IFN-}\gamma$. **4.3A** shows the merged image for the results of staining for ICAM-1 (red) and DAPI (blue) on stimulated HBMECs. **4.3B** shows the merged image for the results of staining for ICAM-1 (red) and DAPI (blue) on unstimulated HBMECs. The scale bars show 100 μm . Inset images show the merged negative control.

4.3.2 Time dependent stimulation of HBMECs with 100ng/ml TNF- α

A time dependent analysis was performed with TNF- α stimulation at 1 hour, 2, 4, 8, 16 and 24 hours (figure 4.4) to determine optimal stimulation time for the HBMECs to generate ICAM-1. Significant increases in intensity when stimulated cells were compared to baseline were seen at each time point. Stimulated cells were also significantly different to unstimulated control cells at each time point. There were no significant differences when unstimulated cells were compared to baseline at each time point. The difference between stimulated and unstimulated cells at baseline for ICAM-1 intensity at 2 hours (figure 4.5) did not significantly increase at further time points up to 24 hours, so 2 hour stimulation was accepted as optimal for ICAM-1 generation for further studies.

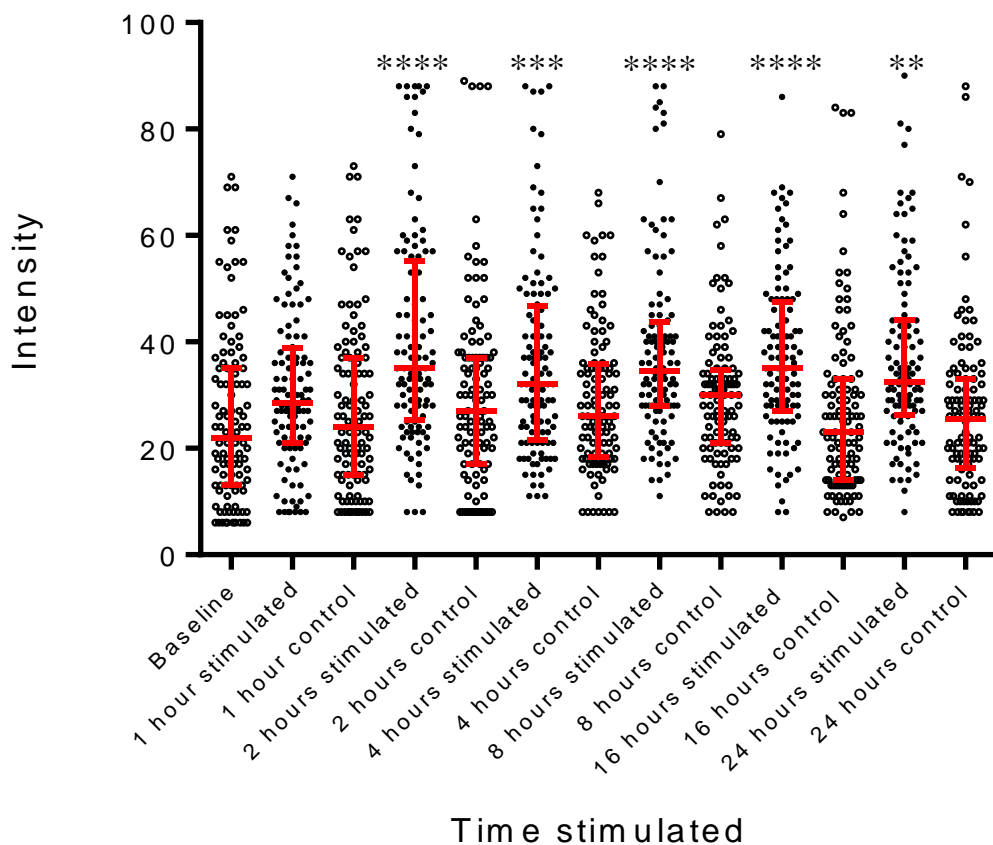


Figure 4.4 Dot plot showing ICAM-1 staining intensity at 0-24 hour TNF- α stimulation of HBMECs. Data shows the median values for intensity of ICAM-1 following TNF- α treatment for 1, 2, 4, 8, 16 and 24 hours. Kruskal-Wallis ANOVA was performed as data were non parametric, the vertical red bar indicates interquartile range, with horizontal red line showing median. * $p < 0.05$, ** $p < 0.01$, *** $p < 0.001$, **** $p < 0.0001$ from baseline using Dunn's post hoc test.

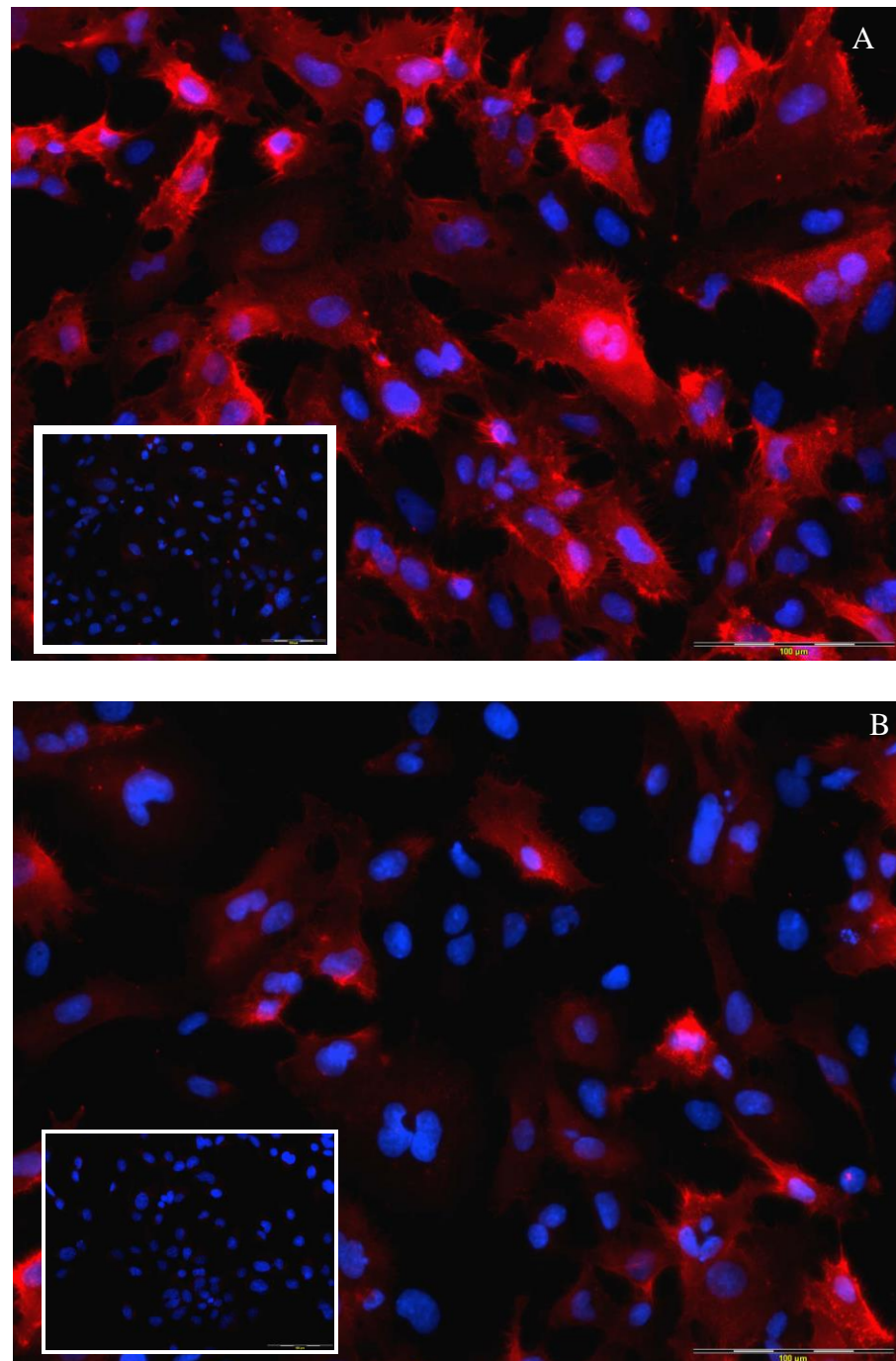


Figure 4.5 Image showing typical ICAM-1 staining of HBMECs stimulated with **100ng/ml TNF- α for 2 hours**. **4.5A** shows the merged image for the results of staining for ICAM-1 (red) and DAPI (blue) in stimulated HBMECs. **4.5B** shows the merged image for the results of staining for ICAM-1 (red) and DAPI (blue) on unstimulated HBMECs. The scale bars show 100 μ m. Inset images show the merged negative control.

4.4 Chemokine generation at activated HBMECs

4.4.1 Time dependent CCL7 generation by HBMECs in the absence and presence of 10ug/ml cycloheximide.

In the absence of cycloheximide a time dependent analysis to assess the generation of CCL7 by HBMECs was performed. Cells were stimulated with TNF- α and chemokine staining then performed at 0, 2, 3, 4, 5 and 6 hours post-stimulation (figure 4.6). Significant differences in CCL7 were observed at 2, 3, 4, 5 and 6 hours when stimulated and unstimulated cells were compared (table 4.2). The greatest increase was seen at 2 hours (figure 4.7A and 4.7B) where median intensity increased by 6.00au from 17.00au under normal conditions (unstimulated) to 23.00au when stimulated (p 0.0001, table 4.2). No non-specific staining was seen on the negative control (figure 4.7C). Trend analysis showed that there was a significant trend of decreasing levels of intensity between 2 and 6 hours post-stimulation (p = 0.016). The negative (unstimulated) control showed no significant changes in staining intensity over the 6 hour time course.

In the presence of cycloheximide the only significant difference in CCL7 between stimulated and unstimulated cells was found at 2 hours (table 4.2, figure 4.6, figure 4.11A, 4.11B). Median intensity increased by 3.75au from 19.25au under normal conditions to 23.00au when stimulated (p = <0.001). Trend analysis showed no significant differences in CCL7 intensity at 3, 4 and 5 hours post stimulation when compared to control. No changes were seen in the staining intensity of unstimulated cells over the 6 hour experimental period.

Table 4.2 Intensity of CCL7 staining following time dependent stimulation of HBMECs by TNF- α in the absence and presence of cycloheximide.

Time stimulated (hours)	Without cycloheximide			With cycloheximide		
	Unstimulated (n=2)	Stimulated	Difference	Unstimulated	Stimulated	Difference
Baseline	16.75 14.00 – 18.00		-	19.25 16.55 – 23.30		-
2	17.00 15.00 - 18.00	23.00**** 17.25 - 29.00	+6.00 $P = 0.0001$	20.00 17.25 - 24.00	23.00*** 19.25 - 27.00	+3.00 $p = 0.41$
3	18.00 15.00 - 21.00	22.50**** 16.00 - 27.00	+4.50 $p = 0.0001$	20.50 18.00 - 23.00	21.00 18.00 - 25.00	+1.50 $p = 0.59$
4	17.00 15.00 - 20.00	20.00**** 17.00 - 24.00	+3.00 $p = 0.001$	20.00 16.00 - 24.00	21.55 18.00 - 26.00	+1.55 $p = 0.065$
5	16.00 14.00 - 18.00	18.00*** 16.00 - 20.00	+2.00 $p = 0.0001$	19.25 15.50 - 22.00	21.50 17.25 - 24.00	+2.25 $p = 0.05$
6	16.00 14.00 - 19.00	17.00 15.00 - 19.75	+1.00 $p = 0.024$	20.00 17.00 - 23.00	21.00 18.00 - 25.00	+1.00 $p = 0.07$

Values are expressed as median values and given in arbitrary units with interquartile range. n = 3 wells throughout unless otherwise specified. Value for ‘difference’ is stimulated median – unstimulated median (TNF- α absent) and p value is from Wilcoxon signed rank test. P value for stimulated intensity compared with baseline (baseline performed in the absence of TNF- α) is from Dunn’s post hoc test, *** $p = <0.001$, **** $p = <0.0001$.

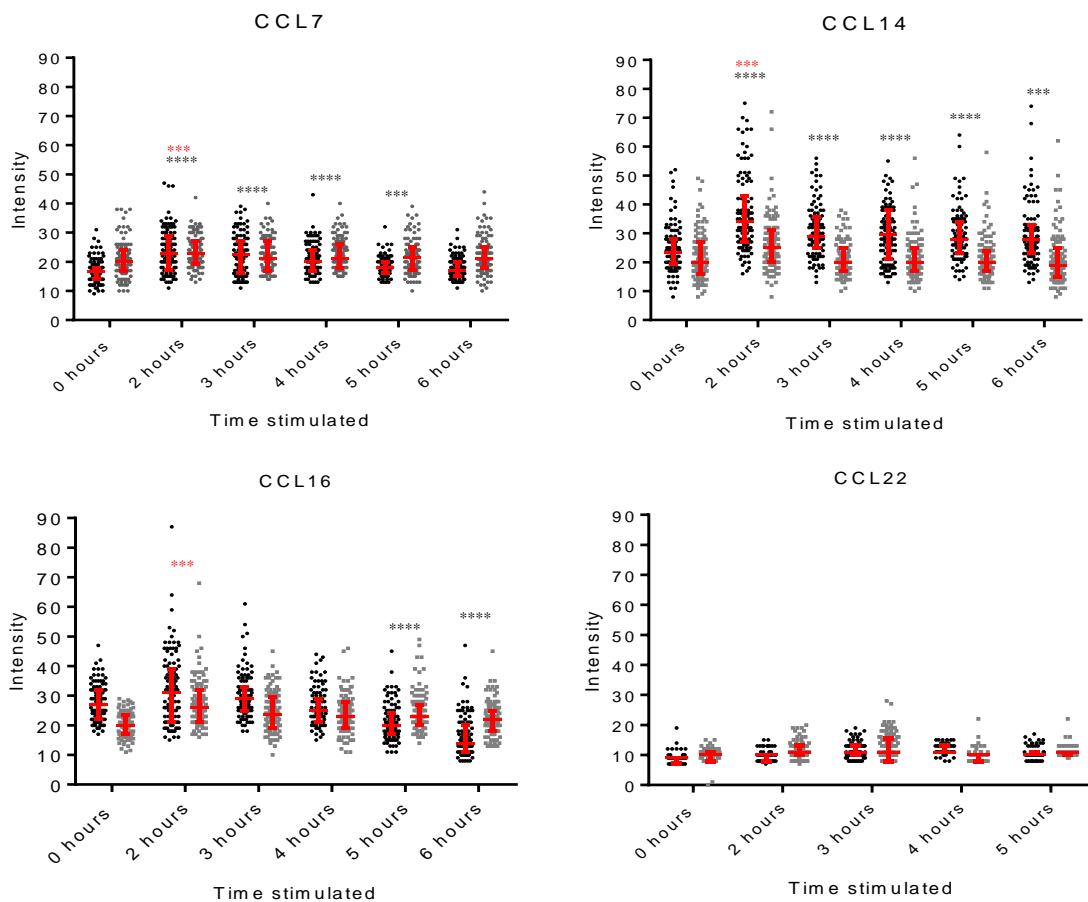


Figure 4.6 CCL7, CCL14, CCL16 and CCL22 staining intensity at 0, 2, 3, 4, 5 and 6 hours TNF- α stimulation of HBMECs in the absence and presence of cycloheximide.

• Shows chemokine in the absence of cycloheximide, • shows chemokine in the presence of cycloheximide. **A** shows CCL7 in the presence and absence of cycloheximide (n = 2 for absence), **B** shows CCL14 in the presence and absence of cycloheximide, **C** shows CCL16 in the presence and absence of cycloheximide, **D** shows CCL22 in the presence and absence of cycloheximide, for each experiment n = 3 unless otherwise stated. All experiments were performed by stopping the experiment for the control (0 hours) in the absence of TNF- α , and simultaneously adding cycloheximide to the remaining cells. The vertical red bar indicates interquartile range and horizontal red line shows median. Kruskal-Wallis ANOVA was used to show overall difference and Dunn's post hoc test was used to assess differences between 0 hours and each time point.*** $p < 0.001$, **** $p < 0.0001$. * indicates significance in the absence of cycloheximide, * indicates significance in the presence of cycloheximide.

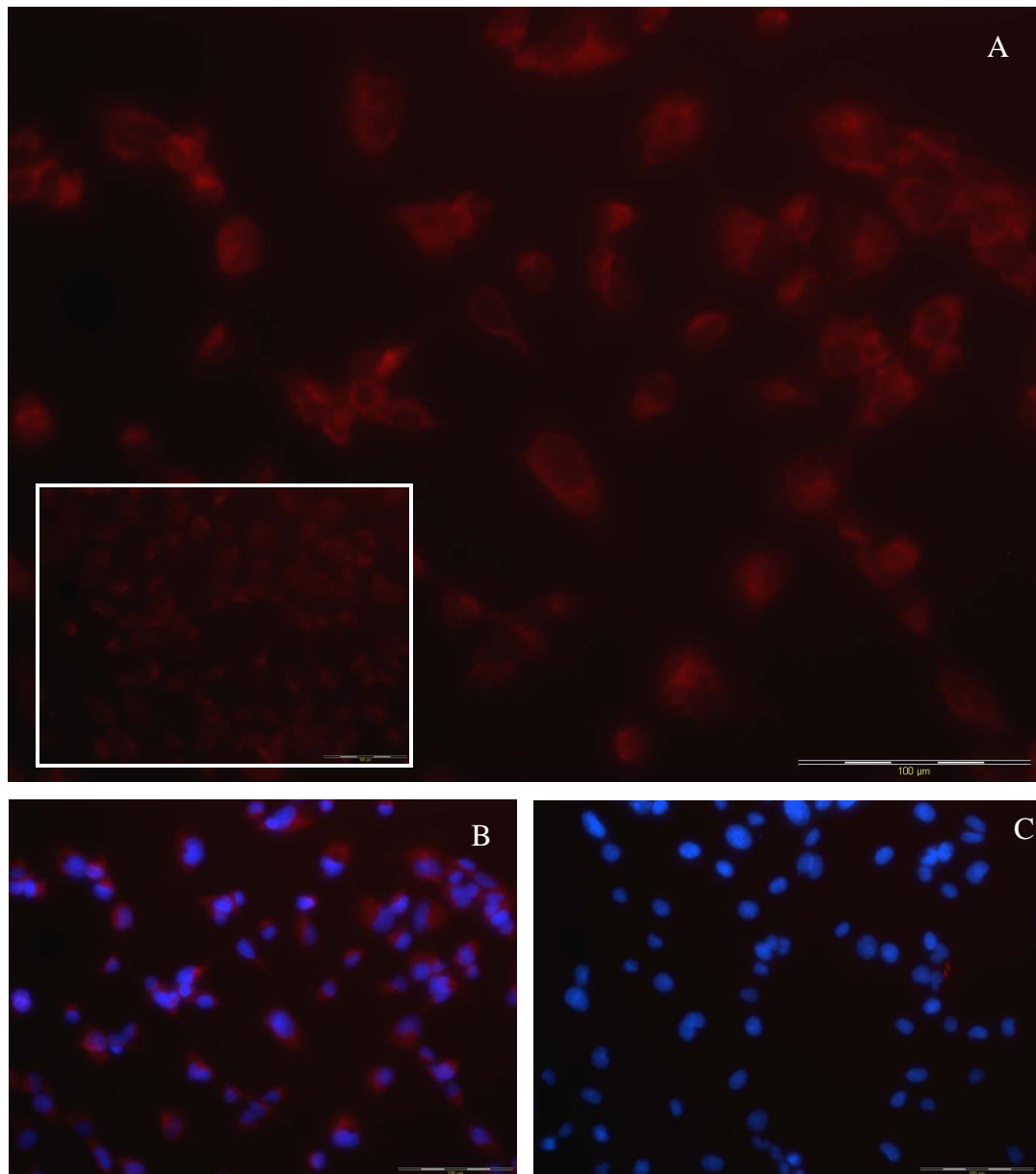


Figure 4.7 Image showing typical CCL7 staining of HBMECs stimulated with 100ng/ml TNF- α for 2 hours in the absence of cycloheximide. **4.7A** shows the image for the results of staining for CCL7 (red) in stimulated HBMECs. The inset image shows CCL7 at 5 hours stimulation. **4.7B** shows the same image merged for the results of staining for CCL7 (red) and DAPI (blue). **4.7C** shows the merged negative control. Scale bars shows 100 μ m.

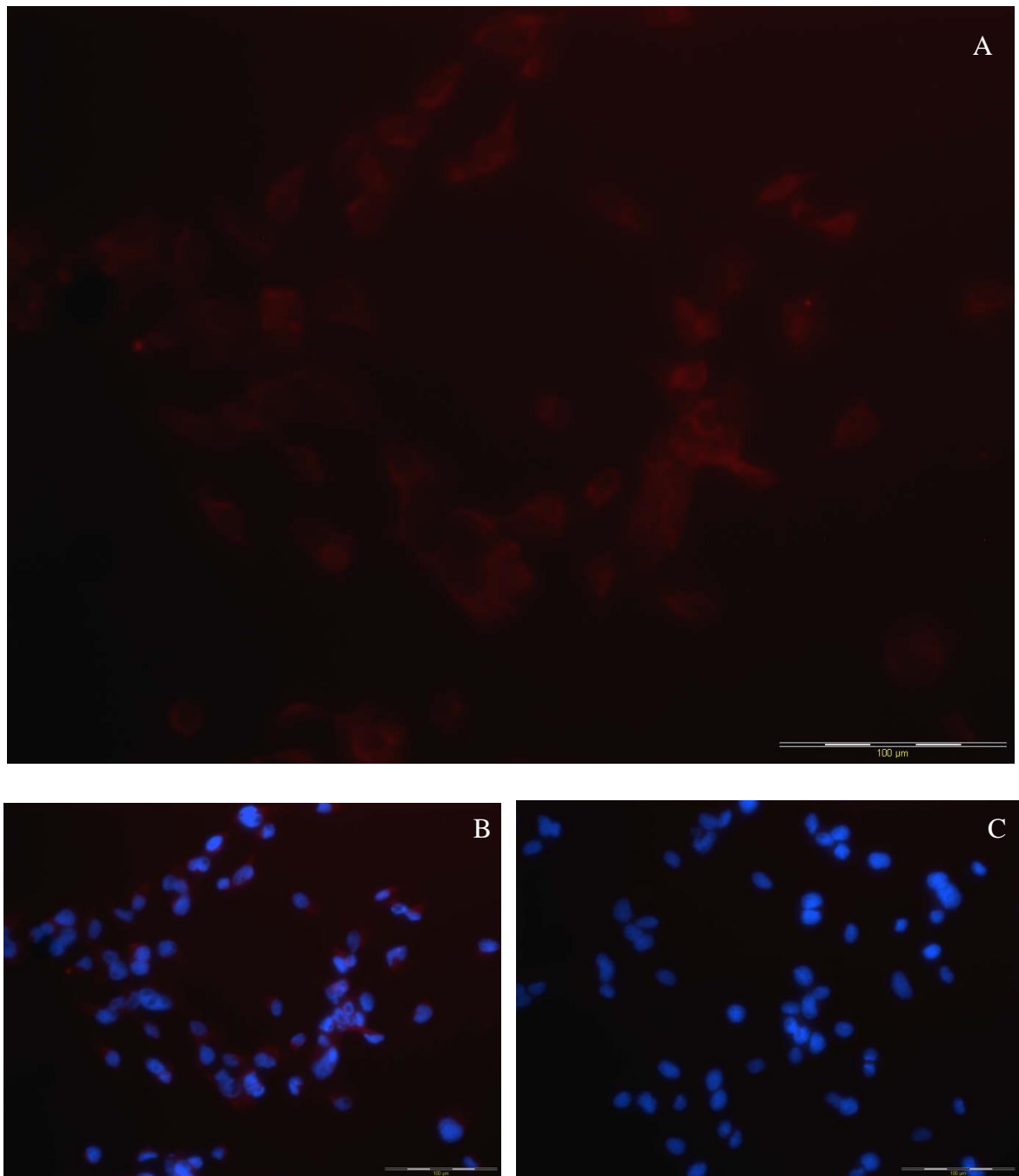


Figure 4.8 Image showing typical CCL7 staining of HBMECs stimulated with 100ng/ml TNF- α for 2 hours in the presence of cycloheximide. **4.8A** shows the image for the results of staining for CCL7 (red) in stimulated HBMECs. **4.8B** shows the same image merged for the results of staining for CCL7 (red) and DAPI (blue). **4.8C** shows the merged negative control. Scale bars shows 100 μ m.

4.4.2 Time dependent CCL14 generation by HBMECs in the absence and presence of 10ug/ml cycloheximide.

In the absence of cycloheximide significant differences in CCL14 were observed at each time point when stimulated and unstimulated cells were compared. The greatest increase was seen at 2 hours (table 4.3, figure 4.6, figures 4.9, 4.10A and 4.10B) where median intensity increased by 10.00au from 24.00au under normal conditions to 34.00au in inflammatory conditions ($p = <0.0001$). This was followed by a gradual decrease in intensity difference over the proceeding time periods. Trend analysis showed an overall significant decrease in intensity between 2 and 6 hours post-stimulation ($p = 0.017$). The negative (unstimulated) control showed no significant changes in staining intensity over the 6 hour time course.

In the presence of cycloheximide a significant difference in CCL14 was observed only at the 2 hour time point when stimulated and unstimulated cells were compared (table 4.3, figure 4.6, figures 4.9, 4.10A and 4.10B). Median intensity increased by 4.50au from 20.50au under normal conditions to 25.00au in inflammatory conditions ($p = 0.0007$). There were no significant differences in the intensity at the other time points.

Table 4.3. Intensity of CCL14 staining following time dependent stimulation of HBMECs by TNF- α in the absence and presence of cycloheximide.

Time stimulated (hours)	Without cycloheximide			With cycloheximide		
	Unstimulated	Stimulated	Difference	Unstimulated	Stimulated	Difference
Baseline	23.00 19.00– 27.00		-	19.50 16.25 – 27.00		-
2	24.00 20.00 - 28.00	34.00**** 27.00 - 43.00	+10 $p = <0.0001$	20.50 17.00 - 27.75	25.00**** 20.00 - 31.00	+4.5 P = 0.0007
3	25.00 20.00 - 30.00	29.00**** 25.00 - 35.75	+4.00 $p = 0.001$	19.00 15.00 - 25.00	20.00 17.00 - 25.00	+1 P = 0.35
4	23.00 18.00 - 29.00	29.5**** 21.99 - 38.00	+6.5 $p = 0.0003$	20.00 17.00 - 25.75	20.00 17.00 - 25.00	0
5	21.00 17.00 - 25.00	28.00**** 23.25 - 34.00	+7.00 $p = <0.0001$	20.00 17.00 - 24.00	20.00 17.00 - 25.00	0
6	n/a	28.00*** 23.25 - 32.75	n/a	18.00 14.25 - 22.00	19.00 15.00 - 25.00	+1

Values are expressed as median values and given in arbitrary units with interquartile range. n = 3 wells throughout unless otherwise specified. Value for ‘difference’ is stimulated median – unstimulated median (TNF- α absent) and p value is from Wilcoxon signed rank test. P value for stimulated intensity compared with baseline (baseline performed in the absence of TNF- α) is from Dunn’s post hoc test, *** $p = <0.001$, **** $p = <0.0001$.

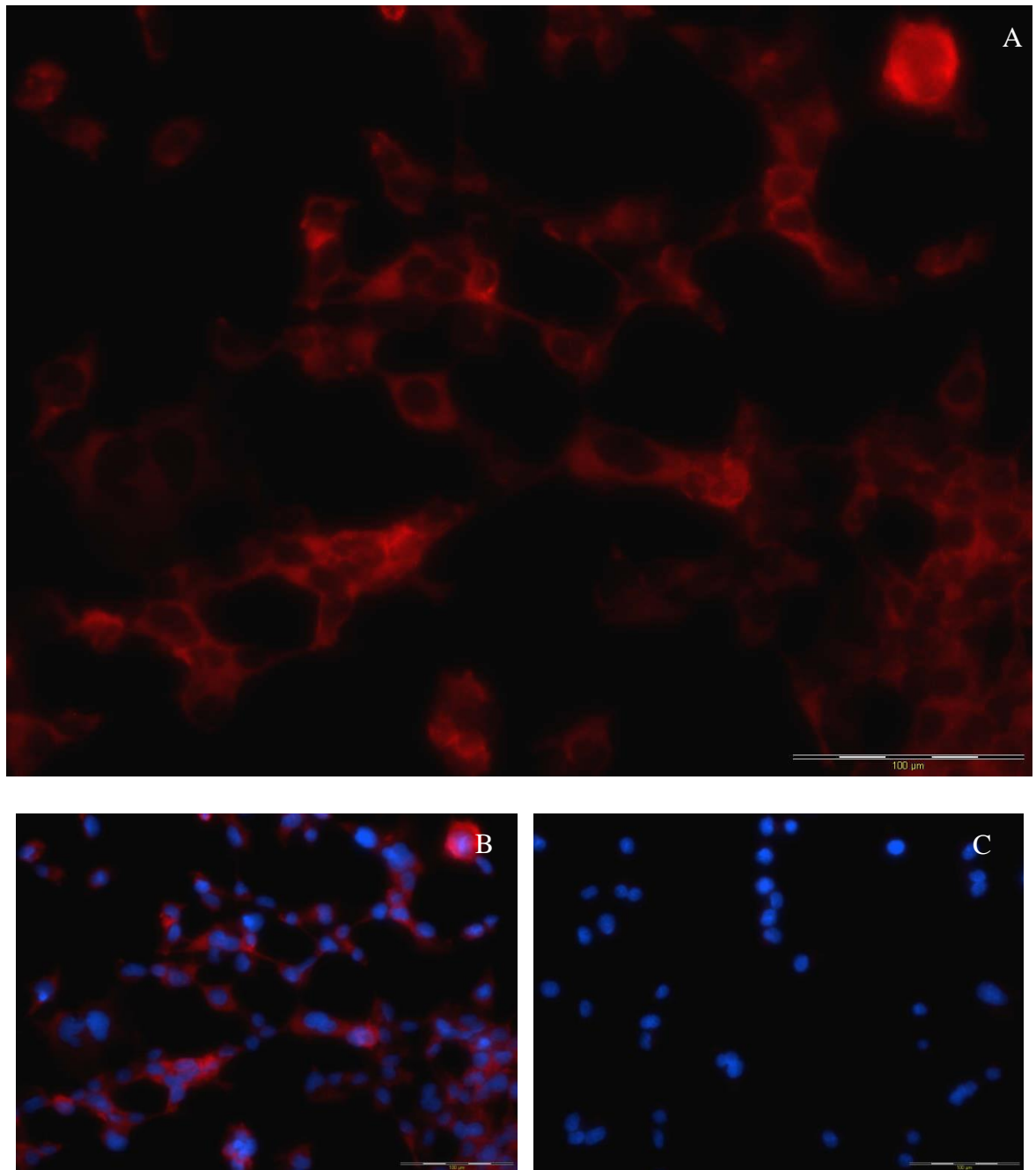


Figure 4.9 Image showing typical CCL14 staining of HBMECs stimulated with 100ng/ml TNF- α for 2 hours in the absence of cycloheximide. **4.9A** shows the image for the results of staining for CCL14 (red) in stimulated HBMECs. **4.9B** is the same image merged for the results of staining for CCL14 (red) and DAPI (blue). **4.9C** shows the merged negative control. Scale bars shows 100 μ m.

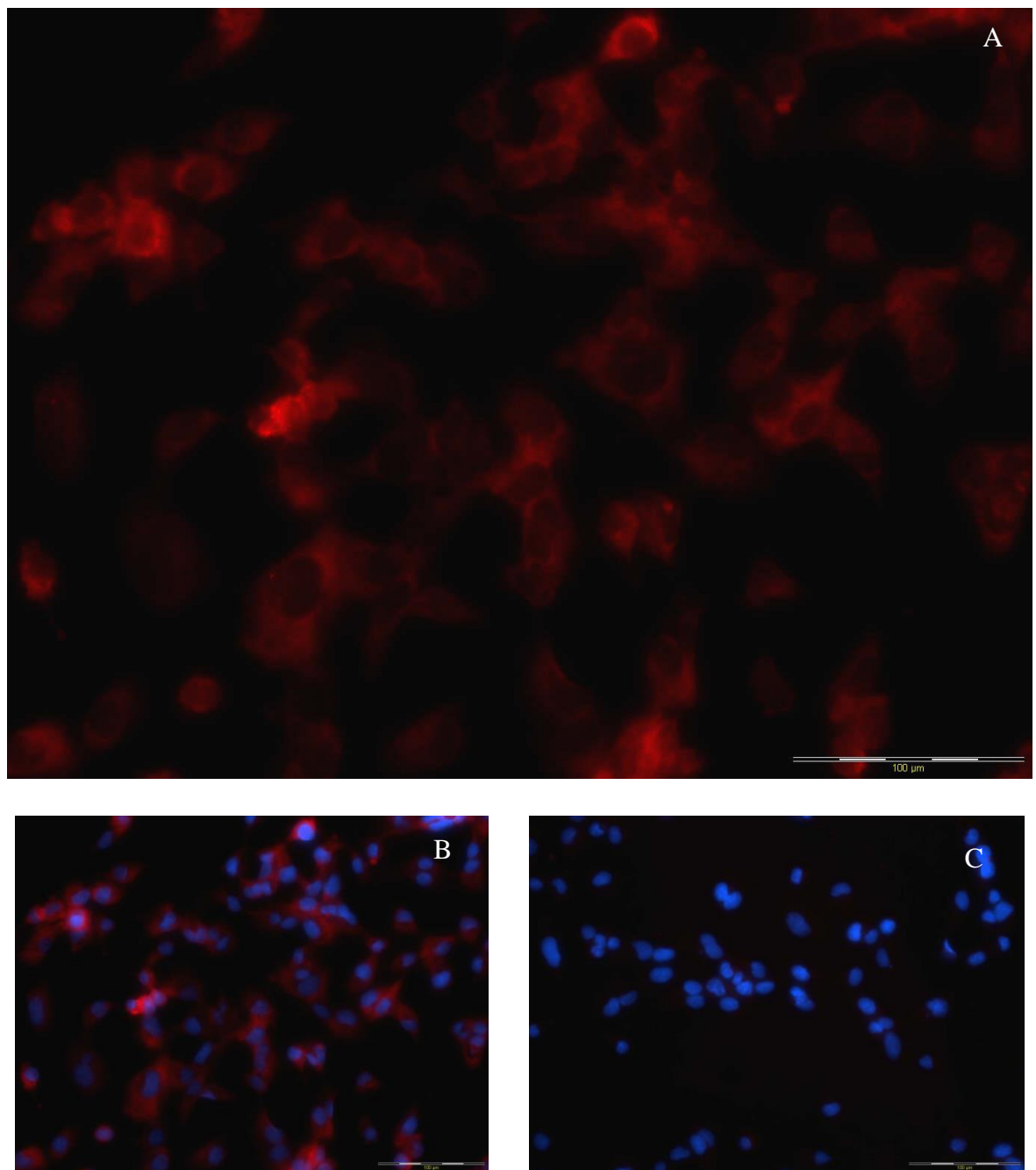


Figure 4.10 Image showing typical CCL14 staining of HBMECs stimulated with 100ng/ml TNF- α for 2 hours in the presence of cycloheximide. **4.10A** shows the image for the results of staining for CCL14 (red) in stimulated HBMECs. **4.10B** shows the same image merged for the results of staining for CCL14 (red) and DAPI (blue). **4.10C** shows the merged negative control. Scale bars shows 100 μ m.

4.4.3 Time dependent CCL16 generation by HBMECs in the absence and presence of 10µg/ml cycloheximide.

In the absence of cycloheximide significant differences in CCL16 were observed at the 5 and 6 hour time points when stimulated and unstimulated cells were compared (table 4.4, $p = 0.001$, $p = 0.0001$, respectively) where the intensity decreased to significantly below control ($p = <0.0001$) (table 4.4, figure 4.6, figure 4.11). There was a near-significant difference in intensity observed at 2 hours post-stimulation ($p = 0.053$) and at 3 hours post-stimulation ($p = 0.05$). At 5 and 6 hours post-stimulation the intensity decreased to significantly below control ($p = <0.001$ and <0.0001 respectively) (table 4.4, figure 4.6, figure 4.11). Trend analysis showed a significant decrease in intensity between 2-6 hours post stimulation ($p = 0.001$). Representative staining is shown in figures 4.15A and 4.15B. The negative (unstimulated) control showed no significant changes in staining intensity over the 6 hour time course.

In the presence of cycloheximide (table 4.4, figures 4.12A and 4.12B) a significant difference was observed at 2 hours when stimulated and unstimulated cells were compared (table 4.4). Trend analysis showed no significant differences from 2-6 hours post-stimulation ($p = 0.1$). As the n number for the unstimulated cells and control cells is low, this data requires repeating for validation and must be considered observational only.

4.4.4 Time dependent CCL22 generation in HBMECs in the absence and presence of 10µg/ml cycloheximide.

No significant differences were observed between data in the presence or absence of cycloheximide (table 4.5, figures 4.6, 4.13)

Table 4.4 Intensity of CCL16 staining following time dependent stimulation of HBMECs by TNF- α in the absence and presence of cycloheximide.

Time stimulated (hours)	Without cycloheximide			With cycloheximide		
	Unstimulated	Stimulated	Difference	Unstimulated (n=2)	Stimulated	Difference
Baseline	27.50 22.50 – 32.50		-	22.00 (n=1) 18.50 – 26.00		-
2	28.00 22.00 – 33.00	31.50 21.00 - 39.00	+3.50 $p = 0.053$	21.00 18.00 - 24.75	26.00**** 21.00 - 32.00	+5.00 $p = 0.03$
3	26.00 22.00 – 32.00	29.00 25.00 - 33.00	+3.00 $p = 0.05$	21.00 17.00 - 23.00	23.50 19.25 – 29.75	+2.50 $p = 0.05$
4	28.00 22.00 - 32.00	25.00 21.00 – 29.00	+2.00 $p = 0.10$	21.00 16.00 - 25.00	23.00 19.00 - 28.00	+2.00 $p = 0.06$
5	26.00 21.00 – 31.00	20.00*** 17.00 - 24.00	-6.00 $p = <0.001$	19.75 17.00 – 23.00	23.00 20.00 - 27.00	+3.25 $p = 0.05$
6	26.00 22.00 – 31.00	14.00**** 11.00 - 20.00	-12.00 $p = <0.0001$	20.00 17.00 – 24.00	22.00 18.00 - 25.00	+2.00 $p = 0.06$

Values are expressed as median values and given in arbitrary units with interquartile range. n = 3 wells throughout unless otherwise specified. Value for ‘difference’ is stimulated median – unstimulated median (TNF- α absent) and p value is from Wilcoxon signed rank test. P value for stimulated intensity from baseline (baseline performed in the absence of TNF- α) is from Dunn’s post hoc test, *** $p = <0.001$, **** $p = <0.0001$.

Table 4.5 Intensity of CCL22 staining following time dependent stimulation of HBMECs by TNF- α in the absence and presence of cycloheximide.

Time stimulated (hours)	Without cycloheximide			With cycloheximide		
	Unstimulated	Stimulated	Difference	Unstimulated (n=2)	Stimulated	Difference
Baseline	11.00 8.00 – 11.50		-	10.50 9.50 – 12.50		-
2	10.00 8.00 – 11.00	11.00 10.00 – 13.00	+1.00 $p = 0.07$	11.00 10.00 – 13.00	11.00 10.00 – 13.00	0
3	10.00 10.00 - 11.00	11.00 8.00 – 15.50	+1.00 $p = 0.06$	10.00 8.00 – 10.00	11.00 11.00 – 13.00	0
4	10.00 8.00 – 10.00	10.00 8.00 – 10.00	0	10.00 8.00 – 10.00	10.00 8.00 - 10.00	0
5	11.00 10.00 – 11.00	11.00 10.00 – 11.00	0	10.00 9.00 – 11.00	10.00 10.00 – 11.00	0

Values are expressed as median values and given in arbitrary units with interquartile range. n = 3 wells throughout unless otherwise specified. Value for ‘difference’ is stimulated median – unstimulated median (TNF- α absent) and p value is from Wilcoxon signed rank test. P value for stimulated intensity from baseline is from Dunn’s post hoc test.

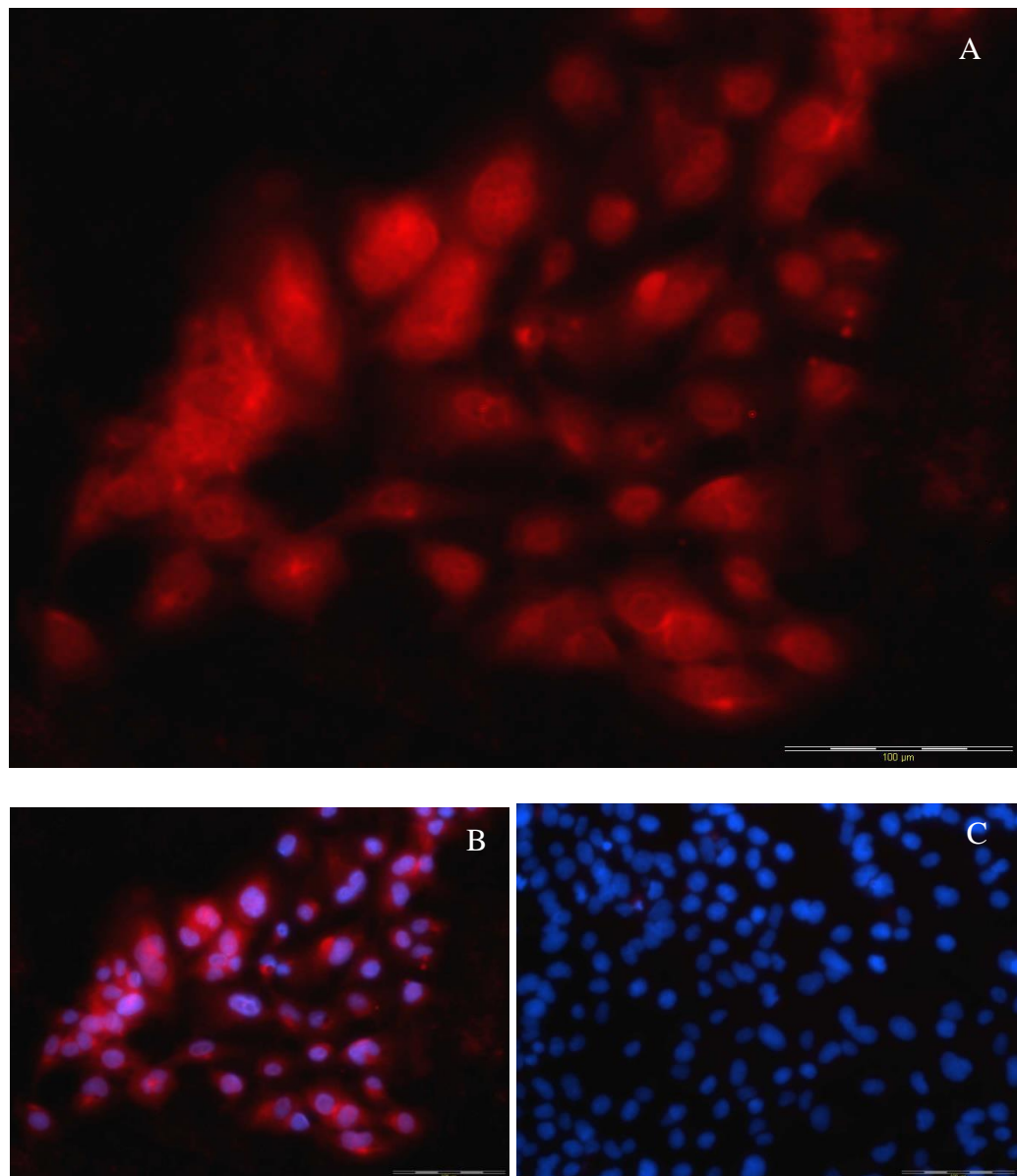


Figure 4.11 Image showing typical CCL16 staining of HBMECs stimulated with **100ng/ml TNF- α** for 2 hours in the absence of cycloheximide. **4.11A** shows the image for the results of staining for CCL16 (red) in stimulated HBMECs. **4.11B** shows the same image merged for the results of staining for CCL16 (red) and DAPI (blue). **4.11C** shows the merged negative control. Scale bars shows 100 μ m.

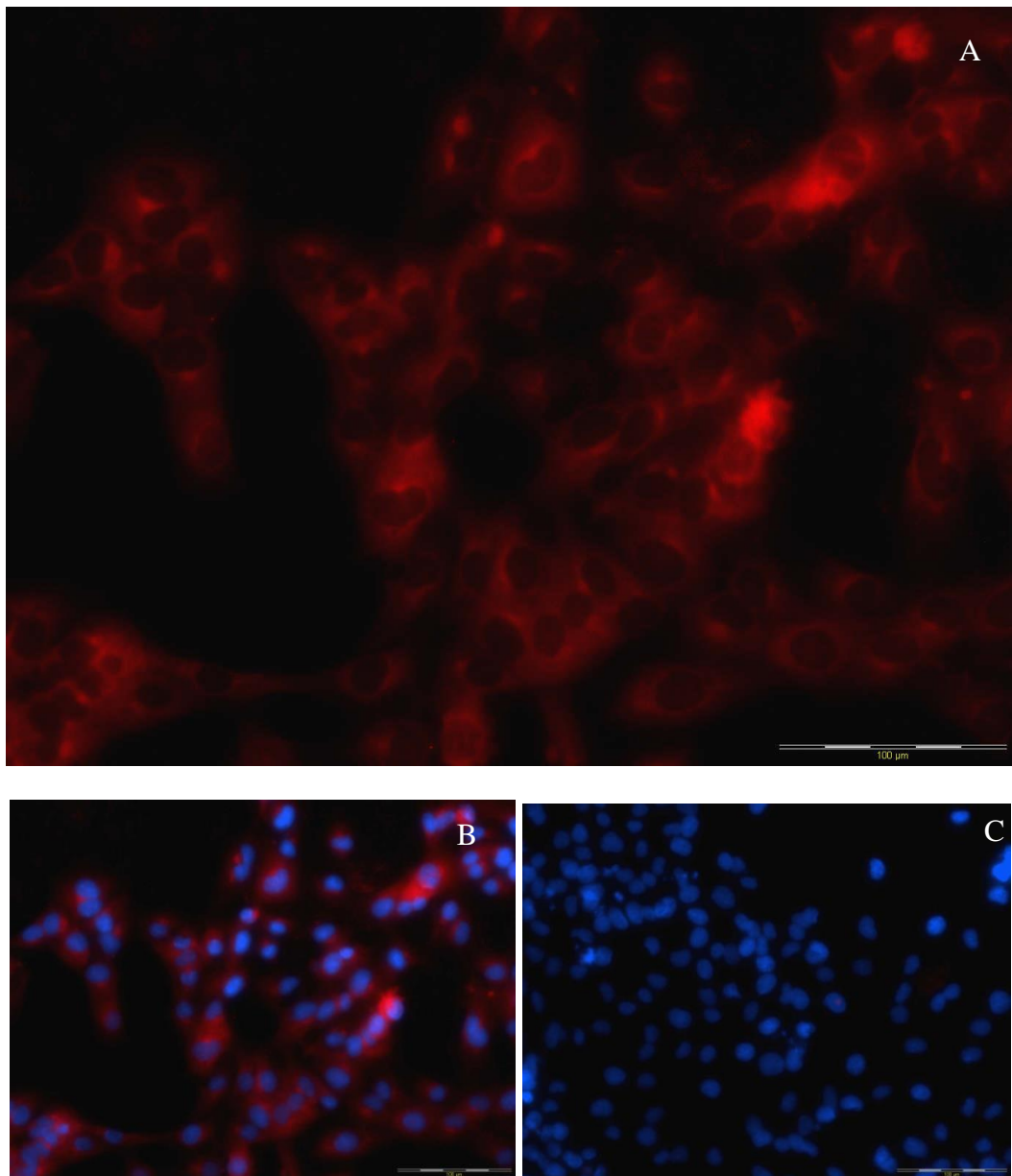


Figure 4.12 Image showing typical CCL16 staining of HBMECs stimulated with 100ng/ml TNF- α for 2 hours in the presence of cycloheximide. **4.12A** shows the image for the results of staining for CCL16 (red) in stimulated HBMECs. **4.12B** shows the same image merged for the results of staining for CCL16 (red) and DAPI (blue). **4.12C** shows the merged negative control. Scale bars shows 100 μ m.

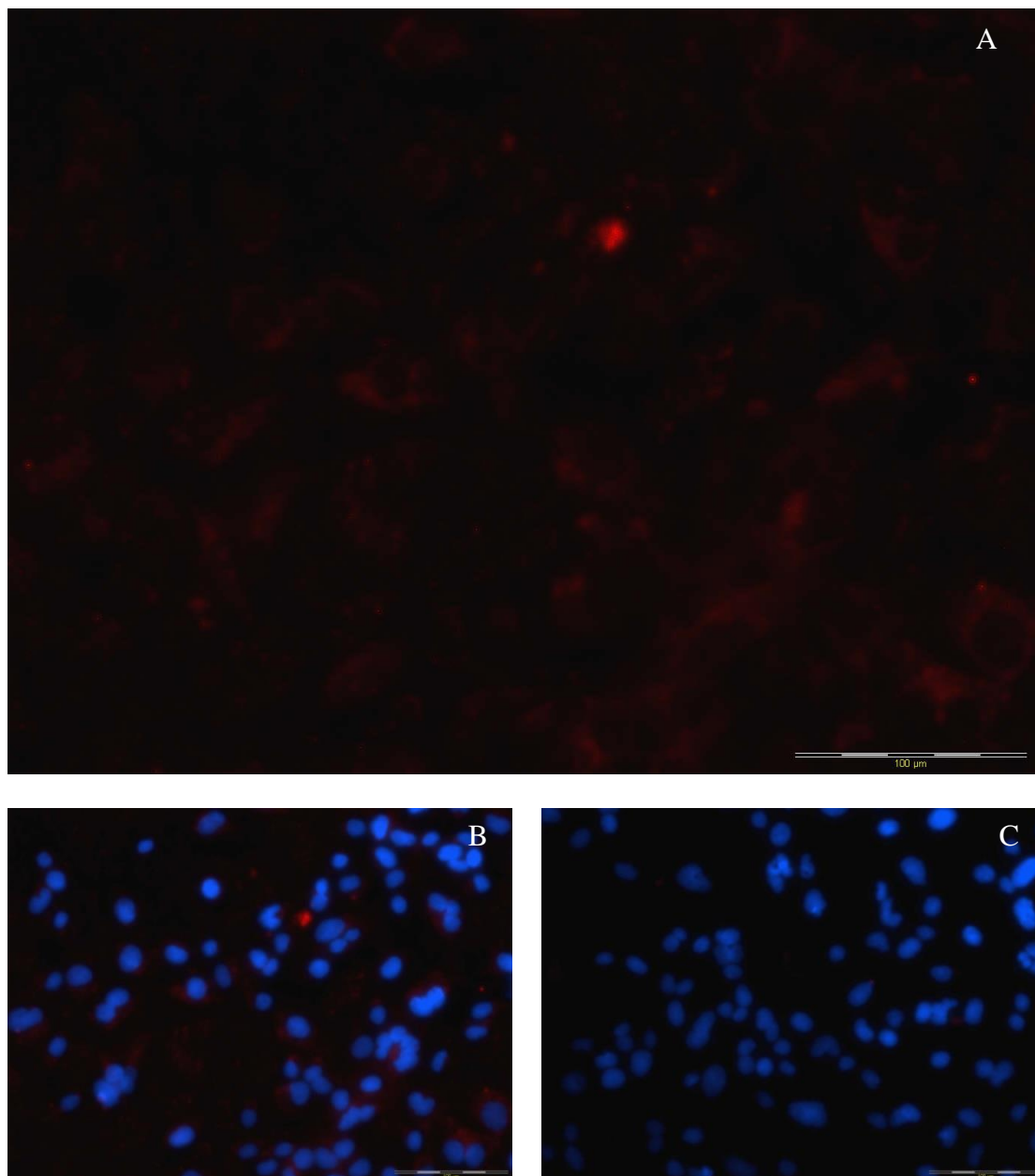


Figure 4.13 Image showing typical CCL22 staining of HBMECs stimulated with 100ng/ml TNF- α for 3 hours in the absence of cycloheximide. **4.13A** shows the image for the results of staining for CCL22 (red) in stimulated HBMECs. **4.13B** shows the same image merged for the results of staining for CCL22 (red) and DAPI (blue). **4.13C** shows the merged negative control. Scale bars shows 100 μ m.

4.5 Cell surface ICAM-1 intensity following 16 hour stimulation of HDLECs.

4.5.1 Stimulation of HDLECs with 100ng/ml TNF- α

There was a significant effect on the generation of ICAM-1 caused by 16 hour stimulation with TNF- α (table 4.6, figure 4.14A). Under normal conditions (figure 4.14B) ICAM-1 intensity was 29.00au which increased by 6.50au to 35.50au following TNF- α stimulation ($p = <0.0001$). Isotype matched controls showed no non-specific staining (inset images).

4.5.2 Stimulation of HDLECs with 100ng/ml IFN- γ

There was a significant effect on the generation of ICAM-1 caused by 16 hour stimulation with IFN- γ (see table 4.6, figure 4.15A). Following IFN- γ stimulation, ICAM-1 intensity increased by 11au from 25.00au under normal conditions to 36.00au ($p = <0.0001$). The increase in ICAM-1 expression was clear once stimulated (figure 4.15A), despite some staining being observed on the unstimulated cells (Figure 4.15B). Isotype matched controls showed minimal non-specific staining (inset images)

4.5.3 Stimulation of HDLECs with 100ng/ml TNF- α and 100ng/ml IFN- γ

There was a significant effect on the generation of ICAM-1 caused by 16 hour stimulation with IFN- γ /TNF- α (see table 4.6, figure 4.16A). Following stimulation with IFN- γ /TNF- α ICAM-1 intensity increased from 24.50au under normal conditions by 19.50au to 44.00au ($p = <0.0001$) (table 4.6). ICAM-1 showed markedly higher expression on stimulated cells (figure 4.16A) than on unstimulated cells (Figure 4.16B). Isotype matched controls showed minimal non-specific staining (inset images).

Table 4.6 Intensity of cell surface ICAM-1 staining following 16 hour stimulation of HDLECs with 100ng/ml TNF- α , 100ng/ml IFN- γ and 100ng/ml IFN- γ /TNF- α .

Stimulation solution	Unstimulated	Stimulated	Difference (<i>p</i> value)
100ng/ml TNF- α	29.00 23.00 – 37.75	35.50 28.50 – 50.00	+6.5 <i>p</i> = < 0.0001
100ng/ml IFN- γ	25.00 19.00 - 33.00	36.00 29.25 – 46.75	+11 <i>p</i> = < 0.0001
100ng/ml TNF- α /IFN- γ	24.50 18.00 – 30.00	44.00 36.25 – 55.00	+19.50 <i>p</i> = < 0.0001

Values are expressed as medians and given in arbitrary units with interquartile range. Values for difference are stimulated median – unstimulated median. Unstimulated analysis was performed in the absence of TNF- α , IFN- γ and TNF- α /IFN- γ as a negative control. Data were non-parametric so *p* values are from the Wilcoxon signed rank test. 3 fields of view per chamber slide well were analysed. n=3 wells throughout.

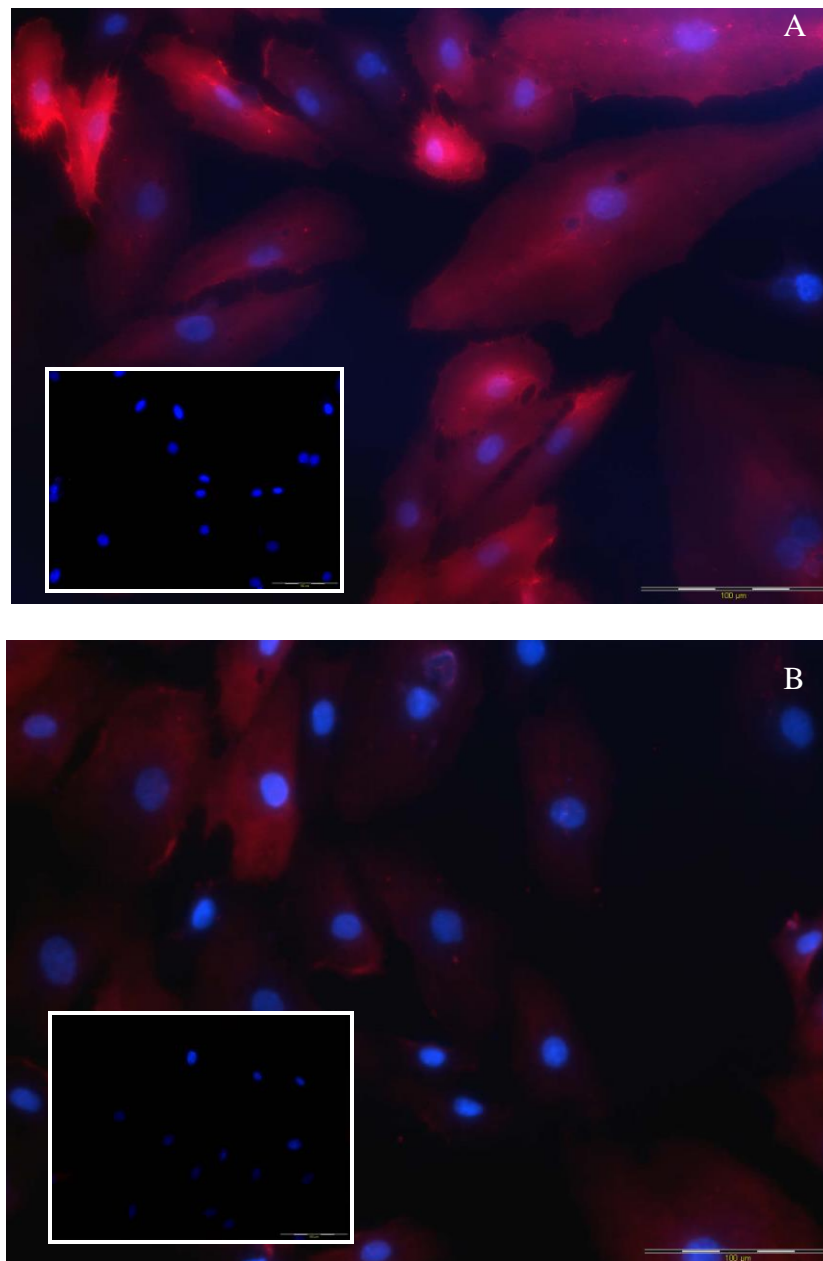


Figure 4.14 ICAM-1 staining of HDLECs stimulated for 16 hours with 100ng/ml TNF- α . **4.14A** shows the merged image for the results of staining for ICAM-1 (red) and DAPI (blue) on stimulated HDLECs. **4.14B.** shows the merged image for the results of staining for ICAM-1 (red) and DAPI (blue) on unstimulated HDLECs. Inset images are the corresponding merged negative control. The scale bars show 100 μ m.

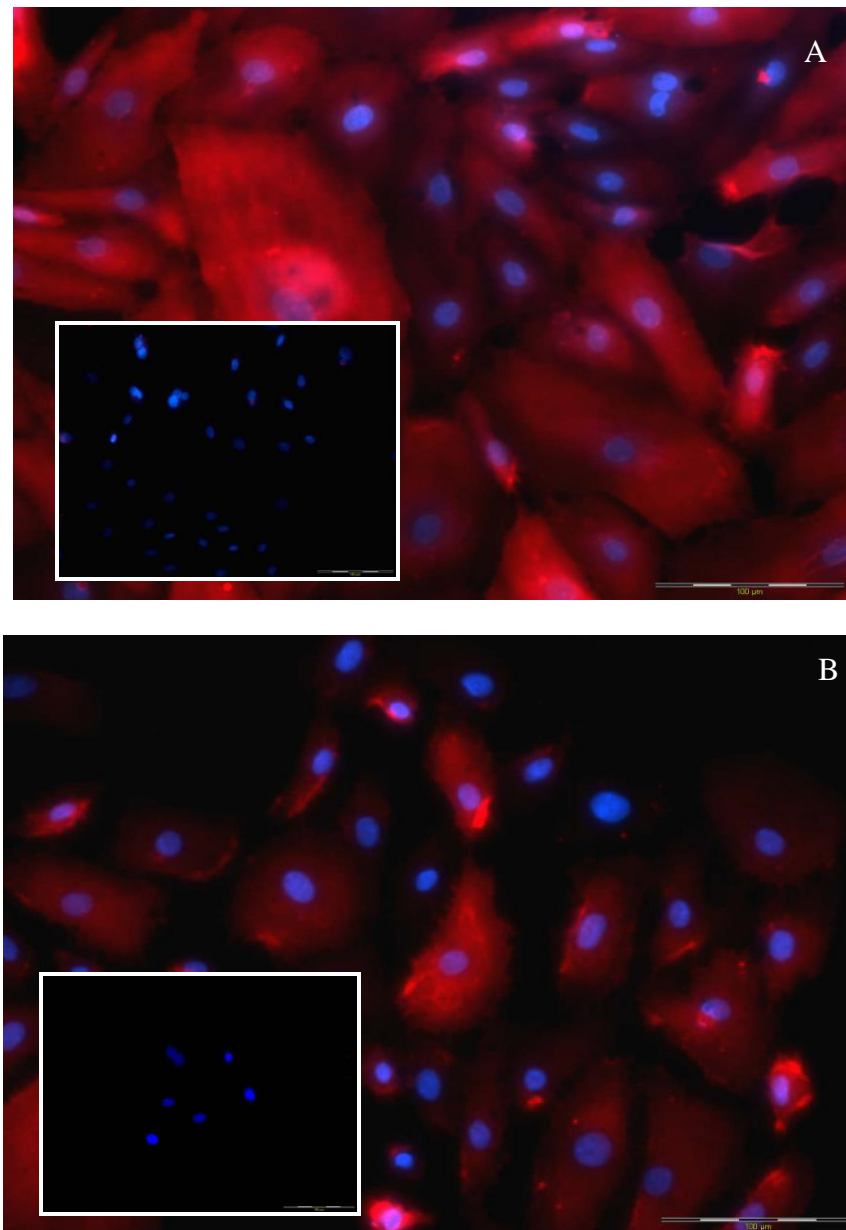


Figure 4.15 ICAM-1 staining of HDLECs stimulated for 16 hours with 100ng/ml IFN- γ **4.15A** shows the merged image for the results of staining for ICAM-1 (red) and DAPI (blue) on stimulated HDLECs. **4.15B.** shows the merged image for the results of staining for ICAM-1 (red) and DAPI (blue) on unstimulated HDLECs. Inset images are the corresponding merged negative control. The scale bars show 100 μ m.

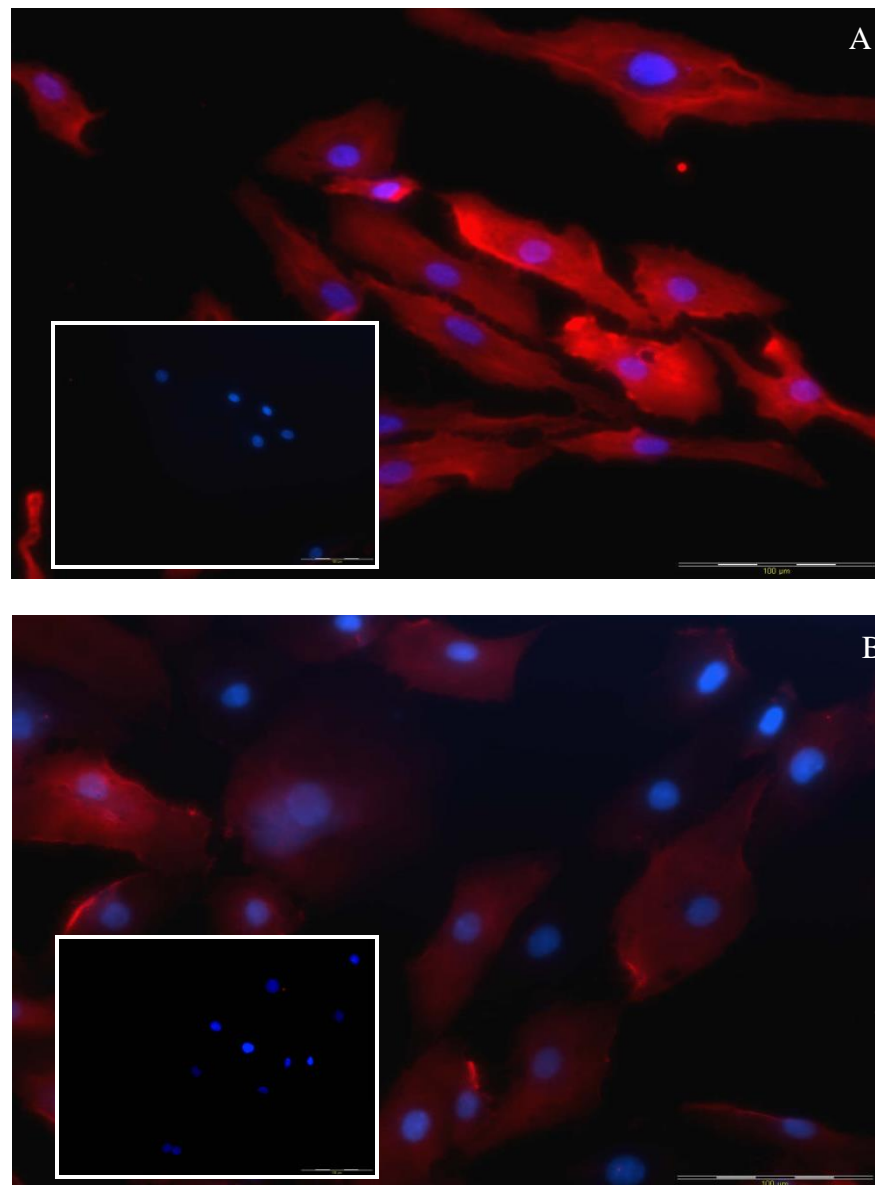


Figure 4.16 ICAM-1 staining of HDLECs stimulated for 16 hours with 100ng/ml TNF- α and 100ng/ml IFN- γ **4.16A** shows the merged image for the results of staining for ICAM-1 (red) and DAPI (blue) on stimulated HDLECs. **4.16B.** shows the merged image for the results of staining for ICAM-1 (red) and DAPI (blue) on unstimulated HDLECs. Inset images show the corresponding merged negative control. The scale bars show 100 μ m.

4.5.4 Time dependent stimulation of HDLECs with 100ng/ml TNF- α and 100ng/ml IFN- γ

A time dependent analysis was performed with TNF- α /IFN- γ stimulation at 1, 2, 4, 8, 16 and 24 hours to determine optimal stimulation time for the HDLECs to generate ICAM-1. There were significant increases in ICAM-1 at 2, 4, 8 and 16 hours post stimulation compared to unstimulated control cells ($p = <0.0001$ throughout) (figure 4.17). Significant spontaneous changes were observed when unstimulated cells were compared to baseline with significant differences observed at 2, 4 and 16 hours (<0.001). However when stimulated and unstimulated cells were compared at each time point there were greater significant differences observed at 2, 4, 8, 16 and 24 hours (all <0.0001). As the differences between these time points when baseline and stimulated cells were compared were negligible the 2 hour stimulation was accepted as optimal (figure 4.18).

Tests were performed to assess the chemokine presence in stimulated HDLECs for 2, 4, 6, 8, 16 and 24 hours. However, it was noted that the cells appeared to be dedifferentiating from passage 5, which were the only cells available, and due to time constraints the tests were unable to be repeated.

4.5.5 ELISA testing of conditioned medium for CCL7, CCL14, CCL16 and CCL22

CCL7 was detected at 4799.59pg/ml in neat medium from stimulated HBMECs and at 427.623pg/ml from simulated HMVEC ($n = 1$ in each case). ELISA testing showed CCL14 at 644.65pg/ml in neat medium from stimulated HMVECs ($n = 1$), but it was not detected in other samples. CCL16 and CCL22 were not detected in any samples. Due to the low n number this data is purely observational and so must be interpreted with caution and repeated for validation.

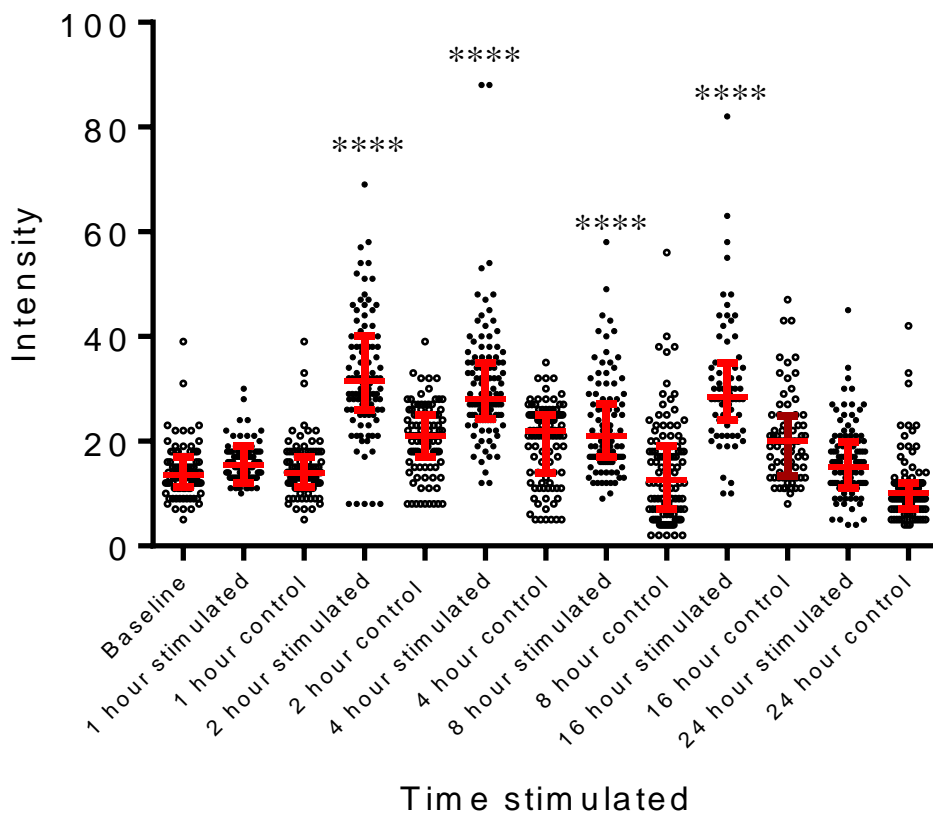


Figure 4.17 Dot plot showing ICAM-1 staining intensity at 0-24 hour TNF- α /IFN- γ stimulation of HDLECs. Data show the values for intensity of ICAM-1 following TNF- α /IFN- γ treatment for 1, 2, 4, 8, 16 and 24 hours. Kruskal-Wallis ANOVA was performed as data were non parametric, the vertical red bar indicates interquartile range with horizontal red line showing the median **** $p = <0.0001$ from baseline using Dunn's post hoc test.

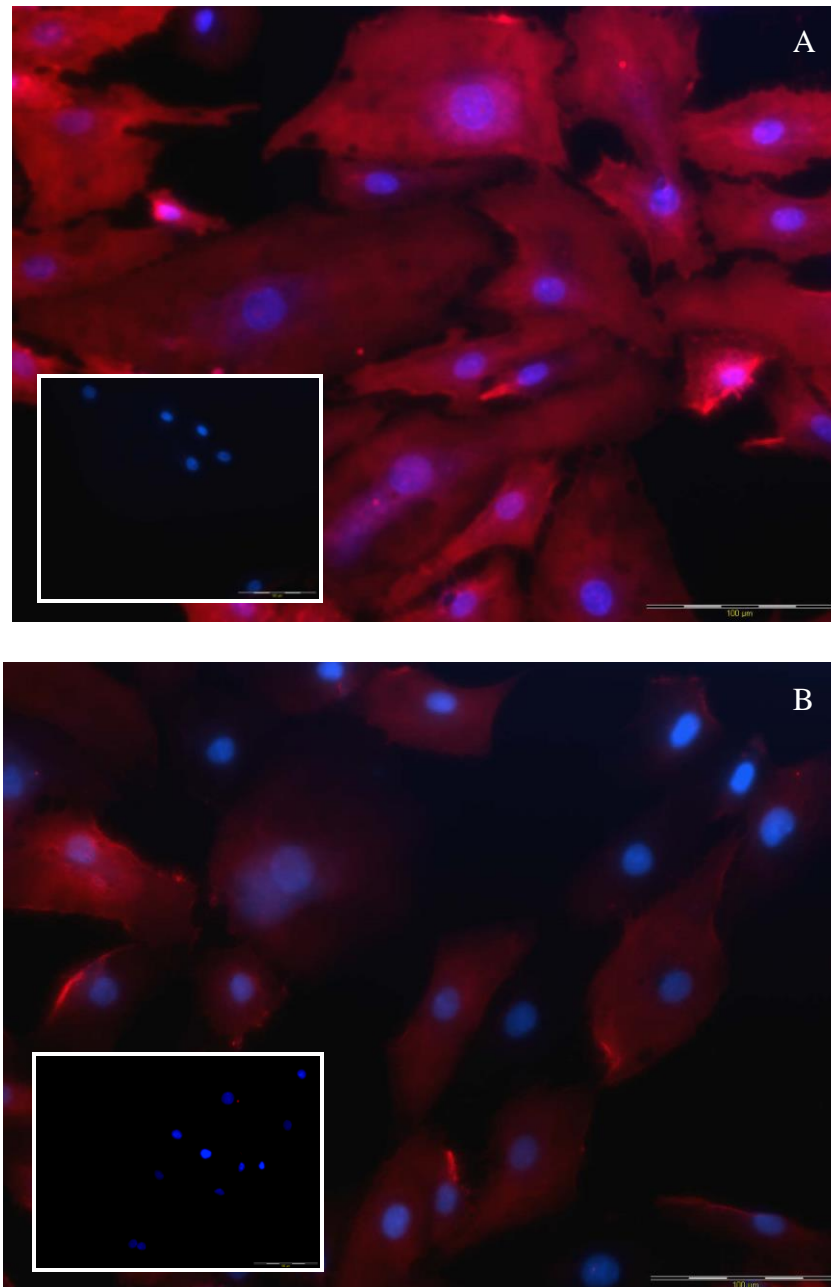


Figure 4.18 ICAM-1 staining of HDLECs stimulated for 2 hours with 100ng/ml TNF- α and 100ng/ml IFN- γ **4.18A** shows the merged image for the results of staining for ICAM-1 (red) and DAPI (blue) on stimulated HDLECs. **4.18B.** shows the merged image for the results of staining for ICAM-1 (red) and DAPI (blue) on unstimulated HDLECs. Inset images show the corresponding merged negative control. The scale bars show 100 μ m.

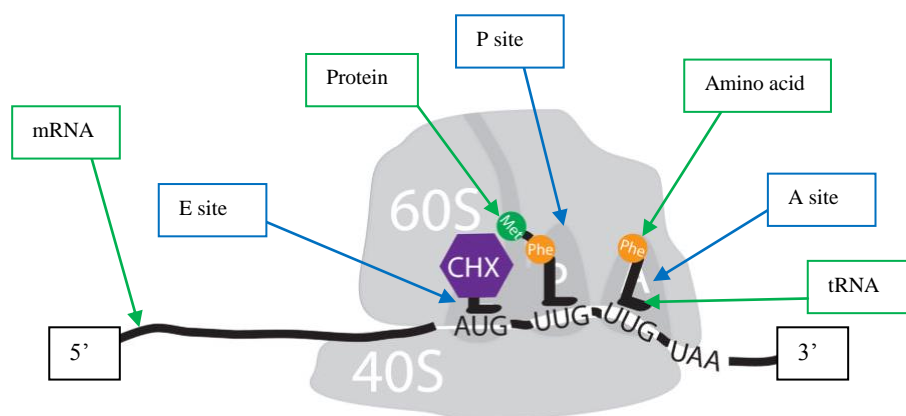
4.6 Discussion

Assessment of ICAM-1 expression was performed to study EC activation by cytokines. Chemokine mediated leukocyte 'crawling' before transmigration is MAC-1 and ICAM-1 dependent (Ley *et al.*, 2007). ICAM-1 reduces the velocity of rolling leukocytes by stabilising the initial transient contact between the leukocytes and the EC (Barreiero and Sanchez-Madrid, 2009), furthermore ICAM (among other adhesion factors), has been shown to regulate the elongation of microvilli (Oh *et al.*, 2007).

In the current study, TNF- α was shown to generate the most significant increase in ICAM-1 at the HBMEC cell surface following 16 hour stimulation compared to IFN- γ or TNF- α /IFN- γ . This supports work by Gimbrone, and Lelke (2003) who state that TNF- α increased ICAM expression to the greatest degree in 8 hours or less when compared to IFN- γ or a combination of the two.

This is the first study to show that for HDLECs, TNF- α in combination with IFN- γ stimulates the most significant increase in ICAM-1. The greatest ICAM-1 expression was observed at 16 hours post stimulation, with highly significant increases seen from 2 hours. Johnson *et al.*, (2006) showed that TNF- α increased ICAM expression in DLECs to the greatest degree when compared to IFN- γ , with maximal expression achieved at 6-12 hours post-stimulation. However, no evidence can be found of combined TNF- α and IFN- γ stimulation performed on HDLECs in the literature.

Cycloheximide disrupts protein synthesis by blocking the translocation step in elongation (Schneider-Poetsch *et al.*, 2010) so in a time dependant manner would affect the levels of the chemokine available for staining (Figure 4.19).

Figure 4.19 Mechanistic model of Cycloheximide inhibition of translation elongation

In the absence of Cycloheximide, a peptide bond would be formed between the amino acid attached to the transfer RNA (tRNA) in site P and the amino acid attached to the tRNA in site A. The growing 'protein' would detach from the tRNA in site P, and as the ribosome moved along the mRNA to the next codon (in a 5' to 3' direction) the tRNA would then translocate from site P to site E allowing another amino acid carrying tRNA to move to the A site. In the presence of Cycloheximide the E site is blocked inhibiting translocation of the tRNA and hence elongation of the protein.

The expected affect if the ECs were actively producing the chemokines in response to TNF- α stimulus in the absence of cycloheximide would be increasing intensity of chemokine staining during the time period, as the concentration of the protein increases, or a rise followed by a plateau in the chemokine production.

In the presence of cycloheximide there would be no increases in intensity as the generation of the chemokine was inhibited at the translational level. However, if the chemokine was constitutively present it would be expected to remain at a 'steady state', or reduce in intensity if the cell was releasing it into the medium over the time frame of the experiment.

The current study is the first to show an increase in intensity of CCL7 in the absence of cycloheximide in ECs. However, given that protein synthesis in the absence of cycloheximide is expected where the ECs are actively generating CCL7, the subsequent trend of CCL7 decreasing in intensity to near baseline suggests that while pre-synthesised

CCL7 may be stored in the ECs, in Weibel-Palade bodies or other secretory vesicles, it is not being generated in an on-going manner in response to inflammatory stimuli. However, given the low n numbers for this data this evidence should be considered as preliminary and all conclusions drawn with caution. The release of CCL7 is partially supported by the observational data from the ELISA tests which showed CCL7 to be detectable in the conditioned medium. The presence of chemokines and other factors such as VWF in Weibel-Palade bodies is well documented (Øynebråten *et al.*, 2005; Rondajj *et al.*, 2006; Hol *et al.*, 2009). Chemokine receptors such as D6 and CCR5 have been shown to rapidly internalise chemokines for recycling (Weber *et al.*, 2004) so it is also possible that CCL7 may have been broken down intracellularly without the cells generating further CCL7 to replenish stores within this timeframe. In the presence of cycloheximide the only significant increases in CCL7 was observed at 2 hours. This suggests that there may be some pre-stimulation by TNF- α occurring prior to the cycloheximide starting to inhibit protein synthesis.

In the absence of cycloheximide the data for CCL14 show a significant increase in intensity followed by a significant decreasing trend which does not reduce to near baseline levels. This indicates that pre-synthesised CCL14 was stored in the ECs and either released into the medium and/or recycled within the cell, primarily between 2 and 6 hours stimulation. These data indicate that further CCL14 was either being generated by the ECs to replenish stores during this process, or CCL14 was not being released and/or recycled to a significant degree within the timeframe. However, the lack of CCL14 in HBMEC conditioned medium, but its presence in HMVEC conditioned medium indicates that the chemokine is not being released by HBMECs. In the presence of cycloheximide the increase in intensity at 2 hours post-stimulation indicates that there was some pre-stimulation occurring prior to the cycloheximide inhibition of protein synthesis. This was

followed by a significant decrease between 2-6 hours post-stimulation which indicates that the cycloheximide had successfully blocked any further chemokine generation and suggests that the cell surface CCL14 may have been released into the medium as the cycloheximide should have prevented cellular recycling.

This study is the first to indicate that ECs may generate CCL14 in response to inflammatory stimuli, as shown by the significantly increased CCL14 levels throughout the 24 hour timeframe in the absence of cycloheximide. Further work is needed to assess the half-life of the different chemokines and their levels of release/recycling within the cell in ECs using pulse-chase experiments (e.g. with ³⁵S-methionine) which would provide more conclusive data.

In the absence of cycloheximide, CCL16 showed a near-significant initial increase from baseline to 2 hours post-stimulation ($p = 0.054$), followed by a significant decrease from baseline at 5 and 6 hours post-stimulation. Trend analysis showed a significant decrease between 2-6 hours post-stimulation. This suggests that pre-synthesised CCL16 was either released into the medium or recycled within the cell. It also suggests that further CCL16 was not being generated by the ECs to replenish stores during this timeframe.

As with CCL7 and CCL14 in the presence of cycloheximide, a significant increase in CCL16 was observed at 2 hours, and as with CCL14 this was followed by a significant decrease at 5-6 hours post-stimulation. However, this was not an overall significant trend between 2-6 hours. This suggests pre-stimulation and (as with CCL14) the release of CCL16 into the medium and/or its intracellular recycling. This is partially supported by Weber *et al.*, (2005) who showed that CCR5 (one of the receptors for CCL16) can rapidly internalise chemokines for recycling. If CCL16 was preferentially bound to CCR5 it is highly possible that CCL16 was rapidly being internalised and degraded.

The significant decrease in CCL22 between 0 and 6 hours in the absence of cycloheximide (overall non-significant with trend analysis), without undergoing a significant increase at any point, indicates that pre-synthesised CCL22 was either released into the medium or recycled within the cell. There was a non-significant increase between 5-6 hours post-stimulation which may be due to normal variation in CCL22 levels. However, the possibility that the cells were starting to generate detectable CCL22 increases at this point cannot be discounted.

The failure to detect CCL16 and CCL22 in conditioned medium may be due to undetectable levels being released in the time frame allowed, or further evidence that these chemokines are recycled intracellularly rather than released.

A number of factors which have a bearing on the analysis of these data became apparent during this section of the study. The first was the low *n* numbers. Given further time it would be important to increase the sample size throughout this section to assess if reductions in the variation seen within the groups were possible.

The second was the loss of HDLECs viability prior to being able to assess their generation of the chemokines. They began to dedifferentiate at around their 15th population doubling and showed a lower than expected survival rate between passages. This led to them becoming unusable for the last part of the study. Given further time I would have attempted to retrieve primary synovial LECs to provide a more sustainable source of cells with the possibility of immortalisation.

The third major problem was the pre-stimulation of the cells prior to the cycloheximide beginning to inhibit protein synthesis. If the work was to be repeated the cycloheximide would be added to the cells for a minimum of 30 minutes prior to the addition of TNF- α to allow the cycloheximide time to arrest protein synthesis. It would also have been beneficial

to have assessed the EC presence of a chemokine such as CXCL8, which is established as being secreted by ECs (Utgaard *et al.*, 1998; Wolff *et al.*, 1998; Øynebråten *et al.*, 2004), in the presence and absence of cycloheximide to act as a positive control for the chemokines investigated in this study. This section of the study would also greatly benefit from repeating the ELISA analysis on the conditioned medium to further elucidate if the chemokines are released into the medium. Further to this, running 'pulse chase' experiments would be able to track chemokine synthesis, to elucidate where they were localised and how they were cycled through the cell in response to stimuli.

Conclusions

The first aim of this section of the study was to establish which cytokine (TNF- α , IFN- γ or a combination) provides optimal simulated inflammatory conditions for HBMECs and HDLECs. The HBMECs were shown to undergo the greatest ICAM-1 intensity increases at two hours stimulation and beyond in the presence of TNF- α . The HDLECs were shown to undergo the greatest intensity increases at two hours stimulation and beyond by a combination of TNF- α and IFN- γ . This is the first study to show such an ICAM increase using these cytokines simultaneously.

The second and third aims of this section of the study were to assess if CCL7, CCL14, CCL16 and CCL22 are present in cultured HBMECs and HDLECs, and if there are changes in the intensity of their expression in the presence of a protein synthesis inhibitor. The data shows that each chemokine is present with CCL14 being present to the greatest degree and CCL22 at the lowest levels. Of each of the chemokines CCL14 underwent the greatest increase in response to TNF- α in the absence of cycloheximide which indicates it to have the greatest potential of the chemokines under investigation to be produced by ECs leading to leukocyte recruitment in RA. The lack of significant changes in the levels of

CCL22 in either the presence or absence of cycloheximide taken with its presence being just within the limits of detection, indicate that CCL22 is least likely of the chemokines under investigation to have an active role in RA pathology via its generation within ECs. These novel findings offer further evidence into the generation of chemokines by ECs.

Chapter 5

Microstructure formation on HBMECS in response to CCL7, CCL14, CCL16 and CCL22

5.1 Introduction and Aims

It has been shown that ECs and mononuclear cells undergo morphological changes in response to inflammatory conditions which facilitate transendothelial migration of inflammatory cells into the tissue (Geiger and Bershadsky, 2002; Barriero and Sanchez-Madrid, 2009; Whittall *et al.*, 2013). Leukocytes are activated by contact with the EC luminal surface bound chemokines and integrins and their ligands enable leukocyte arrest in normal blood flow conditions (Tarrent and Patel, 2006; Barriero and Sanchez-Madrid, 2009). Once firmly adhered the leukocytes change morphology from round to 'polarised' whereby a greater proportion of their surface area is in contact with the EC surface (Barriero and Sanchez-Madrid, 2009). Prior to transmigration across the post capillary ECs leukocytes 'crawl' (mediated by chemokines) on the luminal EC surface in a MAC-1 and ICAM-1 dependent manner (Ley *et al.*, 2007) actively seeking out a suitable transmigration site. Additional evidence from Middleton *et al.*, (1997) using CXCL8 (IL-8) injections into rabbit skin showed that the chemokine was not only internalised abluminally into caveolae by postcapillary and small vein ECs but was also transcytosed and presented on the EC luminal surface, predominantly in association with EC microvilli. As well as the chemokines and chemokine receptors, adhesion molecules such as the selectins, integrins and VCAM are present at the EC surface. Each of these can be localised on microvilli projections of the leukocytes and ECs, and a range of work indicating the importance of microvilli localised adhesion molecule distribution in leukocyte migration has been carried out (reviewed by Middleton *et al.*, 2002).

As well as microvilli providing a greater surface area allowing the presentation of more chemokines and receptors, they have been seen to elongate mediated by specific molecules such as ICAM-1. This was observed by Oh *et al.*, (2007) where ICAM was seen to regulate *de novo* microvilli elongation allowing its clustering at the most apical region of the EC.

The hypothesis from this evidence is that ECs and/or mononuclear cells, in the presence of CCL7, CCL14, CCL16 and CCL22, will increase their generation of microvilli or other microstructures such as podosomes and filopodia. Leukocyte podosomes palpate the EC surface and facilitate transcellular-migration by identifying sites of low EC resistance where an invasive podosome (of >1000nm) can begin penetration (Vijayakumar *et al.*, 2015; Carmen and Spinger, 2008; Wittchen, 2009; reviewed by Carmen *et al.*, 2007). Filopodia are generated by ‘activated’ ECs such as those undergoing angiogenesis (Jakobsson *et al.*, 2010). Furthermore ‘filopodia-like’ protrusions are generated by cerebral ECs, which ‘engulf’ mononuclear cells before forming pores through which the mononuclear cells migrate (Wolburg *et al.*, 2004).

It is further hypothesised that greater numbers of firmly adhered/polarised or actively migrating mononuclear cells may be observed following addition of CCL7, CCL14, CCL16 and CCL22. These effects on EC microstructures would initially enable better presentation of the chemokines to mononuclear cells, followed by crawling and firm adhesion of mononuclear cells to the EC surface, which would in turn better enable transendothelial migration. As inflammatory chemokine production can be induced in response to stimulation by TNF- α (Haringman *et al.*, 2004), it was necessary to reduce the likelihood of increased microvilli generation by ECs being due to the generation of endogenous chemokines in the presence of TNF- α rather than the chemokine under investigation. This was achieved by performing the experiments in the presence of TNF- α and the chemokine rather than with the TNF- α or the chemokine alone. This negates effects on the results due to endogenous chemokine generation and allows more robust comparisons between the presence and absence of each of the chemokines under investigation. By performing the experiments in co-culture rather than monoculture the cell to cell interactions more closely resemble those found in vivo.

The aims were to:

- Activate HBMEC monolayers using TNF- α and perform transendothelial migration assays in the presence and absence of CCL7, CCL14, CCL16 and CCL22 to establish if structural changes occur to the mononuclear cells and/or ECs.
- Differentiate between the structural changes to establish if specific microstructures (for example microvilli and podosomes) are preferentially induced on ECs or mononuclear cells to assess which stage in transmigration the chemokine may be functional.

5.2 Materials and Methods

HBMECs were cultured to approximately 80% confluency on 5 μ m hanging filters in transwells and then activated for 16 hours using 100ng/ml TNF- α . For further details see chapter 2 section 2.4. Mononuclear cells were isolated as described in section 2.5.1.1 and used immediately. Transmigration was carried out as described in section 2.5.2.

Preparation for electron microscopy was carried out as in section 2.5.3. Experiments were performed in triplicate and specific n numbers for images provided are given below tables. The transmission electron microscope images for each data set were scored as positive for the microstructure under investigation (N1) and negative for the microstructure under investigation (N2).

5.2.1 Quantitation of results

Statistical analysis was performed using NCSS (NCSS, Kaysville, UT, USA) software. Mononuclear cells and ECs were scored as being microstructure positive (N1) or microstructure negative (N2) and two proportion tests were performed to calculate the odds ratio (OR) for microstructure generation being due to the presence of the chemokine rather than the TNF- α alone. The confidence interval for the OR was also calculated. Further calculations were carried out to assess podosomes, filopodia, cells in the process of migrating, and firmly adhered cells. Fisher's exact test was also utilised to give *P* values throughout.

For measurements of microstructures the nm per mm of scale bar from the original images were calculated for each image and the microstructure length and width was calculated using Adobe Illustrator (Adobe Systems Software, Ireland, UK).

5.3 Results

5.3.1 Transmission electron micrograph description.

5.3.1.1 Microstructures on mononuclear cells and HBMECs.

The mononuclear cells were seen to have numerous finger like projections (*MCPs*), or microvilli, continuous with the cell membrane ranging from 200nm in length and 50nm wide (see figure 5.1) to 7500nm in length and 330nm wide (figure 5.2).

Podosomes were also seen to be generated by the mononuclear cells and to be penetrating the EC membrane. The usual size range was up to 660nm long and 2660nm in width (figure 5.2) and from 880nm in length and 440nm wide at their widest (figure 5.3). The very wide but shorter podosomes appeared to be associated with transcellular migration and appeared 'foot' like in structure having a flattened base (penetrating end) that appeared to be extending laterally through the EC once it had penetrated by approximately 50% through the EC. The longest podosome observed was 1765nm in length but only 529nm at the widest point, narrowing to 60nm wide at their leading edge (figure 5.4) and had penetrated most of the way through the EC.

Filopodia protruded from the EC apical surface then extended laterally across the surface of the cell, and over the adjacent cell surface (figure 5.5). These reached 12,727nm in length and were 226nm wide. Endothelial cell microvilli like projections were seen to protrude from the apical EC surface and extend into the medium which contained the mononuclear cells. These projections were 266nm long and 200nm wide (figure 5.6). In the absence of the chemokine the EC surface was primarily smooth and lacked microvilli (figure 5.7).

5.3.1.2 Interactions between mononuclear cells and ECs

Mononuclear cell microvilli and endothelial cell microvilli were seen to interact prior to the mononuclear cell becoming adhered to the ECs. In these early interactions the endothelial cell microvilli are seen to ‘reach’ towards the mononuclear cell microvilli (or vice-versa, as seen in figure 5.6, 5.9 and 5.10). Mononuclear cell microvilli were also seen to be in direct contact with the EC surface prior to adherence (figure 5.6).

For statistical analysis mononuclear cells were not categorised as being firmly adhered to the ECs unless the length of mononuclear cell membrane equivalent to approximately 1/3 its overall length was flattened to, and thus in direct contact with, the EC surface (figures 5.2, 5.3 and 5.4). The presence of podosomes at these junctions was also regarded as being evidence of firm adherence.

Mononuclear cells were defined as migrating only if they were in the process of moving through a single EC or between adjacent ECs and/or had podosomes.

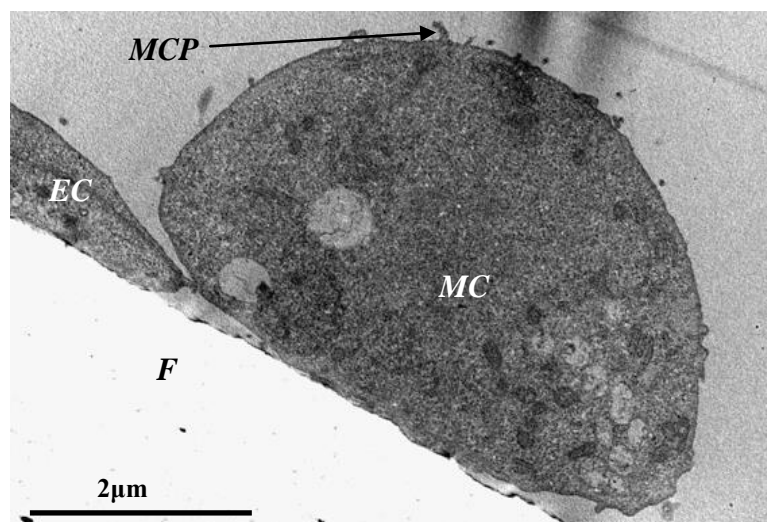


Figure 5.1 TNF- α stimulated HBMEC's (*EC*) grown on a 5 μ m transwell filter (*F*) in close association with mononuclear cell (*MC*) in the absence of chemokine. An example of a mononuclear cell microvillus like projection of 200nm length and 50nm width is indicated (*MCP*).

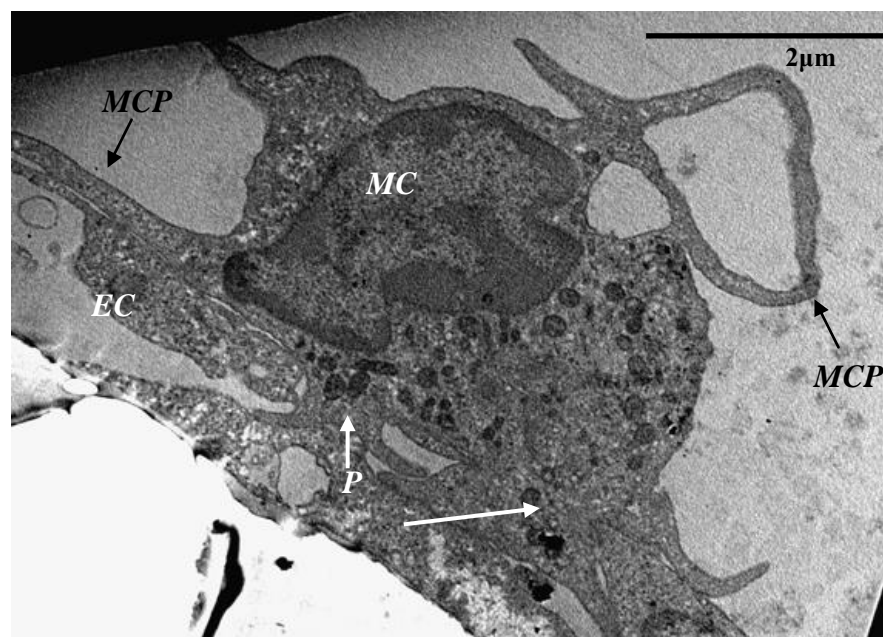


Figure 5.2 Mononuclear cell (*MC*) with long (7500nm long) microvillus (*MCP*) like projection. A wide (>2660nm) podosome like structures (*P*) in the process of migration in the presence of CCL22 and TNF- α .

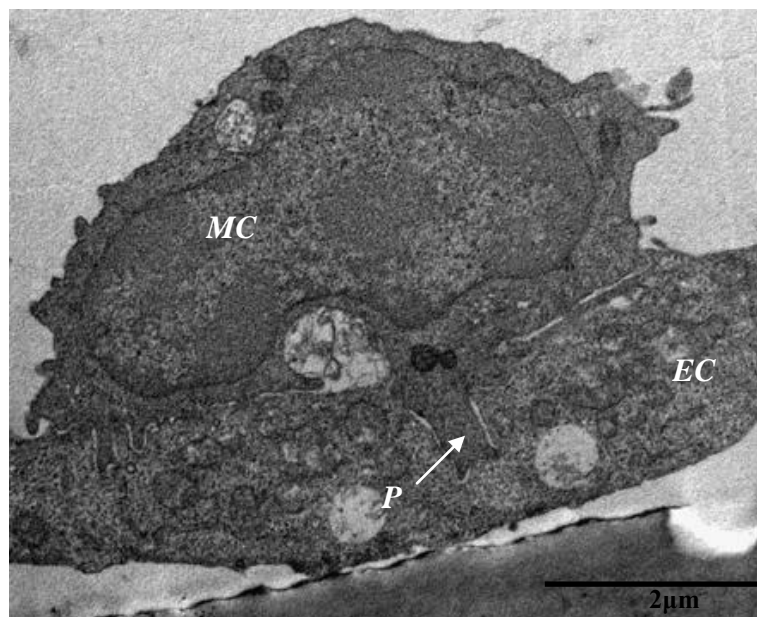


Figure 5.3 Mononuclear cell (*MC*) seen in the polarised conformation with podosome like microstructures (*P*) (880nm length) protruding into the EC in the process of migrating through a HBMEC in the presence of CCL14 and TNF- α .

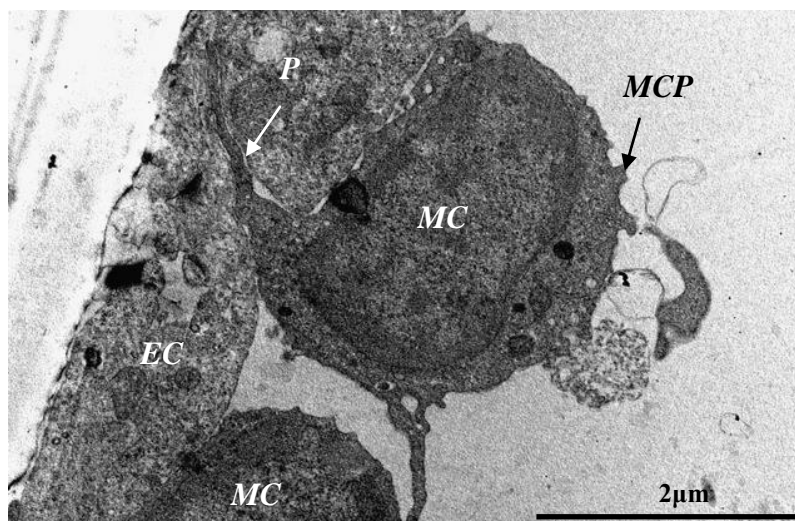


Figure 5.4 Mononuclear cell (*MC*) in the process of migrating through HBMEC monolayer (*EC*). A podosome like structure (1765nm length) is indicated (*P*). Performed in the presence of CCL7 and TNF- α .

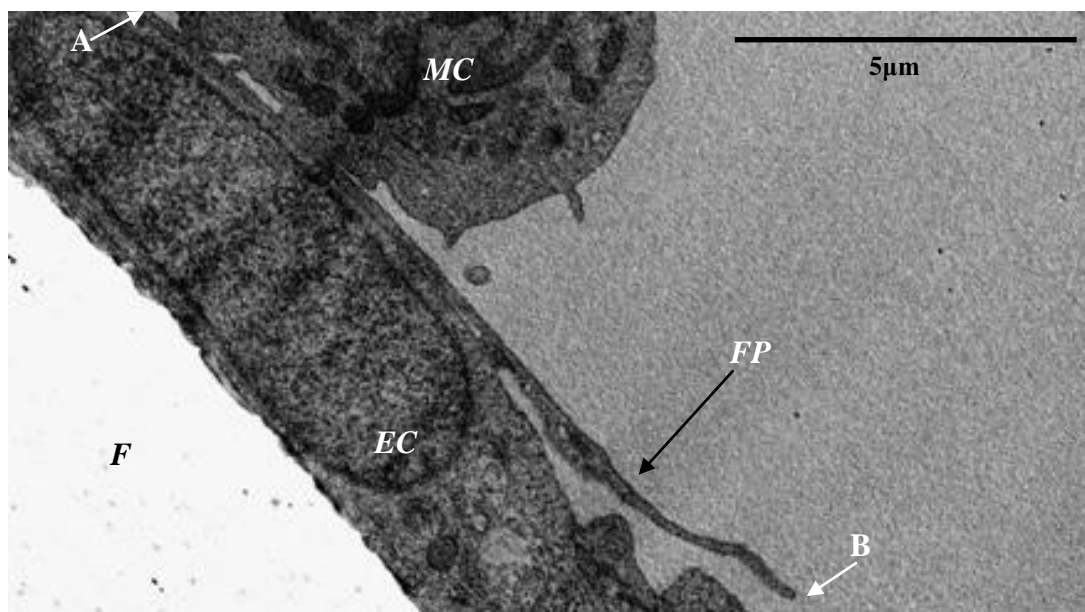


Figure 5.5 Mononuclear cell (*MC*) in close association with an *EC* with a filopodia like microstructure (*FP*) (12,727nm length, measured from A-B) in the presence CCL16 and TNF- α . F = filter.

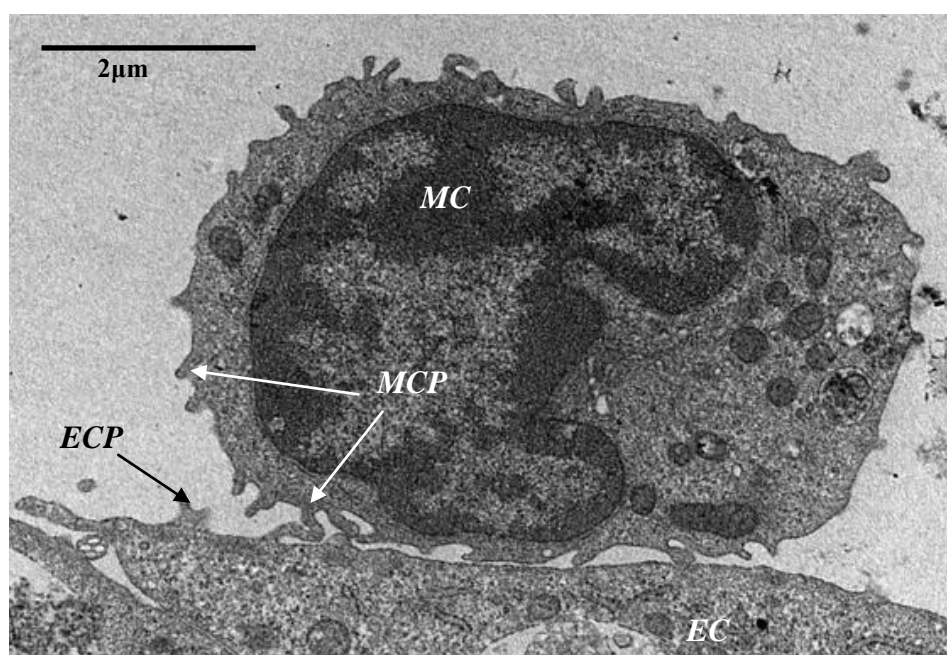


Figure 5.6 Mononuclear cell (*MC*) with microvilli like projections (*MCP*) in close association with microvilli like structures of endothelial cells (*ECP*) in the presence of CCL22 and TNF- α . *ECP* and *MCP* appear to be ‘reaching’ towards each other in lower left of micrograph.



Figure 5.7 TNF- α stimulated HBMEC's (*EC*) grown on a 5 μ m transwell filter (*F*) showing lack of microstructure formation. Chemokine absent.

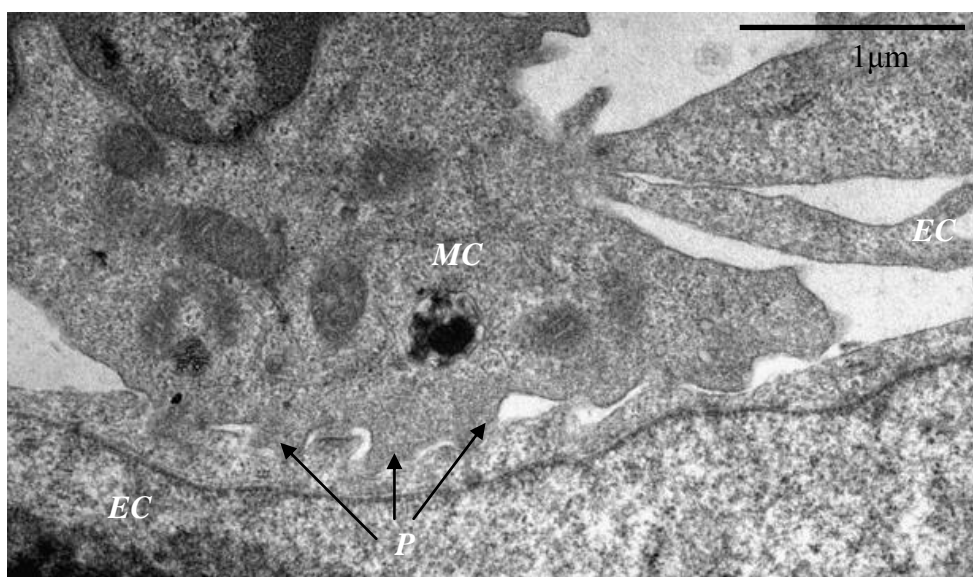


Figure 5.8 Mononuclear cell (*MC*) with podosome like microstructures (*P*). Microstructures are seen protruding into an *EC* in the process of migrating through an HBMEC monolayer in response to CCL16 and TNF- α .

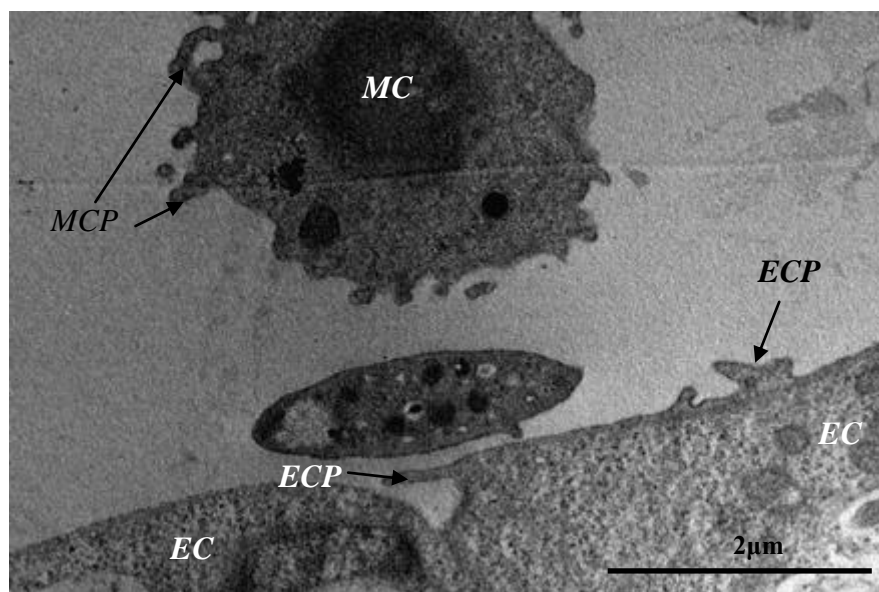


Figure 5.9 A mononuclear cell (*MC*) near HBMEC's where CCL14 was added to the basal transwell filter compartment for 30 minutes. Both endothelial and mononuclear cell microvilli are seen (*MCP* and *ECP*) in the presence of CCL14 and TNF- α .

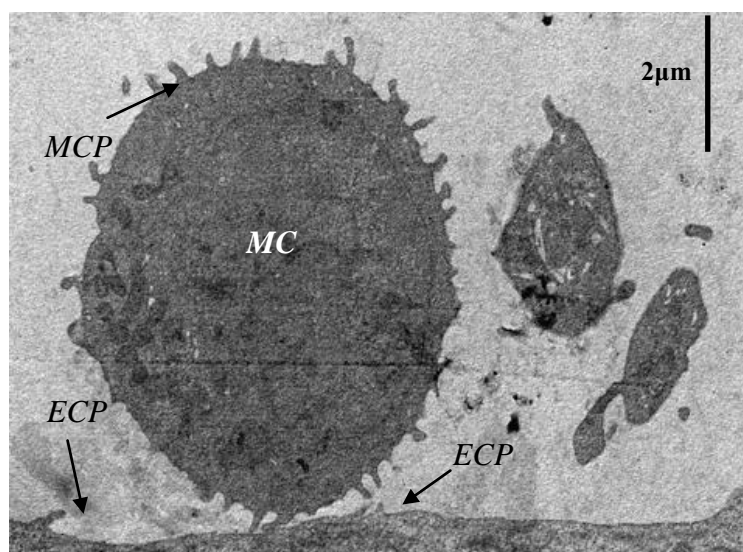


Figure 5.10 A mononuclear cell (*MC*) in association with HBMEC's where CCL7 was added to the basal transwell filter compartment for 30 minutes. A mononuclear cell with numerous microvilli like protrusions (*MCP*) in early association with an endothelial cell which is also showing microvilli like protrusions (*ECP*) in the presence of CCL7 and TNF- α .

5.3.2 Microvilli generation on mononuclear cells in response to chemokines.

A number of chemokines had an effect on generation of microvilli like microstructures on mononuclear cells. The OR and Fishers Exact test results indicated that both CCL14 and CCL22 had a significant effect on the generation of the microvilli on mononuclear cells placed over TNF- α stimulated HBMECs (table 5.1). CCL14 appeared to have the greatest effect. CCL16 showed a non-significant trend towards an increase in microvilli production. CCL7 did not reach significance.

5.3.3 Microvilli generation on HBMECs.

A number of chemokines had an effect on generation of microvilli like microstructures. The OR for CCL16 and CCL22 showed a significant effect on the generation of microvilli on HBMECs stimulated with TNF- α (table 5.2). The OR and Fisher's exact test also indicated a strong positive trend for microstructure generation in the presence of CCL7 and CCL14 with TNF- α compared to TNF- α alone (table 5.2) although the results did not quite reach significance ($p = 0.057$ and 0.054)

Table 5.1 Microvilli generation on mononuclear cells in the presence of TNF- α stimulated HBMECs with and without chemokines

Chemokine	Figure reference	Chemokine treated N1:N2	Control N1:N2	OR (95% CI)	Fisher's Exact Test (<i>p</i> value)
CCL7	5.10	18:8	5:6	2.57 (0.06 – 1.95)	<i>p</i> = 0.26
CCL14	5.9	22:0	5:6	53.18 (3.30 – 263.80)	<i>P</i> = 0.0004
CCL16	5.8	9:1	5:6	7.48 (0.78 – 319.51)	<i>p</i> = 0.070
CCL22	5.6	17:2	5:6	8.27 (1.20 – 109.09)	<i>p</i> = 0.014

Chemokine treated - mononuclear cells incubated with HBMECs which were TNF- α stimulated and had the chemokine placed in the lower transwell chamber for 30 minutes to allow time for the chemokine to be presented by the ECs prior to addition of the mononuclear cells. N1 = number of mononuclear cells with microstructures; N2 = number of mononuclear cells without microstructures. Control – mononuclear cells incubated with HBMECs cultured in the absence of chemokine but stimulated with 100ng/ml TNF- α . OR = odds ratio. CI - confidence interval. For Fisher's exact test $P < 0.05$ is significant. For each chemokine overall $n=3$. For CCL7, CCL14, CCL16 and CCL22, 26, 22, 10 and 19 individual images were produced and analysed respectively. The control experiments produced 11 images for analysis.

Table 5.2 Microvilli generation on HBMECs in response to TNF- α stimulation in the presence of chemokines.

Chemokine	Figure reference	Chemokine treated N1:N2	Control N1:N2	OR (95% CI)	Fisher's Exact Test (p value)
CCL7	5.10	12:14	1:10	6.03 (0.86 – 205.86)	p = 0.057
CCL14	5.9	10:12	1:10	5.90 (0.9 – 205.31)	p = 0.054
CCL16	5.5	7:3	1:10	15.00 (1.52 – 787.30)	p = 0.007
CCL22	5.6	10:9	1:10	7.74 (1.03 – 281.39)	p = 0.023

Chemokine treated - HBMECs which were TNF- α stimulated and had the chemokine placed in the lower transwell chamber for 30 minutes to allow time for the chemokine to be presented by the ECs prior to addition of the mononuclear cells. N1 = number of HBMECs with microstructures; N2 = number of HBMECs without microstructures. Control cells – HBMECs which were cultured in the absence of chemokine but stimulated with 100ng/ml TNF- α . OR - odds ratio. CI - confidence interval. For Fisher's exact test P<0.05 is significant. For each chemokine overall n=3. For CCL7, CCL14, CCL16 and CCL22, 26, 22, 10 and 19 individual images were produced and analysed respectively. The control experiments produced 11 images for analysis.

5.3.4 Filopodia generation on TNF- α stimulated HBMECs in the presence of chemokine.

There was a non-significant positive trend in the generation of filopodia by HBMECs in the presence of each chemokine as indicated by the OR in table 5.4 (see figure 5.5 for filopodia image). The low number of micrographs showing sufficient EC surface area available for analysis of filopodia is likely to have affected the resulting data. Further analysis of micrographs taken at lower magnification may provide more adequate results for statistical analysis of filopodia generation.

5.3.5 Podosome generation, migration and adherence of mononuclear cells.

The number of mononuclear cells firmly adhered to HBMECs in the presence of CCL16 showed a highly positive trend for mononuclear cell adherence with an OR of 6.59 (CI 0.93-87.12) supported by a significant Fisher's exact test giving $p=0.039$ (table 5.3). OR for all other results indicated a positive trend for the generation of podosomes (figures 5.2, 5.4 and 5.8, table 5.3), cells actively migrating and cells firmly adhered, although these were not significant (table 5.3).

Table 5.3 Data for podosome-like structure generation of mononuclear cells, mononuclear cells actively migrating and mononuclear cells adhered to HBMECs treated with TNF- α alone, and in the presence of chemokines.

Chemokine	Structure or activity	Chemokine treated N1:N2	Control N1:N2	OR (95% CI)	Fisher's Exact Test (<i>p</i> value)
CCL7	Podosomes	1:25	2:9	0.22 (0.01 – 3.06)	<i>p</i> = 0.978
	Migrating	4:22	1:10	1.40 (0.14 - 48.56)	<i>p</i> = 0.528
	Adhered	12:14	3:8	2.26 (0.44 – 15.16)	<i>p</i> = 0.207
CCL14	Podosomes	4:18	2:9	0.92 (0.11 – 9.81)	<i>p</i> = 0.692
	Migrating	5:17	1:10	2.20 (0.25 - 76.63)	<i>p</i> = 0.328
	Adhered	10:12	3:8	2.04 (0.37 – 14.40)	<i>p</i> = 0.267
CCL16	Podosomes	2:8	2:9	1.12 (0.08– 15.47)	<i>p</i> = 0.669
	Migrating	2:8	1:10	2.05 (0.13 - 85.48)	<i>p</i> = 0.462
	Adhered	9:3	3:8	6.59 (0.93 – 87.12)	<i>p</i> = 0.039
CCL22	Podosomes	5:14	2:9	1.44 (0.20 – 15.32)	<i>p</i> = 0.485
	Migrating	7:12	1:10	4.20 (0.52 - 148.8)	<i>p</i> = 0.107
	Adhered	9:10	3:8	2.19 (0.38 – 16.31)	<i>p</i> = 0.442

Chemokine treated - mononuclear cells incubated with HBMECs which were TNF- α stimulated and had the chemokine placed in the lower transwell chamber for 30 minutes to allow time for the chemokine to be presented by the ECs prior to addition of the mononuclear cells. N1 = number of mononuclear cells with microstructures; N2 = number of mononuclear cells without microstructures. Control – mononuclear cells incubated with HBMECs cultured in the absence of chemokine but stimulated with 100ng/ml TNF- α . OR - odds ratio. CI - confidence interval. For Fisher's exact test $P < 0.05$ is significant. For each chemokine overall $n=3$. For CCL7, CCL14, CCL16 and CCL22, 26, 22, 10 and 19 individual images were produced and analysed respectively. The control experiments produced 11 images for analysis.

Table 5.4. The generation of filopodia like structures on HBMECs in response to TNF- α stimulation in the presence of chemokines.

Chemokine	Chemokine treated N1:N2	Control N1:N2	OR (95% CI)	Fisher's Exact Test (<i>p</i> value)
CCL7	6:20	1:10	2.22 (0.27 - 75.53)	<i>p</i> = 0.309
CCL14	7:15	1:10	3.38 (0.43 - 117.15)	<i>p</i> = 0.158
CCL16	3:7	1:10	3.26 (0.27 - 133.78)	<i>p</i> = 0.255
CCL22	7:12	1:10	4.20 (0.53 - 148.83)	<i>p</i> = 0.199

Chemokine treated - HBMECs which were TNF- α stimulated and had the chemokine placed in the lower transwell chamber for 30 minutes to allow time for the chemokine to be presented by the ECs prior to addition of the mononuclear cells. N1 = number of HBMECs with microstructures; N2 = number of HBMECs without microstructures. Control cells – HBMECs which were cultured in the absence of chemokine but stimulated with 100ng/ml TNF- α . OR - odds ratio. CI - confidence interval. For Fisher's exact test $P < 0.05$ is significant. For each chemokine overall $n=3$. For CCL7, CCL14, CCL16 and CCL22, 26, 22, 10 and 19 individual images were produced and analysed respectively. The control experiments produced 11 images for analysis.

5.4 Discussion

Middleton *et al.*, (1997) and Pruenster *et al.*,(2009) suggested that membrane bound chemokines acted as facilitators for effective leukocyte transmigration from circulating blood and showed that transcytosed chemokines were presented on EC microvilli. Chemokines in association with EC microvilli, bound via glycosaminoglycans, generate signals via the G protein coupled receptors on leukocytes causing integrin conformational changes contributing to leukocyte activation and arrest (Barriero and Sanchez-Madrid, 2009). Activated leukocytes have been shown to change morphology from round to 'polarised' which allows the intracellular coordination required for crawling and eventual transmigration (Geiger and Bershadsky, 2002).

This study has provided novel data to the field by showing that morphological changes occur in the presence of CCL7 (which generated a positive trend response), and in the presence of CCL14, CCL16 and CCL22 (which generated a significant response). These morphological changes are conducive to transmigration, including the formation of leukocyte and/or EC microvilli which indicates that these chemokines have a functional role in mononuclear cell migration into the synovium. A number of leukocytes were also observed to be in the 'polarised' state. Mononuclear cells were observed to interact with EC microvilli and filopodia like projections. Carmen *et al.*, 2007; Carmen and Spinger, 2008 and Wittchen, 2009 showed that podosome formation is also indicative of transmigration. The podosome palpation of the EC surface identifies suitable migration sites and forces a 'podo-print' into the membrane prior to pore formation. While podosome generation in the presence of the chemokines was not seen to reach significance compared to the absence of chemokine their generation was observed to be increased.

A range of chemokine receptors and adhesion molecules such as L-selectin, P-selectin, PGSL-1 and integrins have been shown to be distributed on leukocyte microvilli where

they facilitate early leukocyte to EC interactions (reviewed by Middleton *et al.*, 2002) important in transmigration. This study is the first to quantify microvilli formation on mononuclear cells due to the presence of chemokines CCL7, CCL14, CCL16 and CCL22. In this study it was shown that CCL14 generated microvilli on mononuclear cells to the greatest degree with CCL22 also having a significant, but lesser effect. CCL16 generated a positive trend in microvilli formation and CCL7 had little effect on mononuclear cell microvilli generation. CCL16 and CCL22 had significant positive effects on HBMEC microvilli formation with CCL16 having the greatest effect. Both CCL7 and CCL14 generated a strong positive trend in HBMEC microvilli formation which fell just short of being statistically significant. Therefore, overall CCL14 was the most effective at generating microvilli on mononuclear cells and CCL16 was the most effective at generating them on ECs.

It has been shown by Brown *et al.*, (2003) that CXCL12 caused lymphocyte microvilli retraction during firm adherence allowing for the conformation to change to a polarised state, further facilitating transmigration. While this study did not find significant increases in adherence in the presence of the chemokine, sampling problems may have affected the data gathering. These problems were low numbers of micrographs showing leukocyte adherence. Thus, increasing the n number and the number of micrographs available for analysis would benefit the study and help confirm these results. CCL16 did increase adherence in the present experiments.

It is known that TNF- α induces the production of a range of chemokines, including CXCL8 and CCL5, and also induces the upregulation of other adhesion factors on ECs (Zhao *et al.*, 2005; Szekanecz and Koch, 2008). Further to this Whittall *et al.*, (2013) showed that CXCL8 increased EC microvilli and filopodia formation. This study extends current knowledge in this field by showing significant increases in microvilli formation of

ECs in the presence of chemokines CCL14, CCL16, CCL22 and TNF- α , compared to the presence of TNF- α alone. Whilst this indicates that the increases may be due to the chemokine alone, the study would have been improved by repetition of the work in the absence of TNF- α but in the presence of the chemokine alone, to assess possible synergistic effects between the chemokine and TNF- α which affected the cell-cell interactions

By performing the experiments in co-culture rather than monoculture the potential synergistic effects between each cell type were not removed from the experimental environment. This allowed for the 'normal' generation of a range of factors such as adhesion molecules vital to transmigration and for cell-cell interactions to more closely resemble those seen in vivo .

In conclusion

The first aim of this section of the study was to establish if structural changes occur to the mononuclear cells and/or ECs associated with transmigration mechanisms. The data show that each of the chemokines have the ability to generate structural changes on both ECs and mononuclear cells to differing degrees

The second aim of this section was to differentiate between structural changes to establish if specific microstructures are preferentially induced on ECs or mononuclear cells to assess which stage in transmigration the chemokine may be functional. The data show that CCL14 preferentially generates microvilli formation on mononuclear cells and CCL16 preferentially generating microvilli formation on ECs. No significant differences could be ascertained for the generation of podosomes, filopodia or the numbers of firmly adhered/migrating cells. This suggests that these chemokines are involved in the activation

of cells prior to firm adherence, however the sampling problem may have negatively affected the data and so this finding should be interpreted with caution until such time as further work has been performed to quantify it.

These findings provide novel evidence of differential activation of ECs and mononuclear cells by these chemokines in an inflammatory environment. Furthermore, it indicates a direct link between the presence of these chemokines and increases in structural changes which may be mechanistic in transmigration.

Chapter 6

Chemokine receptor expression and transendothelial migration.

6.1 Introduction and aims

As discussed in 1.8.2 there are currently 19 identified chemokine receptors (Bonecchi *et al.*, 2009; Bachelierie *et al.*, 2014), many of which bind multiple ligands and are expressed on a range of leukocyte cell types. CCL7 is the ligand for CCR1, 2 and 3; CCL14 is the ligand for CCR1 and CCR5; CCL16 is the ligand for CCR1 and CCR2 and CCL22 is the ligand for CCR4 and CCR8 (Filer *et al.*, 2008; Bonecchi *et al.*, 2009). As the beta chemokines' major targets are monocytes and lymphocytes the hypothesis for this section of the study was that each of the chemokines of interest will generate increases in the transmigration of mononuclear cells across activated HBMEC monolayers. Elucidation of the degree to which transmigration is affected, and the chemokine receptor via which the chemokine may be functional, would identify new potential therapeutic targets.

Previously discussed in chapters 1 and 3 are the increases in production of a range of chemokines including CCL2, CCL5 and CCL20 at blood vessel ECs. In a normal model of inflammation Johnson *et al.*, (2006) showed that TNF- α activated dermal lymphatic endothelial cells (DLECs) show >100 fold increases in CCL2, CCL5 and CCL20. This indicates that in inflammatory conditions lymphatic vessels would be required to upregulate the expression of chemokines chemoactive for the effective removal of the leukocytes in the synovium. Burman *et al.*, (2005) provided evidence of chemokine gradient corruption within the RA synovium and data from chapter 3 showed CCL7 to be markedly decreased on the LECs of RA sufferers while a number of other chemokines were markedly increased on blood vessel ECs. The second hypothesis is that this reduction in CCL7 at RA lymphatic ECs leads to inflammatory cell persistence within the synovium. In order to substantiate this hypothesis it was important to perform transmigration experiments in response to chemokines across both HBMECs, which provide a model for the migration of leukocytes across human vascular ECs into the synovium, and HDLECS

(in the case of CCL7) as they act as a model for the migration of leukocytes from the synovium, into the lymphatic system (as discussed in chapter 4).

The aims of this chapter were to:

- Isolate CD3+, CD14+ and CD20+ leukocyte populations and investigate the presence of chemokine receptors CCR1 (the receptor for CCL7 and CCL14), CCR2 (the receptor for CCL7 and CCL16), CCR4 (the receptor for CCL22), and CCR5 (the receptor for CCL14 and CCL16) in both RA and non-RA blood to determine if the receptors are expressed, and via which receptor(s) CCL7, CCL14, CCL16 and CCL22 may be functional in RA.
- Determine the functionality of CCL7, CCL14, CCL16 and CCL22 in the transmigration of mononuclear cells across vascular HBMECs.
- Determine the functionality of CCL7 in the transmigration of monocytes, B-cells and T-cells from RA blood across HDLECs in inflammatory conditions to establish if CCL7 downregulation on lymphatic ECs in RA may lead to reduced transmigration of mononuclear cells from the synovium and so result in mononuclear cell persistence within the synovial tissue.

6.2 Materials and Methods

Mononuclear cells were separated from whole blood of RA sufferers and normal controls as described in chapter 2, section 2.5.1.1.

CCR and CD marker staining of mononuclear cells was carried out as described in chapter 2, section 2.6.3.1 and 2.6.3.2. Transmigration was carried out as described in section 2.4.

All migrations were carried out 37°C for 1 hour. Flow cytometry was carried out on a Becton Dickinson FACscan flow cytometer (FACs)

6.2.1 Quantitation of results

Statistical analysis was performed using GraphPad. Normality checks were performed for each dataset which showed normal distribution for CD marker staining. Therefore unpaired T-test was utilised for CD analysis. Where normality tests showed non-normal distribution non-parametric analysis was utilised, thus Mann-Whitney U test was used for CCR analysis. RA n=3 and non-RA n=3. Kruskal-Wallis one-way ANOVA on ranks was used for statistical analysis of transmigration data (significant result at $p < 0.05$) followed by Dunn's post hoc test. Details of the precise analysis method are reiterated at the start of each section.

6.3 Results

6.3.1 CD and CCR analysis.

6.3.1.1 Establishing T-cell, B-cell and monocyte populations by flow cytometry.

Forward and side scatter was used to differentiate between the monocyte and lymphocyte populations of RA and non-RA PBMCs (figure 6.1). The percentage of CD3+ (T cells), CD14+ (monocytes) and CD20+ (B cells) cells (section 6.4) was determined as was the percentage of CCR+, CCR2+, CCR4+ and CCR5+ cells for each population (section 6.5). The mean fluorescent intensity (MFI), which shows the cell surface expression of each marker, for CCR1, CCR2, CCR4 and CCR5 for each population was also determined (section 6.5)

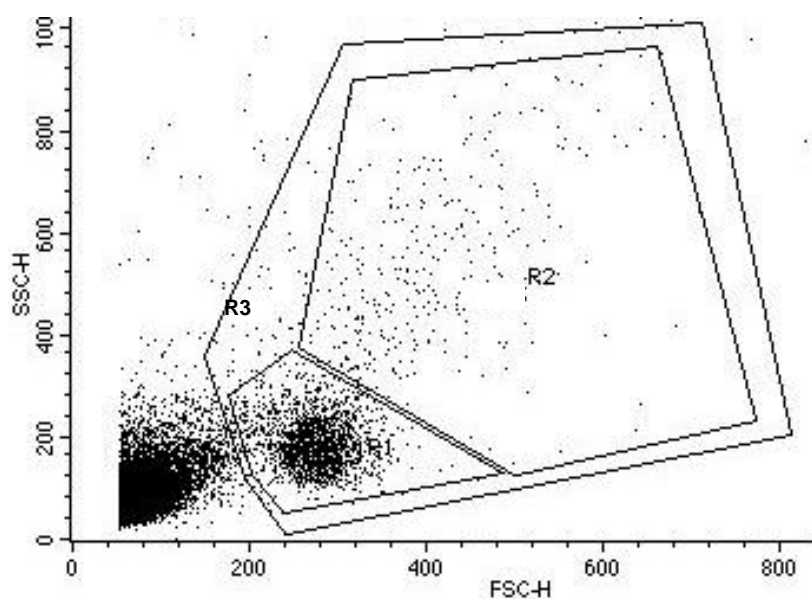


Figure 6.1 Sample dot plot showing forward scatter (FSC) versus side scatter (SSC) for freshly isolated RA mononuclear cells. FSC depicts relative size of cell; SSC depicts relative granularity/density of the cell. These enable the differentiation of different leukocyte populations. R1 gates the B/T cell population, R2 gates the monocyte population. R3 gates total population.

6.3.1.2 Establishing the percentage of cells positive for each marker in the gated populations by FACs.

To establish the percentage of positive cells the quadrant was placed at the point where 95% of the control cells were negative leaving the 5% in the upper right quadrant positive. The stained cells were then superimposed on this dot plot to determine the percentage of positive cells (figure 6.2).

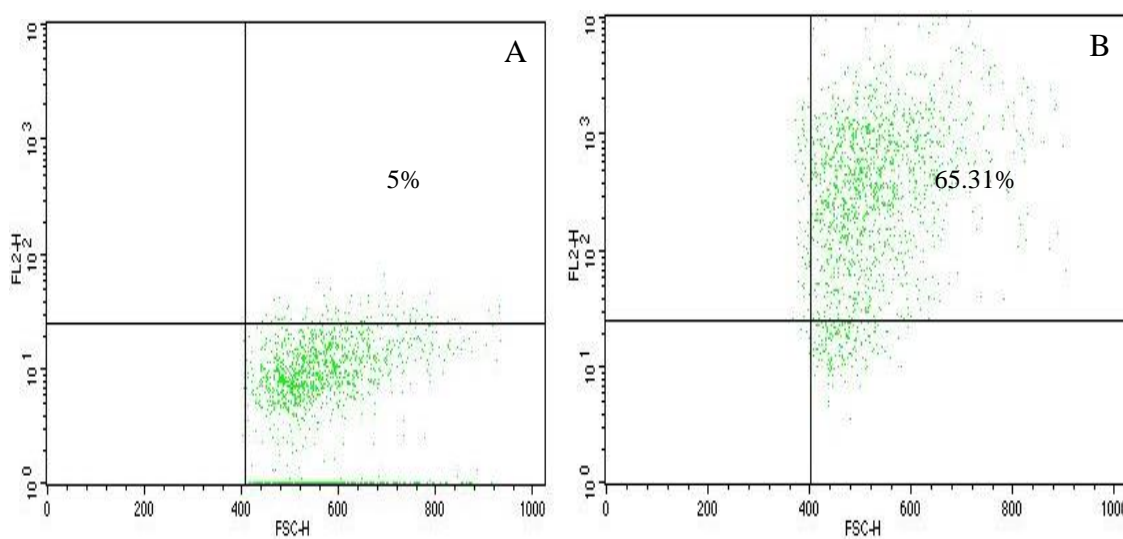


Figure 6.2 Sample dot plots showing FSC versus fluorescence for isotype control and stained cells in PBMCs. **A** shows an isotype matched control dot plot. **B** shows the dot plot for stained cells from, for example, RA PBMCs, using an antibody to CCR1.

6.4 Results of CD3+, CD14+ and CD20+ marker staining on peripheral blood mononuclear cells (PBMCs).

The pink peak shift to the right in each histogram indicates a positive result. Data are given as percentage population (\pm SD). The pink peaks within the control peak indicate a degree of background (non-specific) binding. Data were parametric so Student's T-test was utilised for statistical analysis.

6.4.1 CD3+ marker staining on RA and non-RA PBMCs.

Some background staining was seen using anti-human CD3+ antibodies to stain T-cells (figure 6.3). However, a clear peak shift was still visible. Unpaired T-test showed a significant difference in CD3+ cells observed in RA (figure 6.3A) and non-RA (figure 6.3B) PBMC populations; RA = 64.59% (\pm 1.79), non-RA = 74.40% (\pm 1.28), $p = 0.014$ (figure 6.6).

6.4.2 CD14+ marker staining on RA and non-RA PBMCs

Only small numbers of monocytes were found during FACs analysis following PBMC isolation, transmigration and staining. It is likely that the low volume of blood that it was possible to obtain from patients, followed by cell death during the staining phase of these experiments contributed to the low numbers. Despite the low numbers, and a degree of background staining, a peak shift is still clearly visible. Unpaired T-test showed no difference in CD14+ monocytes in RA (figure 6.4A) and non-RA (figure 6.4B) PBMC populations; RA 75.41% (\pm 5.52), non-RA 81.40% (\pm 2.18), $p = 0.39$ (figure 6.6).

6.4.3 CD20+ marker staining on RA and non-RA PBMCs

Some background staining was seen using anti-human CD20+ antibodies to stain B-cells. However, a clear peak shift was still visible. Unpaired T-test showed no difference between CD20+ cells in RA (figure 6.5A) and non-RA (figure 6.5B) PBMC populations; RA 20.50% (± 0.47), non-RA 16.02% (± 4.08), $p = 0.38$ (figure 6.6).

6.4.4 Monocyte, T-cell and B-cell expression on RA and non-RA monocytes.

In summary, for monocytes (gated in the R2 region), T-cells and B-cells (gated in the R1 region) in PBMCs, only the numbers of T-cells (CD3+) present showed a significant difference between RA and non-RA blood with 74.40% of non-RA PBMCs and 81.40% of RA PBMCs staining for T cells (combined data shown in figure 6.6). There were no significant differences seen in the percentage of B-cell and monocyte populations of RA and non-RA blood.

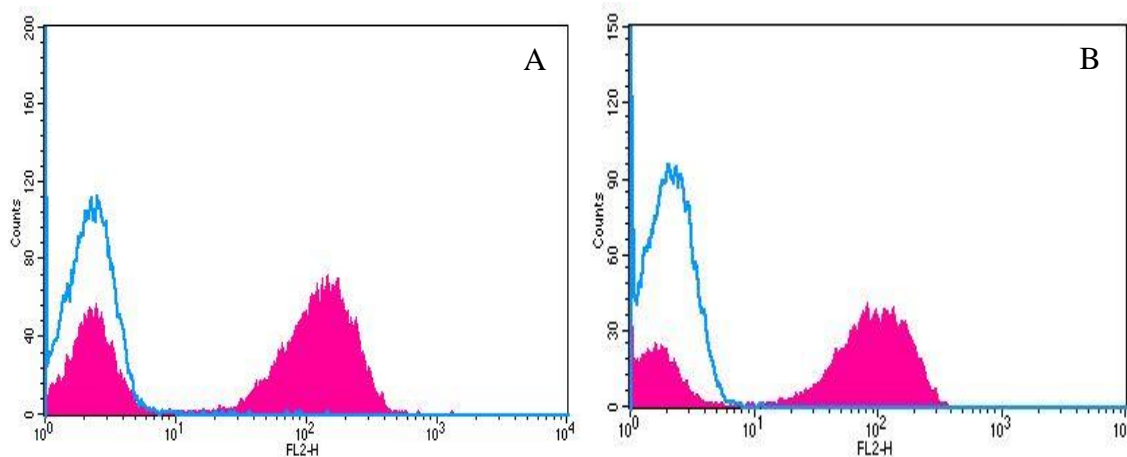


Figure 6.3 Expression of (A) CD3+ on RA blood PBMCs and (B) non-RA blood PBMCs. The histograms in pink show the expression of CD3+ (B/T-cell gated population, R1) with their isotype matched controls (blue line), $n = 3$. The pink peak shift to the right in each histogram indicates a positive result.

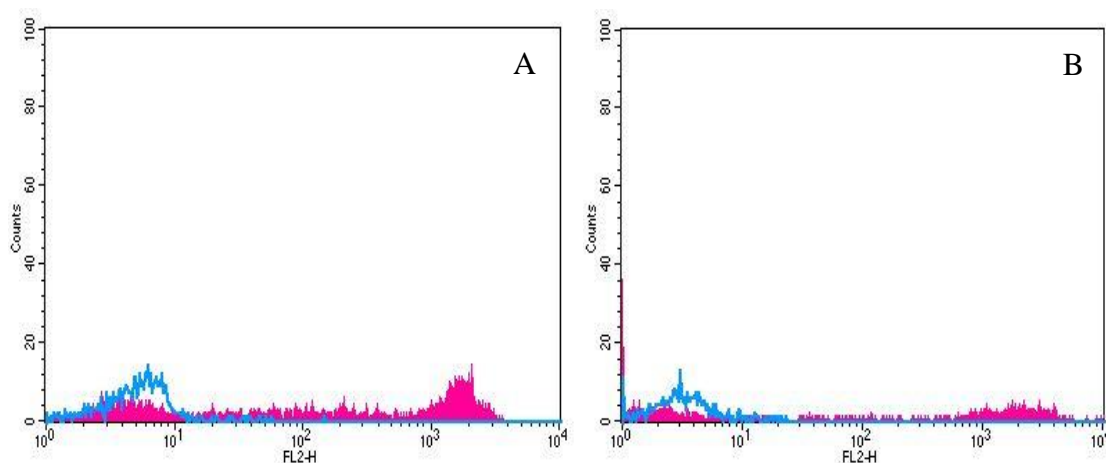


Figure 6.4 Expression of (A) CD14+ on RA blood PBMCs and (B) non-RA blood PBMCs. The histograms in pink show the expression of CD14+ (monocyte cell gated population, R2) with their isotype matched controls (blue line), $n = 3$. The pink peak shift to the right in each histogram indicates a positive result.

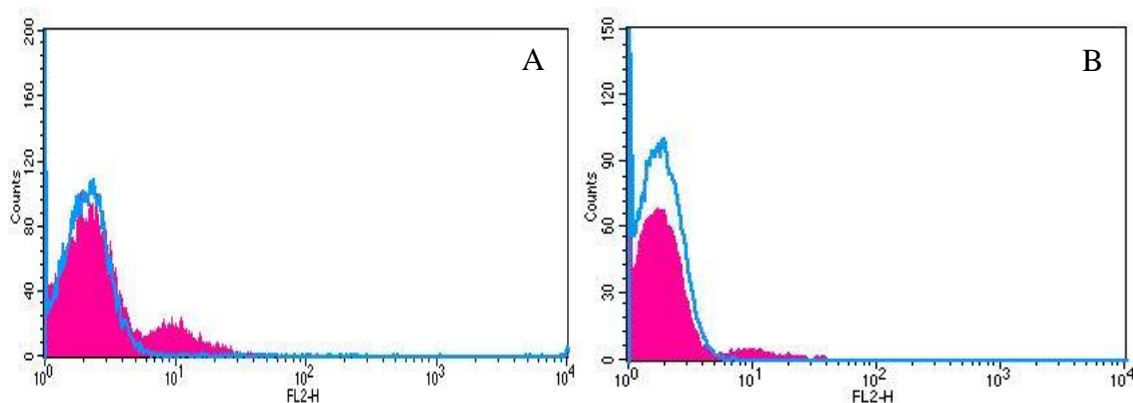


Figure 6.5 Expression of (A) CD20+ on RA blood PBMCs and (B) non-RA blood PBMCs. The histograms in pink show the expression of CD20+ (B/T-cell gated population) with their isotype matched controls (blue line), $n = 3$. The pink peak shift to the right in each histogram indicates a positive result.

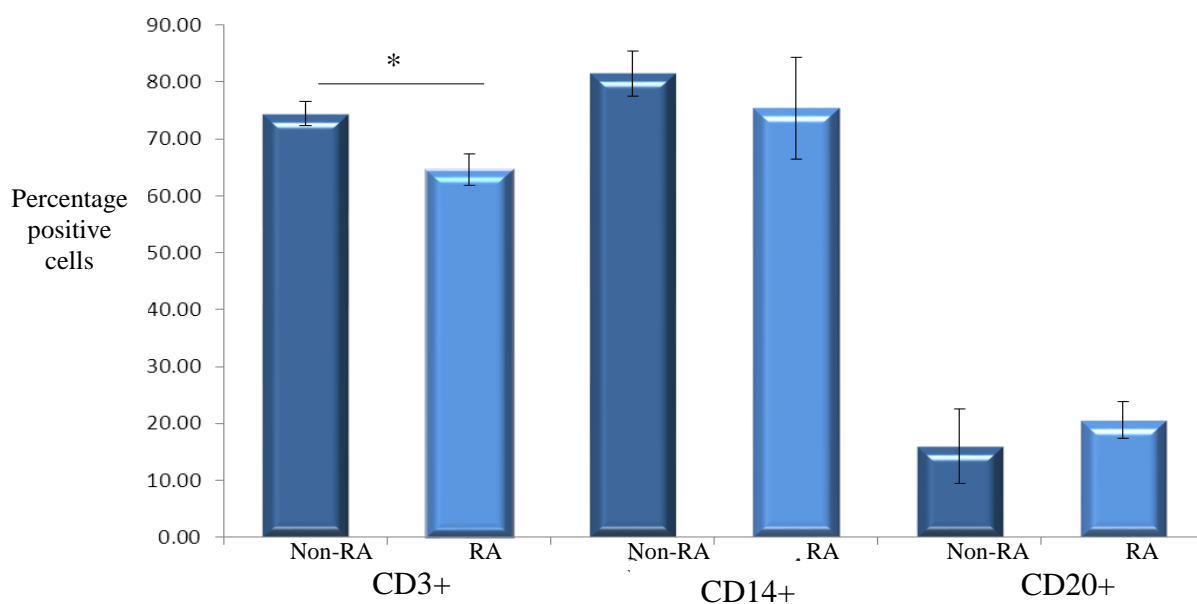


Figure 6.6 Chart showing percentage of CD3+, CD14+ and CD20+ positive RA and non-RA PBMCs. Percentage expression of PBMCs (\pm SD) from RA ($n=3$) and non-RA ($n=3$) PBMCs. Data are given as percentage population (\pm SD). Unpaired student's T-test was utilised for statistical analysis. * $p = <0.05$

6.5 Results of CCR marker staining on PBMCs

The pink peak shift to the right in each histogram (figures 6.7-6.10) indicates a positive result. MFI = mean fluorescent intensity. Gating was performed as described in section 6.3.1.1, figure 6.1. The percentage population positive was ascertained as described in section 6.3.1.2, figure 6.2. Mann-Whitney U test and Kruskal-Wallis ANOVA was utilised for statistical analysis as data were non-parametric.

6.5.1 CCR1 expression in RA and non-RA blood

Both lymphocytes and monocytes expressed CCR1 in RA and non-RA. Unpaired T-test showed no significant difference in CCR1 expression by monocytes (defined in R2) in RA (figure 6.7A) and non-RA (figure 6.7 B); RA 65.31% (± 5.46), non-RA 65.01% (± 13.65), $p = 0.98$ (figure 6.11). In addition, no difference was seen in CCR1 expression in B/T-cells (defined in R1) in RA (figure 6.7C) and non-RA (figure 6.7D); RA 27.25% (± 13.7), non-RA 10.96% (± 3.74), $p = 0.31$ (figure 6.12).

Whilst the percentage of monocytes expressing CCR1 showed no significant differences between RA and non-RA PBMCs the mean fluorescent intensity, indicating the cell surface expression of CCR1, was significantly increased on RA monocytes ($p = <0.001$) compared to non-RA monocytes, as shown by the Mann-Whitney U test (figure 6.13). No significant differences were observed in CCR1 cell surface expression on B/T-cells (figure 6.14).

6.5.2 CCR2 expression in RA and non-RA blood

As with CCR1, both RA and non-RA monocytes and lymphocytes expressed CCR2. The unpaired T-test showed no difference in CCR2 expression by monocytes in RA (figure 6.8A) and non-RA (figure 6.8B); RA 77.42% (± 7.14), non-RA 85.71% (± 3.01), $p = 0.34$ (figure 6.11). Further to this no difference was seen in CCR2 expression by B/T-cells in RA (figure 6.8C) and non-RA (figure 6.8D); RA 24.74% (± 8.05) non-RA 24.42% (± 2.85), $p = 0.97$ (figure 6.12).

Despite the lack of difference in the percentage population expression of CCR2, the cell surface expression on monocytes showed significant differences with CCR2 being increased on non-RA monocytes ($p < 0.001$) compared to RA monocytes (figure 6.13). No significant differences were observed in B/T-cell surface expression of CCR2 (figure 6.14)

6.5.3 CCR4 expression in RA and non-RA blood

CCR4 was seen to be expressed on both RA and non-RA lymphocytes and monocytes. It was ascertained that the difference seen in CCR4 expression by monocytes in RA (figure 6.9A) and non-RA (figure 6.9B); RA 81.68% (± 2.93), non-RA 60.20% (± 21.05), $p = 0.37$ was not statistically significant (figure 6.11). Whilst not reaching significance the results indicate a positive trend in increased CCR4 expression by RA (figure 6.9C) B/T-cells; RA 66.69% (± 12.01), non-RA (figure 6.9D) 32.38% (± 6.39), $p = 0.065$ (figure 6.12). However, the MFI showed that CCR4 cell surface expression was significantly increased on RA monocytes ($p < 0.001$) compared to non-RA monocytes (figure 6.13), and also on RA B/T-cells ($p = 0.049$) (figure 6.14).

6.5.4 CCR5 expression in RA and non-RA PBMCs

CCR5 was expressed by both RA and non-RA PBMCs. A statistical difference was seen in CCR5 expression by monocytes in RA (figure 6.10A) and non-RA (figure 6.10B); RA 59.18% (± 6.08) non-RA 91.15% (± 2.95), $p = 0.009$ (figure 6.11). The results show a significant increase in CCR5 expression by B/T-cells in RA (figure 6.10C) compared to non-RA (figure 6.10D); RA 44.81% (± 10.6) non-RA 36.01% (± 5.17), $p = 0.049$ (figure 6.12).

The MFI showed a significant increase in CCR5 cell surface expression on non-RA monocytes ($p = < 0.001$) compared to RA monocytes (figure 6.13). No significant differences were observed in B/T-cell surface expression of CCR5 (figure 6.14).

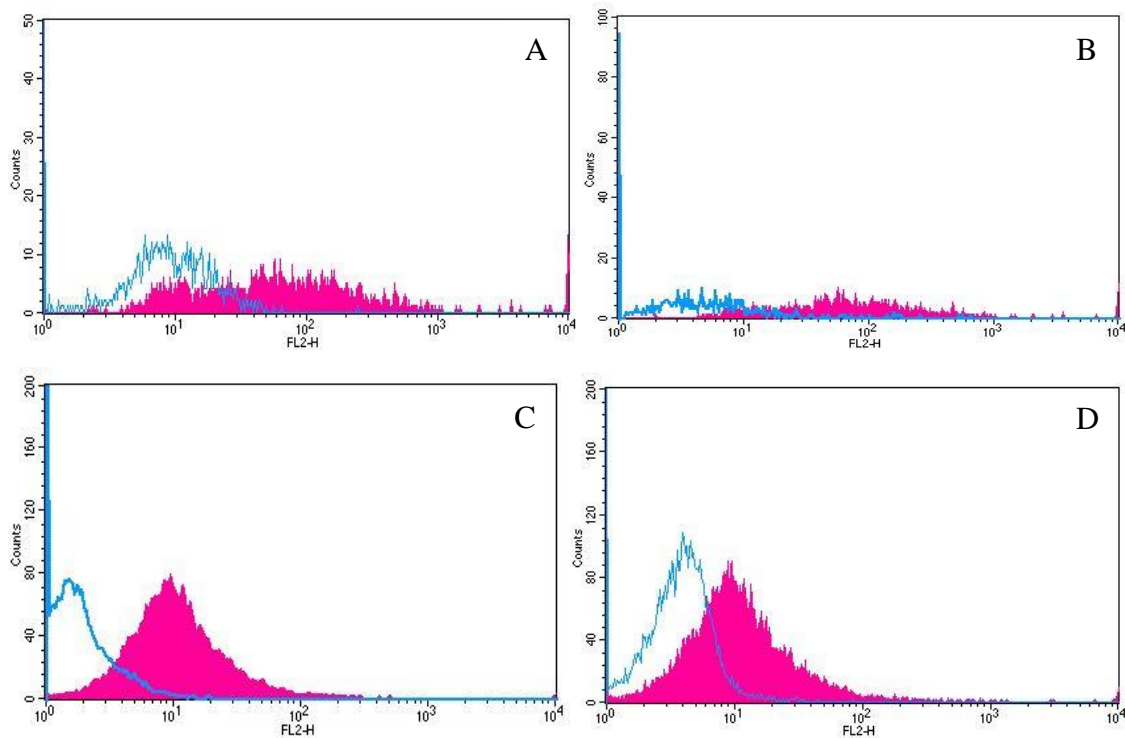


Figure 6.7 Expression of CCR1 in RA and non-RA PBMCs

(A) shows CCR1 on RA monocytes (B) shows CCR1 on non-RA monocytes (C) shows CCR1 on RA B/T-cells. (D) shows CCR1 on non-RA B/T-cells. The histograms in pink show the expression of CCR1 with their isotype matched controls (blue line), $n = 3$. The pink peak shift to the right in each histogram indicates a positive result.

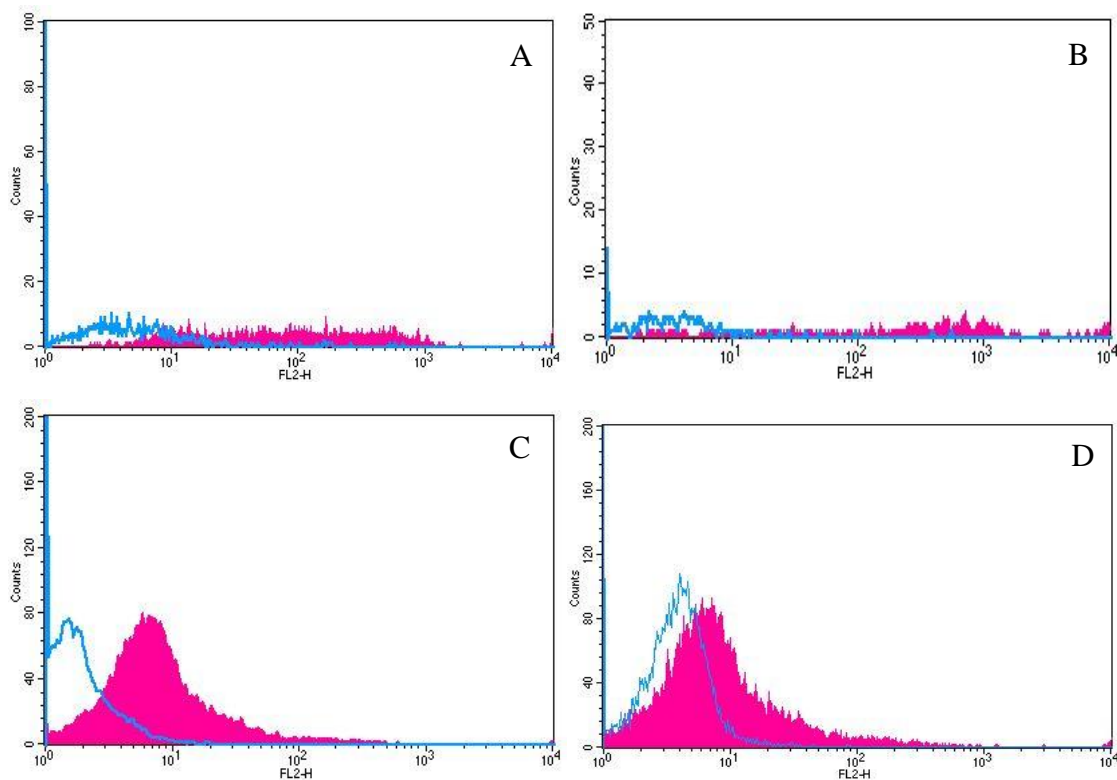


Figure 6.8 Expression of CCR2 in RA and non-RA PBMCs

(A) shows CCR2 on RA monocytes. (B) shows CCR2 on non-RA monocytes. (C) shows CCR2 on RA B/T-cells. (D) shows CCR2 on non-RA B/T-cells. The histograms in pink show the expression of CCR2 with their isotype matched controls (blue line), $n = 3$. The pink peak shift to the right in each histogram indicates a positive result.

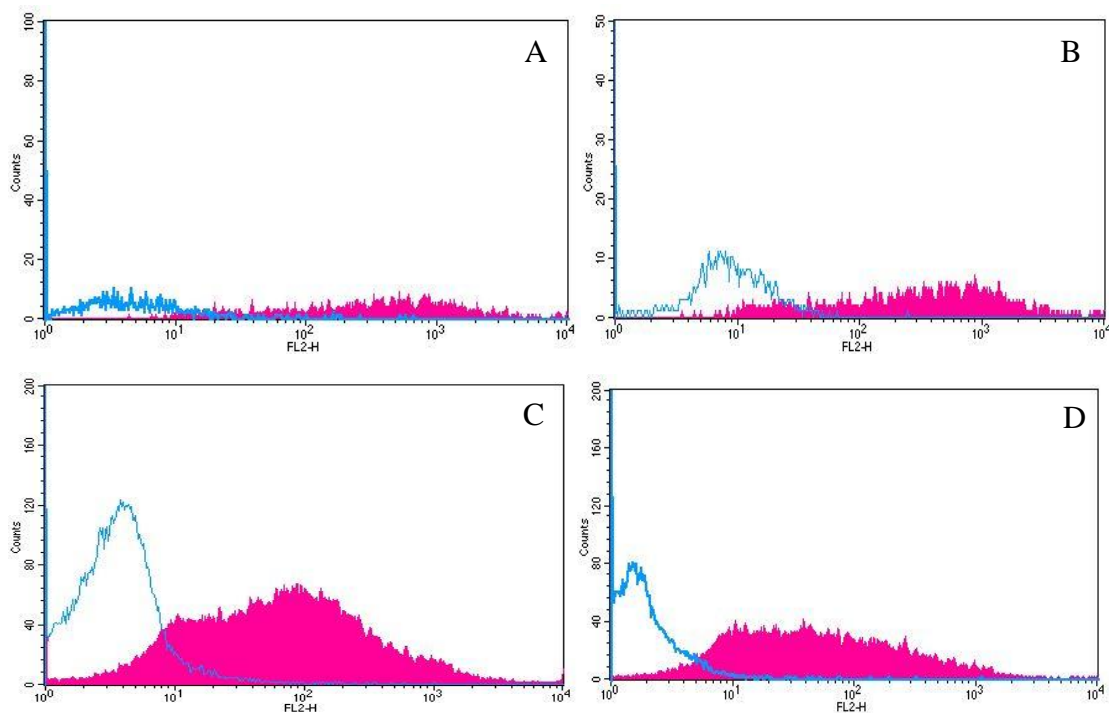


Figure 6.9 Expression of CCR4 in RA and non-RA PBMCs

A shows CCR4 on RA monocytes, **B** shows CCR4 on non-RA monocytes. **C** shows CCR4 on RA B/T-cells. **D** shows CCR4 on non-RA B/T-cells. The histograms in pink show the expression of CCR4 with their isotype matched controls (blue line), $n = 3$. The pink peak shift to the right in each histogram indicates a positive result.

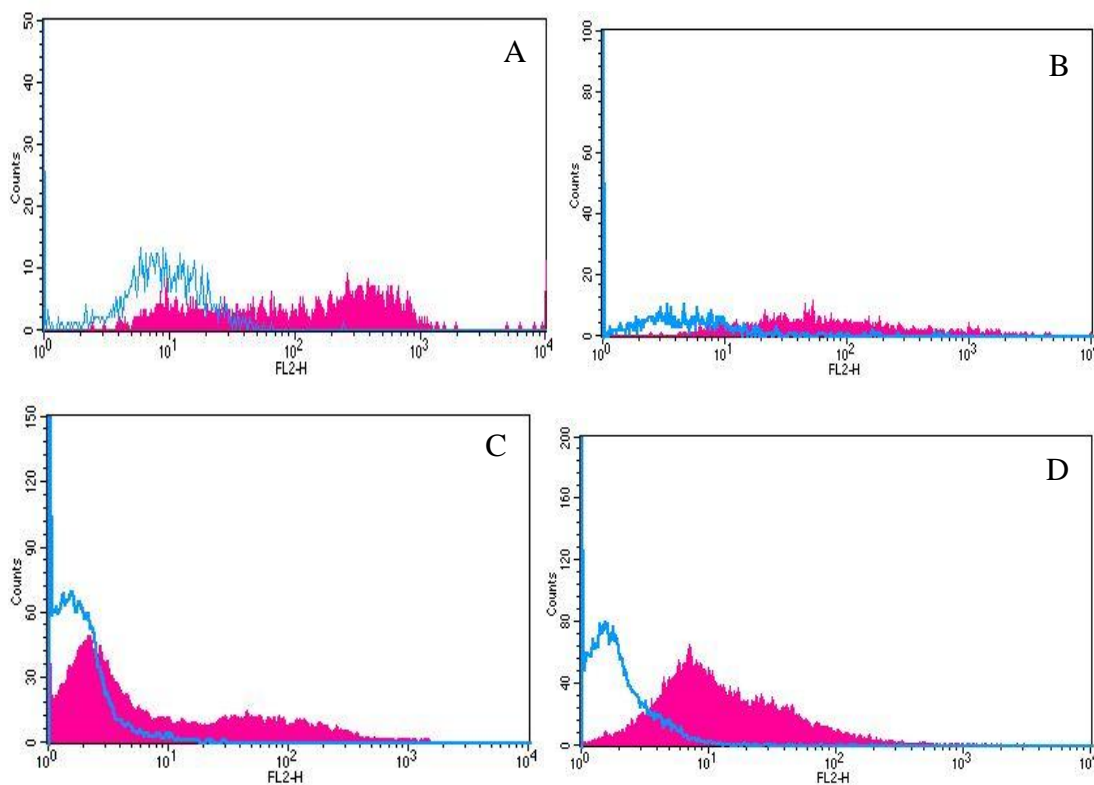


Figure 6.10 Expression of CCR5 in RA and non-RA PBMCs

A shows CCR5 on RA monocytes. **B** shows CCR5 on non-RA monocytes. **C** shows CCR5 on RA B/T-cells. **D** shows CCR5 on non-RA B/T-cells. The histograms in pink show the expression of CCR5 with their isotype matched controls (blue line). The pink peak shift to the right in each histogram indicates a positive result.

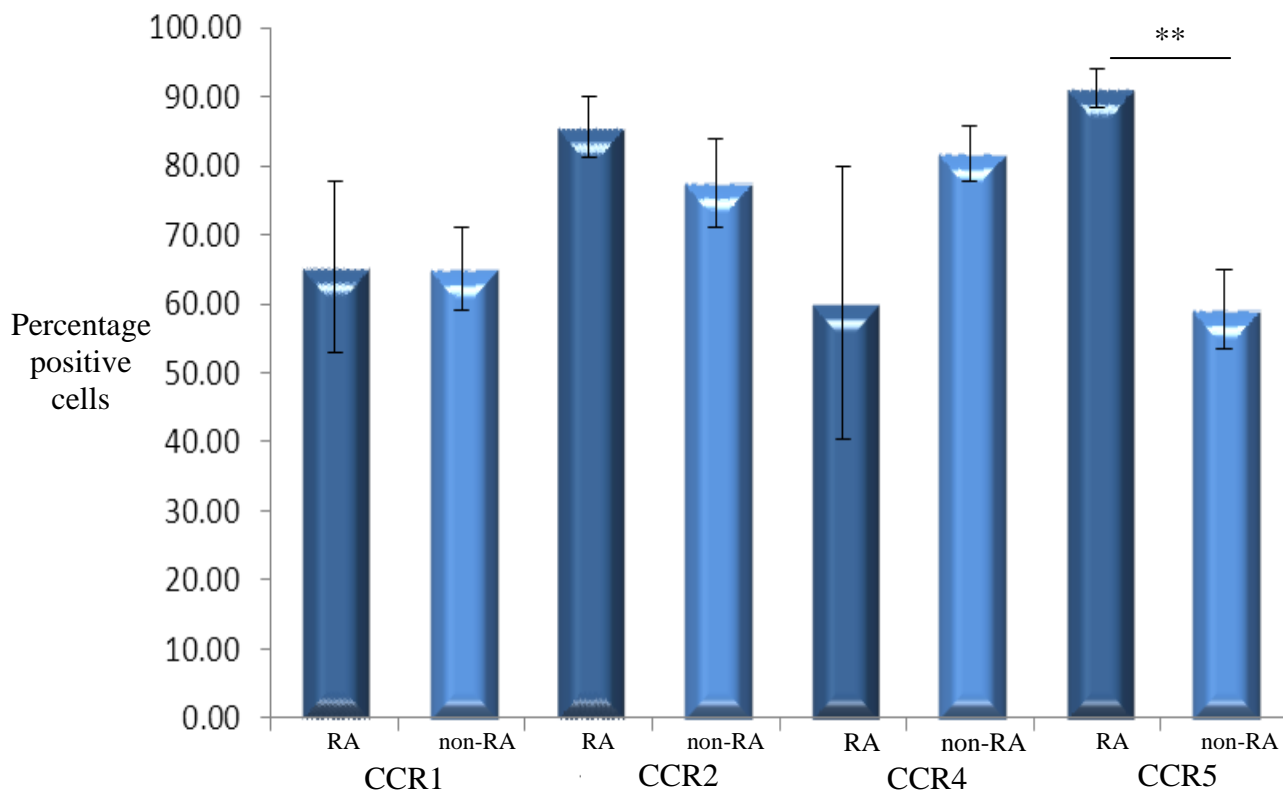


Figure 6.11 Chart showing percentage of CCR1, CCR2, CCR4 and CCR5 positive monocytes in RA and non-RA. Showing average percentage expression of monocytes (\pm SE) from RA (n=3) and non RA (n=3) monocytes. Mann-Whitney U test was utilised, ** p = <0.01

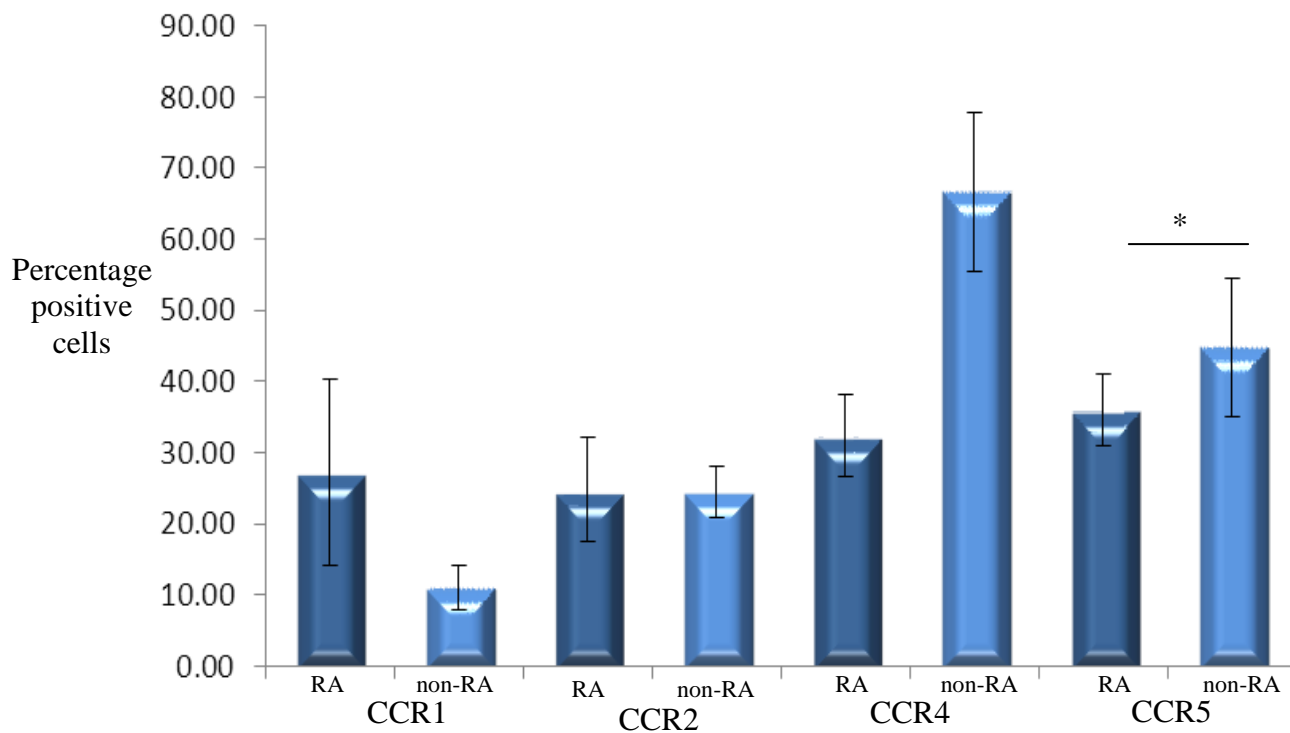


Figure 6.12 Chart showing percentage of CCR1, CCR2, CCR4 and CCR5 positive B/T cells in RA and non-RA. Percentage expression of B/T-cells (\pm SE) from RA (n=3) and non-RA(n=3) PBMCs. Mann-Whitney U test was utilised, * $p < 0.05$

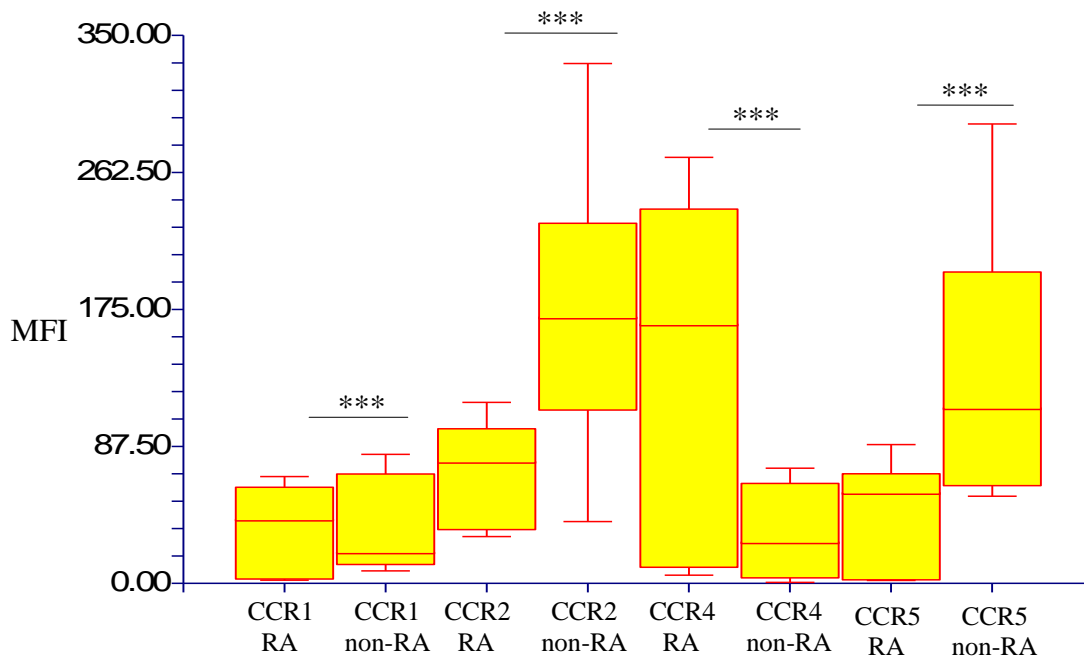


Figure 6.13 Box plot showing mean fluorescent intensity (MFI) of CCR1, CCR2, CCR4 and CCR5 on RA and non-RA monocytes. The vertical red bar indicates overall range, yellow box shows interquartile range with horizontal red line in yellow box showing median values. RA n =3, non-RA n=3. IgG controls were subtracted from the data. Mann-Whitney U test was utilised, *** $p = <0.001$.

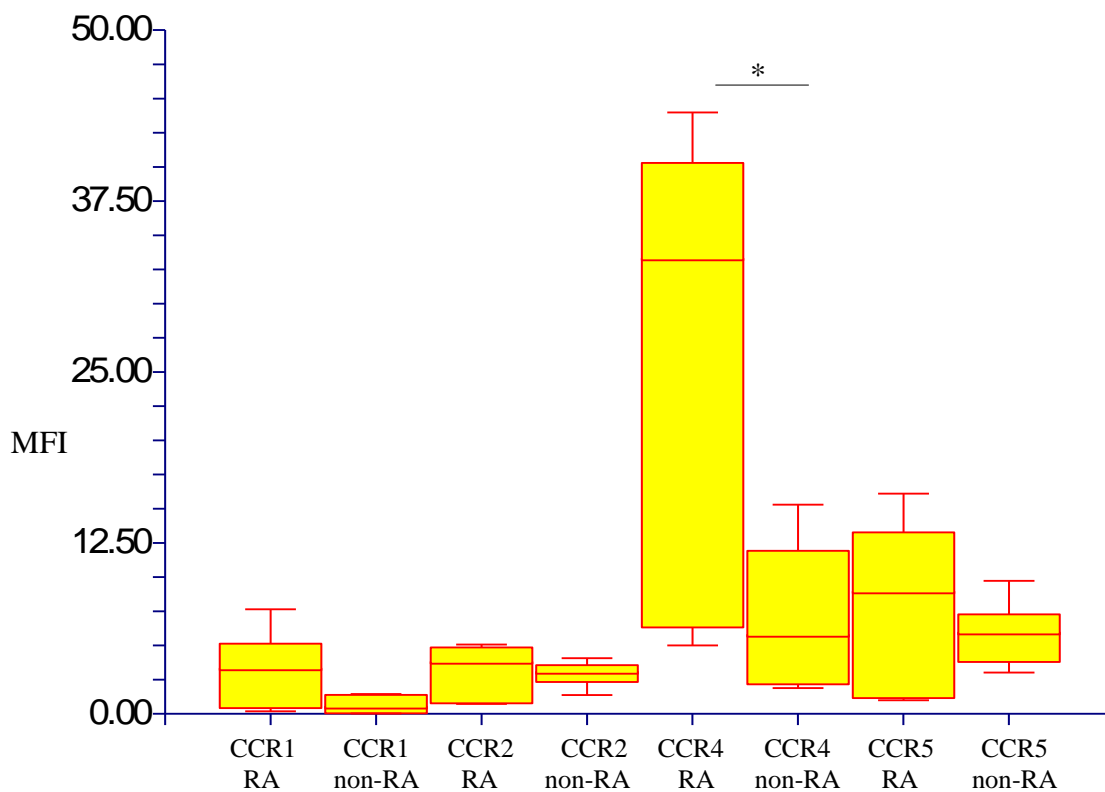


Figure 6.14 Box plot showing mean fluorescent intensity (MFI) of CCR1, CCR2, CCR4 and CCR5 on RA and non-RA B/T-cells. The vertical red bar indicates overall range, yellow box shows interquartile range with horizontal red line in yellow box showing median values. RA n =3, non-RA n=3. IgG controls were subtracted from the data. Mann-Whitney U test was utilised, * p = <0.05

6.6 PBMC migrations across HBMEC's

Having found expression of the receptors for the chemokines of interest it was decided to assess the functionality of each chemokine with HBMECs using non-RA blood PBMCs which were more readily available at the time. Following these tests it was decided to test the functionality of CCL7 for migration across HDLECs using RA blood as a better example of the total inflammatory environment to test potential lymphatic clearance in RA, and due to the significant increases in the CCL7 receptors CCR1 and CCR4 seen in RA blood monocytes (figure 6.13). As CCL7 was the only chemokine to show a significant decrease on RA LECs it was decided to only assess CCL7 chemokine in this way due to time constraints. Kruskal-Wallis ANOVA was used for statistical analysis as data were non-parametric.

6.6.1 Mononuclear cell migration across TNF- α activated HBMECs.

A comparison was made between the different chemokines for monocyte migration (figure 6.15) and B/T-cell migration (figure 6.16).

Kruskal-Wallis ANOVA test showed an overall significant difference in monocyte migration in the presence of 100ng/ml chemokine ($p = 0.002$). When data were compared using Dunn's post hoc test it was shown that CCL7 gave the greatest response for monocyte migration ($p = 0.0045$) followed by the positive control CCL2 ($p = 0.014$), CCL14 ($P = 0.026$) and CCL22 ($p = 0.026$) when compared to the 0 ng/ml chemokine control. Statistical analysis for CCL16 did not reach significance (figure 6.15).

Kruskal-Wallis one-way ANOVA on ranks showed no overall significant difference in B/T cell migration (figure 6.16) in the presence of 100ng/ml chemokine ($p = 0.28$).

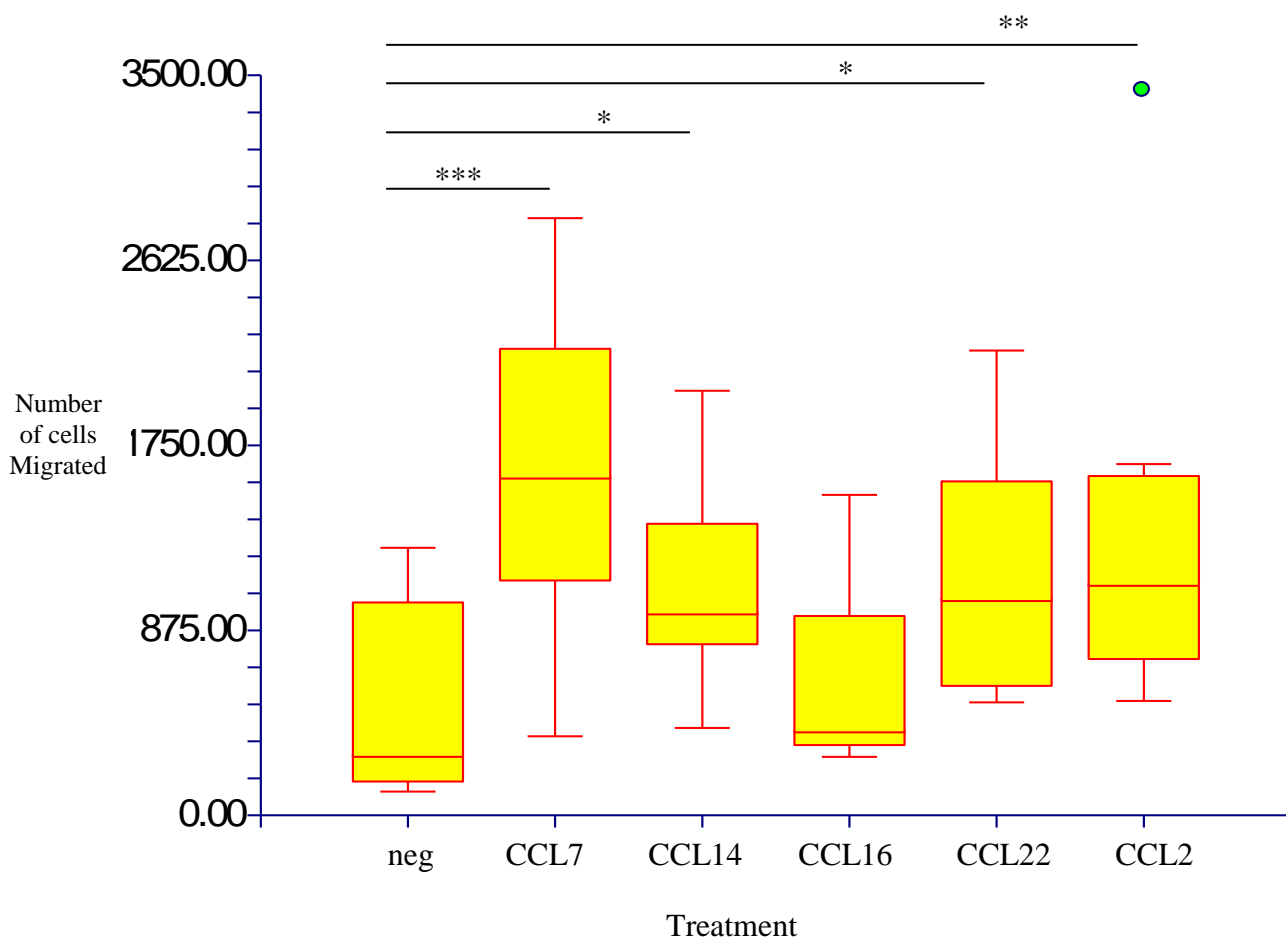


Figure 6.15 Box plot showing numbers of monocytes migrated in response to 100ng/ml chemokine across TNF- α activated HBMECs. Negative control (neg) was performed in the presence of TNF- α and the absence of chemokine. Positive control (CCL2) was performed in the presence of TNF- α and 100ng/ml CCL2. The vertical red bar indicates overall range, yellow box shows interquartile range with horizontal red line in yellow box showing median, and the outlier values are shown in green ($n = 3$). Kruskal-Wallis ANOVA was used followed by the Wilcoxon signed-rank test * $p = <0.05$, ** $p = <0.01$, *** $p = <0.001$.

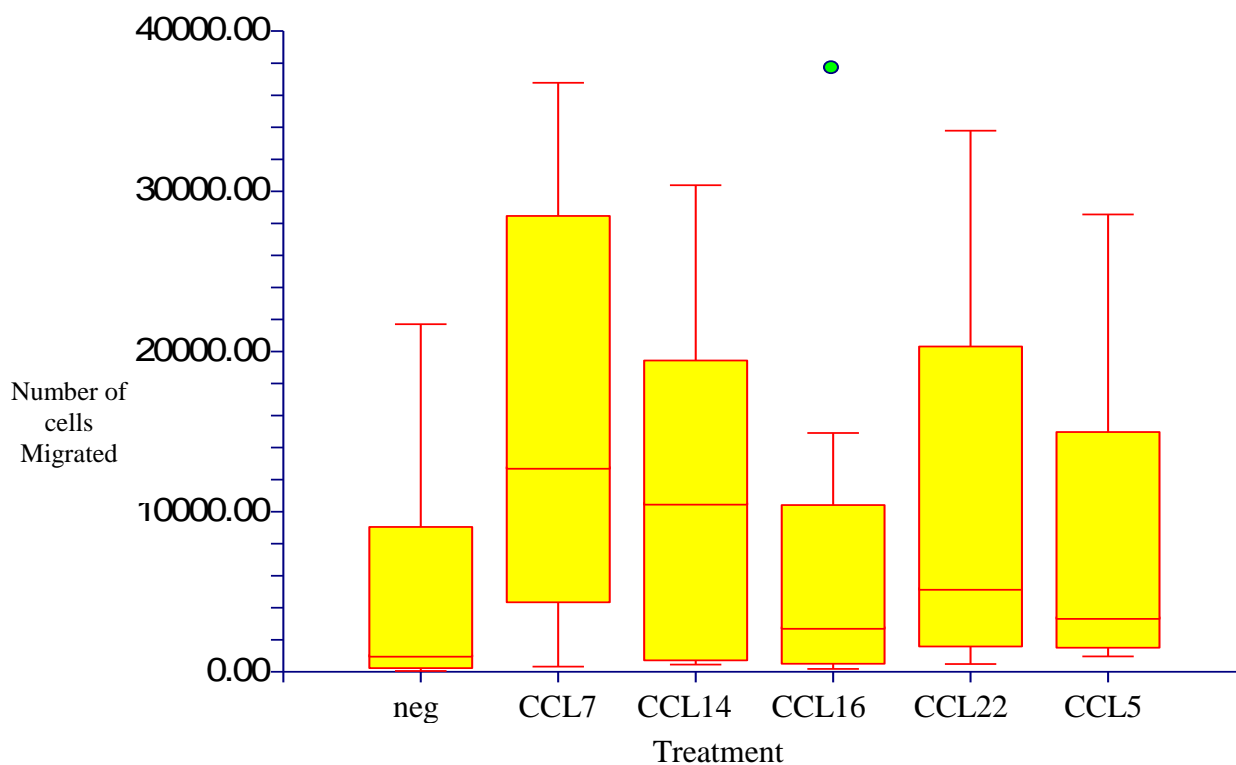


Figure 6.16 Box plot showing numbers of B/T-cells migrated in response to 100ng/ml chemokine across TNF- α activated HBMECs. Negative control (neg) was performed in the absence of chemokine. Positive control (CCL5) was performed in the presence of TNF- α and CCL5. The vertical red bar indicates overall range, yellow box shows interquartile range with horizontal red line in yellow box showing median, and the outlier values are shown in green (n = 3). Kruskal-Wallis ANOVA was used followed by the Wilcoxon signed-rank test.

6.7 CCL7 HDLEC dose response.

In section 3.3.1.7 it was shown that there was a significant reduction in the percentage of LEC's stained for CCL7 in RA synovium ($p = 0.011$). TNF- α /IFN- γ was used to activate the cells as this was shown to generate the greatest ICAM increase in HDLECs (section 4.5).

In this section of the study when HDLECs were incubated with increasing concentrations of CCL7 in transwells significant increases in RA monocyte migration were observed. Kruskal-Wallis one way ANOVA on ranks showed a significant difference in monocyte migration in response to CCL7 ($p = 0.002$) The Mann-Whitney U test was also performed and showed the greatest increase to be at 250ng/ml CCL7 ($p = 0.013$) with a significant increase in monocyte migration also seen at 100ng/ml CCL7 ($p = 0.037$) compared to 0ng/ml (see figure 6.17).

In the same conditions increases in B/T-cell migration which peaked at 10ng/ml were observed. Kruskal-Wallis one way ANOVA on ranks showed no significant differences when compared to 0ng/ml, however a significant difference in B/T cell migration in response to CCL7 ($p = 0.030$) compared to the negative control was observed using the Mann-Whitney U test (figure 6.18).

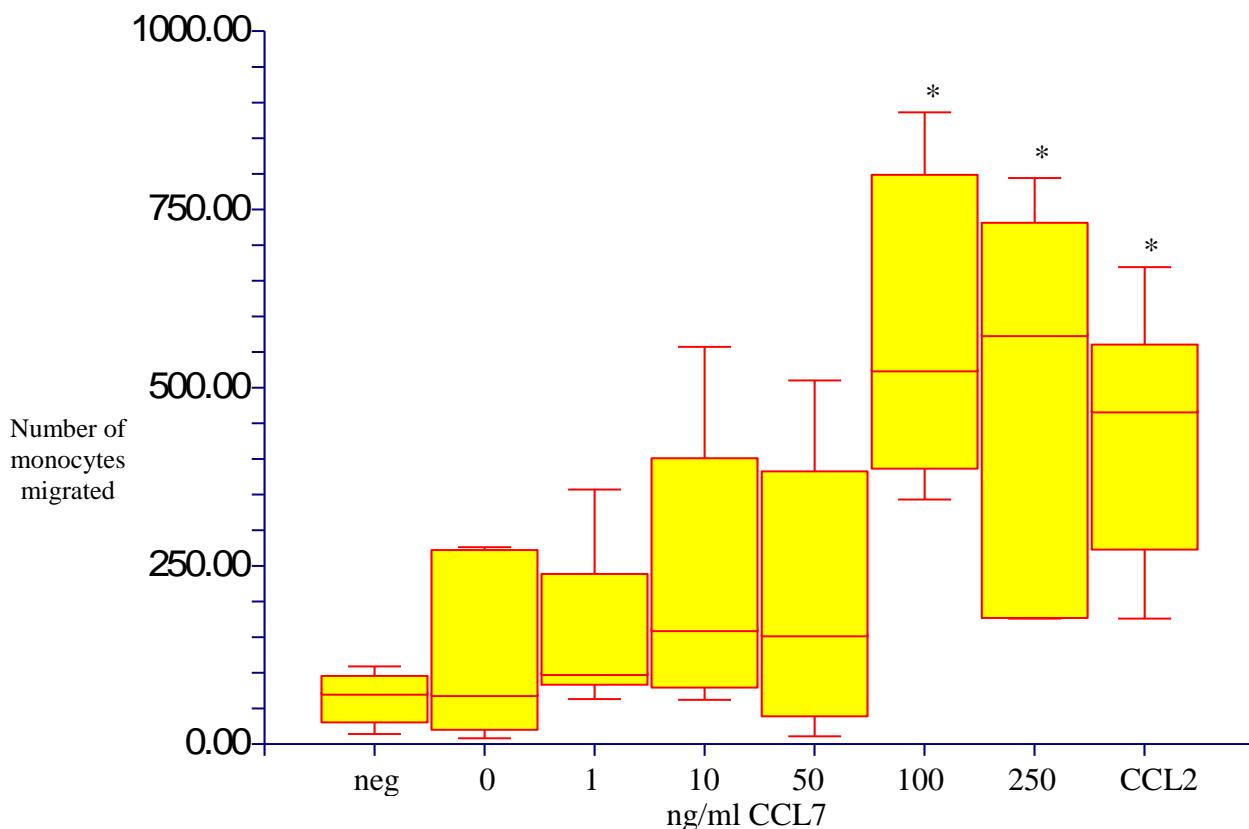


Figure 6.17 Box plot showing numbers of monocytes migrated in response to CCL7 through TNF- α /IFN- γ activated HDLECs. Negative control (neg) was performed in the absence of TNF- α /IFN- γ and CCL7. Positive control (CCL2) was performed in the presence of TNF- α /IFN- γ and 100ng/ml CCL2. The vertical red bar indicates overall range, yellow box shows interquartile range with horizontal red line in yellow box showing median ($n = 3$). Kruskal-Wallis ANOVA was used followed by the Wilcoxon signed-rank test * $p = <0.05$ compared to 0ng/ml CCL7.

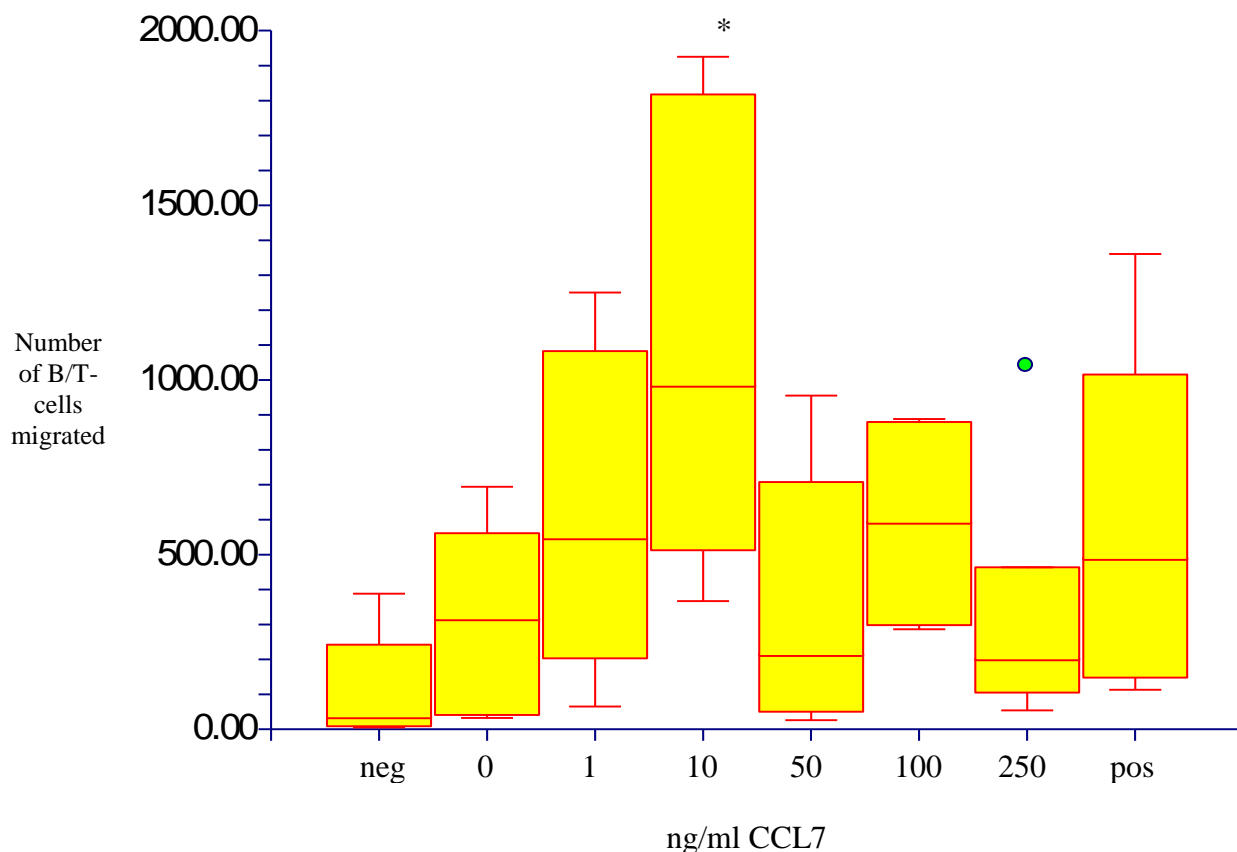


Figure 6.18 Box plot showing numbers of B/T-cells migrated in response to CCL7 across TNF- α /IFN- γ activated HDLECs. Negative control (neg) was performed in the absence of TNF- α /IFN- γ and CCL7. 0ng/ml was performed in the presence of TNF- α /IFN- γ . Positive control (pos) was performed in the presence of TNF- α /IFN- γ and 100ng/ml CCL5. The vertical red bar indicates overall range, yellow box shows interquartile range with horizontal red line in yellow box showing median, and the outlier values are shown in green. Kruskal-Wallis ANOVA was used followed by the Wilcoxon signed-rank test * $p \leq 0.05$ compared to negative control.

6.8 Discussion

Monocytes differentiate into macrophages, which in the normal intima are a minority cell type. However, they have been shown to increase to up to 80% of the intimal cell population in RA (Bartholome *et al.*, 2004). Macrophages express a range of chemokines, cytokines, chemokine receptors, and secrete a range of cytokines, chemokines, growth factors, proteases and further mediators (reviewed by Szekanecz and Koch, 2007).

In this study transmigration analysis of non-RA mononuclear cells across TNF- α stimulated HBMECs in response to CCL7, CCL14 and CCL22 indicated that whilst each have a positive effect on monocyte migration the greatest effect was seen to be in response to CCL7. However, the similar degrees to which CCL7 were identified on both RA and non-RA ECs (as shown in chapter 3) indicates that synovial infiltration via CCL7 is most likely not primarily responsible in driving the pathology of RA. This is the first study to show the significant increase in the cell surface expression of CCR1 in RA monocytes and indicate that CCR1 is the preferential receptor through which CCL7 functions in RA.

CCR1 and CCR5 are known CCL14 receptors. The high expression of CCR1 by RA monocytes and the significant increases in the percentage of B/T-cells expressing CCR5 in non-RA in this study indicate that monocyte recruitment most likely occurs via CCR1. However, the lack of significant response by B/T-cells to CCL14 indicates that B/T-cells migrating via CCL14 are not of great significance to RA pathology.

Increases in the numbers of monocytes migrating, such as seen in this study with CCL22, suggest that CCL22 may be functional in monocyte migration in RA, and hence the presence of large numbers of macrophages in the synovium. Furthermore, CCR4 (the receptor for CCL22), was significantly increased in RA; specifically in RA monocytes. This indicates that CCL22 may be important in driving monocyte migration in RA.

In RA, monocytes also differentiate into osteoclasts via signals from activated T-cells and synovial fibroblast-like cells. Osteoclasts are essential for bone remodelling throughout life as the primary bone resorbing cells, enabling remodelling and old age bone loss (Schett, 2007 and references therein). It is possible that the increases in monocyte recruitment seen in the current study due to CCL7, CCL14 and CCL22 may be exacerbating the generation of osteoclasts, which have been shown to be abundant in the RA synovial membrane (Schett, 2007 and references therein) and hence increasing bone loss in RA. Further work to substantiate this hypothesis is required,

No significant effects on monocyte migration or B/T-cell migration in response to CCL16, and no significant B/T-cell migration in response to CCL7, CCL14 or CCL16 were observed in the same conditions.

Whilst not reaching significance when compared to 0ng/ml where TNF- α was present, CCL7 generated a positive trend in T-cell migration at 10ng/ml. This trend declined after this point and it is possible that the T-cell receptors became saturated and desensitised at this point resulting in the decline in migratory response. The transmigration analysis of RA monocytes across TNF- α /IFN- γ stimulated HDLECs in response to CCL7 showed significant increases at 100ng/ml and 250ng/ml CCL7 when compared to 0ng/ml

The data presented here have shown higher numbers of T-cells (CD3+) and monocytes (CD14+) in the PBMCs of both RA sufferers and normal control blood, compared with B-cells (CD20+) in both populations, but proportionally similar values to Eggleton *et al.*, (2011).

However, the results show that non-RA PBMCs have more T-cells (CD3+) and monocytes (CD14+) present. It is likely that increased trafficking of these cells into the rheumatoid joints is resulting in fewer numbers being present in the blood.

In agreement with Katschke *et al.*, (2001) the data presented here indicate that a high percentage of both RA and non-RA monocytes express CCR1 and CCR2 with no significant differences in the values. However, the present study also analysed the MFI of the monocytes for the receptors and showed a significant increase in the MFI for CCR1 (the receptor for CCL7 and CCL14) in RA monocytes and a significant increase in the MFI for CCR2 (the receptor for CCL7 and CCL16) in non-RA monocytes. However, CCR1 cell surface expression in RA was lower than that of each of the other tested receptors. While this study showed that CCR4 is expressed by a greater percentage of RA monocytes compared to non-RA monocytes, the increase is not significant, unlike the results in Katschke's study. However, this study showed a significant increase in the monocyte MFI for CCR4 (the receptor for CCL22) in RA blood. The present study shows a significant increase in both the percentage of RA monocytes expressing CCR5 compared to non-RA monocytes, and a significant increase in the monocyte MFI for CCR5 in non-RA blood. However, the increase in CCR5 expressing CD14⁺ monocytes in normal blood shown in this study is supported by a study carried out by Harringman *et al.*, (2006). This group who also found lower CCR5 expression in the RA group compared to healthy controls with the paired synovial tissue samples and showed 'abundantly expressed' CCR5. CCR5 positive macrophages have been found to accumulate in the synovial tissue. It is likely that in RA, CCR5 positive monocytes are being actively trafficked into the joint where they have been implicated to be involved in monocyte/macrophage retention (Katschke., *et al*, 2001). Further to this, differences in circulating cytokine population between the RA and non-RA groups may be affecting CCR5 cell surface expression.

This section of the study was limited by the low n number and volume of blood allowed by the ethical approval. These issues reduce the reliability of the data and hence the conclusions which are drawn from it. This low n number and blood volume was

particularly pertinent in the analysis of the CD/CCR data as monocyte numbers were particularly low, potentially due to their increased trafficking to the joints. Given more time this section would benefit from repetition using increased sample numbers and greater volumes of blood from each participant to allow for greater monocyte numbers to be analysed. This would also have allowed for greater numbers of transmigrations to be performed to further benefit the study.

It was not possible to put the histograms on the same axis due to changes in the computer system where not all data transferred. Further work would be carried out to repeat these analyses prior to their use in publications.

In conclusion:

The first aim of this section of the study was to establish if the receptors for the chemokines CCL7, CCL14, CCL16 and CCL22 were expressed in RA. The data suggested that CCR1 was the preferential receptor through which B/T cells are recruited by CCL14 in RA and that monocyte recruitment most likely occurs via CCR1 also. No conclusions can be drawn as to CCR2 or CCR5 being the preferential receptor for CCL16. As the MFI for CCR4 (the receptor for CCL22) was increased in RA blood this is the best candidate for the CCL22 receptor in RA. As stated earlier, further work is required to substantiate these conclusions.

The second aim of this section of the study was to quantify the potential of CCL7, CCL14, CCL16 and CCL22 to act as chemoattractants within the rheumatoid synovium. It was shown that CCL7 has the greatest effect on monocyte migration, but that synovial infiltration via CCL7 is most likely not primarily responsible in driving the pathology of RA.

The third aim of this section of the study was to determine the functionality of CCL7 across HDLECs. This chemokine stimulated monocyte migration. When considered with

the decreased expression of *CCL7* at synovial LECs ascertained in chapter 3, this section of the study indicates that the decreased expression of *CCL7* at LECs in inflammatory conditions may reduce CD14⁺ cell removal from synovial tissue via migration across lymphatic ECs as part of lymphatic clearance. This provides further novel evidence for the role of blood:lymphatic vessel dysregulation in the persistence of inflammatory cells within the synovium.

Chapter 7

**CCL7, CCL14, CCL16 and
CCL22 in matched serum
and synovial fluid.**

7.1 Introduction and Aims

The presence of CCL7, CCL14, CCL16 and CCL22 in RA synovium and cultured ECs were studied in chapter 3 and chapter 4. The effects of the same chemokines on mononuclear and endothelial cell morphological changes conducive to leukocyte migration were analysed in chapter 5, while chapter 6 analysed the functionality of these chemokines in mononuclear cell migration. The relationship of the levels of these particular chemokines with disease pathogenesis has not been previously examined so it was important to determine their levels within the circulation and the joint, and to investigate whether particular chemokine profiles are associated with disease features and/or different types of arthritis.

It is fully accepted that certain chemokines are found in the serum and/or synovial fluid (SF) of arthritis sufferers (Opdenakker *et al.*, 1993; Koch *et al.*, 1995; Flytie *et al.*, 2010; McNearny *et al.*, 2011). Furthermore, it is accepted that the chemokine profiles in serum/SF differ between different arthritides which allows for the identification of potential disease markers. For example, SF levels of cytokines in patients with early RA have been shown to have differing cytokine profiles at different disease stages (Raza *et al.*, 2005; Yoshihara *et al.*, 2000). However, CCL7, CCL14, CCL16 and CCL22 have not previously been studied in the range of arthritide SF and serum seen in the current study.

A wide range of clinical variables are assessed in arthritis patients. Variables such as erythrocyte sedimentation rate (ESR), joint scores and disease activity scores (DAS44) are used to assess systemic inflammation and overall disease activity. Further variables such as early morning stiffness (EMS), grip strength and Health Assessment Questionnaire (HAQ) can be used to assess pain and loss of function at the different disease stages, while the damage scale of the Overall Status in Rheumatoid Arthritis (OSRA) has been strongly correlated with articular damage as determined by radiographs using the Larsen score.

The hypothesis is that the chemokines CCL7, CCL14, CCL16 and CCL22 occur in RA serum and SF and show differential expression between arthritides. These chemokines may have correlations with specific clinical variables of the diseases and may indicate a role in the pathology of later stage disease.

The aims of this section were to;

- Examine if CCL7, CCL14, CCL16 and CCL22 occur in human RA serum and SF in support of chapters 3-6 showing their expression in RA synovium and function in stimulating leukocyte migration.
- Compare the presence of CCL7, CCL14, CCL16 and CCL22 in matched samples of serum and SF from patients with RA, psoriatic arthritis (PsA), OA and reactive arthritis (ReA) to establish whether different chemokine profiles are associated with different types of arthritis.
- Examine correlations between levels of these chemokines and clinical variables to ascertain their potential role in disease pathogenesis.

7.2 Materials and Methods

Matched SF and serum were collected as described in section 2.7.1. All samples were kindly donated by Dr Derek Matthey (Keele University, Guy Hilton Research Centre, Stoke-on-Trent, UK). ELISA was performed as described in section 2.7.2 -2.7.4.

7.2.1 Quantitation of results

Statistical analysis was performed using GraphPad software and WinPepi (Abramson, 2011). Normality testing showed the data was not normally distributed. Kruskal-Wallis ANOVA followed by the Holm-Bonferroni post hoc test was utilised to analyse differences in serum and SF levels for each chemokine between each arthritis type. The Mann-Whitney U test was used to assess differences in chemokine serum and SF levels within

each disease type. Spearman's rank correlations were performed followed by the Holm-Bonferroni post hoc test.

7.3 Results

7.3.1 CCL7 in the serum and SF of RA, OA, PsA and ReA patients.

In serum CCL7 was detected almost solely in RA, being detected in the serum of only 1 OA (table 7.1), 1 PsA and no ReA sufferers (table 7.2). Kruskal-Wallis ANOVA for non-parametric data indicated a significant difference between groups ($p = 0.0025$). Further analysis showed significant difference between CCL7 levels in RA and ReA serum, $p = 0.021$, (figure 7.1A). In the SF, CCL7 was present in the majority of RA but no OA (table 7.1), and the majority of ReA but only 1 PsA sufferer (table 7.2). CCL7 in the SF was shown to be significantly different between groups ($p = 0.0005$). Further analysis showed significant differences between CCL7 SF in RA and OA ($p = 0.028$), RA and ReA ($p = 0.020$) and RA and PsA ($p = 0.0042$) (figure 7.1B).

There was a significant differences between CCL7 levels in serum and SF (median levels, 23.78 pg/ml in serum v 345.37 pg/ml in SF, $p = 0.0045$) in both RA and ReA sufferers. No significant differences were seen in the serum and SF in OA and PsA.

Table 7.1 Chemokines present in serum and synovial fluid from RA and OA.

Test	RA			OA		
	Serum	SF	<i>p</i> value	Serum	SF	<i>p</i> value
CCL7	23.78 0.00 – 109.78 (n=16)	345.37 80.98 – 1379.36 (n=15)	0.0045	0.00♦ 0.00 - 2.81	°	-
CCL14	91510.7 52527.8 – 142502.3	63059.5 49237.8 – 91143.4	0.15	107170.0 93376.6 – 221806.8	55688.7 44517.8 – 91335.0	<i>p</i> = 0.010
CCL16	15264.5 11945.85 – 22827.2	3185.9 2277.3 – 8198.2	0.00016	17892.6 14556.3 – 35236.1	7863.7 6971.1 – 9426.1	<i>p</i> = 0.0042
CCL22	662.65 519.13 – 1004.58	363.21 280.5 - 470.21	0.010	526.7 340.3 – 934.1	189.2 161.3 – 205.4	<i>p</i> = 0.010

Median values are given as pg/ml with inter-quartile range. ♦ indicates CCL7 was present in only 1 of the samples tested, ° indicates chemokine not present in any sample. For RA n=17 and OA serum n=6, OA SF n=7, unless otherwise stated in table, *p* value by Mann-Whitey U test.

Table 7.2 Chemokines present in serum and synovial fluid from ReA and PsA.

Test	ReA			PsA		
	Serum	SF	<i>p</i> value	Serum	SF	<i>p</i> value
CCL7	° (n=12)	322.84▪ 196.47 – 438.80 (n=13)	0.040	0.00♦ 0.00 – 467.5 (n=6)	0.00♦ 0.00– 0.001	0.82
CCL14	78426.7 73365.25 – 92636.25	47401.6 40058.1 – 72219.7	0.0019	72447.3 68221.1 – 84806.3	40565.8 56388.8 – 42911.6	0.0017
CCL16	11093.3 9497.68 – 14887.0	6663.44 5368.29 – 8175.63	0.000053	12696.5 9925.2 - 17995.1	8160.5 4452.9 – 11706.4	0.14
CCL22	498.06 353.21 – 655.42	299.4 160.8 – 342.9	0.0044	480.8 272.7 – 621.4 (n=13)	226.06 183.42 – 272.24 (n=13)	0.010

Median values are given as pg/ml with inter-quartile range. ▪ indicates CCL7 was detected in 4 of the samples tested, ♦ indicates CCL7 was present in only 1 of the samples tested. ° indicates chemokine not present in any sample. For ReA n=14 and PsA n=7 unless otherwise stated in table, *p* values calculated by Mann-Whitney U test.

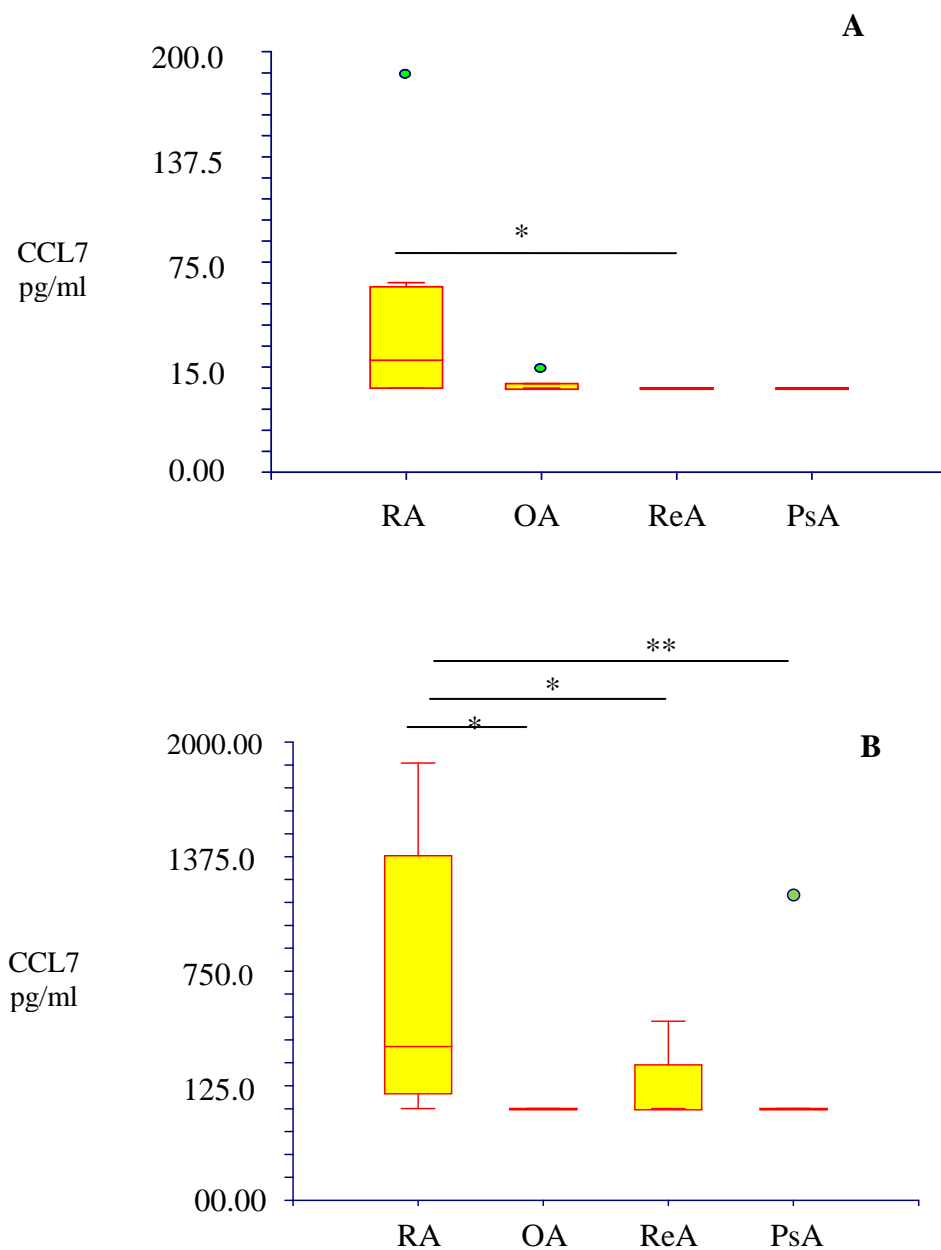


Figure 7.1 CCL7 in RA, OA, ReA and PsA serum and synovial fluid. 7.1A shows the median values for CCL7 in pg/ml in serum. RA n = 16, OA n = 6, ReA n = 12, PsA n = 6. **7.1B** shows the median values for CCL7 in pg/ml in synovial fluid. RA n = 15, OA n = 7, ReA n = 13, PsA n = 7. The yellow boxes show interquartile range with horizontal red in box showing median and the outlier values are shown in green * p < 0.05, ** p < 0.01, as calculated by Holm-Bonferroni post hoc test.

7.3.2 CCL14 in the serum and SF of RA, OA, PsA and ReA patients.

CCL14 was detected in the serum and SF of RA, OA (table 7.1), ReA and PsA (table 7.2) at comparatively high levels. The results indicated no significant differences between the groups for CCL14 in serum ($p = 0.20$), (figure 7.2A).

CCL14 in the SF was shown to be significantly different between groups ($p = 0.034$) and further analysis showed significant differences between CCL14 SF in RA and PsA ($p = 0.012$), (figure 7.2B). Significant differences in SF levels of CC14 were not observed between the other groups

Within the disease groups, OA, ReA and PsA, CCL14 was observed to be significantly higher in the serum compared to the SF (table 7.1 and 7.2).

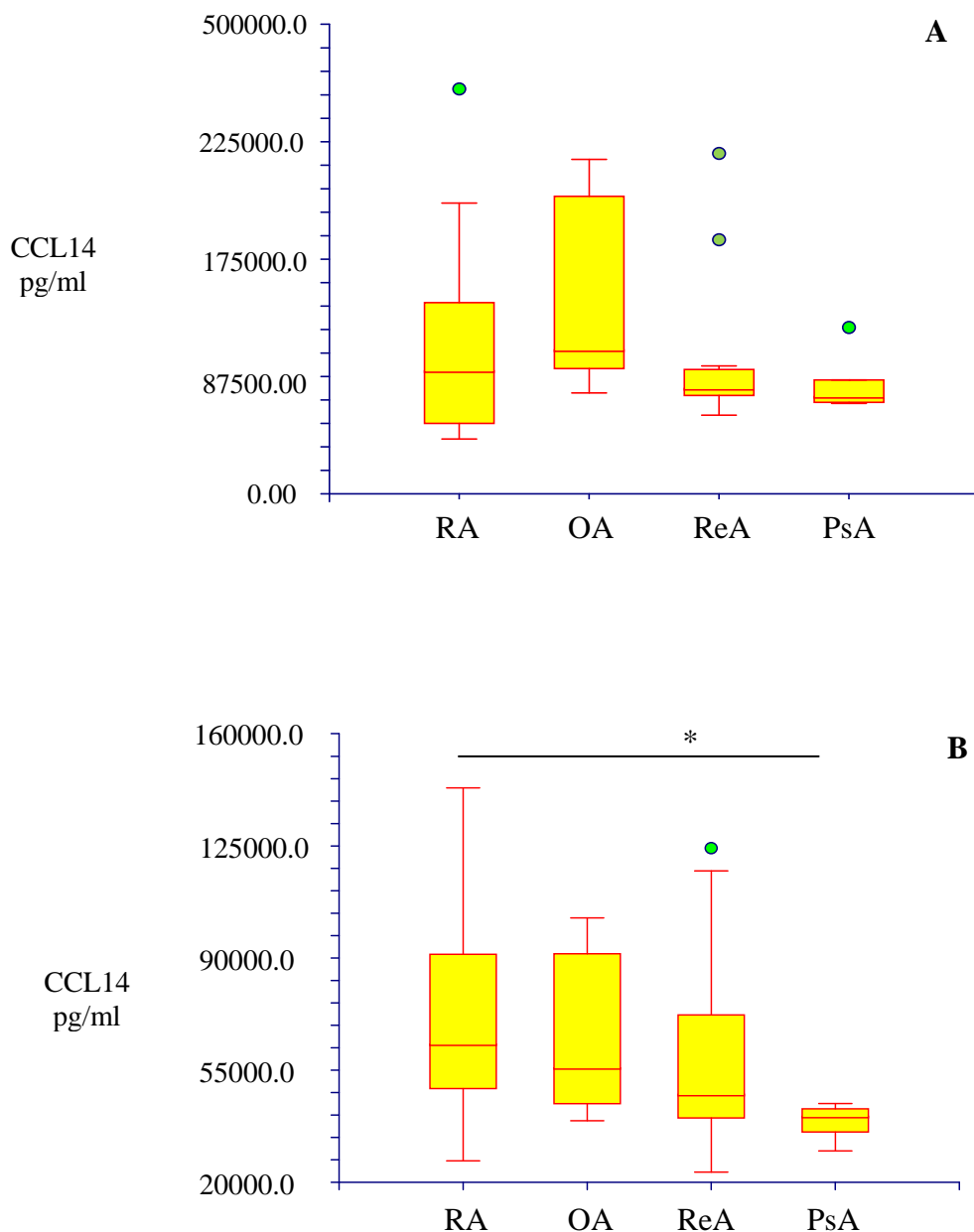


Figure 7.2 CCL14 in RA, OA, ReA and PsA serum and synovial fluid. 7.2A shows the median values for CCL14 in pg/ml in serum. RA n = 16, OA n = 6, ReA n = 12, PsA n = 6. 7.2B shows the median values for CCL14 in pg/ml in synovial fluid. RA n = 17, OA n = 7, ReA n = 14, PsA n = 7. The yellow boxes show the interquartile range with the horizontal red line in the box showing median, and the outlier values are shown in green. * p < 0.05, as calculated by Holm-Bonferroni post hoc test.

7.3.3 CCL16 in the serum and SF of RA, OA, PsA and ReA patients.

As with CCL14, CCL16 was detected in both the serum and SF of RA, OA (table 7.1), ReA and PsA (table 7.2). Kruskal-Wallis ANOVA showed a significant difference between groups for serum CCL16 ($p = 0.049$). However, further analysis showed no significant differences between CCL16 levels in the serum of any group (figure 7.3A). A significant difference in CCL16 in SF as analysed by Kruskal-Wallis was observed ($p = 0.049$). However, further analysis again showed no significant pair-wise differences (figure 7.3B).

Within the disease groups there was a significant difference between CCL16 levels in serum and SF in RA, OA and ReA (tables 7.1 and 7.2) with higher levels being present in the serum. There was no significant difference observed for CCL16 in PsA serum and SF.

7.3.4 CCL22 in the serum and SF of RA, OA, PsA and ReA patients.

CCL22 was detected in the serum and SF of RA, OA (table 7.1), ReA and PsA (table 7.2). Kruskal-Wallis ANOVA analysis indicated no significant differences between the groups for CCL22 in serum ($p = 0.29$), this was supported by Mann-Whitney U test (figure 7.4A). CCL22 in the SF was shown to be significantly different between groups ($p = 0.049$) (figure 7.4B). While further analysis showed no significant differences in SF CCL22 between individual groups, the difference between RA and PsA was approaching significance ($p = 0.058$).

Within the disease groups, CCL22 was observed to be significantly higher in the serum compared to the SF (table 7.1 and 7.2).

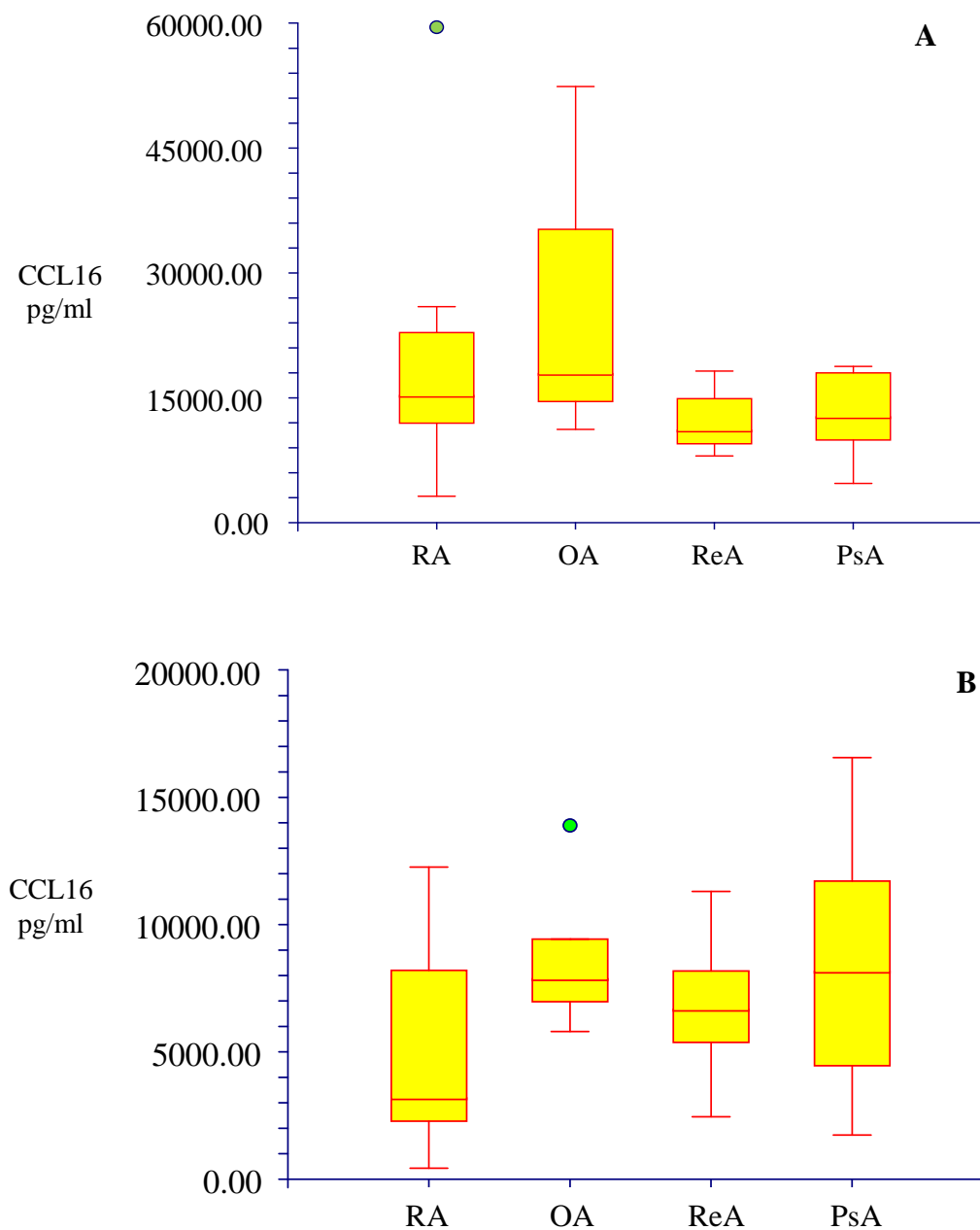


Figure 7.3 CCL16 in RA, OA, ReA and PsA serum and synovial fluid. 7.3A shows the median values for CCL16 in pg/ml in serum. RA n = 16, OA n = 6, ReA n = 12, PsA n = 6. 7.3B shows the median values for CCL16 in pg/ml in synovial fluid. RA n = 17, OA n = 7, ReA n = 14, PsA n = 7. The yellow boxes show the interquartile range with horizontal red line in the box showing median. Outlier values are shown in green. No significant differences were observed.

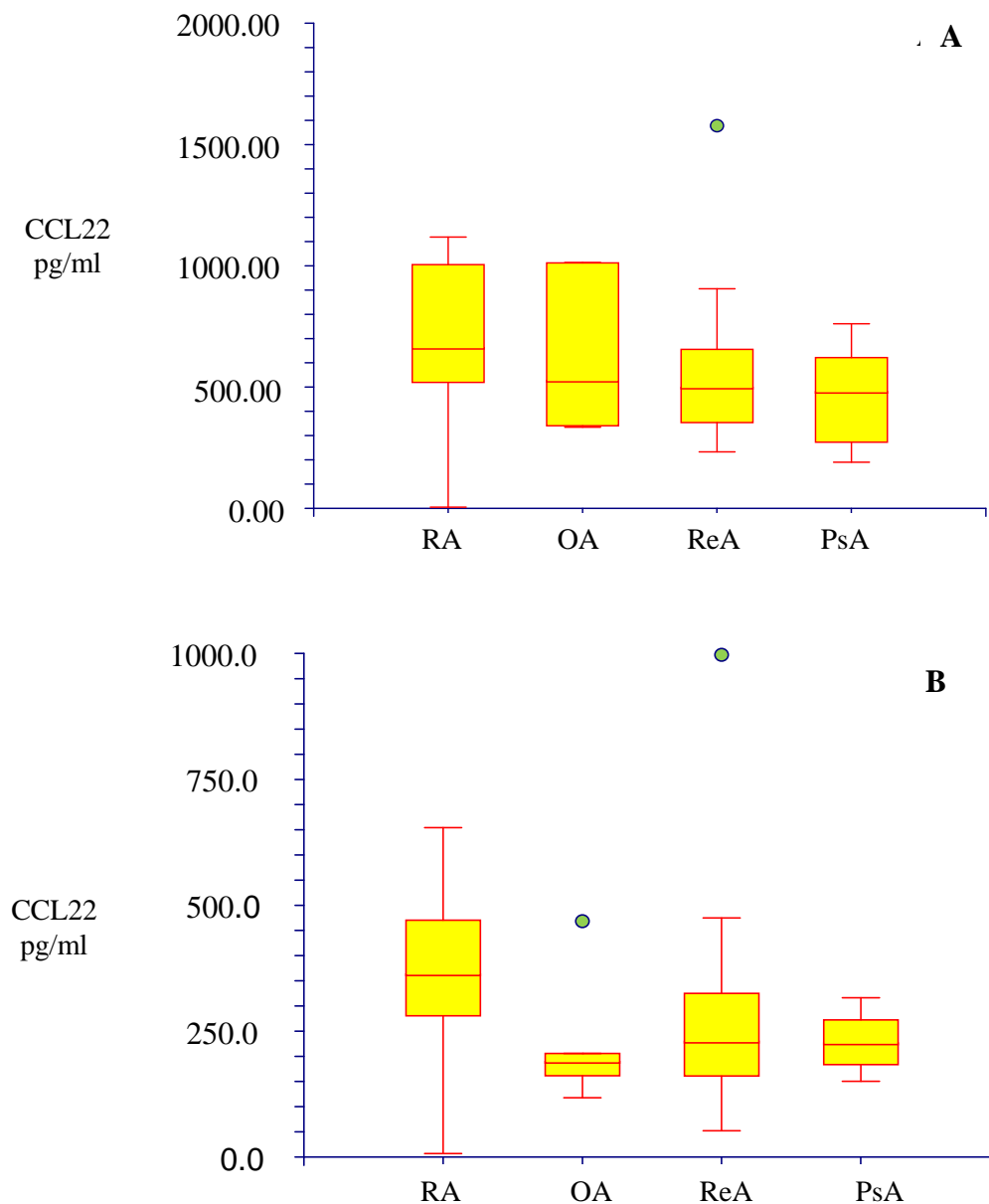


Figure 7.4 CCL22 in RA, OA, ReA and PsA serum and synovial fluid. 7.4A shows the median values for CCL22 in pg/ml in serum. RA n = 16, OA n = 6, ReA n = 12, PsA n = 6. 7.4B shows the median values for CCL22 in pg/ml in synovial fluid. RA n = 17, OA n = 7, ReA n = 14, PsA n = 7. The yellow boxes show the interquartile range with horizontal red line in the box showing median. The outlier values are shown in green. No significant differences were observed.

7.3.5 Analysis of correlations in RA, ReA and PsA SF and serum.

7.3.5.1 CCL7, CCL14, CCL16 and CCL22 in RA

Spearman rank correlation analysis followed by the Holm-Bonferroni test on serum and SF showed a significant correlation between serum levels of CCL7 and CCL16 ($p = 0.001$). A highly significant correlation between CCL7 levels and anti-CCP units was also observed ($p = 0.001$) (table 7.3). No correlations were observed between levels of CCL14, CCL16 or CCL22 and clinical variables.

7.3.5.2 CCL7, CCL14, CCL16 and CCL22 in ReA

For CCL7 in ReA there were no significant correlations for serum. However, there were a number of significant correlations for SF. The most significant correlations were between CCL7 SF levels and the number of tender joints ($p = 0.009$), and the number of swollen joints ($p = 0.006$). There were also correlations with the damage index ($p = 0.01$) and the Richie index ($p = 0.021$). Further correlations for SF CCL7 levels were observed with DAS44 ($p = 0.024$), the health assessment questionnaire (HAQ) ($p = 0.031$), early morning stiffness (EMS) ($p = 0.031$) and erythrocyte sedimentation rate (ESR) ($p = 0.036$) (table 7.3). No correlations were observed between levels of CCL14, CCL16 or CCL22 in ReA and clinical variables.

7.3.5.3 CCL7, CCL14, CCL16 and CCL22 in PsA

No significant correlations were observed. However serum CCL14 levels approached a significant correlation with grip strength ($p = 0.050$), as did SF CCL22 levels with the numbers of monocytes and macrophages ($p = 0.050$) (table 7.3). No correlations for CCL7 or CCL16 levels were observed.

7.3.5.4 CCL7, CCL14, CCL16 and CCL22 in OA.

No significant correlations between chemokines or clinical variables were found.

Table 7.3 List of correlations for serum and SF CCL7, CCL14, CCL16 and CCL22 in serum RA, ReA and PsA.

Chemokine (SF/S)	Correlation	<i>p</i> value (R value)
Rheumatoid arthritis		
CCL7 (SF)	anti-CCP units	<i>p</i> = 0.001 (R = 0.93)
CCL7 (S)	CCL16 (S)	<i>p</i> = 0.016 (R = 0.64)
Reactive arthritis		
CCL7 (SF)	ESR	<i>p</i> = 0.036 (R = 0.69)
CCL7 (SF)	EMS	<i>p</i> = 0.031 (R = 0.57)
CCL7 (SF)	Tender joints	<i>p</i> = 0.009 (R = 0.76)
CCL7 (SF)	Swollen joints	<i>p</i> = 0.006 (R = 0.79)
CCL7 (SF)	OSRA-D	<i>p</i> = 0.010 (R = 0.73)
CCL7 (SF)	Richie index	<i>p</i> = 0.021 (R = 0.72)
CCL7 (SF)	HAQ	<i>p</i> = 0.030 (R = 0.69)
CCL7 (SF)	DAS44	<i>p</i> = 0.024 (R = 0.73)
Psoriatic arthritis		
CCL14 (S)	GRIP	<i>p</i> = 0.05 (R = 0.68)
CCL22 (SF)	MO/M	<i>p</i> = 0.05 (R = 0.097)

R value given by Spearman Rank correlation analysis with *p* value following Holm-Bonferroni post hoc test. S – serum. SF – synovial fluid. ESR – erythrocyte sedimentation rate, EMS – early morning stiffness, HAQ – health assessment questionnaire. DAS44 – disease activity score (44 joint). GRIP – grip strength, MO/M – monocyte and macrophage numbers in SF, OSRA-D – damage scale of the “Overall Status in Rheumatoid Arthritis”. No correlations for OA were observed.

7.4 Discussion

McNearney *et al.*, (2011) showed that a number of chemokines and chemoattractants are found in the SF of RA patients and a number of chemokines, such as CCL3 and CCL5, have been shown to be upregulated in RA compared to other arthropathies (reviewed by Iwamoto *et al.*, 2008). Further to this CCL7 has been shown to be upregulated in the serum of systemic sclerosis patients and associated with the severity of sclerosis and pulmonary fibrosis (Yanaba *et al.*, 2006).

Whilst comparisons have been made for levels of CCL7, CCL14 and CCL16 in paired synovial tissue and peripheral blood mononuclear cells in RA, ReA and OA (Haringman *et al.*, 2006) this is the first study to compare levels of these chemokines in paired serum and SF from RA, ReA, OA and PsA. CCL7 level was shown to be significantly increased in the serum of RA compared to ReA, and approached a significant difference with OA serum. Furthermore, the CCL7 level was significantly increased in the SF of RA compared to OA, ReA and PsA. This study is also the first to show significant correlations between CCL7 levels in RA SF and anti-CCP antibodies in RA. This finding, combined with the lack of CCL7 in OA and PsA, suggests that CCL7 may be a novel marker for RA. However, the current study also shows that SF CCL7 levels correlate with a range of both clinical variables (such as tender joints, swollen joints and the Richie index) and inflammatory variables (such as ESR, DAS and EMS) in ReA. This suggests that SF CCL7 may be a novel general marker for inflammation in ReA and RA.

The significant increase in CCL7 in the SF compared to the serum of RA and ReA suggests that CCL7 may be active in the recruitment of mononuclear cells to the inflamed joint. This relates to work by Koch *et al.*, (1994) who showed that SF CCL3 in RA was significantly increased compared to OA, and significantly increased monocyte recruitment to the RA joint. The increase in SF CCL7 in RA and ReA may also be due to CCL7

generation by macrophages (Opdenakker *et al.*, 1993) which are abundant in the RA joint (Kinne *et al.*, 2000).

The current study is the first to assess the levels of CCL14 and CCL16 in serum and SF of RA, OA, ReA and PsA. It shows no significant differences in serum CCL14 levels between patient groups. However, in SF, the CCL14 level was significantly higher in RA than in PsA which would suggest that it may be chemoactive in the RA joint.. The data showing that the CCL14 level in OA, ReA and PsA was significantly greater in serum than SF suggests that it is generated within the circulation rather than in the joint

CCL16 in serum and SF showed no significant differences between the patient groups, although it was significantly higher in the serum of RA, OA and ReA compared to the matched SF. As with CCL14, this suggests that it is generated within the circulation rather than the joint.

CCL22 in serum and SF also showed no significant differences between the patient groups. This may be due to insufficient patient numbers as Flytie *et al.*, (2010) showed significant differences in SF CCL22 levels between RA and PsA, as well as CCL22 levels being increased in RA and PsA plasma compared to OA and healthy plasma. The current study showed that CCL22 levels were significantly increased in the serum of RA, OA, ReA and PsA compared to the matched SF with no significant correlations other than CCL22 SF levels approaching a significant correlation with SF monocyte and macrophage numbers in PsA. Like CCL14 and CCL16 this suggests that CCL22 is generated within the circulation rather than being locally produced at the site of any specific joint disease.

This section of the study was limited by only having access to samples from a relatively small number of patients, and mainly those with late stage disease. It would benefit from repetition using larger numbers of patients as well as early serum samples to compare chemokine levels and clinical variables. Furthermore, the SF tested was removed from a

single joint (knee), and so it is impossible to assess if the levels would be significantly different for any of the chemokines had it been removed from other joints. Ideally the same analysis would be performed in a longitudinal study whereby serum samples were taken at baseline (at diagnosis or before) and then at set intervals over 5 years. This would help to establish chemokine profile alterations in line with the clinical manifestations and changes in clinical variables.

In conclusion:

The first aim of this section of the study was to establish whether CCL7, CCL14, CCL16 and CCL22 were present in RA, OA, ReA and PsA and whether there were any differences in chemokine profile between the different arthritides. The study is the first to indicate that serum CCL7 is seen almost solely in RA where it may be a novel RA disease marker. No significant differences were observed between patient groups for levels of CCL14, CCL16 and CCL22 in serum or SF apart from a difference between RA and PsA in the level of SF CCL14. The levels of these 3 chemokines were higher in serum than SF, suggesting their generation within the circulation rather than the joint.

The second aim was to examine whether there were any correlations between clinical variables and SF and serum levels of these chemokines. Apart from significant correlations between SF CCL7 levels and anti-CCP levels in RA and a range of clinical variables in ReA there was little or no correlation of CCL14, CCL16 and CCL22 levels in serum or SF with any clinical variables. These data suggest that CCL14, CCL16 and CCL22 have little or no association with disease pathology in different types of arthritis, although CCL7 may be a general marker for inflammation in ReA. Further work is required to substantiate this hypothesis.

Chapter 8

Final Discussion

8.1 General discussion

8.1.1 Background

Whilst much is known about the functionality of a range of chemokines in RA, a significant proportion remain unstudied at the blood vessel endothelial cell wall across which all transmigration occurs. The work in this study aimed to elucidate the RA endothelial presentation of the beta-family (CC) chemokines, and to establish the potential functionality of the most highly represented, novel, chemokines.

The CC chemokines are so named because the first two of four cysteine residues are adjacent to each other. They constitute the largest of the chemokines groups whose major target is monocytes and lymphocytes (Bonecchi *et al.*, 2009) and are represented in the constitutive, inflammatory, dual function/heterologous and angiogenic sub groups (Filer *et al.*, 2008; Bonecchi *et al.*, 2009).

CCL7 (MCP-3) is an inflammatory chemokine which is a chemoattractant for mononuclear cells, specifically monocytes (Oppenheim *et al.*, 1991; Taub *et al.*, 1993) and T-cells (Taub *et al.*, 1995) and plays a role in macrophage regulation (Opdenakker *et al.*, 1993). It is produced by a range of cells including FLS, macrophages (Harringman *et al.*, 2006), cancerous tumour cells (Jung *et al.*, 2010) and astrocytes (Renner *et al.*, 2011), where it has been suggested as the primary source for increased monocyte trafficking to the CNS in neuroAIDS. CCL7 belongs to the MCP monocyte chemoattractant protein (MCP) subfamily which includes CCL2 (MCP-1), CCL8 (MCP-2) and CCL13 (MCP-4). It binds the receptors CCR1, CCR2, CCR3 and CCR5, which allows it to activate numerous cell types, including monocytes, T-cells and basophils (Menten *et al.*, 2001).

CCL14, originally known as haemofiltrate CC-1 (HCC-1), is found in high levels in

plasma and was initially detected during protein isolation of haemofiltrate (Schulz-Knappe *et al.*, 1997). It has been found in a range of tissue types, including liver, muscle and kidney (Schulz-Knappe *et al.*, 1997) and requires post-translational modification to enhance biological activity for receptor binding to CCR1, CCR3 (low affinity binding only) and CCR5 (Detheux *et al.*, 2000; Forssman *et al.*, 2001; Mortier *et al.*, 2008; Richter *et al.*, 2009). Furthermore, it has been shown to chemoattract monocytes, eosinophils and T cells (Munch *et al.*, 2002).

CCL16, previously known as liver expressed chemokine (LEC) is expressed in a range of tissues including the liver and spleen and is expressed by hepatocytes (Youn *et al.*, 1998). Via binding to CCR1, CCR2, CCR5 and CCR8 (Howard *et al.*, 2000; Nomiya *et al.*, 2001) CCL16 can activate a range of inflammatory cells and shows chemotactic ability for both lymphocytes and monocytes (Youn *et al.*, 1998). It is an angiogenic chemokine (Strasly *et al.*, 2004; Filer., 2008) but has not yet been designated as being inflammatory, constitutive/heterologous or dual-function.

CCL22 is a dual-function chemokine (Loetscher., 2005) which is produced by macrophages and monocyte derived dendritic cells. It is also expressed in the thymus, lymph nodes, appendix and Langerhans' cell histiocytosis with a functional role in atopic dermatitis. (Vulcano *et al.*, 2001; Kwon *et al.*, 2011; Hirota *et al.*, 2011).

8.1.2 Presence of CCL7, CCL14, CCL16 and CCL22 in RA and non-RA ECs.

In RA, both CCL7 and CCL14 were first observed within the synovial tissue by Haringman *et al.*, (2006). The current study provided novel data to the field by showing that both CCL7 and CCL14 are widely expressed by the ECs of both RA and non-RA synovial vessels and throughout the RA synovium on infiltrates, with CCL7 not showing a significant difference between RA and non-RA synovial ECs. The current study shows CCL14 to be significantly upregulated on RA ECs compared to non-RA ECs ($p = 0.0041$) indicating that CCL14 may play a role in the recruitment of inflammatory cells to the RA synovium. This study shows that CCL7 is significantly decreased on lymphatic ECs in RA compared to non-RA lymphatic ECs. These findings are in contrast with the findings for CCL14, which the current study shows to be upregulated in RA blood vessel ECs but to have no significant differences between RA and non-RA lymphatic ECs. The non-significant difference between RA and non-RA ECs presence of CCL7 suggests that CCL7 may not be of primary importance in the transmigration of monocytes and T-cells into the synovium in RA. However, this is the first study to show CCL7 on RA lymphatic ECs, furthermore, it shows CCL7 to be significantly decreased in the RA lymphatic vessel ECs compared to non-RA lymphatic ECs. This indicates that CCL7 may be of greater importance in the removal of infiltrates via lymphatic vessels. T22 experiments he lack of significant differences between RA and non-RA lymphatic ECs for CCL14 indicates that while CCL14 may be of importance in the recruitment of monocytes and T-cells into the RA joint, it may not be responsible for their lymphatic removal.

CCL16 was identified in RA tissue in multiple studies (Radstake *et al.*, 2005; Van-Lieshout *et al.*, 2005; Haringman *et al.*, 2006), however this is the first study to identify its presence in RA ECs. With the current study there were no significant differences in CCL16 in RA and non-RA ECs, thus monocyte and lymphocyte recruitment via CCL16 at

the EC: blood interface is not likely to be primarily responsible for their elevated recruitment in RA. The presence of CCL16 in infiltrates (Radstake *et al.*, 2005; Van-Lieshout *et al.*, 2005; Haringman *et al.*, 2006) is most likely the source of the CCL16 mediated transmigration.

In contrast to the other chemokines CCL22 was not only significantly increased in RA blood vessel ECs compared to non-RA ECs but also significantly increased in lymphatic RA ECs compared to non-RA. The significant increase seen in RA in the current study is supported by Flytie *et al.*, (2010) who found abundant CCL22 in the RA synovium. This may indicate that CCL22 is important in the pathology of RA inflammatory cell recruitment from the blood. It may also be an example of lymphatic EC CCL22 upregulation in response to inflammatory stimuli as a compensatory mechanism for increased CCL22 on blood vessel ECs. In order to analyse these hypothesis further work is required to compare early and late RA tissue for differential blood vessel and lymphatic EC chemokine expression.

The differential expression of the chemokines on blood vessel ECs and lymphatic ECs led to the possibility that synovial dysregulation of chemokine expression has a greater role than previously discerned in the pathology of RA. The dysregulation of the chemokine gradient was documented by Burman *et al.*, (2005) who showed chemokines to be present at high levels on both lymphatic and blood vessel ECs within the rheumatoid synovium, and suggested that the chemokine gradient disruption plays a vital role in RA. Further evidence that lymphatic ECs are of vital importance in RA came from Johnson *et al.*, (2006) who showed >100 fold increases in inflammatory chemokines such as CCL5 and CCL20 in TNF- α activated HDLECs. As synovial lymphatic vessel formation has been shown to decrease during the chronic phase of RA (Zhou *et al.*, 2010), this compensatory mechanism of chemokine upregulation in lymphatic vessels may be less effective.

Particularly if chemokines, such as with CCL7, are also downgraded in RA lymphatic ECs. The current study is the first to show CCL7, CCL14, CCL16 and CCL22 in RA lymphatic ECs. It shows significant decreases in lymphatic CCL7 (chapter 3) and provides further evidence that in RA the chemokine gradient is disrupted. Furthermore, the current study shows that blood: lymphatic dysregulation of CCL7 may play an important role in the pathology of RA. The importance of lymphatic CCL7 in relation to transmigration analysis was explored in chapter 6. Following activation of HDLECs a dose response was performed using PBMCs isolated from RA blood. The results showed that at increasing concentrations of CCL7 generated increasing monocyte migration across activated HDLECS, with the greatest responses being significant at 100ng/ml and 250ng/ml chemokine compared to the absence of CCL7. There were no significant differences in T-cell migration seen under the same conditions, however a significant difference in T-cell migration at 10ng/ml compared to unstimulated HDLECs in the absence of CCL7 was observed. It is possible that the receptors became desensitised in the case of T-cell migration at each CCL7 dose and for monocyte migration at over 250ng/ml. It is known that TNF- α induces the generation of a range of chemokines in ECs (Haringman *et al.*, 2004) and HDLECs (Johnson *et al.*, 2006) and the presence of TNF- α /IFN- γ would most likely generate the release of endogenous chemokines and/or other factors which were pro-migratory. This may also account for the significant difference in T-cell migration in response to CCL7 at 10ng/ml when compared only to the negative control which was performed in the absence of both TNF- α /IFN- γ and the chemokine.

These experiments show that CCL7 is functional in monocyte migration across LECs. Thus that the reduced expression of CCL7 on lymphatic ECs in RA may have functional significance, whereby reduced lymphatic clearance of monocytes leads to their accumulation and persistence in the RA synovium. This hypothesis is partially supported

by Ibrahim *et al.*, (2014) who showed that CCL7 reduction in the lymph nodes of malnourished mice results in reduced dendritic cells and monocytes/macrophages in the same area which suggested the importance of CCL7 in their clearance in this disease state. Further work to establish the effect of CCL7 on monocyte lineage cell migration in RA would be beneficial.

8.1.3 CCL7, CCL14, CCL16 and CCL22 in cultured cells

As CCL7, CCL14, CCL16 and CCL22 were so highly represented in ECs in RA ECs; it was decided to establish if they were present in cultured ECs in simulated inflammatory conditions. These experiments would provide evidence for the potential of ECs to synthesise, store and release the chemokines under inflammatory conditions. Following establishing the optimum conditions for HBMEC stimulation, it was decided to perform whole cell staining to establish the presence of chemokines to establish their cellular expression as chemokines and other factors, such as VWF, in Weibel-Palade bodies are well documented (Øynebråten *et al.*, 2005; Rondaij *et al.*, 2006; Hol *et al.*, 2009). In chapter 4 of this study it was shown that in the absence of cycloheximide, over a six hour time frame, CCL7 staining increased in intensity with TNF- α from 0-2 hours before a significant decreasing trend in intensity occurred. In order for the observed decrease in CCL7 to occur the chemokine must have been either released in to the medium or otherwise recycled intracellularly. The data also indicates that CCL7 is pre-synthesised in HBMECs prior to TNF- α stimulation and released/recycled in response to inflammatory stimuli. This is supported by the non-significant reductions in CCL7 in the presence of cycloheximide due to protein synthesis arrest. However, there was a significant increase in CCL7 intensity over the first 2 hours of combined stimulation and cycloheximide addition. CCL14 was also observed to undergo significant intensity increases, followed by a non-significant trend in decreasing CCL14 intensity. As with CCL7 this indicates that

ECs pre-synthesise and store CCL14 which is mobilised under inflammatory stimuli. Unlike CCL7, the decrease in CCL14 intensity did not reduce to near baseline levels, instead remaining significantly increased at each time point compared to baseline. This indicated that the ECs were either synthesising more CCL14 which was replenishing the stores as they were depleted, or it was being recycled intracellularly. In this study ELISA tests showed that CCL14 was detectable in HMVEC conditioned medium at 644.65pg/ml at 2 hours, but was not detectable in HBMEC conditioned medium at 2 hours. It is possible that it was simply not at a detectable level in the HBMEC medium within this time frame. However, the fact that a 2 hour time frame provided detectable CCL14 levels in HMVEC conditioned medium which was not detectable in HBMEC conditioned medium suggests that ECs differentially generate chemokines. Further work to assess the potential of different EC types to generate each of the tested chemokines to confirm these conclusions are required. Unlike CCL7 and CCL14, CCL16 and CCL22 showed no initial significant increase in intensity. This would indicate that while pre-synthesised CCL16 is present within HBMECs, it was not significantly synthesised in response to inflammatory stimuli. There was, however, a significant trend in decreasing CCL16 which reduced to below baseline. This suggests that while CCL16 was being released into the medium or intracellularly recycled, it was either not being synthesised, or was being synthesised at levels below those required to adequately replenish intracellular stores. This is supported by the lack of detectable CCL16 in the HBMEC and HMVEC conditioned medium. CCL22 showed only a significant decrease from baseline which was not a significant trend. As with CCL7, CCL14 and CCL16 the evidence may suggest that there is CCL22 being released into the medium or that is being recycled/ degraded without intracellular stores being replenished in a timely manner. Alternatively CCL22 may be being released/recycled while the intracellular stores are replenished in an ongoing process over

the tested timeframe. However, given that CCL22 was not detected in the conditioned medium it is likely that it is recycled rather than released. In order to better analyse the generation of these chemokines it would be beneficial to perform pulse chase experiments with radiolabelled amino acids (e.g. ^{35}S -methionine). This would be followed by immunoprecipitation to establish the half-life and/or release of newly synthesised chemokines in primary microvascular ECs and HDLECs.

Further research indicates that the stimulation in the presence of cycloheximide seen in chapter 4 for each tested chemokine was due to a delay in the protein synthesis arrest effect of cycloheximide, during which time stimulation by TNF- α would have generated the initial intensity increases. This delay is most likely responsible for the initial increases seen throughout these particular experiments for CCL7, CCL14, CCL16 and CCL22. In future work I would pre-incubate with cycloheximide before the addition of the TNF- α to reduce/remove this effect.

Following the exploration of cellular CCL7, CCL14, CCL16 and CCL22 in chapters 3 and 4 it was decided to establish the effects the chemokines had on the microvilli formation of stimulated HBMECs and non-RA PBMCs. Microvilli formation on ECs in arthritis was first observed by Sattar *et al.*, (1986) and has since been reported by numerous sources. Middleton *et al.*, (1997) showed that EC microvilli appear to present CXCL8 to leukocytes, and most recently, Whittall *et al.*, (2013) showed that CXCL8 stimulates cytoskeletal remodelling in ECs which lead to microvilli formation and preferential chemokine presentation. Further to this, the presence of chemokines such as CXCL8 in the rheumatoid synovium (Szekanecz and Kock., 2008; Whittall *et al.*, 2013) indicates that chemokine-stimulated microvilli formation may be relevant to leukocyte transmigration in RA and that the chemokine stimulation may lead to preferential chemokine presentation at the apical

tips of microvilli (Middleton et al., 1997; Whittall *et al.*, 2013). The current study showed that CCL7 generated a positive trend for EC microvilli formation that did not reach significance ($p = 0.057$) and had little observed effect on leukocyte microvilli formation. In the presence of CCL14, significant increases in mononuclear cell microvilli generation occurred ($P = 0.0004$) and the generation of microvilli by HBMECs approached significance ($p = 0.057$). This potential for monocyte microvilli formation is supported by Schulz-Knappe *et al.*, (1997), who showed that CCL14 was capable of monocyte activation. CCL16 generated a positive trend in mononuclear cell microvilli formation which was non-significant, but had the greatest significant effect on EC microvilli generation of each of the tested chemokines ($p = 0.007$). CCL22 gave a significant increase in both mononuclear cell and EC microvilli formation ($p = 0.023$ and 0.014 respectively). This is the first study to show microvilli generation in response to CCL7, CCL14, CCL16 and CCL22 and their preferential stimulation of HBMECs or leukocytes. It is known that chemokines respond differently in response to inflammatory activators such as TNF- α and IFN- γ . For example, CCL16 is induced strongly by IFN- γ (Nomiya *et al.*, 1999) and it is therefore highly possible that different results may have been obtained had the experiments been performed under a range of conditions such as assessing each chemokine using TNF- α and IFN- γ rather than TNF- α alone. Further work would include further optimisation of the conditions with a range of EC types.

The generation of podosomes which are also influential in transmigration processes (Carmen *et al.*, 2007; Carmen and Spinger, 2008; Wittchen, 2009), were also examined. Increases in the numbers of podosomes formed in the presence of the chemokines were observed, however they failed to reach significance. This may have been due to sampling errors. In future work, greater numbers of micrographs at a greater range of magnifications would provide more data for better analysis, as would scanning electron microscopy

(SEM), in addition to the TEM in this thesis, to better analyse the topography of the leukocyte: EC interactions. SEM would also aid the examination of filopodia.

While little work has been done on the chemotactic responses to CCL7 in inflammatory disease, Ali *et al.*, (2005) showed significant increases in leukocyte migration in response to CCL7 across human microvascular endothelial cells ($p < 0.001$), supporting the findings of this study which shows that CCL7 generates significant increases in monocyte migration across HBMECs in a dose dependent manner at 100ng/ml ($p = 0.037$) and 250ng/ml ($p = 0.031$). Again, this would suggest that CCL7 is active in the recruitment of monocytes to the RA joint. However, as stated earlier, the RA and non-RA blood vessel ECs showed similar degrees of CCL7 expression (chapter 3) and so monocyte recruitment via CCL7 is unlikely to be a pathological driving factor in RA. This is partially supported by the presence of other chemokines such as CCL5 and CCL2, which have been shown to be highly expressed in the RA synovium and are also adept at monocyte and T-cell recruitment (Charo and Ransohoff., 2006).

Schulz-Knappe *et al.*, (1997) stated that CCL14 generated no chemotactic response for monocytes, however the methods and actual results which provided that conclusion were not shown and no further work showing chemotactic responses to CCL14 could be found. The data in this study opposes that data, as it shows that at a concentration of 100ng/ml CCL14 generates a significant increase in monocyte migration. Furthermore, the significant upregulation of CCL14 at RA ECs compared to non-RA ECs suggests that CCL14 may be active in monocyte recruitment in RA. Further work to assess CCL14 chemotactic responses in a dose dependent manner are required to further elucidate the full potential of CCL14 to act as a chemoattractant in RA. CCL16 showed no significant effect on either monocyte or B/T-cell migration in the presence of TNF- α . As stated earlier, CCL16 is most strongly induced by IFN- γ (Nomiya *et al.*, 1999) and so it is possible

that significant effects on migration in response to CCL16 would be seen under different conditions which time restraints prevented analysis of during this study.

CCL22 was shown to stimulate significant increases in monocyte migration across activated HBMECs compared to the absence of CCL22, further to this CCR4 (the receptor for CCL22), was significantly increased in RA monocytes. While this indicates that CCL22 may be of importance in driving monocyte recruitment in RA, the significant increase in CCL22 at blood vessel ECs in RA was accompanied by a significant increase in RA lymphatic vessel ECs. This would likely act as a compensatory factor where CCL22 mediated transmigration is occurring. However, this mechanism would be beneficial during the earlier stages of RA only, as during latter stage RA lymphangiogenesis has stopped and normal lymphatic drainage has reduced as movement has become more restricted (Polzer *et al.*, 2008).

This is the first study to observe the presence of LYVE-1 macrophages in the RA synovium (chapter 3). While their presence is well documented in cancer cells, particularly those with a high metastatic rate (reviewed by Ran and Montgomery, 2012), they are believed to be involved in lymphangiogenesis (reviewed by Ran and Montgomery, 2012), which plays a role in the lymphatic movement of cancerous cells around the body. The presence of these cells implies that even in the very end stage of RA there is the potential for lymphangiogenesis within the RA joint. However, given the reduction in lymphatic vessels seen in the RA tissue (Zhou *et al.*, 2010) in comparison to the blood vessels these 'lymphatic progenitors' do not appear to develop into mature vessels. This may be due to a number of factors, such as a downstream signalling cascade failure which prevents maturation of the progenitors, or environmental factors within the joint which are anti-lymphangiogenic. Further work to assess these cells in synovial tissue would be beneficial.

8.1.4 CCL7, CCL14, CCL16 and CCL22 in matched serum and synovial fluid

Following analysis of CCL7, CCL14, CCL16 and CCL22 in synovial tissue and cultured cells it was decided to assess their presence in matched serum and synovial fluid samples (chapter 7). The demonstration of the chemokines by ELISAs supported the detection of the chemokines by immunofluorescence. While CCL7 did not reach significant difference between RA and OA serum it was approaching significance at $p = 0.054$, and given that CCL7 was only detectable in one of the OA patients tested it would be expected the data to become significant given greater patient numbers. CCL7 was also shown to be significantly increased in RA SF compared to OA, ReA and PsA. This relates to work by by Piere *et al.*, (2004) who showed that CCL5 was significantly increased in RA compared to OA, ReA and PsA. As with CCL7, CCL5 is an inflammatory chemokine which is a ligand for CCR1 and CCR3. The current study shows significant correlations of SF CCL7 in RA with anti-CCP antibodies, and a range of clinical markers in ReA (table 7.3), including ESR, disease activity score, and tender and swollen joints. Given the lack of serum CCL7 in the other arthropathies tested, and the significant correlation with anti-CCP in RA, CCL7 may be a novel marker for RA diagnosis. However, due to the numbers of correlations for CCL7 in SF in ReA, it is likely to be a general inflammatory marker in this disease. The presence of CCL7 in SF at significantly greater concentrations than in serum, indicates that the synovial tissue is a primary source of CCL7, which may be released into the serum via ECs

The current study shows CCL14 to be significantly increased in the serum of RA, ReA and PsA compared to the SF, the OA levels were approaching significance. CCL14 has been shown to be expressed at high concentrations of 10nM in the plasma of healthy individuals which significantly increases up to 80nM in patients with renal disease (Schulz-Knappe *et al.*, 1997). It is unusual for a chemokine to reach such levels, even in a disease state (Koch

et al., 1992). However, the serum CCL14 concentration observed in the current study of up to 91510.7pg/ml are still surprisingly high when compared to serum levels of chemokines such as CCL2 who Koch *et al.*, (1992) showed to be present at ~251500.0pg/ml and CCL5, which has been shown to be ~1000pg/ml in RA (Hidaka *et al.*, 2001). It is possible that the high levels of CCL14 observed in the serum in this study are the result of interplay between normally occurring levels and disease exacerbated levels. Also, the increased likelihood of renal complications in arthritis patients taking certain drugs (such as disease modifying anti-rheumatic drugs, DMARDS) may relate to the very high plasma CCL14 concentration seen in this study. High levels were also observed in SF which were significantly increased in RA compared to PsA, however the lack of significant differences with OA and ReA indicate that CCL14 would not be a suitable disease marker.

As with CCL14, CCL16 was shown to be present at relatively high concentrations in serum at up to 15264.5g/ml in RA. This is lower than chemokines such as CCL2, which was found at ~251500pg/ml by Koch *et al.*, (1992) but as it is higher than CCL5 at ~1000pg/ml in RA (Hidaka *et al.*, 2001). However, there were no significant increases in CCL16 in RA serum compared to OA, PsA or ReA shown in the current study, suggesting it is not a marker of RA. Due to a lack of correlations between serum/SF levels and clinical variables it is unlikely to be of significance as a marker of disease activity or severity, but may be a general marker of inflammation. As with CCL14, CCL16 is generated by the liver it is also possible that the high levels were the result of liver complications exacerbated by the use of DMARDS (Selmi *et al.*, 2011).

CCL22 was shown to be significantly increased in serum compared SF in RA, OA, ReA and PsA at up to 662.65pg/ml (in RA), however these levels are below chemokines such as CCL2 at ~251500pg/ml (Koch *et al.*, 1992). However, different studies have shown other chemokines of importance in RA such as CCL5 (~1000pg/ml) to be at much lower levels

in RA serum. The significant increases in serum CCL14, CCL16 and CCL22 compared to SF indicate that the synovial tissue of the joints sampled are not the primary source of these chemokines in RA.

Overall, this study has identified a range of chemokines to be present in RA ECs and has shown that the functionality of a number of them, particularly CCL7, may have significance in the RA disease process.

8.2 Final main conclusions

1. There is known to be a high degree of heterogeneity between the chemokines present in RA, which is reflected by high heterogeneity in synovial ECs. The most highly represented 7 chemokines in RA ECs are (in increasing prevalence in RA ECs):

CCL22 - CCL4 - CCL8 - CCL7 - CCL14 - CCL16 - CCL19.

2. While each of the chemokines studied are pre-synthesised in ECs, CCL14 has the greatest potential to be synthesised in an ongoing manner in response to inflammatory stimuli. Furthermore, as well as generating the most significant effect on leukocyte microvilli formation, CCL14 generated significant increases in monocyte migration. This suggests that CCL14 may be highly active in RA pathology.

3. The significant decrease of CCL7 in lymphatic ECs, combined with it having the greatest chemotactic ability for monocytes suggests it may be of importance in the lymphatic removal of infiltrates in the inflamed RA synovium. This would lead to leukocyte persistence and accumulation in the RA synovium. Further to this serum CCL7 may be a novel marker for RA.

4. The presence of LYVE-1+ macrophages indicate the potential for lymphangiogenesis in later stage RA and with further study may prove to be a target in RA to increase lymphangiogenesis and thus reduce inflammation.

8.3 Further work

- Establish if the chemokines are present in HDLECs in response to inflammatory stimuli.
- Perform pulse chase experiments with radiolabeled amino acids (e.g. ³⁵S-methionine) followed by immunoprecipitation to establish the half-life and/or release of newly synthesised chemokines in primary microvascular ECs and HDLECs.
- Assess the effects of the chemokines on primary synovial ECs and lymphatic ECs.
- Increase the sample number for further micrograph analysis of firm adherence/filopodia.
- Assess the effect of CCL7, CCL14 and CCL22 on monocyte differentiation to macrophage using CD68+ marker.
- Assess the effect of CCL7 on macrophage migration across HDLECs.
- Assess the effect of CCL7, CCL14, CCL16 and CCL22 on migration of mononuclear cells from RA blood across HBMECs in a dose response assay.
- Assess the effect of CCL7 on the migration of mononuclear cells from non-RA blood across HDLECs
- Increase monocyte numbers for repeat CCR and CD14+ analysis.
- Analysis of SF and serum from healthy controls to establish if the levels present were the result of upregulation in the disease or reflected the steady state in circulation at any given time.
- Assess the prevalence of LYVE-1+ macrophages in a range of arthritis tissue sample to better establish if they are increased in specific environments.

Chapter 9

References

9.1 Journal references

Abreo K, Glass J. (1993). Cellular, biochemical, and molecular mechanisms of aluminium toxicity. *Nephrol Dial Transplant.* ;8 Suppl 1:5-11.

Akhavani MA, Madden L, Buyschaert I, Sivakumar B, Kang N, Paleolog EM. (2009) Hypoxia upregulates angiogenesis and synovial cell migration in rheumatoid arthritis. *Arthritis Res Ther.* 11(3):R64. Epub 2009 May 8.

Aletaha D, Neogi T, Silman AJ, Funovits J, Felson DT, Bingham CO 3rd, Birnbaum NS, Burmester GR, Bykerk VP, Cohen MD, Combe B, Costenbader KH, Dougados M, Emery P, Ferraccioli G, Hazes JM, Hobbs K, Huizinga TW, Kavanaugh A, Kay J, Kvien TK, Laing T, Mease P, Ménard HA, Moreland LW, Naden RL, Pincus T, Smolen JS, Stanislawska-Biernat E, Symmons D, Tak PP, Upchurch KS, Vencovský J, Wolfe F, Hawker G. (2010) 2010 Rheumatoid arthritis classification criteria: an American College of Rheumatology/European League Against Rheumatism collaborative initiative. *Arthritis Rheum.* 2010 Sep;62(9):2569-81

Aloisi, F. and Pujol-Borrell, R. (2006). Lymphoid neogenesis in chronic inflammatory diseases. *Nature Rev. Immunol.* 6, 205–217

Alon R, Ley K. (2008). Cells on the run: shear-regulated integrin activation in leukocyte rolling and arrest on endothelial cells. *Curr Opin Cell Biol.* 20(5):525-32

Alon R, Shulman Z. (2011). Chemokine triggered integrin activation and actin remodeling events guiding lymphocyte migration across vascular barriers. *Exp Cell Res.* 317(5):632-41.

Amin AK, Huntley JS, Simpson AH, Hall AC. (2009). Chondrocyte survival in articular cartilage; the influence of subchondral bone in a bovine model. *J Bone Joint Surg Br.* 91(5);691-9.

Andersson SE, Lexmüller K, Johansson A, Ekström GM. (1999). Tissue and intracellular pH in normal periarticular soft tissue and during different phases of antigen induced arthritis in the rat. *J Rheumatol.* 1999 Sep;26(9):2018-24.

Andreas K, Lübke C, Häupl T, Dehne T, Morawietz L, Ringe J, Kaps C, Sittlinger M. (2008). Key regulatory molecules of cartilage destruction in rheumatoid arthritis; an in vitro study. *Arthritis Res Ther.* 10(1);R9.

Arnett FC, Edworthy SM, Bloch DA, McShane DJ, Fries JF, Cooper NS, Healey LA, Kaplan SR, Liang MH, Luthra HS, et al.(1988). The American Rheumatism Association 1987 revised criteria for the classification of rheumatoid arthritis. *Arthritis Rheum.* 31(3);315-24.

Baekkevold ES, Yamanaka T, Palframan RT, Carlsen HS, Reinholt FP, von Andrian UH, Brandtzaeg P, Haraldsen G. (2001). The CCR7 ligand elc (CCL19) is transcytosed in high endothelial venules and mediates T cell recruitment. *J Exp Med.* 193(9):1105-12.

- Baggiolini M. (2001). Chemokines in pathology and medicine. *Journal of internal medicine*. 250. 91-104.
- Baker EN, Lindley PF. (1992). New perspectives on the structure and function of transferrin. *J Inorg Biochem* 47, 147–160.
- Barland P, Novikoff A B, Hamerman D. (1962). Electron microscopy of the human synovial membrane. *J Cell Biol*. 14; 207-216
- Bartholome B, Spies CM, Gaber T, Schuchmann S, Berki T, Kunkel D, Bienert M, Radbruch A, Burmester GR, Lauster R, Scheffold A, Buttgereit F. (2004) Membrane glucocorticoid receptors (mGCR) are expressed in normal human peripheral blood mononuclear cells and up-regulated after in vitro stimulation and in patients with rheumatoid arthritis. *FASEB J*. 18. 70–80.
- Barreiro O and Sánchez-Madrid F. (2009). Molecular Basis of Leukocyte–Endothelium Interactions During the Inflammatory Response. *Rev Esp Cardiol*. 62(5);552-62
- Becker J, Winthrop KL. 2010. Update on rheumatic manifestations of infectious diseases. *Curr Opin Rheumatol*. 22(1);72-7.
- Beglova N, Blacklow SC, Takagi J, Springer TA. (2002). Cysteine-rich module structure reveals a fulcrum for integrin rearrangement upon activation. *Nat Struct Biol*. 9;282-7.
- Bernardini G, Spinetti G, Ribatti D, Camarda G, Morbidelli L, Ziche M. I-309 binds to and activates endothelial cell functions and acts as an angiogenic molecule in vivo. *Blood* 2000;96:4039e45.
- Biemond P, Swaak AJ, van Eijk HG, Koster JF. (1986) Intraarticular ferritin-bound iron in rheumatoid arthritis. A factor that increases oxygen free radical-induced tissue destruction. *Arthritis Rheum*. 29(10):1187-93.
- Biniecka M, Kennedy A, Fearon U, Ng CT, Veale DJ, O'Sullivan JN.(2010). Oxidative damage in synovial tissue is associated with in vivo hypoxic status in the arthritic joint. *Ann Rheum Dis*. Jun;69(6):1172-8.
- Blades MC, Ingegnoli F, Wheller SK, Manzo A, Wahid S, Panayi GS, Perretti M, Pitzalis C. (2002). Stromal cell-derived factor 1 (CXCL12) induces monocyte migration into human synovium transplanted onto SCID Mice. *Arthritis Rheum*. 46(3);824-36.
- Blaschke S, Koziolk M, Schwarz A, Benöhr P, Middel P, Schwarz G, Hummel KM, Müller GA. (2003). Proinflammatory role of fractalkine (CX3CL1) in rheumatoid arthritis. *J Rheumatol*. 30(9);1918-27
- Bonecchi R, Galliera E, Borroni EM, Corsi MM, Locati M, Mantovani A.(2009). Chemokines and chemokine receptors; an overview. *Front Biosci*. 1;14;540-51.
- Bonnet CS, Williams AS, Gilbert SJ, Harvey AK, Evans BA, Mason DJ. (2013). AMPA/kainate glutamate receptors contribute to inflammation, degeneration and pain

- related behaviour in inflammatory stages of arthritis. *Ann Rheum Dis.* 2013 Oct 15. doi: 10.1136/annrheumdis-2013-203670. [Epub ahead of print]
- Book C, Karlsson MK, Akesson K, Jacobsson LT. (2009). Early rheumatoid arthritis and body composition. *Rheumatology (Oxford)*. 48(9);1128-32.
- Borthwick NJ, Akbar AN, MacCormac LP, Lowdell M, Craigen JL, Hassan I, Grundy JE, Salmon M, Yong KL. (1997). Selective migration of highly differentiated primed T-cells, defined by low expression of CD45RB, across human umbilical vein endothelial cells; effects of viral infection on transmigration. *Immunology*. 90(2);272-80.
- Brown MJ, Nijhara R, Hallam JA, Gignac M, Yamada KM, Erlandsen SL, Delon J, Kruhlak M, Shaw S. (2003). Chemokine stimulation of human peripheral blood T lymphocytes induces rapid dephosphorylation of ERM proteins, which facilitates loss of microvilli and polarization. *Blood*. Dec 1;102(12):3890-9.
- Brühl H, Mack M, Niedermeier M, Lochbaum D, Schölmerich J, Straub RH. (2008). Functional expression of the chemokine receptor CCR7 on fibroblast-like synoviocytes. *Rheumatology (Oxford)*.47(12):1771-4.
- Buckley CD, Amft N, Bradfield PF, Pilling D, Ross E, Arenzana-Seisdedos F, Amara A, Curnow SJ, Lord JM, Scheel-Toellner D, Salmon M. (2000). Persistent induction of the chemokine receptor CXCR4 by TGF-beta 1 on synovial T-cells contributes to their accumulation within the rheumatoid synovium. *J Immunol*. 165(6);3423-9.
- Burman A, Haworth O, Hardie DL, Amft EN, Siewert C, Jackson DG, Salmon M, Buckley CD. (2005). A chemokine-dependent stromal induction mechanism for aberrant lymphocyte accumulation and compromised lymphatic return in rheumatoid arthritis. *J Immunol*. 174(3):1693-700.
- Bystry RS, Aluvihare V, Welch KA, Kallikourdis M, Betz AG. (2001). "B cells and professional APCs recruit regulatory T-cells via CCL4". *Nat. Immunol*. 2 (12): 1126–32
- Cai C, La Cava A. (2009). Mimicking self-antigens with synthetic peptides in systemic autoimmune rheumatic diseases. *Curr Clin Pharmacol*. 4(2);142-7.
- Campbell JJ, Hedrick J, Zlotnik A, Siani MA, Thompson DA, Butcher EC. (1998). Chemokines and the arrest of lymphocytes rolling under flow conditions. *Science*. 279;381-4.
- Cañete JD, Celis R, Moll C, Izquierdo E, Marsal S, Sanmartí R, Palacín A, Lora D, de la Cruz J, Pablos JL. (2009). Clinical significance of synovial lymphoid neogenesis and its reversal after anti-tumour necrosis factor- α therapy in rheumatoid arthritis. *Ann. Rheum. Dis.* 68, 751–756.
- Carman CV, Sage PT, Sciuto TE, de la Fuente MA, Geha RS, Ochs HD, Dvorak HF, Dvorak AM, Springer TA. (2007). Transcellular diapedesis is initiated by invasive podosomes. *Immunity*. 26(6);784-97.

Carman CV, Springer TA. (2008). Trans-cellular migration: cell-cell contacts get intimate. *Curr Opin Cell Biol.* 20(5):533-40.

Castor CW, Smith EA, Hossler PA, Bignall MC, Aaron BP. (1992). Connective tissue activation. XXXV. Detection of connective tissue activating peptide-III isoforms in synovium from osteoarthritis and rheumatoid arthritis patients; patterns of interaction with other synovial cytokines in cell culture. *Arthritis Rheum.* 35(7);783-93.

Castor CW, Andrews PC, Swartz RD, Ellis SG, Hossler PA, Clark MR, Matteson EL, Sachter EF. (1993). Connective tissue activation. XXXVI. The origin, variety, distribution, and biologic fate of connective tissue activating peptide-III isoforms; characteristics in patients with rheumatic, renal, and arterial disease. *Arthritis Rheum.* 36(8);1142-53.

Charo IF, Ransohoff RM. (2006). The many roles of chemokines and chemokine receptors in inflammation. *N Engl J Med.* 9;354(6);610-21.

Chen A, Dong L, Leffler NR, Asch AS, Witte ON, Yang LV. (2011). Activation of GPR4 by acidosis increases endothelial cell adhesion through the cAMP/Epac pathway. *PLoS One.* 6(11):e27586.

Cinamon G, Shinder V, Shamri R, Alon R. (2004). Chemoattractant signals and beta integrin occupancy at apical endothelial contacts combine with shear stress signals to promote transendothelial neutrophil migration. *J Immunol.* 173(12):7282-91.

Congiu-Castellano A, Boffi F, Della Longa S, Giovannelli A, Girasole M, Natali F, Pompa M, Soldatov A, Bianconi A. (1997). Aluminum site structure in serum transferrin and lactoferrin revealed by synchrotron radiation X-ray spectroscopy. *Biometals.* Oct;10(4):363-7.

Cross A, Barnes T, Bucknall RC, Edwards SW, Moots RJ. (2006). Neutrophil apoptosis in rheumatoid arthritis is regulated by local oxygen tensions within joints. *J Leukoc Biol.* Sep;80(3):521-8. Epub 2006 Jun 22.

Dabbagh AJ, Trenam CW, Morris CJ, Blake DR. Iron in joint inflammation. *Ann Rheum Dis.* 1993 Jan;52(1):67-73.

D'Ambrosio D, Albanesi C, Lang R, Girolomoni G, Sinigaglia F, Laudanna C. (2002). Quantitative differences in chemokine receptor engagement generate diversity in integrin-dependent lymphocyte adhesion. *J Immunol.* 2002 Sep 1;169(5):2303-12.

D'Aura-Swanson C, Paniagua RT, Lindstrom TM, Robinson WH. (2009). Tyrosine kinases as targets for the treatment of rheumatoid arthritis. *Nat Rev Rheumatol.* 5(6);317-24.

Detheux, M., L. Standker, J. Vakili, J. Munch, U. Forssmann, K. Adermann, S. Pohlmann, G. Vassart, F. Kirchhoff, M. Parmentier, W. G. Forssmann. (2000). Natural proteolytic processing of hemofiltrate CC chemokine 1 generates a potent CC chemokine receptor (CCR)1 and CCR5 agonist with anti-HIV properties. *J. Exp. Med.* 192: 1501-1508

- Dong L, Li Z, Leffler NR, Asch AS, Chi JT, Yang LV. (2013). Acidosis activation of the proton-sensing GPR4 receptor stimulates vascular endothelial cell inflammatory responses revealed by transcriptome analysis. *PLoS One*. 16;8(4):e61991
- Drexler SK, Kong PL, Wales J and Foxwell BM. 2008. Cell signalling in macrophages, the principal innate immune effector cells of rheumatoid arthritis. *Arthritis Research & Therapy* 10;216
- Dye JR, Ullal AJ, Pisetsky DS.(2013). The role of microparticles in the pathogenesis of rheumatoid arthritis and systemic lupus erythematosus. *Scand J Immunol*. 2013 Aug;78(2):140-8.
- Ebringer A, Rashid T. (2009). Rheumatoid arthritis is caused by Proteus ; the molecular mimicry theory and Karl Popper. *Front Biosci (Elite Ed)*. 1;577-86.
- Edwards JC, Leandro MJ. (2008). Lymphoid follicles in joints: what do they mean?. *Arthritis Rheum.*;58(6):1563-5.
- Elsaid KA, Fleming BC, Oksendahl HL, Machan JT, Fadale PD, Hulstyn MJ, Shalvoy R, Jay GD. (2008). Decreased lubricin concentrations and markers of joint inflammation in the synovial fluid of patients with anterior cruciate ligament injury. *Arthritis Rheum*. 58(6);1707-15.
- Elsner J, Mack M, Brühl H, Dulkys Y, Kimmig D, Simmons G, Clapham PR, Schlöndorff D, Kapp A, Wells TN, Proudfoot AE. (2000). Differential activation of CC chemokine receptors by AOP-RANTES. *J Biol Chem*. 17;275(11):7787-94.
- El-Jawhari JJ, El-Sherbiny YM, Jones EA, McGonagle D. (2014). Mesenchymal Stem Cells, Autoimmunity & Rheumatoid Arthritis. *QJM*. Feb 10. [Epub ahead of print]
- Endres M, Andreas K, Kalwitz G, Freymann U, Neumann K, Ringe J, Sittinger M, Häupl T, Kaps C. (2010). Chemokine profile of synovial fluid from normal, osteoarthritis and rheumatoid arthritis patients: CCL25, CXCL10 and XCL1 recruit human subchondral mesenchymal progenitor cells. *Osteoarthritis Cartilage*. Nov;18(11):1458-66. Epub 2010 Aug 13.
- Erdem H, Pay S, Musabak U, Simsek I, Dinc A, Pekel A, Sengul A. (2007). Synovial angiostatic non-ELR CXC chemokines in inflammatory arthritides; does CXCL4 designate chronicity of synovitis?. *Rheumatol Int.*;27(10);969-73.
- Eriksson C, Rantapää-Dahlqvist S, Sundqvist K. (2013). Changes in chemokines and their receptors in blood during treatment with the TNF inhibitor infliximab in patients with rheumatoid arthritis. *Scand J Rheumatol.* 2013;42(4):260-5.
- Essouma M, Noubiap JJ. (2015). Is air pollution a risk factor for rheumatoid arthritis?. *J Inflamm (Lond)*. Jul 30;12:48. doi: 10.1186/s12950-015-0092-1. eCollection 2015.
- Exley C. (2003). A biogeochemical cycle for aluminium?. *J Inorg Biochem*. 2003 Sep 15;97(1):1-7.

- Farr M, Garvey K, Bold AM, Kendall MJ, Bacon PA.(1985). gnificance of the hydrogen ion concentration in synovial fluid in rheumatoid arthritis. *Clin Exp Rheumatol.* 3(2):99-104.
- Filer A, Raza K, Salmon M, Buckley CD. (2008). The role of chemokines in leucocyte-stromal interactions in rheumatoid arthritis. *Front Biosci.* 1;13:2674-85.
- Filer A, Bik M, Parsonage GN, Fitton J, Trebilcock E, Howlett K, Cook M, Raza K, Simmons DL, Thomas AM, Salmon M, Scheel-Toellner D, Lord JM, Rabinovich GA, Buckley CD. (2009). Galectin 3 induces a distinctive pattern of cytokine and chemokine production in rheumatoid synovial fibroblasts via selective signaling pathways. *Arthritis Rheum.* 60(6):1604-14.
- Firestein G. (1999). Starving the synovium: angiogenesis and inflammation in rheumatoid arthritis. *J Clin Invest.*1; 103(1): 3–4.
- Firestein GS. (2003). Evolving concepts of rheumatoid arthritis. *Nature.* 423(6937);356-61.
- Flytlie HA, Hvid M, Lindgreen E, Kofod-Olsen E, Petersen EL, Jørgensen A, Deleuran M, Vestergaard C, Deleuran B. (2010). Expression of MDC/CCL22 and its receptor CCR4 in rheumatoid arthritis, psoriatic arthritis and osteoarthritis. *Cytokine.* 49(1):24-9. Epub 2009 Nov 25.
- Förster R, Emrich T, Kremmer E, Lipp M. (1994). Expression of the G-protein--coupled receptor BLR1 defines mature, recirculating B cells and a subset of T-helper memory cells. *Blood.* 84(3):830-40.
- Förster R, Mattis AE, Kremmer E, Wolf E, Brem G, Lipp M. (1996). A putative chemokine receptor, BLR1, directs B cell migration to defined lymphoid organs and specific anatomic compartments of the spleen. *Cell.* 87(6):1037-47.
- Forssmann U, Mägert HJ, Adermann K, Escher SE, Forssmann WG.(2001). Hemofiltrate CC chemokines with unique biochemical properties: HCC-1/CCL14a and HCC-2/CCL15. *J Leukoc* 70(3):357-66.
- Gardner L, Patterson AM, Ashton BA, Stone MA, Middleton J. (2004). The human Duffy antigen binds selected inflammatory but not homeostatic chemokines. *Biochem Biophys Res Commun.* 321(2):306-12.
- Gardner L, Wilson C, Patterson AM, Bresnihan B, FitzGerald O, Stone MA, Ashton BA, Middleton J. (2006). Temporal expression pattern of Duffy antigen in rheumatoid arthritis: up-regulation in early disease. *Arthritis Rheum.* 54(6):2022-6.
- Gravallese E M. (2002). Bone destruction in Arthritis. *Ann Rheum Dis.* 61(Suppl II);ii84–ii86

Gregory JL, Morand EF, McKeown SJ, Ralph JA, Hall P, Yang YH, McColl SR, Hickey MJ. (2006). Macrophage migration inhibitory factor induces macrophage recruitment via CC chemokine ligand 2. *J Immunol.* 177(11):8072-9.

Geiger B, Bershadsky A. Exploring the neighbourhood: adhesion-coupled cell mechanosensors. *Cell.* 2002;110:139-42.

Grespan R, Fukada SY, Lemos HP, Vieira SM, Napimoga MH, Teixeira MM, Fraser AR, Liew FY, McInnes IB, Cunha FQ. (2008). CXCR2-specific chemokines mediate leukotriene B4-dependent recruitment of neutrophils to inflamed joints in mice with antigen-induced arthritis. *Arthritis Rheum.* 58(7);2030-40.

Gimbrone MA, Lelkes P. (2003). Mechanical Forces and the Endothelium, volume 6 of *Endothelial Cell Research*. Lelkes P ed. *Hardwood Academic Publishers*. The Netherlands

Goldring S R. (2003). Pathogenesis of bone and cartilage destruction in rheumatoid arthritis. *Rheumatology.* 42(Suppl. 2);ii11–ii16

Gong W, Howard OM, Turpin JA, Grimm MC, Ueda H, Gray PW, Raport CJ, Oppenheim JJ, Wang JM. (1998). Monocyte chemotactic protein-2 activates CCR5 and blocks CD4/CCR5-mediated HIV-1 entry/replication. *J Biol Chem.* 273(8):4289-92.

Goronzy JJ, Weyand CM. (2009). Developments in the scientific understanding of rheumatoid arthritis. *Arthritis Res Ther.* 11(5):249. Epub 2009 Oct 14.

Guillén C, McInnes IB, Kruger H, Brock JH. (1998). Iron, lactoferrin and iron regulatory protein activity in the synovium; relative importance of iron loading and the inflammatory response. *Ann Rheum Dis.* May;57(5):309-14.

Hajalilou M, Noshad H, Khabbazi AR, Kolahi S, Azari MH, Abbasneghad M. (2012). Familial rheumatoid arthritis in patients referred to rheumatology clinics of Tabriz, Iran. *Int J Rheum Dis.* Feb;15(1):110-5. doi: 10.1111/j.1756-185X.2011.01664.x. Epub 2011 Sep 14.

Halloran MM, Woods JM, Strieter RM, Szekanecz Z, Volin MV, Hosaka S, Haines GK 3rd, Kunkel SL, Burdick MD, Walz A, Koch AE. (1999). The role of an epithelial neutrophil-activating peptide-78-like protein in rat adjuvant-induced arthritis. *J Immunol.* 162(12):7492-500.

Hamann J, Wishaupt JO, van Lier RA, Smeets TJ, Breedveld FC, Tak PP. (1999). Expression of the activation antigen CD97 and its ligand CD55 in rheumatoid synovial tissue. *Arthritis Rheum.* 42(4);650-8.

Hao Q, Wang L, Tang H. (2009). Vascular endothelial growth factor induces protein kinase D-dependent production of proinflammatory cytokines in endothelial cells. *Am J Physiol Cell Physiol.* 296(4):C821-7.

Hallett MB, Williams AS. (2008). Stopping the traffic: a route to arthritis therapy. *Eur J Immuno.*; 38(10):2650-3.

Haringman JJ, Ludikhuizen J, Tak PP. (2004). Chemokines in joint disease; the key to inflammation? *Ann Rheum Dis.* 63(10):1186-94..

Haringman JJ, Smeets TJ, Reinders-Blankert P, Tak PP. (2006). Chemokine and chemokine receptor expression in paired peripheral blood mononuclear cells and synovial tissue of patients with rheumatoid arthritis, osteoarthritis, and reactive arthritis. *Ann Rheum Dis.* 65(3):294-300.

Hart JE, Laden F, Puett RC, Costenbader KH, Karlson EW. (2009). Exposure to traffic pollution and increased risk of rheumatoid arthritis. *Environ Health Perspect.* 117(7):1065-9

He M, Liang X, He L, Wen W, Zhao S, Wen L, Liu Y, Shyy JY, Yuan Z. (2013). Endothelial dysfunction in rheumatoid arthritis: The role of monocyte chemoattractant protein-1-induced protein. *Arterioscler Thromb Vasc Biol.* 33(6):1384-91.

Hemminki K, Li X, Sundquist J, Sundquist K. (2009). Familial associations of rheumatoid arthritis with autoimmune diseases and related conditions. *Arthritis Rheum.* 60(3):661-8.

Hidaka T, Suzuki K, Kawakami M, Okada M, Kataharada K, Shinohara T, Takamizawa-Matsumoto M, Ohsuzu F. (2001). Dynamic changes in cytokine levels in serum and synovial fluid following filtration leukocytapheresis therapy in patients with rheumatoid arthritis. *J Clin Apher.* 16(2):74-81.

Hillyer P, Mordet E, Flynn G, Male D. (2003). Chemokines, chemokine receptors and adhesion molecules on different human endothelia: discriminating the tissue-specific functions that affect leucocyte migration. *Clin Exp Immunol.* 134(3):431-41.

Hillyer P, Male D. (2005). Expression of chemokines on the surface of different human endothelia. *Immunol Cell Biol.* 83(4):375-82

Hintzen C, Quaiser S, Pap T, Heinrich PC, Hermanns HM. (2009). Induction of CCL13 expression in synovial fibroblasts highlights a significant role of oncostatin M in rheumatoid arthritis. *Arthritis Rheum.* 60(7):1932-43.

Hirota T, Saeki H, Tomita K, Tanaka S, Ebe K, Sakashita M, Yamada T, Fujieda S, Miyatake A, Doi S, Enomoto T, Hizawa N, Sakamoto T, Masuko H, Sasaki T, Ebihara T, Amagai M, Esaki H, Takeuchi S, Furue M, Noguchi E, Kamatani N, Nakamura Y, Kubo M, Tamari M. (2011). Variants of C-C motif chemokine 22 (CCL22) are associated with susceptibility to atopic dermatitis: case-control studies. *PLoS One.* 6(11)

Hitchon CA, El-Gabalawy HS. (2004). Oxidation in rheumatoid arthritis. *Arthritis Res Ther.* 6(6):265-78. Epub 2004 Oct 13.

Hofnagel O, Luechtenborg B, Plenz G, Robenek H. (2002). Expression of the novel scavenger receptor SR-PSOX in cultured aortic smooth muscle cells and umbilical endothelial cells. *Arterioscler Thromb Vasc Biol.* 22(4):710-1.

Hol J, Küchler AM, Johansen FE, Dalhus B, Haraldsen G, Oynebråten I.(2009). Molecular requirements for sorting of the chemokine interleukin-8/CXCL8 to endothelial Weibel-Palade bodies. *J Biol Chem.* Aug 28;284(35):23532-9

Hosaka S, Akahoshi T, Wada C, Kondo H. (1994). Expression of the chemokine superfamily in rheumatoid arthritis. *Clin Exp Immunol.* 97(3);451-7.

House E, Esiri M, Forster G, Ince PG, Exley C. (2012). Aluminium, iron and copper in human brain tissues donated to the Medical Research Council's Cognitive Function and Ageing Study. *Metallomics.* 4(1):56-65.

Hueber W, Tomooka BH, Zhao X, Kidd BA, Drijfhout JW, Fries JF, van Venrooij WJ, Metzger AL, Genovese MC, Robinson WH. (2007). Proteomic analysis of secreted proteins in early rheumatoid arthritis; anti-citrulline autoreactivity is associated with up regulation of proinflammatory cytokines. *Ann Rheum Dis.* 66(6);712-9.

Hui AY, McCarty WJ, Masuda K, Firestein GS, Sah RL. (2012) A systems biology approach to synovial joint lubrication in health, injury, and disease. *WIREs Syst Biol Med.* Jan-Feb;4(1):15-37. doi: 10.1002/wsbm.157. Epub 2011 Aug 8.

Hosaka S, Akahoshi T, Wada C, Kondo H. (1994). Expression of the chemokine superfamily in rheumatoid arthritis. *Clin Exp Immunol.* 97(3);451-7.

Humby F, Manzo A, Kirkham B, Pitzalis C. (2007). The synovial membrane as a prognostic tool in rheumatoid arthritis. *Autoimmun Rev.* 6(4):248-52.

Hwang TL, Lee LY, Wang CC, Liang Y, Huang SF, Wu CM. CCL7 and CCL21 overexpression in gastric cancer is associated with lymph node metastasis and poor prognosis.(2012). *World J Gastroenterol.* Mar 21;18(11):1249-56.

Hwang J, Kim CW, Son KN, Han KY, Lee KH, Kleinman HK, et al. Angiogenic activity of human CC chemokine CCL15 in vitro and in vivo. *FEBS Lett* 2004;570:47e51.

Hyduk S J javascript:popRef('end-a1') and Cybulsky javascript:popRef('end-a1')javascript:popRef('cn1') M I. (2009). Role of $\alpha 4\beta 1$ Integrins in Chemokine-Induced Monocyte Arrest under Conditions of Shear Stress. *Microcirculation.* 16, 1, 17-30

Ibrahim MK1, Barnes JL, Osorio EY, Anstead GM, Jimenez F, Osterholzer JJ, Travi BL, Ahuja SS, Clinton White A Jr, Melby PC. (2014). Deficiency of lymph node resident dendritic cells and dysregulation of DC chemoattractants in a malnourished mouse model of *Leishmania donovani* infection. *Infect Immun.* 2014 May 12.

Iikuni N, Okamoto H, Yoshio T, Sato E, Kamitsuji S, Iwamoto T, Momohara S, Taniguchi A, Yamanaka H, Minota S, Kamatani N. (2006). Raised monocyte chemotactic protein-1 (MCP-1)/CCL2 in cerebrospinalfluid of patients with neuropsychiatric lupus.*Ann Rheum Dis.* 65(2):253-6.

- Imboden JB. (2009). The immunopathogenesis of rheumatoid arthritis. *Annu Rev Pathol.* 4:417-34.
- Iwamoto T, Okamoto H, Iikuni N, Takeuchi M, Toyama Y, Tomatsu T, Kamatani N, Momohara S. (2006). Monocyte chemoattractant protein-4 (MCP-4)/CCL13 is highly expressed in cartilage from patients with rheumatoid arthritis. *Rheumatology (Oxford).* 45(4);421-4. Epub 2005 Nov 22.
- Iwamoto T, Okamoto H, Toyama Y, Momohara S. (2008). Molecular aspects of rheumatoid arthritis; chemokines in the joints of patients. *FEBS J.* 275(18);4448-55.
- Takuji Iwamoto T, Okamoto H, Toyama Y, Momohara S. (2008). Molecular aspects of rheumatoid arthritis; chemokines in the joints of patients. *FEBS Journal.* 275. 4448–4455
- Jay GD, Torres JR, Warman ML, Laderer MC, Breuer KS. (2007). The role of lubricin in the mechanical behavior of synovial fluid. *Proc Natl Acad Sci U S A.* 104(15);6194-9.
- Jeong HG, Pokharel YR, Lim SC, Hwang YP, Han EH, Yoon JH, Ahn SG, Lee KY, Kang KW. (2009). Novel role of Pin1 induction in type II collagen-mediated rheumatoid arthritis. *J Immunol.* 183(10);6689-97
- Jin C, Ekwall AK, Bylund J, Björkman L, Estrella RP, Whitelock JM, Eisler T, Bokarewa M, Karlsson NG.(2012). Human synovial lubricin expresses sialyl Lewis x determinant and has L-selectin ligand activity. *J Biol Chem.* 2012 Oct 19;287(43):35922-33.
- Johnson LA, Clasper S, Holt AP, Lalor PF, Baban D, Jackson DG. (2006). An inflammation-induced mechanism for leukocyte transmigration across lymphatic vessel endothelium. *J Exp Med.* 27;203(12):2763-77.
- Keeley EC, Mehrad B, Strieter RM. (2008). Chemokines as mediators of neovascularization. *Arterioscler Thromb Vasc Biol.* 28(11):1928-36.
- Kennedy A, Ng CT, Biniiecka M, Saber T, Taylor C, O'Sullivan J, Veale DJ, Fearon U. (2010). Angiogenesis and blood vessel stability in inflammatory arthritis. *Arthritis Rheum.* Mar;62(3):711-21.
- Key J A. (1932). The synovial membrane of joints and bursae. In; *Special Cytology*, Vol 2. New York; PB Hoeber; 1055-1076
- Strand V, Kimberly R and Isaacs J D. (2007). Biologic therapies in rheumatology; lessons learned, future directions. *Nature Reviews Drug Discover.* 6. 75-92
- Kinne RW, Stuhlmüller B and Gerd-R Burmester G. (2007). Cells of the synovium in rheumatoid arthritis Macrophages. *Arthritis Research & Therapy.* 9;224
- Koch AE, Kunkel SL, Burrows JC, Evanoff HL, Haines GK, Pope RM, Strieter RM. (1991). Synovial tissue macrophage as a source of the chemotactic cytokine IL-8. *J Immunol.* 147(7);2187-95.

Koch AE, Kunkel SL, Harlow LA, Johnson B, Evanoff HL, Haines GK, Burdick MD, Pope RM, Strieter RM. (1992). Enhanced production of monocyte chemoattractant protein-1 in rheumatoid arthritis. *J Clin Invest.* 90(3);772-9.

Klimiuk PA, Sierakowski S, Latosiewicz R, Skowronski J, Cylwik JP, Cylwik B, Chwiecko J. (2005). Histological patterns of synovitis and serum chemokines in patients with rheumatoid arthritis. *J Rheumatol.* 32(9):1666-72.

Koch AE, Kunkel SL, Harlow LA, Mazarakis DD, Haines GK, Burdick MD, Pope RM, Walz A, Strieter RM. (1994a). Epithelial neutrophil activating peptide-78; a novel chemotactic cytokine for neutrophils in arthritis. *J Clin Invest.* 94(3);1012-8.

Koch AE, Kunkel SL, Harlow LA, Mazarakis DD, Haines GK, Burdick MD, Pope RM, Strieter RM. (1994b). Macrophage inflammatory protein-1 alpha. A novel chemotactic cytokine for macrophages in rheumatoid arthritis. *J Clin Invest.* 93(3);921-8.

Koch AE, Kunkel SL, Shah MR, Hosaka S, Halloran MM, Haines GK, Burdick MD, Pope RM, Strieter RM. (1995a). Growth-related gene product alpha. A chemotactic cytokine for neutrophils in rheumatoid arthritis. *J Immunol.* 1;155(7);3660-6.

Koch AE, Kunkel SL, Shah MR, Fu R, Mazarakis DD, Haines GK, Burdick MD, Pope RM, Strieter RM. (1995b). Macrophage inflammatory protein-1 beta; a C-C chemokine in osteoarthritis. *Clin Immunol Immunopathol.* 77(3);307-14.

Koch AE, Volin MV, Woods JM, Kunkel SL, Connors MA, Harlow LA, Woodruff DC, Burdick MD, Strieter RM. (2001). Regulation of angiogenesis by the C-X-C chemokines interleukin-8 and epithelial neutrophil activating peptide 78 in the rheumatoid joint. *Arthritis Rheum.* 44(1);31-40.

Koch AE. (2003). Angiogenesis as a target in rheumatoid arthritis. *Ann Rheum Dis.* 62 Suppl 2:ii60-7.

Koizumi K, Saitoh Y, Minami T, Takeno N, Tsuneyama K, Miyahara T, Nakayama T, Sakurai H, Takano Y, Nishimura M, Imai T, Yoshie O, Saiki I. (2009). Role of CX3CL1/fractalkine in osteoclast differentiation and bone resorption. *J Immunol.*;183(12);7825-31.

König A, Krenn V, Toksoy A, Gerhard N, Gillitzer R. (2000). Mig, GRO alpha and RANTES messenger RNA expression in lining layer, infiltrates and different leucocyte populations of synovial tissue from patients with rheumatoid arthritis, psoriatic arthritis and osteoarthritis. *Virchows Arch.* 436(5);449-58.

Krzysiek R, Lefèvre EA, Zou W, Foussat A, Bernard J, Portier A, Galanaud P, Richard Y. (1999). Antigen receptor engagement selectively induces macrophage inflammatory protein-1 alpha (MIP-1 alpha) and MIP-1 beta chemokine production in human B cells. *J Immunol.* 162(8);4455-63.

Kuan WP, Tam LS, Wong CK, Ko FW, Li T, Zhu T, Li EK. (2010). CXCL9 and CXCL10 as Sensitive Markers of Disease Activity in Patients with Rheumatoid Arthritis. *J Rheumatol.* (2009 Dec 23 e pub ahead of print)

Kuschert GS, Coulin F, Power CA, Proudfoot AE, Hubbard RE, Hoogewerf AJ, Wells TN. (1999). Glycosaminoglycans interact selectively with chemokines and modulate receptor binding and cellular responses. *Biochemistry.* 38(39);12959-68.

Kwon DJ, Bae YS, Ju SM, Goh AR, Youn GS, Choi SY, Park J. (2012). Casuarinin suppresses TARC/CCL17 and MDC/CCL22 production via blockade of NF- κ B and STAT1 activation in HaCaT cells. *Biochem Biophys Res Commun.* 27;417(4):1254-9.

Lardner A The effects of extracellular pH on immune function. (2001). *J Leukoc Biol.* 69(4):522-30.

Laurent L, Clavel C, Lemaire O, Anquetil F, Cornillet M, Zabraniecki L, Nogueira L, Fournié B, Serre G, Sebbag M. (2011). Fc γ receptor profile of monocytes and macrophages from rheumatoid arthritis patients and their response to immune complexes formed with autoantibodies to citrullinated proteins. *Ann Rheum Dis.* Jun;70(6):1052-9. Epub 2011 Mar 15.

Lebre MC. And Tak PP. (2009). Dendritic cells in rheumatoid arthritis; Which subset should be used as a tool to induce tolerance?. *Human Immunology.* 70. 321-324

Lee YH, Rho YH, Choi SJ, Ji JD, Song GG. (2007). PADI4 polymorphisms and rheumatoid arthritis susceptibility; a meta-analysis. *Rheumatol Int .* 27;827-833.

Ley K., Laudanna C, Cybulsky M I, Nourshargh S.(2007). Getting to the site of inflammation; the leukocyte adhesion cascade updated. *Nat Rev Immunol.* 7(9);678-89.

Li GQ, Liu D, Zhang Y, Qian YY, Zhu YD, Guo SY, Sunagawa M, Hisamitsu T, Liu YQ. (2013). Anti-invasive effects of celastrol in hypoxia-induced fibroblast-like synoviocyte through suppressing of HIF-1 α /CXCR4 signaling pathway. *Int Immunopharmacol.* 17(4):1028-36

Lisignoli G, Manferdini C, Codeluppi K, Piacentini A, Grassi F, Cattini L, Filardo G, Facchini A. (2009). CCL20/CCR6 chemokine/receptor expression in bone tissue from osteoarthritis and rheumatoid arthritis patients; different response of osteoblasts in the two groups. *J Cell Physiol.* 221(1);154-60.

Loetscher P, Seitz M, Clark-Lewis I, Baggiolini M, Moser B. (1994). Monocyte chemotactic proteins MCP-1, MCP-2, and MCP-3 are major attractants for human CD4+ and CD8+ T lymphocytes. *FASEB J.* 8. 1055–1060.

Loetscher P and Moser B. (2002). Homing chemokines in rheumatoid arthritis. *Arthritis Res.* 4;233-236

Loetscher P. (2005). Chemokines in rheumatoid arthritis. *Drug Discovery Today; Disease Mechanisms.* 2 (3). 377-382

- Longato L, Anania A, Calosso L, Corino D, Tarocco RP.(2005). [Histogenic characterization of the cells forming RA pannus]. *Recenti Prog Med.* 96(1);16-22.
- Lu Y, Levick J R and Wang W. (2005). The Mechanism of Synovial Fluid Retention in Pressurized Joint Cavities. *Microcirculation.* 12.7.581-595.
- Lundy SK, Sarkar S, Tesmer LA and Fox DA. (2007). Cells of the synovium in rheumatoid arthritis, T lymphocytes. *Arthritis Research & Therapy* . 9;202
- Luster AD, Greenberg SM, Leder P. (1995). The IP-10 chemokine binds to a specific cell surface heparan sulfate site shared with platelet factor 4 and inhibits endothelial cell proliferation. *J Exp Med.* 182(1):219-31.
- Lutzky V, Hannawi S and Thomas R. (2007). Cells of the synovium in rheumatoid arthritis Dendritic cells. *Arthritis Research & Therapy* . 9;219
- Malinin T, Ouellette EA. (2000). Articular cartilage nutrition is mediated by subchondral bone; a long-term autograft study in baboons. *Osteoarthritis and Cartilage.* 8. 483–491
- Malmstrom V, Trollmo C, Klareskog L (2005). Modulating co-stimulation: a rational strategy in the treatment of heumatoid arthritis? *Arthritis Res Ther* , 7 Suppl 2:S15-S20.
- Manzo A, Vitolo B, Humby F, Caporali R, Jarrossay D, Dell'accio F, Ciardelli L, Uguccioni M, Montecucco C, Pitzalis C. (2008). Mature antigen-experienced T helper cells synthesize and secrete the B cell chemoattractant CXCL13 in the inflammatory environment of the rheumatoid joint. *Arthritis Rheum.* 58(11):3377-87.
- Manzo A, Bombardieri M, Humby F., Pitzalis, C. (2010). Secondary and ectopic lymphoid tissue responses in rheumatoid arthritis: from inflammation to autoimmunity and tissue damage/remodeling. *Immunol. Rev.* 233, 267–285
- Marcelino J, Carpten JD, Suwairi WM, Gutierrez OM, Schwartz S, Robbins C, Sood R, Makalowska I, Baxevanis A, Johnstone B, Laxer RM, Zemel L, Kim CA, Herd JK, Ihle J, Williams C, Johnson M, Raman V, Alonso LG, Brunoni D, Gerstein A, Papadopoulos N, Bahabri SA, Trent JM, Warman ML. (1999). CACP, encoding a secreted proteoglycan, is mutated in camptodactyly-arthropathy-coxa vara-pericarditis syndrome. *Nat Genet.* 23(3):319-22.
- Mapp PI, Grootveld MC, Blake DR. (1995). Hypoxia, oxidative stress and rheumatoid arthritis. *Br Med Bull.* Apr;51(2):419-36.
- Marsland BJ, Bättig P, Bauer M, Ruedl C, Lässig U, Beerli RR, Dietmeier K, Ivanova L, Pfister T, Vogt L, Nakano H, Nembrini C, Saudan P, Kopf M, Bachmann MF. (2005). CCL19 and CCL21 induce a potent proinflammatory differentiation program in licensed dendritic cells. *Immunity.* 22(4):493-505.
- Martini G, Cabrelle A, Calabrese F, Carraro S, Scquizzato E, Teramo A, Facco M, Zulian F, Agostini C. (2008). CXCR6-CXCL16 interaction in the pathogenesis of Juvenile Idiopathic Arthritis. *Clin Immunol.* 129(2):268-76.

- Mauri C and Ehrenstein MR. (2007). Cells of the synovium in rheumatoid arthritis B cells. *Arthritis Research & Therapy*. 9;205
- Matloubian M, David A, Engel S, Ryan JE, Cyster JG. (2000). A transmembrane CXC chemokine is a ligand for HIV-coreceptor Bonzo. *Nat Immunol*. 1(4):298-304.
- Matsui T, Akahoshi T, Namai R, Hashimoto A, Kurihara Y, Rana M, Nishimura A, Endo H, Kitasato H, Kawai S, Takagishi K, Kondo H. (2001). Selective recruitment of CCR6-expressing cells by increased production of MIP-3 alpha in rheumatoid arthritis. *Clin Exp Immunol*. 125(1);155-61.
- Matsunawa M, Isozaki T, Odai T, Yajima N, Takeuchi HT, Negishi M, Ide H, Adachi M, Kasama T. (2006). Increased serum levels of soluble fractalkine (CX3CL1) correlate with disease activity in rheumatoid vasculitis. *Arthritis Rheum*. 54(11);3408-16.
- Mauri C, Ehrenstein MR. (2007). Cells of the synovium in rheumatoid arthritis. B cells. *Arthritis Res Ther*. 9(2):205.
- McEver RP. (2002). Selectins: lectins that initiate cell adhesion under flow. *Curr Opin Cell Biol*. 14:581-586.
- McNearny T, Baethge BA, Cao S, Alam R, Lisse JR and Westlund KN. (2011). Excitatory amino acids, TNF- α , and chemokine levels in synovial fluids of patients with active arthropathies. *Clin Exp Immunol*. 137(3): 621–627.
- Mellado M, Martínez-Muñoz L, Cascio G, Lucas P, Pablos JL, Rodríguez-Frade JM. (2015). T Cell Migration in Rheumatoid Arthritis. *Front Immunol*. 27;6:384.
- Menten, P, Wuyts, A, Van Damme, J. (2001) Monocyte chemotactic protein-3. *Eur. Cytokine Netw*. 12, 554–560
- Messemaker TC, Huizinga TW, Kurreeman F. (2015). Immunogenetics of rheumatoid arthritis: Understanding functional implications. *J Autoimmun*. 2015 Jul 24. pii: S0896-8411(15)30010-X. doi: 10.1016/j.jaut.2015.07.007. [Epub ahead of print]
- Middleton J, Neil S, Wintle J, Clark-Lewis I, Moore H, Lam C, Auer M, Hub E, Rot A. (1997). Transcytosis and surface presentation of IL-8 by venular endothelial cells. *Cell*. 91(3);385-95.
- Middleton J, Patterson AM, Gardner L, Schmutz C, Ashton BA. (2002). Leukocyte extravasation; chemokine transport and presentation by the endothelium. *Blood*. 100(12);3853-60.
- Middleton J, Americh L1, Gayon R1, Julien D1, Aguilar L1, Amalric F and Girard J. (2004). Endothelial cell phenotypes in the rheumatoid synovium; activated, angiogenic, apoptotic and leaky. *Arthritis Res Ther*. 6;60-72

- Miossec P. (2008). Dynamic interactions between T-cells and dendritic cells and their derived cytokines/chemokines in the rheumatoid synovium. *Arthritis Res Ther.* 10 Suppl 1:S2.
- Mittler RS. (2004). Suppressing the self in rheumatoid arthritis. *Nat Med.* 10(10):1047-9.
- Mogi C, Tobo M, Tomura H, Murata N, He XD, Sato K, Kimura T, Ishizuka T, Sasaki T, Sato T, Kihara Y, Ishii S, Harada A, Okajima F. (2009). Involvement of proton-sensing TDAG8 in extracellular acidification-induced inhibition of proinflammatory cytokine production in peritoneal macrophages. *J Immunol.* 1;182(5):3243-51.
- Momohara S, Okamoto H, Iwamoto T, Mizumura T, Ikari K, Kawaguchi Y, Takeuchi M, Kamatani N, Tomatsu T. (2007). High CCL18/PARC expression in articular cartilage and synovial tissue of patients with rheumatoid arthritis. *J Rheumatol.* 34(2);266-71.
- Moore BB, Keane MP, Addison CL, Arenberg DA, Strieter RM. (1998). CXC chemokine modulation of angiogenesis; the importance of balance between angiogenic and angiostatic members of the family. *J Investig Med.* 46(4);113-20.
- Morales-Ducret J, Wayner E, Elices MJ, Alvaro-Gracia JM, Zvaifler NJ, Firestein GS. (1992). Alpha 4/beta 1 integrin (VLA-4) ligands in arthritis. Vascular cell adhesion molecule-1 expression in synovium and on fibroblast-like synoviocytes. *J Immunol.* 149(4);1424-31.
- Morris CJ, Earl JR, Trenam CW, Blake DR. (1995). Reactive oxygen species and iron--a dangerous partnership in inflammation. *Int J Biochem Cell Biol.* Feb;27(2):109-22.
- Moser B, Willmann K. (2004). Chemokines: role in inflammation and immune surveillance. *Ann Rheum Dis.* 63. Suppl 2:ii84-ii89.
- Mostaghi AA and Skillen A W. (1990). Comparative Binding Studies of Aluminium and Iron to Serum Transferrin. *J of I Acad of Sci* 3:4, 280-283
- Mortier A, Van Damme J, Proost P. (2008). Regulation of chemokine activity by posttranslational modification. *Pharmacol Ther.*;120(2):197-217.
- Mowat AG, Hothersall TE. (1968). Nature of anaemia in rheumatoid arthritis. VIII. Iron content of synovial tissue in patients with rheumatoid arthritis and in normal individuals. *Ann Rheum Dis* 27:345-350
- Müller-Ladner U, Ospelt C, Gay S, Distler O, Pap T. (2007). Cells of the synovium in rheumatoid arthritis. Synovial fibroblasts. *Arthritis Res Ther.* 9(6):223.
- Münch J1, Ständker L, Pöhlmann S, Baribaud F, Papkalla A, Rosorius O, Stauber R, Sass G, Heveker N, Adermann K, Escher S, Klüver E, Doms RW, Forssmann WG, Kirchhoff F. (2002). Hemofiltrate CC chemokine 1[9-74] causes effective internalization of CCR5 and is a potent inhibitor of R5-tropic human immunodeficiency virus type 1 strains in primary T cells and macrophages. *Antimicrob Agents Chemother.*;46(4):982-90.

- Murata N, Mogi C, Tobo M, Nakakura T, Sato K, Tomura H, Okajima F. (2009). Inhibition of superoxide anion production by extracellular acidification in neutrophils. *Cell Immunol.* 259(1):21-6
- Murphy PM. (1994). The molecular biology of leukocyte chemoattractant receptors. *Annu Rev Immunol.* 12;593-633.
- Murphy D A and Courtneidge S A. (2011). The 'ins' and 'outs' of podosomes and invadopodia: characteristics, formation and function. *Nat Rev Mol Cell Biol.* 23;12(7):413-26
- Murphy G and Nagase H. (2008). Reappraising metalloproteinases in rheumatoid arthritis and osteoarthritis: destruction or repair? *Nat Clin Pract Rheumatol.*;4(3):128-35.
- Nakken B, Munthe LA, Konttinen YT, Sandberg AK, Szekanecz Z, Alex P, Szodoray P. (2011). B-cells and their targeting in rheumatoid arthritis--current concepts and future perspectives. *Autoimmun Rev.* 11(1):28-34. Epub 2011 Jul 14.
- Nanki T, Hayashida K, El-Gabalawy HS, Suson S, Shi K, Girschick HJ, Yavuz S, Lipsky PE. (2000). Stromal cell-derived factor-1-CXC chemokine receptor 4 interactions play a central role in CD4+ T cell accumulation in rheumatoid arthritis synovium. *J Immunol.* 165(11);6590-8.
- Nanki T, Shimaoka T, Hayashida K, Taniguchi K, Yonehara S, Miyasaka N. (2005). Pathogenic role of the CXCL16-CXCR6 pathway in rheumatoid arthritis. *Arthritis Rheum.* 52(10):3004-14.
- Nanki T, Takada K, Komano Y, Morio T, Kanegane H, Nakajima A, Lipsky PE, Miyasaka N. (2009). Chemokine receptor expression and functional effects of chemokines on B cells; implication in the pathogenesis of rheumatoid arthritis. *Arthritis Res Ther.* 11(5);R149.
- Napoli C, Ignarro LJ. (2001). Nitric oxide and atherosclerosis. *Nitric Oxide* 2001;5(2):88e97.
- Narumi S. Tominaga Y. Tamaru M . Shimai S. Okumura O. Nishioji K. Itoh Y. Okanoue T. (1997). Expression of IFN-inducible protein-10 in chronic hepatitis. *The Journal of Immunology.* 158. 11 5536-5544.
- Neote K, Darbonne W, Ogez J, Honk R, and Schall T J. (1993). Identification of a Promiscuous Inflammatory Peptide Receptor on the Surface of Red Blood Cells. *The Journal of Biological Chemistry.* 268. 17. 12247-12249,
- Newton P, O'Boyle G, Jenkins Y, Ali S, Kirby JA. (2009). T cell extravasation: demonstration of synergy between activation of CXCR3 and the T cell receptor. *Mol Immunol.* 47(2-3):485-92.
- Neyt K, Perros F, GeurtsvanKessel CH, Hammad H, Lambrecht BN.(2012). Tertiary lymphoid organs in infection and autoimmunity. *Trends Immunol.* Jun;33(6):297-305.

Ng CT, Biniecka M, Kennedy A, McCormick J, Fitzgerald O, Bresnihan B, Buggy D, Taylor CT, O'Sullivan J, Fearon U, Veale DJ. (2010). Synovial tissue hypoxia and inflammation in vivo. *Ann Rheum Dis*. 2010 Jul;69(7):1389-95

Nibbs R, Graham G, Rot A. (2003). Chemokines on the move; control by the chemokine "interceptors" Duffy blood group antigen and D6. *Semin Immunol*. 15(5);287-94.

Nishida N, Xie C, Shimaoka M, Cheng Y, Walz T, Springer TA. (2006). Activation of leukocyte beta2 integrins by conversion from bent to extended conformations. *Immunity*. 25; 583-94.

Nomiyama H, Fukuda S, Iio M, Tanase S, Miura R, Yoshie O. (1999). Organization of the chemokine gene cluster on human chromosome 17q11.2 containing the genes for CC chemokine MIP1-1, HCC-2, HCC-1, LEC, and RANTES. *J Interferon Cytokine Res*. 19(3):227-34.

Niu J, Azfer A, Zhelyabovska O, Fatma S, Kolattukudy P E. (2008). Monocyte chemotactic protein (MCP) promotes angiogenesis via a novel transcription factor, MCP-1-induced protein (MCPIP). *J Biol Chem*. 283(21):14542-51.

Oh HM, Lee S, Na BR, Wee H, Kim SH, Choi SC, Lee KM, Jun CD. (2007). RKIKK motif in the intracellular domain is critical for spatial and dynamic organization of ICAM-1; functional implication for the leukocyte adhesion and transmigration. *Mol Biol Cell*. 18(6);2322-35.

Okamoto H, Koizumi K, Yamanaka H, Saito T, Kamatani N. (2003). A role for TARC/CCL17, a CC chemokine, in systemic lupus erythematosus. *J Rheumatol*. 30(11);2369-73.

Oliver JE, and Silman AJ. (2009a). Why are women predisposed to autoimmune rheumatic diseases?. *Arthritis Res Ther*. 11(5);252..

Oliver JE, and Silman AJ. (2009b). What epidemiology has told us about risk factors and aetiopathogenesis in rheumatic diseases. *Arthritis Res Ther*. 11;223

Olszewski WL, Pazdur J, Kubasiewicz E, Zaleska M, Cooke CJ, Miller NE. (2001). Lymph draining from foot joints in rheumatoid arthritis provides insight into local cytokine and chemokine production and transport to lymph nodes. *Arthritis Rheum*. 44(3):541-9.

Opdenakker G, Froyen G, Fiten P, Proost P, Van Damme J (1993). "Human monocyte chemotactic protein-3 (MCP-3): molecular cloning of the cDNA and comparison with other chemokines". *Biochem. Biophys. Res. Commun*. 191 (2): 535-42.

Øynebråten I, Barois N, Hagelsteen K, Johansen FE, Bakke O, Haraldsen G.(2005). Characterization of a novel chemokine-containing storage granule in endothelial cells: evidence for preferential exocytosis mediated by protein kinase A and diacylglycerol. *J Immunol*. 2005 Oct 15;175(8):5358-69.

- Otero M and Goldring MB. (2007). Cells of the synovium in rheumatoid arthritis Chondrocytes. *Arthritis Research & Therapy*. 9;220
- Pablos JL, Santiago B, Galindo M, Torres C, Brehmer MT, Blanco FJ, García-Lázaro FJ. (2003). Synoviocyte-derived CXCL12 is displayed on endothelium and induces angiogenesis in rheumatoid arthritis. *J Immunol*. 170(4):2147-52.
- Page G, Lebecque S, Miossec P. (2002). Anatomic localization of immature and mature dendritic cells in an ectopic lymphoid organ: correlation with selective chemokine expression in rheumatoid synovium. *J Immunol*. 168(10):5333-41
- Patel DD, Zachariah JP, Whichard LP. (2001). CXCR3 and CCR5 Ligands in Rheumatoid Arthritis Synovium. *Clinical Immunology*. 98. 1. 39–45.
- Patterson AM, Siddall H, Chamberlain G, Gardner L, Middleton J. (2002). Expression of the duffy antigen/receptor for chemokines (DARC) by the inflamed synovial endothelium. *J Pathol*. 197(1):108-16.
- Patterson AM, Gardner L, Shaw J, David G, Loreau E, Aguilar L, Ashton BA, Middleton J. (2005). Induction of a CXCL8 binding site on endothelial syndecan-3 in rheumatoid synovium. *Arthritis Rheum*. 52(8):2331-42.
- Pease JE, Williams TJ. (2006). The attraction of chemokines as a target for specific anti-inflammatory therapy. *British journal of Pharmacology*. 147 Suppl 1;S212-21.
- Peters CL, Morris CJ, Mapp PI, Blake DR, Lewis CE, Winrow VR. (2004) The transcription factors hypoxia-inducible factor 1alpha and Ets-1 colocalize in the hypoxic synovium of inflamed joints in adjuvant-induced arthritis. *Arthritis Rheum* 50:291–6.
- Pelletier M, Maggi L, Micheletti A, Lazzeri E, Tamassia N, Costantini C, Cosmi L, Lunardi C, Annunziato F, Romagnani S, Cassatella MA. (2010). Evidence for a cross-talk between human neutrophils and Th17 cells. *Blood*. 115. 2. 335-343. Epub 2009 Nov 4.
- Pérez G, Pregi N, Vittori D, Di Risio C, Garbossa G, Nesse A. (2005). Aluminum exposure affects transferrin-dependent and -independent iron uptake by K562 cells. *Biochim Biophys Acta*. Aug 15;1745(1):124-30. Epub 2005 Jan 5.
- Pickens SR, Chamberlain ND, Volin MV, Pope RM, Mandelin AM 2nd, Shahrara S. (2011) Characterization of CCL19 and CCL21 in rheumatoid arthritis. *Arthritis Rheum*. Apr;63(4):914-22. doi: 10.1002/art.30232.
- Pierer M, Rethage J, Seibl R, Lauener R, Brentano F, Wagner U, Hantzschel H, Michel BA, Gay RE, Gay S, Kyburz D. (2004). Chemokine secretion of rheumatoid arthritis synovial fibroblasts stimulated by Toll-like receptor 2 ligands. *J Immunol*. 172(2):1256-65.
- Pitsillides A A. (2003). Identifying and characterizing the joint cavity-forming cell. *Cell Biochem Funct*. 21(3);235-40.

Polzer K, Baeten D, Soleiman A, Distler J, Gerlag DM, Tak PP, Schett G, Zwerina J. (2008). Tumour necrosis factor blockade increases lymphangiogenesis in murine and human arthritic joints. *Ann Rheum Dis.* 67(11):1610-6. Epub 2008 Jan 3.

Pretzel D, Pohlers D, Weiner S and Raimund W Kinne RW. (2009). In vitro model for the analysis of synovial fibroblast-degradation of intact cartilage. *Arthritis Research & Therapy* . 11;R25

Proost P, Wuyts A, Van Damme J. (1996). Human monocyte chemotactic proteins-2 and -3: structural and functional comparison with MCP-1. *J Leukoc Biol.* 59(1):67-74.

Pruenster M, Mudde L, Bombosi P, Dimitrova S, Zsak M, Middleton J, Richmond A, Graham GJ, Segerer S, Nibbs RJ, Rot A. (2009). The Duffy antigen receptor for chemokines transports chemokines and supports their promigratory activity. *Nat Immunol.* 10(1):101-8

Radstake TRDJ, van der Voort R, ten Brummelhuis M, de Waal Malefijt M, Looman M, Figdor CG, van den Berg WB, Barrera P, Adema GJ. (2005). Increased expression of CCL18, CCL19, and CCL17 by dendritic cells from patients with rheumatoid arthritis, and regulation by Fc gamma receptors. *Ann Rheum Dis.* 64;359–367.

Ran S, Montgomery KE. (2012). Macrophage-mediated lymphangiogenesis: the emerging role of macrophages as lymphatic endothelial progenitors. *Cancers (Basel)*. Sep;4(3):618-57.

Ramos CD, Canetti C, Souto JT, Silva JS, Hogaboam CM, Ferreira SH, Cunha FQ. (2005). MIP-1alpha[CCL3] acting on the CCR1 receptor mediates neutrophil migration in immune inflammation via sequential release of TNF-alpha and LTB4. *J Leukoc Biol.* 78(1):167-77.

Rathanaswami P, Hachicha M, Sadick M, Schall TJ, McColl SR. (1993). Expression of the cytokine RANTES in human rheumatoid synovial fibroblasts. Differential regulation of RANTES and interleukin-8 genes by inflammatory cytokines. *J Biol Chem.* 268(8):5834-9.

Rauner M, Stein N, Winzer M, Goettsch C, Zwerina J, Schett G, Distler JH, Albers J, Schulze J, Schinke T, Bornhäuser M, Platzbecker U, Hofbauer LC. (2012) WNT5A is induced by inflammatory mediators in bone marrow stromal cells and regulates cytokine and chemokine production. *J Bone Miner Res.* Dec 8. doi: 10.1002/jbmr.1488. [Epub ahead of print]

Raza K, Scheel-Toellner D, Lee CY, Pilling D, Curnow SJ, Falciani F, Trevino V, Kumar K, Assi LK, Lord JM, Gordon C, Buckley CD, Salmon M. (2006). Synovial fluid leukocyte apoptosis is inhibited in patients with very early rheumatoid arthritis. *Arthritis Res Ther.* 8;R120.

Rhee DK, Marcelino J, Baker M, Gong Y, Smits P, Lefebvre V, Jay GD, Stewart M, Wang H, Warman ML, Carpten JD (2005) The secreted glycoprotein lubricin protects cartilage surfaces and inhibits synovial cell overgrowth. *J Clin Invest.* 115; 622-631.

Richter R, Casarosa P, Ständker L, Münch J, Springael JY, Nijmeijer S, Forssmann WG,

Vischer HF, Vakili J, Detheux M, Parmentier M, Leurs R, Smit MJ. (2009). Significance of N-terminal proteolysis of CCL14a to activity on the chemokine receptors CCR1 and CCR5 and the human cytomegalovirus-encoded chemokine receptor US28. *J Immunol.* 183(2):1229-37

Rioja I, Hughes FJ, Sharp CH, Warnock LC, Montgomery DS, Akil M, Wilson AG, Binks MH, Dickson MC. (2008). Potential novel biomarkers of disease activity in rheumatoid arthritis patients: CXCL13, CCL23, transforming growth factor alpha, tumor necrosis factor receptor superfamily member 9, and macrophage colony-stimulating factor. *Arthritis Rheum.* 58(8):2257-67.

Robinson E, Keystone EC, Schall TJ, Gillett N, Fish EN. (1995). Chemokine expression in rheumatoid arthritis (RA); evidence of RANTES and macrophage inflammatory protein (MIP)-1 beta production by synovial T-cells. *Clin Exp Immunol.* 101(3):398-407.#

Rondaij MG, Bierings R, Kragt A, van Mourik JA, Voorberg J. (2006). Dynamics and plasticity of Weibel-Palade bodies in endothelial cells. *Arterioscler Thromb Vasc Biol.* 2006 May;26(5):1002-7.

Rondeau V, Iron A, Letenneur L, Commenges D, Duchêne F, Arveiler B, Dartigues JF. (2006). Analysis of the effect of aluminum in drinking water and transferrin C2 allele on Alzheimer's disease. *Eur J Neurol.* Sep;13(9):1022-5.

Rot A. (2005) Cointribution of Duffy antigen/receptor chemokine function. *Cytokine Growth Factor Rev.* 16:687-694.

Rovenská E, Rovenský J. (2012). Structure and function of lymphatic capillaries in synovial joint. *Cas Lek Cesk.* 2151(11):520-2.

Ruschpler P, Lorenz P, Eichler W, Koczan D, Hänel C, Scholz R, Melzer C, Thiesen HJ, Stiehl P.(2005). High CXCR3 expression in synovial masT-cells associated with CXCL9 and CXCL10 expression in inflammatory synovial tissues of patients with rheumatoid arthritis. *Arthritis Res Ther.* 5(5);R241-52.

Ruth JH, Volin MV, Haines GK 3rd, Woodruff DC, Katschke KJ Jr, Woods JM, Park CC, Morel JC, Koch AE. (2001). Fractalkine, a novel chemokine in rheumatoid arthritis and in rat adjuvant-induced arthritis. *Arthritis Rheum.* 44(7);1568-81.

Santiago B, Baleux F, Palao G, Gutiérrez-Cañas I, Ramírez JC, Arenzana-Seisdedos F, Pablos JL. (2006). CXCL12 is displayed by rheumatoid endothelial cells through its basic amino-terminal motif on heparan sulfate proteoglycans. *Arthritis Res Ther.* 8(2);R43.

Salcedo R, Young HA, Ponce ML, Ward JM, Kleinman HK. Eotaxin (CCL11) induces in vivo angiogenic responses by human CCR3C endothelial cells. *J Immunol* 2001;166:7571e8.

Schall TJ, Bacon K, Toy KJ, Goeddel DV. (1990). Selective attraction of monocytes and T lymphocytes of the memory phenotype by cytokine RANTES. *Nature.* 347(6294);669-71.

- Schett G, Tohidast-Akrad M, Steiner G, Smolen J. (2001). The stressed synovium. *Arthritis Res.* 3(2):80-6. Epub 2001 Jan 9.
- Schett G. (2007). Cells of the synovium in rheumatoid arthritis Osteoclasts. *Arthritis Research & Therapy.* 9;20
- Schmutz C, Hulme A, Burman A, Salmon M, Ashton B, Buckley C, Middleton J. (2005). Chemokine receptors in the rheumatoid synovium; upregulation of CXCR5. *Arthritis Res Ther.* 7(2);R217-29.
- Schneider-Poetsch T, Ju J, Eyler DE, Dang Y, Bhat S, Merrick WC, Green R, Shen B and Liu JO. (2010). Inhibition of Eukaryotic Translation Elongation by Cycloheximide and Lactimidomycin. *Nat Chem Biol.* Mar 2010; 6(3): 209–217.
- Schutyser E, Struyf S, Van Damme J. (2003). The CC chemokine CCL20 and its receptor CCR6. *Cytokine Growth Factor Rev.* 14(5);409-26.
- Scotton C, Milliken D, Wilson J, Raju S, Balkwill F. (2001). Analysis of CC chemokine and chemokine receptor expression in solid ovarian tumours. *Br J Cancer.* 85(6): 891–897.
- Selmi C, Santis M, Gershwin E. (2011). Liver involvement in subjects with rheumatic disease. *Arthritis Res Ther.* 13(3): 226.
- Senator GB, Muirden KD. (1968). Concentration of iron in synovial membrane, synovial fluid, and serum in rheumatoid arthritis and other joint diseases. *Ann Rheum Dis.* Jan;27(1):49-54.
- Semerano L, Clavel G, Assier E, Denys A, Boissier MC. (2011). Blood vessels, a potential therapeutic target in rheumatoid arthritis?. *Joint Bone Spine.* 78(2):118-23.
- Shamri R, Grabovsky V, Gauguet JM, Feigelson S, Manevich E, Kolanus W, Robinson MK, Staunton DE, von Andrian UH, Alon R (2005). Lymphocyte arrest requires instantaneous induction of an extended LFA-1 conformation mediated by endothelium bound chemokines. *Nat Immunol.* 6:497-506.
- Shashkin P, Simpson D, Mishin V, Chesnutt B, Ley K. (2003). Expression of CXCL16 in human T-cells. *Arterioscler Thromb Vasc Biol.* 23(1):148-9.
- Shimaoka T, Kume N, Minami M, Hayashida K, Kataoka H, Kita T, Yonehara S. (2000). Molecular cloning of a novel scavenger receptor for oxidized low density lipoprotein, SR-PSOX, on macrophages. *J Biol Chem.* 275(52):40663-6.
- Shimaoka T, Nakayama T, Fukumoto N, Kume N, Takahashi S, Yamaguchi J, Minami M, Hayashida K, Kita T, Ohsumi J, Yoshie O, Yonehara S. (2004). Cell surface-anchored SR-PSOX/CXC chemokine ligand 16 mediates firm adhesion of CXC chemokine receptor 6-expressing cells. *J Leukoc Biol.* 75(2):267-74.
- Shulman Z, Shinder V, Klein E, Grabovsky V, Yeger O, Geron E, Montresor A, Bolomini-Vittori M, Feigelson S W, Kirchhausen T, Laudanna C, Shakhar G,

Alon R. (2009). Lymphocyte crawling and transendothelial migration require chemokine triggering of high-affinity LFA-1 integrin. *Immunity*. 30:384–396.

Smith MD, Barg E, Weedon H, Papangelis V, Smeets T, Tak PP, Kraan M, Coleman M, Ahern MJ. (2003). Microarchitecture and protective mechanisms in synovial tissue from clinically and arthroscopically normal knee joints. *Ann Rheum Dis*. 62(4):303-7.

Smith E, McGettrick HM, Stone MA, Shaw JS, Middleton J, Nash GB, Buckley CD, Ed Rainger G. (2008). Duffy antigen receptor for chemokines and CXCL5 are essential for the recruitment of neutrophils in a multicellular model of rheumatoid arthritis synovium. *Arthritis Rheum*. 58(7):1968-73.

Smolen JS, Steiner G. (2003). Therapeutic strategies for rheumatoid arthritis. *Nat Rev Drug Discov*. 2:473-88.

Smolen JS, Aletaha D, Koeller M, Weisman MH, Emery P. (2007). New therapies for treatment of rheumatoid arthritis. *Lancet*. 370:1861_74.

Song Y W and Kang E H. (2009). Autoantibodies in rheumatoid arthritis; rheumatoid factors and anticitrullinated protein antibodies. *QJM*. Advance Access published November 19, 2009

Stanford M M, Issekutz T B.(2003). The relative activity of CXCR3 and CCR5 ligands in T lymphocyte migration: concordant and disparate activities in vitro and in vivo. *J Leukoc Biol*. 74(5):791-9.

Strand V, Kimberly R and Isaacs J D. (2007). Biologic therapies in rheumatology; lessons learned, future directions. *Nature Reviews Drug Discover*. 6. 75-92

Strasly M, Doronzo G, Capello P, Valdembri D, Arese M, Mitola S, et al. (2004), CCL16 activates an angiogenic program in vascular endothelial cells. *Blood* 103:40e9.

Subileau EA, Rezaie P, Davies HA, Colyer FM, Greenwood J, Male DK, Romero IA. (2009). Expression of chemokines and their receptors by human brain endothelium: implications for multiple sclerosis. *J Neuropathol Exp Neurol*. 68(3):227-40.

Szekanecz Z, Strieter RM, Kunkel SL, Koch AE. (1998). Chemokines in rheumatoid arthritis. *Springer Semin Immunopathol*. 20(1-2);115-32.

Szekanecz Z, Koch AE. (2001). Chemokines and angiogenesis. *Curr Opin Rheumatol*. 13(3);202-8.

Szekanecz Z, Kim J, Koch A E. (2003). Chemokines and chemokine receptors in rheumatoid arthritis. *Seminars in Immunology* 15. 15–21

Szekanecz Z, Koch AE. (2004). Vascular endothelium and immune responses; implications for inflammation and angiogenesis. *Rheum Dis Clin North Am*. 30(1);97-114.

- Szekanecz Z, Koch AE. (2005). Endothelial cells in inflammation and angiogenesis. *Curr Drug Targets Inflamm Allergy*. 4(3);319-23.
- Szekanecz Z, Szucs G, Szántó S, Koch AE. (2006). Chemokines in Rheumatic Diseases. *Current Drug Targets*. 7. 91-102.
- Szekanecz Z and Koch AE. (2007). Macrophages and their products in rheumatoid arthritis. *Current Opinion in Rheumatology*. 19(3). 289-295
- Szekanecz Z and Koch A E. (2008). Vascular involvement in rheumatic diseases; ‘vascular rheumatology’. *Arthritis Research & Therapy*. 10;224
- Szekanecz Z, Besenyei T, Paragh G, Koch AE.(2009). Angiogenesis in rheumatoid arthritis. *Autoimmunity*. 42(7);563-73.
- Szekanecz Z, Besenyei T, Paragh G, Koch AE. (2010). New insights in synovial angiogenesis. *Joint Bone Spine*. Jan;77(1):13-9. Epub 2009 Dec 21.
- Szekanecz Z, Besenyei T, Szentpétery A, Koch AE. (2010). Angiogenesis and vasculogenesis in rheumatoid arthritis. *Curr Opin Rheumatol*. 22(3):299-306.
- Tadokoro S, Shattil SJ, Eto K, Tai V, Liddington RC, de Pereda JM, Ginsberg MH, Calderwood DA. (2003). Talin binding to integrin beta tails: a final common step in integrin activation. *Science*. 02:103-106.
- Tak P P. (2001). Is early rheumatoid arthritis the same disease process as late rheumatoid arthritis?. *Best Practice & Research Clinical Rheumatology*. 15(1). 17-26,
- Takemura S, Braun A, Crowson C, Kurtinc P J, Cofield R H, O’Fallon W M, Goronzy J J and Weyand C M. (2001). Lymphoid Neogenesis in Rheumatoid Synovitis. *The Journal of Immunology*, 167; 1072–1080.
- Talbot J, Bianchini FJ, Nascimento DC, Oliveira RD, Souto FO, Pinto LG, Peres RS Silva JR, Almeida SC, Louzada-Junior P, Cunha TM, Cunha FQ, Alves-Filho JC. (2015). CCR2 Expression in Neutrophils Plays a Critical Role in their migration into the joints in rheumatoid arthritis. *Arthritis Rheumatol*. 67(7):1751-9.
- Tanaka Y, Fujii K, Hübscher S, Aso M, Takazawa A, Saito K, Ota T, Eto S. (1998). Heparan sulfate proteoglycan on endothelium efficiently induces integrin-mediated T cell adhesion by immobilizing chemokines in patients with rheumatoid synovitis. *Arthritis Rheum*. 41(8):1365-77.
- Tarrant TK, Patel DD. (2006). Chemokines and leukocyte trafficking in rheumatoid arthritis. *Pathophysiology*. 13(1);1-14. Epub 2005 Dec 27.
- Telfer JF, Brock JH. (2004). Proinflammatory cytokines increase iron uptake into human monocytes and synovial fibroblasts from patients with rheumatoid arthritis. *Med Sci Monit*. Apr;10(4):BR91-5.

Thurlings RM, Wijbrandts CA, Mebius RE, Cantaert T, Dinant HJ, van der Pouw-Kraan TC, Verweij CL, Baeten D, Tak PP. (2008). Synovial lymphoid neogenesis does not define a specific clinical rheumatoid arthritis phenotype. *Arthritis Rheum.* 58(6):1582-9.

Thurlings RM, Wijbrandts CA, Bennink RJ, Dohmen SE, Voermans C, Wouters D, Izmailova ES, Gerlag DM, van Eck-Smit BL, Tak PP. (2009). Monocyte scintigraphy in rheumatoid arthritis: the dynamics of monocyte migration in immune-mediated inflammatory disease. *PLoS One.* 4(11):e7865.

Tiku ML, Shah R, Allison GT. (2000). Evidence linking chondrocyte lipid peroxidation to cartilage matrix protein degradation. Possible role in cartilage aging and the pathogenesis of osteoarthritis. *J Biol Chem.* Jun 30;275(26):20069-76.

Torikai E, Kageyama Y, Suzuki M, Ichikawa T, Nagano A. (2007). The effect of infliximab on chemokines in patients with rheumatoid arthritis. *Clin Rheumatol.* 26(7):1088-93.

Toussiroit E, Roudier J. (2008). Epstein-Barr virus in autoimmune diseases. *Best Pract Res Clin Rheumatol.* 22(5):883-96.

Tsubaki T, Takegawa S, Hanamoto H, Arita N, Kamogawa J, Yamamoto H, Takubo N, Nakata S, Yamada K, Yamamoto S, Yoshie O, Nose M. (2005). Accumulation of plasma cells expressing CXCR3 in the synovial sublining regions of early rheumatoid arthritis in association with production of Mig/CXCL9 by synovial fibroblasts. *Clin Exp Immunol.* 141(2):363-71.

Uhlig T and Kvien T. (2005). Is rheumatoid arthritis disappearing?. *Ann Rheum Dis.* 64(1); 7-10.

Ueno A, Yamamura M, Iwahashi M, Okamoto A, Aita T, Ogawa N, Makino H. (2005). The production of CXCR3-agonistic chemokines by synovial fibroblasts from patients with rheumatoid arthritis. *Rheumatol Int.* 25(5);361-7.

van der Voort R, van Lieshout AW, Toonen LW, Sløetjes AW, van den Berg WB, Figdor CG, Radstake TR, Adema GJ. (2005). Elevated CXCL16 expression by synovial macrophages recruits memory T-cells into rheumatoid joints. *Arthritis Rheum.* 52(5):1381-91.

van Lieshout AW, Barrera P, Smeets RL, Pesman GJ, van Riel PL, van den Berg WB, Radstake TR. (2005). Inhibition of TNF alpha during maturation of dendritic cells results in the development of semi-mature cells; a potential mechanism for the beneficial effects of TNF alpha blockade in rheumatoid arthritis. *Ann Rheum Dis.* 64(3);408-14.

van Lieshout AW, Fransen J, Flendrie M, Eijsbouts AM, van den Hoogen FH, van Riel PL, Radstake TR. (2007). Circulating levels of the chemokine CCL18 but not CXCL16 are elevated and correlate with disease activity in rheumatoid arthritis. *Ann Rheum Dis.* 66(10);1334-8.

van Lieshout AW, van der Voort R, Toonen LW, van Helden SF, Figdor CG, van Riel PL, Radstake TR, Adema GJ. (2009). Regulation of CXCL16 expression and secretion by myeloid cells is not altered in rheumatoid arthritis. *Ann Rheum Dis*. 68(6):1036-43.

Volin MV, Woods JM, Amin MA, Connors MA, Harlow LA, Koch AE. (2001). Fractalkine; a novel angiogenic chemokine in rheumatoid arthritis. *Am J Pathol*. 159(4):1521-30.

Vulcano M, Albanesi C, Stoppacciaro A, Bagnati R, D'Amico G, Struyf S, Transidico P, Bonecchi R, Del Prete A, Allavena P, Ruco LP, Chiabrandi C, Girolomoni G, Mantovani A, Sozzani S (2001). "Dendritic cells as a major source of macrophage-derived chemokine/CCL22 in vitro and in vivo". *Eur. J. Immunol*. 31 (3): 812–22.

Walz A, Kunkel SL, Strieter RM. (1996). in "Chemokines in disease" . Koch AE and Strieter RM eds. RG Landes Company, Austin. 1-25.

Wang CR, Liu MF, Huang YH, Chen HC. (2004). Up-regulation of XCR1 expression in rheumatoid joints. *Rheumatology (Oxford)*. 43(5):569-73.

Wang Y, Cui L, Gonsiorek W, Min SH, Anilkumar G, Rosenblum S, Kozlowski J, Lundell D, Fine JS, Grant EP. (2009). CCR2 and CXCR4 regulate blood peripheral monocyte pharmacodynamics and link in experimental autoimmune encephalitis. *J Inflamm (Lond)*. 11;6:32.

Webb LM, Walmsley MJ, Feldmann M: (1996). revention and amelioration of collagen-induced arthritis by blockade of the CD28 costimulatory pathway: requirement for both B7-1 and B7-2. *Eur J Immunol*, 26:2320-2328.

Weber M, Blair E, Simpson CV, O'Hara M, Blackburn PE, Rot A, Graham GJ, Nibbs RJ. (2004). The chemokine receptor D6 constitutively traffics to and from the cell surface to internalize and degrade chemokines. *Mol Biol Cell*. 2004 May;15(5):2492-508.

Wedepohl S¹, Beceren-Braun F, Riese S, Buscher K, Enders S, Bernhard G, Kilian K, Blanchard V, Dervede J, Tauber R.(2012). L-selectin--a dynamic regulator of leukocyte migration. *Eur J Cell Biol*. 2012 Apr;91(4):257-64. doi: 10.1016/j.ejcb.2011.02.007. Epub 2011 May 4.

Wedepohl S, Beceren-Braun F, Riese S, Buscher K, Enders S, Bernhard G, Kilian K, Blanchard V, Dervede J, Tauber R. (2012). L-selectin--a dynamic regulator of leukocyte migration. *Eur J Cell Biol*. 91(4):257-64.

Weninger W, Carlsen HS, Goodarzi M, Moazed F, Crowley MA, Baekkevold ES, Cavanagh LL, von Andrian UH. (2003). Naive T cell recruitment to nonlymphoid tissues: a role for endothelium-expressed CC chemokine ligand 21 in autoimmune disease and lymphoid neogenesis. *J Immunol*. 170(9):4638-48.

Weyand CM, Goronzy JJ. (2003). Ectopic germinal center formation in rheumatoid synovitis. *Ann N Y Acad Sci*. 987:140-9.

Whittall C, Kehoe O, King S, Rot A, Patterson A, Middleton J. (2013). A chemokine self-presentation mechanism involving formation of endothelial surface microstructures. *J Immunol.* 2013 Feb 15;190(4):1725-36.

Wilkinson L S. Pitsillides A A. Worrall J G. Edwards J C W. (1992). Light microscopic characterisation of the fibroblastic synovial lining cell (synoviocyte). *Arthritis Rheum.* 35. 1179-1184

Wilbanks A, Zondlo SC, Murphy K, Mak S, Soler D, Langdon P, Andrew DP, Wu L, Briskin M. (2001). Expression cloning of the STRL33/BONZO/TYMSTR ligand reveals elements of CC, CXC, and CX3C chemokines. *J Immunol.* 166(8):5145-54.

Wittchen E S. (2009). Endothelial signaling in paracellular and transcellular leukocyte transmigration. *Front Biosci.* 14. 2522–2545.

Wong SH. Francis N. Chahal H. Raza K. Salmon M. Scheel-Toellner D and Lord JM. (2009). Lactoferrin is a survival factor for neutrophils in rheumatoid. *Rheumatology.* 48. 39–44

Woodfin A, Voisin M, Imhof B, Dejana E, Engelhardt B, Nourshargh S. (2009). Endothelial cell activation leads to neutrophil transmigration as supported by the sequential roles of ICAM-2, JAM-A, and PECAM-1. *Blood.* 113(24); 6246–6257.

Woolf E, Grigorova I, Sagiv A, Grabovsky V, Feigelson S W, Shulman Z, Hartmann T, Sixt M, Cyster J.G., Alon R. (2007). Lymph node chemokines promote sustained T lymphocyte motility without triggering stable integrin adhesiveness in the absence of shear forces, *Nat. Immunol.* 8.1076–1085.

Wright HL, Moots RJ, Edwards SW (2014). The multifactorial role of neutrophils in rheumatoid arthritis. *Nat Rev Rheumatol.* 10(10):593-601.

Wu HX, Zhang Y, Zhu YL. Serum levels of several chemokines in patients with rheumatoid arthritis. *Zhonghua Yi Xue Za Zhi.* 2;85(8):534-7

Xu H, Edwards J, Banerji S, Prevo R, Jackson DG, Athanasou NA. (2003). Distribution of lymphatic vessels in normal and arthritic human synovial tissues. *Ann Rheum Dis.* 62(12):1227-9

Yamanishi Y, Boyle DL, Rosengren S, Green DR, Zvaifler NJ, Firestein GS. (2002). Regional analysis of p53 mutations in rheumatoid arthritis synovium. *Proc Natl Acad Sci U S A.* Jul 23;99(15):10025-30. Epub 2002 Jul 15.

Yang MH, Wu FX, Xie CM, Qing YF, Wang GR, Guo XL, Tang Z, Zhou JG, Yuan GH. (2009). Expression of CC chemokine ligand 5 in patients with rheumatoid arthritis and its correlation with disease activity and medication. *Chin Med Sci J.* 24(1);50-4.

Yarwood A, Huizinga TW, Worthington J. (2014). The genetics of rheumatoid arthritis: risk and protection in different stages of the evolution of RA. *Rheumatology (Oxford).* Sep 18. pii: keu323. [Epub ahead of print]

Yeo L, Toellner KM, Salmon M, Filer A, Buckley CD, Raza K, Scheel-Toellner D. (2011). Cytokine mRNA profiling identifies B cells as a major source of RANKL in rheumatoid arthritis. *Ann Rheum Dis*. 70(11):2022-8.

Yin G, Wang Y, Cen XM, Yang M, Liang Y, Xie QB. (2015). Lipid peroxidation-mediated inflammation promotes cell apoptosis through activation of NF- κ B pathway in rheumatoid arthritis synovial cells. *Mediators Inflamm*. 2015:460310.

Youn BS, Zhang S, Broxmeyer HE, Antol K, Fraser MJ Jr, Hangoc G, Kwon BS. (1998). Isolation and characterization of LMC, a novel lymphocyte and monocyte chemoattractant human CC chemokine, with myelosuppressive activity. *Biochem Biophys Res Commun*. 18;247(2):217-22.

Zarbock A, Deem TL, Burcin TL, Ley K. (2007). Galphai2 is required for chemokine-induced neutrophil arrest. *Blood*. 110:37733779.

Zhao X, Yue Y, Cheng W, Li J, Hu Y, Qin L, Zhang P. (2013). Hypoxia-inducible factor: a potential therapeutic target for rheumatoid arthritis. *Curr Drug Targets*. 1;14(6):700-7.

Zhou Q, Wood R, Schwarz EM, Wang YJ, Xing L. (2010). Near-infrared lymphatic imaging demonstrates the dynamics of lymph flow and lymphangiogenesis during the acute versus chronic phases of arthritis in mice. *Arthritis Rheum*. 62(7):1881-9.

Zhu SL, Luo MQ, Peng WX, Li Q X, Feng ZY, Li ZX, Wang MX, Feng XX, Liu F, Huang JL. (2015). Sonic hedgehog signalling pathway regulates apoptosis through Smo protein in human umbilical vein endothelial cells. *Rheumatology (Oxford)*. 54(6):1093-102

Zvaifler NJ, Tsai V, Alsalameh S, von Kempis J, Firestein GS, Lotz M. (1997). Pannocytes; distinctive cells found in rheumatoid arthritis articular cartilage erosions. *Am J Pathol*. 150(3):1125-38.

9.2 Book references

Edwards JCW. (1998). "The Synovium", in *Rheumatology* 2nd edn. Vol 1. Klippel JH and Dieppe PA eds. Mosby Publishers. London

Edwards JCW. (2003). "The synovium", in *Rheumatology*, 3rd edn, vol 1. Hochberg MC, Silman AJ, Smolen JS, Weinblatt ME, Weisman MH, eds. Mosby Publishers. London.

Gimbrone MA, Lelkes P. (2003). Mechanical Forces and the Endothelium, volume 6 of *Endothelial Cell Research*. Lelkes P ed. Hardwood Academic Publishers. The Netherlands

Strieter RM, Kunkel SL, Shanafelt AB. (1996a). in "Chemokines in disease" (Koch AE and Strieter RM eds). RG Landes Company, Austin. 1-25.

Strieter RM, Kunkel SL, Shanafelt AB. (1996b). in “*Chemokines in disease*” (Koch AE and Strieter RM eds). RG Landes Company, Austin. 95-209.

9.3 Web site references

Pubmed: NCBI Entrez gene. URL: <http://www.ncbi.nlm.nih.gov/sites/entrez>

free image database Original image at
http://training.seer.cancer.gov/module_anatomy/images/illu_lymph_capillary.jpg

Abramson, J.H. (2011) WINPEPI updated: computer programs for epidemiologists, and their teaching potential. *Epidemiologic Perspectives & Innovations* 8:1.

ChemGaroo URL:

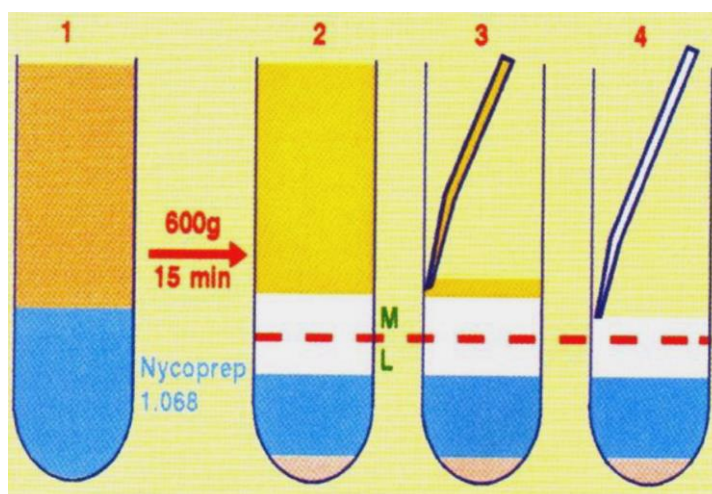
http://www.chemgapedia.de/vsengine/vlu/vsc/en/ch/25/orgentec/autoimmun.vlu/Page/vsc/en/ch/25/orgentec/autoimmun_ra_en.vscml.html

Appendix

Materials and methods additions

Monocyte isolation using NycoPreo™

Monocytes were isolated using the density medium NycoPrep™ 1.068 (Nycomed Pharma AS Diagnostics, Oslo, Norway). The osmolality of this density medium generated a slightly hypertonic solution that enabled the monocytes to be separated from the lymphocytes. Because lymphocytes are more susceptible to this hypertonicity, they expel more water and increase in density, thus they migrated and sedimented further during centrifugation. Following this the monocyte layer at the interface of the NycoPrep and the plasma was aspirated. The density gradient centrifugation procedure was performed using full sterile technique in a biological safety cabinet. Approximately 12ml of fresh peripheral blood was collected, transferred to a universal tube and 1.2 ml of 6% Dextran 500 (Sigma-Aldrich), prepared in 0.9% NaCl saline solution, was added. After mixing, the sample was incubated at room temperature for a minimum of 40 minutes to allow for plasma separation and erythrocyte sedimentation. The leukocyte-rich plasma was then carefully removed and layered over 3 ml of NycoPrep™ 1.068 in a 15 ml centrifuge tube. This was then centrifuged for 15 minutes at 1300rpm at room temperature. Following this the plasma was removed to within 3–4 mm of the interface and immediately aliquoted for storage at –20°C. The remaining plasma and the top half of the NycoPrep™ 1.068 layer which contained the enriched monocytes, was then aspirated. The cells were then washed twice by being centrifuged at 1300rpm for 7 minutes at room temperature in 0.9% NaCl saline solution containing 0.13% EDTA and 1% FBS. Figure 2.4 shows a flow diagram of the procedure.



Appendix figure 1. Flow diagram of the NycoPrep 1.068 monocyte isolation protocol.

1 NycoPrep 1.068 with the leukocyte-rich plasma layered on top. 2. Separation of mononuclear cell fractions 3. Removal of the plasma. 4. Collection of monocyte (M) cell layer. (Figure reproduced from the Nycomed Density Gradient Media Applications and Products catalogue 2000).

2. Principles of Transverse Heated-Graphite Furnace Atomic Absorption Spectrometry (T H-GFAAS)

In atomic absorption (AA) spectrometry, light of a specific wavelength is passed through the atomic vapour of an element of interest, and measurement is made of the attenuation of the intensity of the light because of absorption. Quantitative analysis by AA depends on: 1, accurate measurement of the intensity of the light and 2, the assumption that the radiation absorbed is proportional to atomic concentration.

Samples to be analysed by AA must be vaporised or atomised, typically by using a flame or graphite furnace (figure 2.5). The graphite furnace is an electro-thermal atomiser system that can produce temperatures as high as 3,000°C. The heated graphite furnace provides the thermal energy to break chemical bonds within the sample and produce free ground-state atoms. Ground-state atoms then are capable of absorbing energy, in the form of light, and are elevated to an excited state. The amount of light energy absorbed increases as the concentration of the selected element increases.

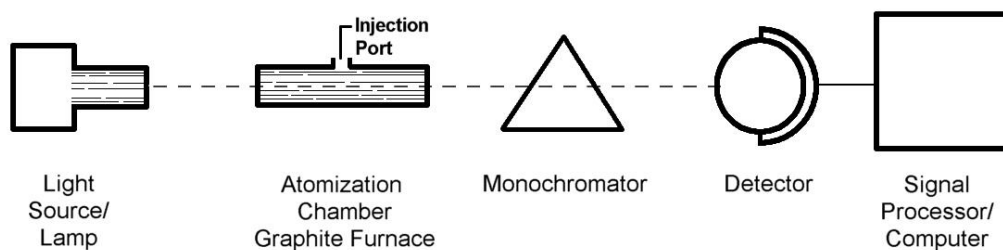


Diagram of the basic components of a Graphite Furnace Atomic Absorption Spectrometer.

Appendix Figure 2. Diagram showing the basic GFAAS components

3 Chemotaxis

The blood was prepared according to whether using PBMCs, monocytes only, or whole blood leukocytes (2.11.1) a sterile 24 well plate (Scientific Laboratory Supplies). The chemokine solutions required were made with serum free DMEM-F12 made up to 800µl for each well. 5µm pore filters (Merck Chemicals, Nottingham, UK) were suspended in each well and approximately 100,000 leukocytes were added to the well of each filter well to give a final volume of 400µl with serum free DMEM-F12. The plate was then left for 30 minutes for migration to occur. All of the above was carried out using solutions at 37°C. Following the migration the medium from the bottom well was removed and a FACS analysis was performed. Negative controls were the same as above with the exception of omitting the chemokine in the bottom well. Positive controls were as above with the chemokine replaced with a suitable chemoattractant.

4 Endothelial cell isolation from fresh synovium

4.1 Separation of endothelial cells from fresh synovium with collagenase and DNaseI.

The tissue sample was collected by the surgeon after informed consent was gained from the patient and stored at 4°C for use within 18 hours. The digestion solution was prepared by placing 39.5ml DMEM-F12 medium with penicillin and streptomycin, FBS and fungizone (as in section 2.5, herein referred to as complete medium) in a 50ml falcon tube 500µl of DNaseI was added (giving a final concentration of 40µg/ml) and 10ml of 10mg/ml collagenase XI was added giving a final concentration of 2mg/ml.

The tissue sample was rinsed in fresh complete medium to eliminate blood clots and was then placed in a petri dish and cut up into pieces approximately 3mm². A region of the tissue which appeared highly vascularised was cut up where possible to maximise the

chance of isolating ECs. A metallic mesh was cut to a size which would fit over the petri dish, then wetted with complete medium. The diced tissue sample was transferred to the mesh which was placed over a clean petri dish where the tissue was rinsed with complete medium again.

The diced tissue was split between 2 x 50ml falcon tubes containing 10ml of the digestion solution and incubated at 37°C for 15 minutes whilst shaking at 230rpm. The supernatant was removed and the pellet resuspended before placing back on the mesh and rinsing with complete medium, at which stage the lymphocytes should have been fully eliminated. The tissue was split between 2 x 50ml falcon tubes containing 15ml of the digestion solution and incubated at 37°C for 45 minutes whilst shaking on a roller.

After this the mesh was rinsed well and placed over a clean petri dish and wetted with fresh complete medium. The tissue sample was poured from the falcon tube back onto the mesh and the eluate was allowed to pass through the mesh into the petri dish. The eluate was then transferred from the petri dish into a clean 50ml falcon tube by passing it through a 40µm sterile filter. The exact volume of eluate was recorded and a cell count was performed. The cell suspension was then transferred into 2 x 15ml falcon tubes and centrifuged at 1600rpm for 5 minutes ready for magnetic labelling.

4.2 Magnetic labelling of isolated EC cells

The supernatant was removed from the pellet resuspended in 80µl PBS/BSA/EDTA per 10^7 total cells. Following this, mouse anti-human Duffy antigen IgG1 (Dako) was added (at 1:200 concentration) and incubated at 8-10°C for one hour. 20µl rat anti-mouse IgG1 micro-beads per 10^7 total cells was then added and once well mixed was incubated at 6-12°C for 15 minutes.

PBS/BSA/EDTA labelling buffer was added at 10-20 x the total volume to wash the cells and they were centrifuged at 1100RPM for 10 minutes. The supernatant was removed and the cells were resuspended in 500µl of buffer per 10^8 total cells.

4.3 Magnetic separation of isolated EC cells

The column was placed in the magnetic field of the MACs separator and prepared by washing with 500µl of the buffer. The cell suspension was added to the column for selection to occur and the column then rinsed with 500µl of the buffer three times. The column was removed from the separator and placed in a 15ml falcon tube where 1ml of buffer was added to the column and the positive cell fraction was removed using the plunger. The positive fraction was transferred to a freshly prepared column and rinsed as above. The positive cells were then transferred to a T25 culture flask containing the pre warned appropriate amount of EGM-2 complete medium and placed in the incubator at 37°C with 5% CO².

Appendix table A. Patient immunofluorescent data (continued on next page)

Chemokine	RA Sample							
	1	2	3	4	5	6	7	8
	% VWF+ Ch +	%VWF + Ch +						
CCL1	0%*	8%*	31%	3%*	23%*	14%*	9%*	na
CCL2	41%	29%*	43%	50%	45%	71%*	89%*	44%
CCL3	11%*	31%	60%*	9%*	30%	8%*	61%*	10%*
CCL4	25%*	6%*	75%*	71%*	71%*	100%*	73%*	78%*
CCL5	55%	61%*	67%*	57%	45%	50%	9%*	15%*
CCL7	58%	49%	87%*	48%	91%*	68%*	85%*	68%*
CCL8	43%	78%*	74%*	69%*	65%*	67%*	89%*	25%*
CCL10	36%	61%*	89%*	38%	73%*	3%*	76%*	44%
CCL11	7%*	0%*	13%*	15%*	57%	18%*	13%*	5%*
CCL12	5%*	3%*	30%*	6%*	2%*	13%*	6%*	12%*
CCL13	65%*	41%	8%*	76%*	46%	55%	54%	26%*
CCL14	37%	71%*	98%*	58%	69%*	94%*	82%*	76%*
CCL15	52%	13%*	56%	44%	63%*	64%	56%	31%

Chemokine	RA Sample							
	1	2	3	4	5	6	7	8
	% VWF+ Ch +	%VWF + Ch +						
CCL15	52%	13%	56%	44%	63%*	64%	56%	31%
CCL16	100%*	47%	83%*	98%*	75%*	71%*	74%*	45%*
CCL17	4%	7%	86%*	0%	5%	33%	3%	0%
CCL18	30%	13%	44%	41%	70%*	24%	47%	36%
CCL19	58%	98%*	80%*	72%*	95%*	81%*	83%*	73%*
CCL20	10%	19%	11%	28%	16%	18	31%	15%
CCL21	5%	40%	48%	4%	8%*	34%	76%*	74%*
CCL22	46%	62%*	73%*	8%	74%*	72%*	74%*	67%*
CCL23	15%	41%	32%	27%	49%	37%	54%	46%
CCL24	28%	22%	39%	6%	29%	43%	44%	19%
CCL25	16%	9%	37%	37%	39%	43%	29%	17%
CCL26	74%*	56%	86%*	59%	95%*	60%*	50%	29%
CCL27	4%	5%	6%	11%	12%	13%	10%	6%
CCL28	43%	35%	70%*	40%	25%	64%*	40%	12%

synovial ECs. * indicates chemokines present on $\geq 60\%$ of vessels.